The potential of biomarkers for reconstructing long-term ecohydrological and microbial community changes in newly discovered Amazonian peatlands

BSc Anca Elena Amariei

Submitted in the fulfilment of the requirements for the degree of Master (by Research)

School of Geographical and Earth Sciences

College of Science and Engineering

University of Glasgow

October 2018

Supervised by Prof. Jaime L. Toney and Dr. Katherine Roucoux

Abstract

The existence of extensive tropical peatlands (i.e. 35,600 ± 2133 km^2) was recently confirmed in Amazonia (Lähteenoja et al., 2009 a, b; 2011; Draper et al., 2014). These peatlands appear to be hydrologically intact but are at risk of degradation from anthropogenic impacts and climate change (Roucoux et al., 2017). Furthermore, their discovery represents a new potential source or sink of atmospheric gas budgets and a new component of the CH_4 global map that need to be considered in future climate change scenarios.

Our main interests are to test the applicability of biomarkers within these settings, to describe CH_4 production in Amazonian peatlands and the changes in CH_4 efflux through time, as a function of various environmental parameters, as this information is currently lacking for this area. We focused on surface and core samples from Pastaza-Marañón Foreland Basin, northern Peru with samples associated with three vegetation types, providing thus a wide view over these dynamic ecosystems.

Vegetation and environment related biomarkers (i.e. n-alkanes; hopanes; GDGTs) and proxies are in agreement with changes depicted in pollen records from Quistococha and San Jorge peatland (Roucoux et al., 2013; Kelly et al., 2017). Thus, they can be used to describe shifts in vegetation or environment in the third peatland, Buena Vista. Furthermore, since present day CH_4 are not predictable from a water-table depth point of view as, for example, higher effluxes occur during the dry season in black-water seasonally flooded forest (i.e. Bunea Vista; Teh et al., 2017), several biomarker groups were used to further our understanding of processes that lead to these discrepancies. Thus, short chain and monosaturated fatty acids were employed alongside hopanoids and GDGTs, in order to test and understand how the archaea and bacteria, and more specifically, methanogen and methanotroph communities, responded to changes in the ecohydrology. Furthermore, we provide new temperature and pH palaeorecords for each peatland that were previously lacking for these environments and compared them to present-day instrumental measurements in surface samples.

By employing a multi-biomarker approach, we can explore the relationship between environmental parameters via direct and proxy observations of fluctuations in water table depth, changes in vegetation, hydrology and CH_4 production potential, gaining a further insight into tropical peatland dynamics and carbon biogeochemical cycles within them. Finally, we encourage higher-resolution biomarker analysis and provide ideas for further research within these peatlands.

Acknowledgments

Firstly, I would like to thank my supervisors, Prof Jaime L. Toney and Dr Katherine Roucoux for their guidance, support and mentorship during this project. Many of the great things that happened to me this year are due to your combined effort. Thank you!

Thank you to everyone in the BECS group, I have learned many things from everyone! Thanks Ali for providing training, assistance and guidance from my first days in the lab to the final analysed samples, thanks to Charlotte and Mike for being so helpuful and resourceful, to Bianca for showing me how to understand and write about the data-probably this is why the GDGT chapter was so long!, to Elsa and Julien for their help in the lab and feedback! Thanks are also going to Cairns, Tingwen and Scott for sharing this master experience together, tips and knowledge, combusted vials and joy along the way.

Special thanks are going to David, Gordon, Ioanna, Jérôme and Profesor Richard Pancost in the OGU lab at the University of Bristol and for allowing me to use their facilities and for providing guidance and support!

This research was possible with the financial support from SAGES and the School of Geographical and Earth Science, University of Glasgow, to which I am grateful.

Finally, I want to thank my mom, dad and Răzvan for their support in every aspect!

List of Tables

Table of Figures

Abbreviations

QT=Quistococha peatland

SJO=San Jorge peatland

BVA=Buena Vista peatland

PMFB= Pastaza-Marañón Foreland Basin

CH_4 = methane

CO_2= carbon dioxide

OM=organic matter

GHG= greenhouse gas(es)

C_{30}-hop= hopane with 30 carbons

GDGTs= glycerol dialkyl glycerol tetraethers

Mha= mega hectars

Gt= giga tonnes

μg= micro grams

MOB= methane oxidising bacteria

Cal yr BP = radiocarbon age

yr bp = extrapolated age from radiocarbon ages

Declaration

"I declare that, except where explicit reference is made to the contribution of others, that this dissertation is the result of my own work and has not been submitted for any other degree at the University of Glasgow or any other institution."

Printed Name: Anca Elena Amariei

Signature: _____

Contents

1. Introduction

1.1. Wetland environments and ecology

Wetlands are highly valuable ecosystems due to their multiple ecological and biodiversity, hydrological, carbon sequestration, habitat and human health functions (Figure 1; Russi et al., 2013). These functions together with their classifications and landscape values are detailed elsewhere (Whiteoak and Binney, 2012, Stefanakis et al., 2014; The Ramsar Conventions Manual, 6th edition) and here their global extent and status are briefly discussed (Hu et al., 2017).

Given their complex nature, wetlands have been and are still difficult to define and geographically delimitate. They are generally thought as zones of transition between terrestrial and aquatic/deep-water environments (Cowardin et al., 1979). As both environments are influencing them, their study requires an interdisciplinary approach that combines elements of hydrology, geomorphology, climate, soil and biota science (Figure 1). In common speech, they have been referred to as "fens", "bogs", "marsh", "swamps", "mires" or "peatlands" ("moors", "muskegs") yet these terms are now used to classify wetland types

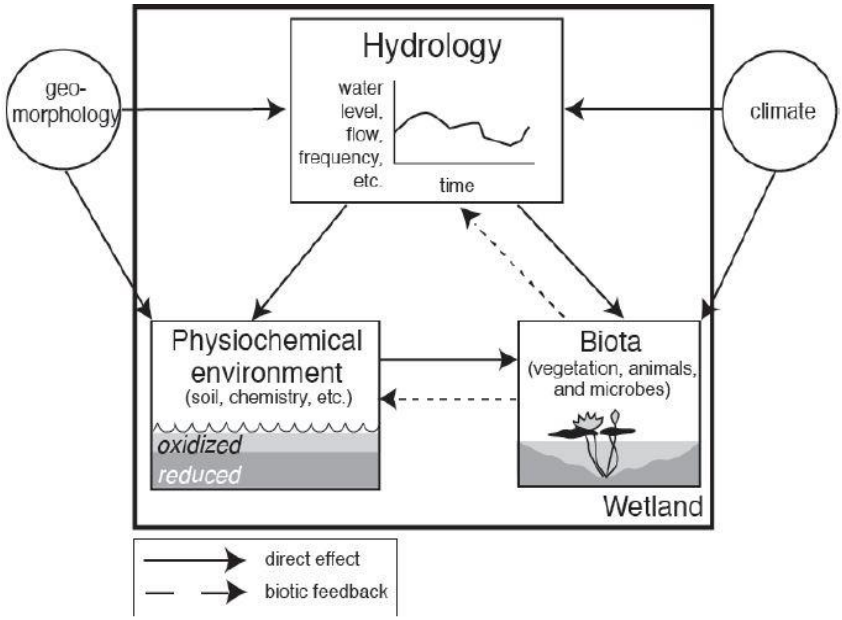

Figure 1 Interactions between main environmental spheres within the wetland classification. Notice the direct effects of geomorphology and climate on hydrology, physiochemical parameters and biota. These effects and feedbacks are currently true for Amazonian peatlands, and influence the carbon cycle within these settings (taken from Mitsch and Gosselink, 2015).

as throughout the literature they have received more precise definitions that distinguish, in broad terms, one from another (Charman, 2002; Mitsch and Gosselink, 2015).

Recently, as conservation and preservation laws emerged in the '70s, a clear definition and classification of a wetland was needed (e.g. The Ramsar Convention on Wetlands, Iran, 1971). The first use of the term "wetland" dates back to 1956 (Shaw and Fredine, 1956) and provided a straightforward definition ("lowlands covered with shallow and sometimes temporary or intermittent waters"-Shaw and Fredine, 1956), giving examples of ecosystems that fall under this category and ecosystems that do not (i.e. "permanent water of streams, reservoir, and deep lakes"- Shaw and Fredine, 1956). The term covers today ecosystems such as palustrine (i.e. swamps, peatlands, marshes), estuaries, deltas, floodplains, rivers, seagrasses, coral reefs, coastal flats, rocky shores (Finlayson and Davidson, 1999; Ramsar Convention, 1971). In addition, artificial settings such as ponds, irrigated rice fields, reservoirs and water treatment settings fall under the same category and are also defined as "wetlands" (Ramsar Convention, 1971) however, their special attributes and environmental functions will not be explored here. Today, the definition of "wetlands" is still highly subjective to the science field or stakeholders involved, yet it encompasses areas that are defined by three main characteristics, generally agreed on (Mitsch and Gosselink, 2015):

1. Areas where the water table is either at the surface or close to the surface (hydric or waterlogged/water-saturated soils, Mitsch and Gosselink and references therein, 2015). Here, the water table divides the wetland into two layers, one that it is oxygen-rich (i.e. actotelm-above water table) and one oxygen-poor (i.e. catotelm-below water table; see further discussion in subchapter 1.3.; Charman, 2002);

2. The vegetation (hydrophytes) within the wetland is highly adapted to periodic flooding events and wet conditions;

3. They differ in terms of soil conditions from surrounding uplands.

The hydrological status is the main characteristic for wetland definition as it influences floristic and biologic components and leads to the formation of physico-chemical proprieties of the soil and morphology of the peatland (Mitsch and Gosselink, 2000; Figure 1). This also ties closely to their role in the natural water cycle (i.e. hydrologic cycle), with services extending from flood mitigation, water filtering and groundwater replenishment to waste water treatment (Russi et al., 2013).

1.1.1. Global extent of wetlands

Their extent varies greatly due to 1) uncertain definitions that also include uneven hydrological fluctuations and consequently, vegetation-types and species characteristic to wetlands, 2) recent inclusion of new ecosystems in the category of "wetlands", 3) techniques used (i.e. remotely sensing, field observations); 4) scale of survey, 5) purpose of research (i.e. carbon/CH_4 budgets; vegetation assessment; hydrological studies; habitat creation and urban development etc.), 6) propagation of un-verified and inaccurate data throughout literature and 7) geographical bias (Davidson, 2014). These results in the failure of recognizing the level of pressure and extent of loss wetlands suffered as a direct consequence of human activities.

Multiple papers attempted to estimate the extent of global wetland area (Figure 2), yet due to above discussed issues, data varies greatly and there is little agreement on a figure reached by two or more individual studies. The overall trend, however, is that previous reported figures are lower than those reported more recently, as the definition of wetlands became broader, new areas were re-assessed and identified as wetlands (or new ones were discovered, e.g. Amazonia, equatorial Africa) and as the accuracy of remote sensing techniques has improved.

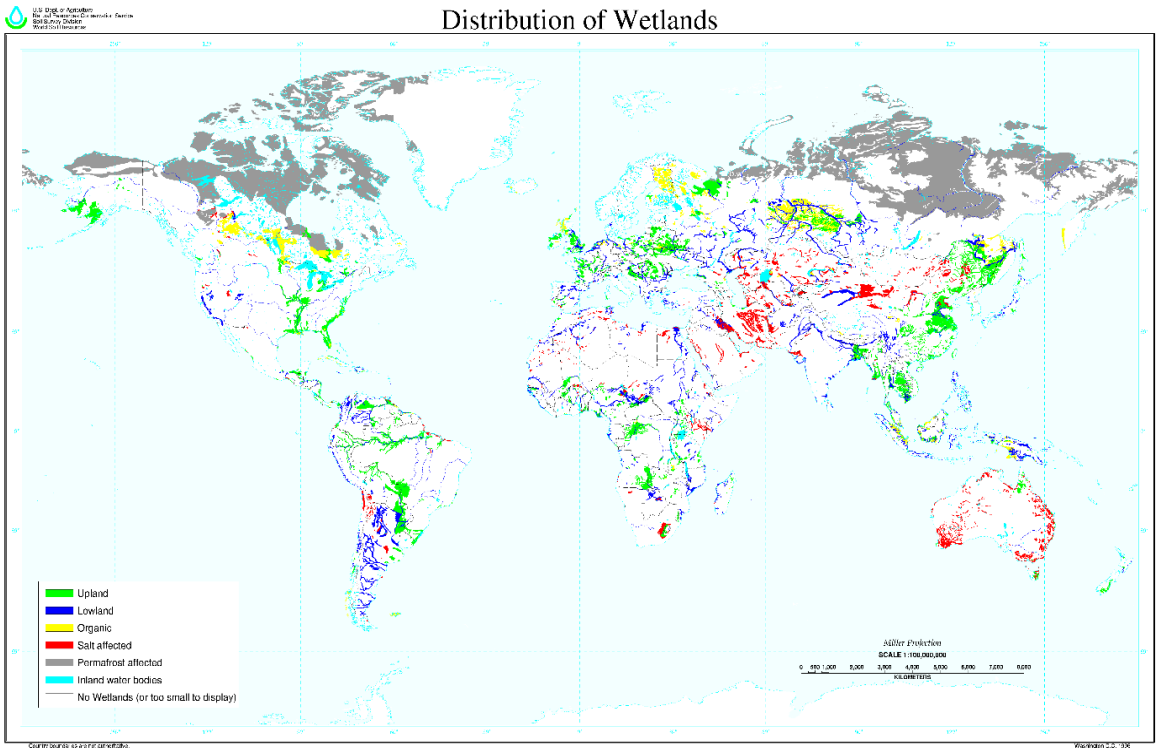

Figure 2 Global distribution of wetlands as of 1997 with 5 major types of wetland classes being represented as provided based on FAO-UNESCO Soil Map of the World and soil climate map. Higher quality figure can be found under the license of USDA (website 1).

One of the earliest cited figures was that of Twenhofel (1926; 1951), who investigated global wetlands from a CH_4 budget point of view. The area reported was of 2.6 million km^2. For the same research purpose (i.e. CH_4 budgets estimates), Sebacher et al. (1986) reported a figure between 4.5-9.0 million km^2 for boreal peatlands solely (Mathews and Fung, 1987 and references therein).

A good agreement seemed to be between Mathews and Fung (1987), Aselmann and Crutzen (1989) and Dugan (1993) who provided global estimates of 5.3 million km^2 (i.e. twice the area previously reported in similar studies), 5.7 million km^2 and 5.6 million km^2, respectively. Furthermore, Mathews and Fung (1987) presented the first global-scale model of wetlands and CH_4 cycling. However, they divided wetlands into 5 categories (i.e. forested bog, non-forested bog, forested swamp, non-forested swamp and alluvial-formations), based on environmental parameters influencing CH_4 emissions while Aselmann and Crutzen's global model (1989) into 6, based on common terminology ("bog, fen, swamp, marsh, floodplain and shallow lake"). From their classifying system alone, discrepancies in the accuracy of presented data can be inferred.

Due to the fact that methodologies were inconsistent, research done in this field that presents very similar data for global extent of wetlands cannot confirm the fact that an average value in close to reality. As various aspects that were taken into consideration by some authors and dismissed by others, the real global extent of wetlands is most of the times underestimated and individual research report, in turn, minimum values.

Finlayson et al. (1999) reassessed previous estimates (i.e. between 5.3 and 9.7 million km^2) to an actual minimum area of 12.8 million km^2 (i.e. inland and coastal wetlands), of which 9.5 million km^2 were classified as inland wetlands (i.e. not affected by marine input; non-tidal-Ramsar definition).

A further summary of reported global estimates of wetlands extent can be found in Melton et al. (2013; Figure 3) who presented data generated by 9 models and remote sensing surveys that spanned between 1993-2004 and participated in WETCHIMP experiments (i.e. Wetland and Wetland CH_4 Inter-comparison of Models Project) and compared the results with observational.

Model	Global (10^6 km$^2 \pm 1\sigma$)	Tropics (30° S–30° N) (10^6 km$^2 \pm 1\sigma$)	Extratropics (> 35° N)[a] (10^6 km$^2 \pm 1\sigma$)
CLM4Me	8.8 ± 1.5	2.6 ± 0.2	5.1 ± 1.4
DLEM	7.1 ± 1.1	3.1 ± 0.4	3.3 ± 0.8
IAP-RAS	20.3	1.3	18.9
LPJ-Bern[a]	81.7 ± 2.4	38.8 ± 1.8	36.4 ± 2.8
	(7.9 ± 0.8)[b]	(2.7 ± 0.2)[b]	(4.5 ± 0.6)[b]
LPJ-WHyMe	2.7[c]	.n.a.	2.7[c]
LPJ-WSL	9.0 ± 1.1	3.8 ± 0.3	4.2 ± 0.9
ORCHIDEE	8.6 ± 0.9	4.3 ± 0.3	3.4 ± 0.7
SDGVM	26.9 ± 3.6	13.2 ± 1.1	12.0 ± 3.8
UVic-ESCM	16.3 ± 1.4	10.6 ± 0.4	5.0 ± 1.2
Observational estimates:			
Matthews and Fung (1987)	5.3		
Williams (1991)[d]	8.6		
Cogley (1994)	4.3		
Stillwell-Soller et al. (1995)	4.8		
GLCC[d]	10.9		
MODIS[d]	12.9		
Finlayson et al. (1999)	min. 12.8		
Mitsch and Gosselink (2000)[d]	7.0–9.0		
GLWD-3 in Lehner and Döll (2004)	9.2		
Gross wetlands map in Lehner and Döll (2004)[e]	11.7		
K07 in Bergamaschi et al. (2007)	6.2	2.8	2.8
GIEMS[f]	12.6 ± 0.8	6.0 ± 1.4	5.2 ± 1.2

Figure 3 Wetland global estimates based on 9 models and remote sensing methodologies (Melton et al., 2013).

1.1.2. South America - Wetland areas and underestimated values

Global approximations of wetland area are difficult to assess and conflicting data can be found throughout literature (Figure 3). Moreover, gaps in data exist for certain parts of the world. For example, Davidson (2014), after reviewing 189 papers on wetland loss, noticed that only 3% of reported data comes from Amazonia (Maltchik, 2003; Bohn et al., 2015) and recognized the importance of in depth studies of large flooded forest regions, with one of the primary examples being the Neotropics (Dixon, 2016) and Amazon basin (see e.g. Finlayson et al. 1999; Maltchik 2003; Keddy et al. 2009). Although this area was included in some global remote sensing surveys, its wetland extent was commonly underestimated due to possible factors such as signal loss due to dense vegetation and seasonal or non-cyclic flooding events that do not allow a permanent above the ground water-table to be detected by microwave signals (Prigent et al., 2007; Hess et al., 2015).

More recently, Hu et al. (2017) estimated through the use of a new Precipitation Topographic Wetness Index (PTWI) that the global value ***would be*** today approximatively 29.83 million km^2 (i.e. divided into 11.41 million km^2 water wetlands and 18.42 million km^2 non-marine wetlands). This was calculated only by taking into account natural parameters (i.e.

topography, precipitation data, drainage basin area, global water table distribution, vegetation type) and in the absence of the human impact on wetlands (Figure 4). From this analysis, it resulted that South America would be the second by largest area of wetlands, with 7.95 million km^2, following Asia.

1.1.3. Wetland loss estimates

The importance of accurate estimates of global wetlands stands not only in mitigation and conservation efforts but also in the need to appreciate loss of wetlands ecosystem alongside CO_2 and CH_4 emission budgets. All 189 reports of long-term changes in wetland ecosystems reviewed by Davidson (2014) show a decreasing trend of areal extend in all parts of the world (Figure 5) and rates of loss higher than long-term rates during the 20th and early 21st centuries (Figure 6). However, loss budgets are again proven to be either overestimated (Winker and DeWitt, 1985) or underestimated, due to time-span of survey and unawareness of areas that fall under the definition of wetlands in addition to similar factors discussed above (see subchapter 1.1.1.). For example, the statement made by Winkler and DeWitt (1985) that the global loss of wetlands has been of 50% since 1900 has been used throughout

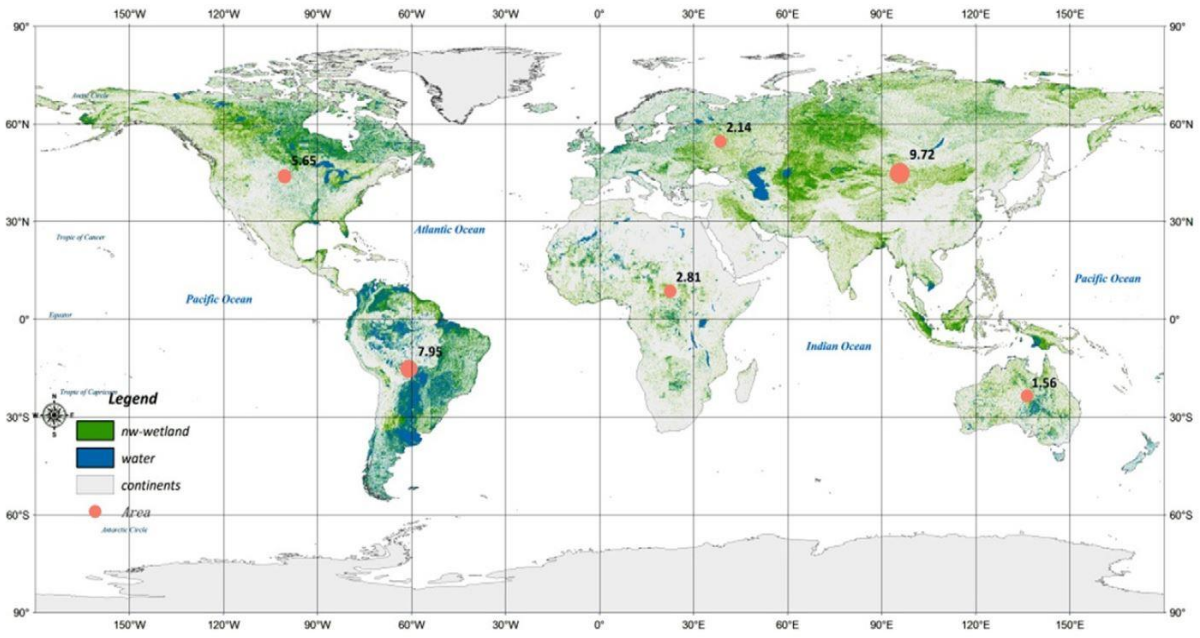

Figure 4 Potential global distribution of wetlands in the absence of human impact as modeled through the Precipitation Topographic Wetness Index (Hu et al., 2017). Green areas are defined as "non-water wetlands" and blue areas as "water wetlands". Approximate area is given for each continent, with Asia on the first place, followed by South America and North America.

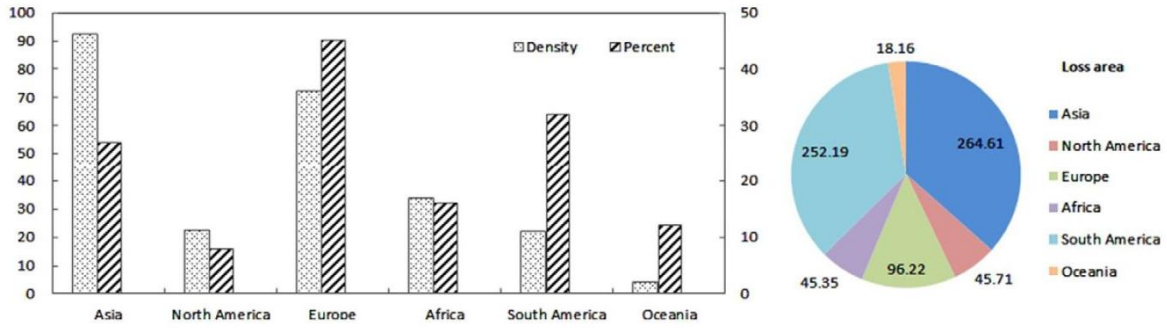

Figure 5 Percentage of lost wetlands on a global scale (Hu et al., 2017). Notice the correlation between population density and wetland loss in graph a) and the scale of loss of Asian peatlands, well above scaled population size. South America has the lowest loss-population ratio (excluding Oceania) indicating the "intact" nature of wetlands on this continent.

literature with little validation of initial methodology while containing only a part of the ecosystems defined as wetlands (Davidson, 2014). In an attempt to reassess the generally accepted "50% loss" that was previously based on USA wetland estimates during the mid-20th century, Davidson (2014) stated that global loss of wetland ecosystems is between 54% and 57% since 1900 AD (i.e. yet initial global extent proved to lack important wetland areas, for example Amazon and Congo). Furthermore, in the 20th century, loss estimates are now at 64-71%, with a higher loss of inland wetlands (i.e. 69-75%) compared to coastal wetlands (62-63%) over the same period of time. This rate of loss shifted since the 1980s, with coastal wetland loss being considerably higher (i.e. 4.2 times) than inland ones (i.e. 3.0 times) compared to long-term values (Davidson, 2014).

Furthermore, it is interesting to appreciate the rate of loss over time with that from the last 100 years (Figure 6; Davidson, 2014) where a 3.7-fold increase in loss was observed. This

Table 1. Changes in the area of all types of natural wetlands over different time periods
n = the number of records for each time period. s.d. = Standard Deviation

Period	*n*	Average no. of years	Average area change (%)	Average rate of change (%.y^{-1})	s.d.	No. & percentage of reports with average change >−1%.y^{-1}
Long-term:						
up to and including the 20th century (start year):						
Pre-18th century	14[A]	n/a[B]	−55.4	−0.113	0.079	0
18th century	6	224.3	−56.9	−0.239	0.081	0
19th century	20	137.6	−48.9	−0.422	0.312	2 (10%)
all long-term	63	n/a[B]	−53.5	−0.296[C]	0.278	2 (5%)
20th and early 21st century (start year):						
1900–1944	23	77.7	−55.8	−0.782	0.475	7 (30%)
1945–1974	38	37.9	−49.3	−1.363	1.446	23 (61%)
1975–1989	28	20.0	−27.8	−1.308	1.261	12 (43%)
1990 or later	17	13.0	−6.5	−0.565	0.803	4 (24%)
all 20th–early 21st century	117	38.6	−38.5	−1.085	1.163	49 (42%)

Figure 6 Different percentages of wetland loss on different periods at a global scale based on presented literature reviews (Davidson, 2014).

has a further positive correlation with the increase in population when assessed at a continental scale (Davidson 2014; Hu et al., 2017).

1.2. Peatlands and processes

As a general characteristic, peatlands are governed by organic matter accumulation and decomposition processes. The balance between carbon accumulation through primary productivity and carbon loss (i.e. gaseous emissions to atmosphere or as dissolved organic carbon) through decomposition is mediated by microbial communities in relationship with water table fluctuations (Clymo et al., 1998). In unaltered peatlands, this is due to changing conditions in the peat column with depth, as a combined result of changes in oxygen and substrate availability, increased acidity, decreasing temperatures and increasing humification degrees (Andersen et al., 2013). These variations lead to stratifications in microbial communities, with different levels of specializations associated to organic matter decomposition levels (Thormann et al., 2003; Artz et al., 2006). Furthermore, CH_4 is produced in anaerobic conditions through incomplete breakdown of organic matter by

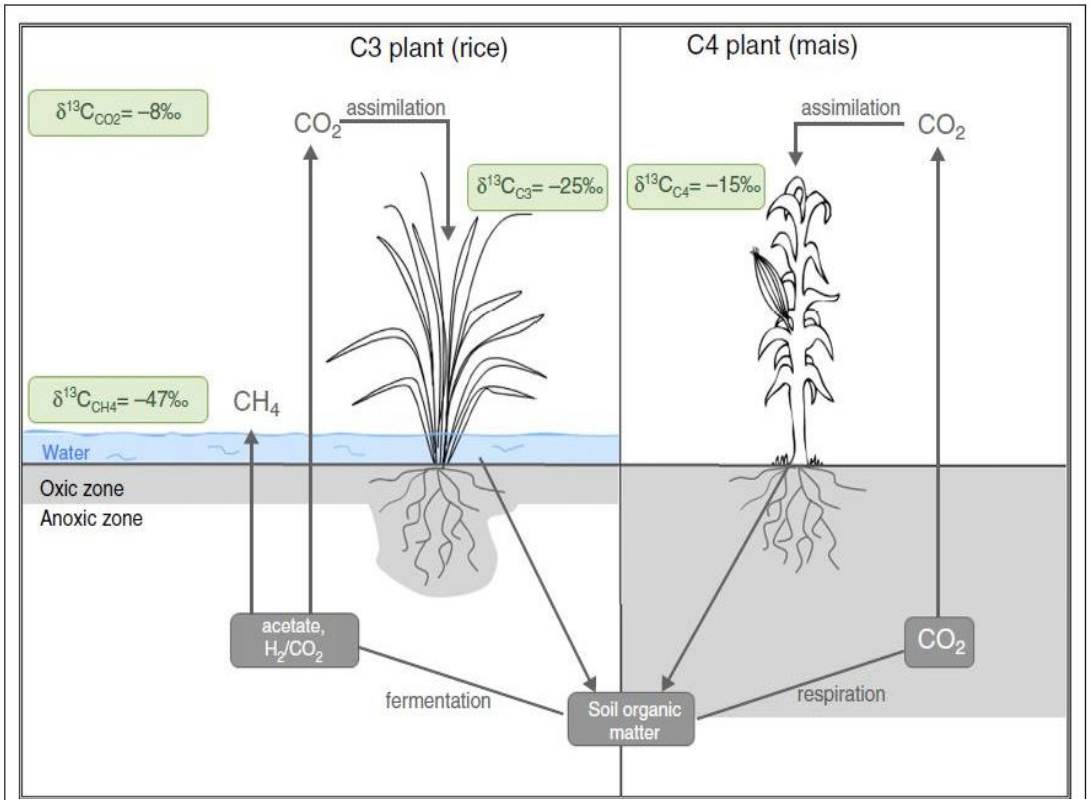

Figure 7 Comparison between organic matter decomposition in flooded and non-flooded systems, by C3 and C4 plants (Blaser and Conrad, 2016). Notice methane production from acetate or H_2/CO_2 (Eq. 1 and Eq. 2.2).

methanogens (see subchapter 1.3.). This critical component of greenhouse gases is further explored in this thesis by assessing its relationships to further constituents of peatland ecosystems (Figure 7).

1.2.1. Methane production

In the anoxic part of the peat column, below water table, organic matter is decomposed by methanogens, a specialized subdivision of archaea. Anaerobic microbes increase their biomass by incorporating carbon-based constituents while producing CH_4 as a by-product of decomposition (Andersen et al., 2013 and references therein).

Methanogens are grouped into 5 divisions based on the terminal electron donors (i.e. substrates) that they use: acetate, H_2 + CO_2, formate, compounds containing methyl groups (methanol, dimethylsulfur) and alcohols (Hanson and Hanson, 1996). However, methanogenesis is usually regarded to take place from fermentation of acetate (Eq. 1) that predominates in the surface layers (where methanogens consume carbon from compounds that contain a methyl radical) and/or reduction of CO_2 with H_2 (Eq. 2.2) that dominates at depth (Figure 7, Hornibrook et al., 1997, 2000 a, b; Chasar et al., 2000a, b). CH_4 is considered a perfect end product in these settings as it is non-toxic and insoluble in water and thus can be easily consumed, transported via ebullition (i.e. bubbles-form) or via plant systems-aerenchymaes (Chanto et al., Ch.6 and references therein; see subchapter 1.5.2.). Furthermore, methanogenesis was shown to be influenced by the quality and availability of organic matter type (i.e. higher in litter-dominated than in wood-dominated; Arai et al. 2014) and root exudates (i.e. substrate availability; Walker et al., 2003).

$$\boldsymbol{CH_3COOH \rightarrow CH_4 + CO_2} \qquad (Eq.1)$$

$$2CH_2O + 2H_2O \rightarrow CO_2 + 4H_2 \qquad (Eq.2.1)$$

$$\boldsymbol{CO_2 + 4H_2 \rightarrow CH_4 + 2H_2O} \qquad (Eq.2.2)$$

1.2.2. Consumption

Aerobic organic matter decomposition is restricted to the section above the water table depth (i.e. acrotelm) and to aerobic microsites. Here, aerobic bacteria and saprotrophic fungi compete over available substrate with several studies debating about their relative biomasses

and predominant roles in organic matter decomposition (Andersen et al., 2013 and references therein). Moreover, organic matter is further decayed in the anaerobic part of the peat by highly adapted microbes.

1.2.2.1. Aerobic methane oxidation

In the oxic layer, the presence of the CH_4 monooxygenase enzyme (i.e. MMO) in methanotrophs allows them to consume CH_4 as a carbon source for energy and biomass. The by-product of this process leads to CO_2 atmospheric emissions (Hanson and Hanson, 1996). Oxygen appears to be the main limiting factor such that in the anaerobic rhizosphere, presence of aerenchyma within roots can provide oxygen from the atmosphere and allow oxidation and further aerobic decomposition (Chowdhury and Dick, 2013; see subchapter 1.5.2.). Furthermore, a part of the CH_4 emitted from the anaerobic layer is being consumed in the top parts of the peat column, limiting atmospheric emissions.

1.2.2.2. Methanotrophs types

Methanotroph bacteria belong to the methylotrophs physiological bacteria group (Hanson and Hanson, 1996). They use CH_4 and its conjugated forms (i.e. methanol, methylated amines, halomethanes, methylated sulphur-containing compounds) as their primarily source of carbon and energy (Hanson and Hanson, 1996; Jahnke et al., 1999) and can be subdivided into various categories, based on its proprieties.

First, based on the criteria and laborious experiment done by Whittenbury et al. (1970), bacteria were divided into 5 groups: *Methylomonas*, *Methylobacter*, *Methylococcus*, *Methylocystis* and *Methylosinus* and later on, *Methyomicrobium* (Bowman et al., 1991, 1993), *Methylocapsa* (Dedysh et al., 2002) and *Methylobacterium* (Patt et al., 1976) were added to the genera list. From here on, and based on criteria reviewed by Hanson and Hanson (1999), they were further divided into two main groups: **type I** and **type II** (Figure 9). *Methylomonas* and *Methylobacter* were first classified as type I (Whittenbury et al., 1970) methanotrophs followed by *Methylococcus*, *Methylomicrobium* that were added later to the group (Bowman et al., 1991, 1993).

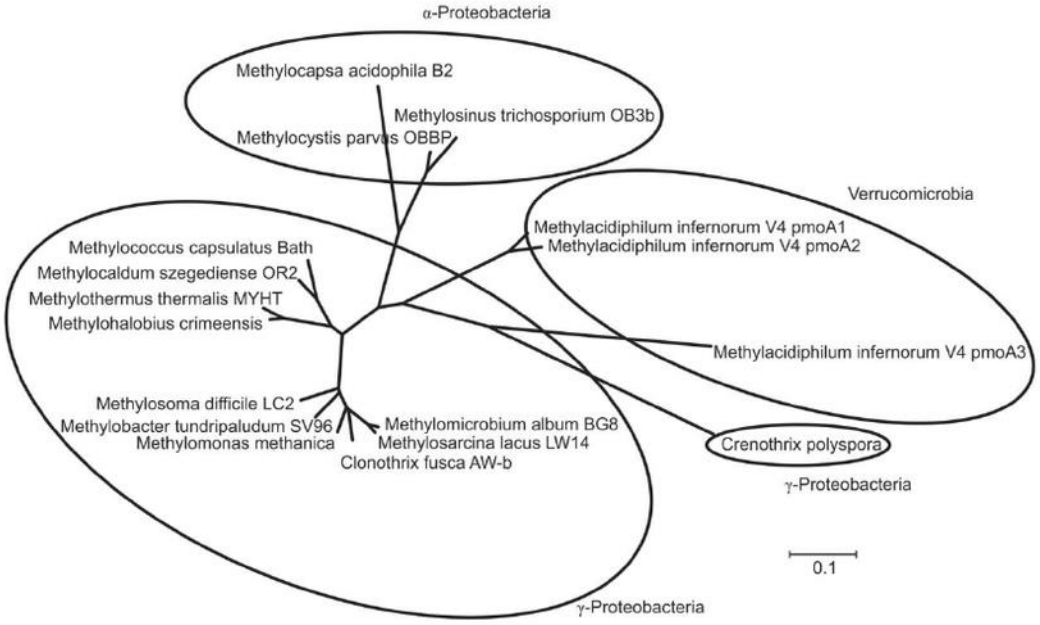

Figure 8 Proterobacteria classification and components of the α-, ϒ- and Verrucomicrobia (Hanson and Hanson, 1996).

Type I (or ϒ-proteobacteria) is known to oxidize CH_4 and assimilate formaldehyde through the ribulose monophosphate pathway (i.e. RuMP, Figure 9). It has a **high affinity** to CH_4 concentrations (i.e. thrives in soils where CH_4 concentrations are similar to atmospheric concentrations), a preference to high oxygen levels (Bull et al., 2000; Bender and Conrad, 1992, 1993; Cai et al., 2016) and shallow depths within the environment.

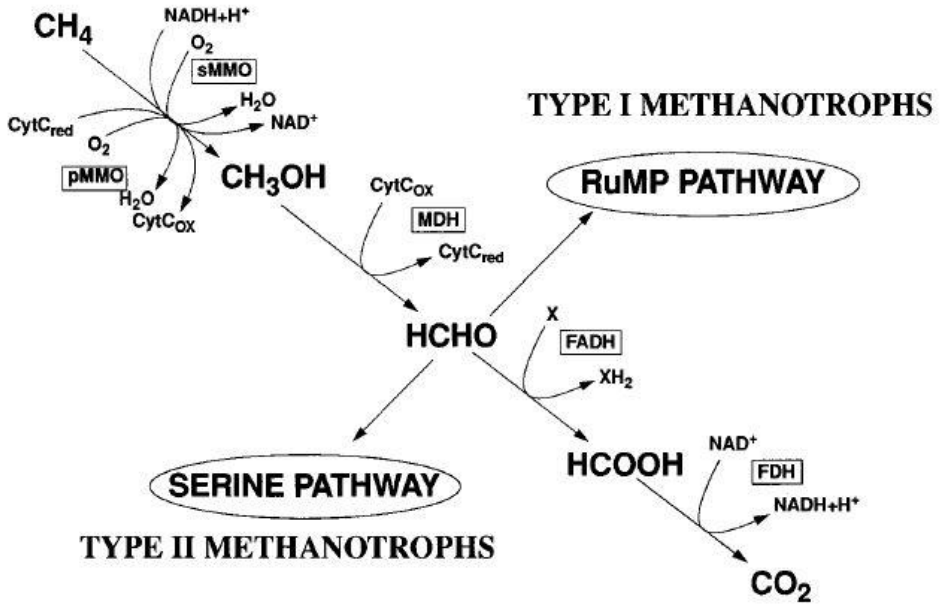

Figure 9 Main pathways through which CH_4 is being processed by methanotrophs and intermediated steps (Hanson and Hanson, 1996).

Methylosinus and *Methylocystis* genera were classified as **type II** (or **α-Proterobacteria**) which utilise the serine pathway for formaldehyde assimilation (Figure 9; Hanson and Hanson, 1999 and references therein). They are known as **low affinity** methanotrophs (Bull et al., 2000), meaning they live in environments where CH_4 concentrations are higher than atmospheric concentrations, having thus a preference for low oxygen concentrations and deeper settings within the environment. A third group exists, **type X**, that uses an altered serine pathway process (i.e. through the use of the ribulosebisphosphate carboxylase pathway) (Hanson and Hanson, 1999; and references therein). This group is however, commonly associated with type I.

1.2.2.3. Competition relationships between type I and II

Competitive relationships between type I and II methanotrophs were observed in relationship to several factors. For example, Knief et al. (2003) found evidence of type I in pH neutral soils while type II were confined to more acidic environments. Type I prefers oxygen-rich environments, lower CH_4 effluxes rates and the presence of copper and nitrogen nutrients for development while type II prefers oxygen-limited and CH_4-rich settings and can develop in the absence of copper and nitrogen (Amaral and Knowles, 1995; Graham et al., 1993).

Furthermore, based on the substrate on which they grow, methanotrophs have been divided into **obligate** and **facultative** types (Anthony, 1982 and references therein). Almost all genera are defined as obligate, meaning that they can only grow on CH_4 substrates, yet past (Patt et al., 1974) and more recent experiments (Dedysh et al. 2002; Theisen and Murrell, 2005; Dedysh and Dunfield, 2011) showed that some members of the *Methylocella*, *Methylocystis, Methylobacterium* and *Methylocapsa* genera can use both CH_4, CO_2 (i.e. one-carbon substrate) and compounds containing C-C bonds (i.e. multicarbon compounds). However, the current assumption is that type I (**or ϒ-proteobacteria)** are obligate methanotrophs and can consume only CH_4 while type II (**α-Proterobacteria)** can are facultative and can consume both CO_2 and CH_4 (Hanson and Hanson, 1996 and references therein).

1.2.2.4. Methane oxidation pathways and fractionation behaviours

In order for CH_4 oxidation and methanol (i.e. CH_3OH) formation process to take place, methanotrophs use an enzyme called **methane monooxygenases** (i.e. MMO) and the two pathways related to this enzyme are showed in Figure 9.

1) **Serine pathway** is specific to type II and is one of the routes through which formaldehyde is assimilated and biosynthesised into cell material by its combination with glycine which leads to serine formation (i.e. via particulate MMO-pMMO). During this process, formaldehyde and CO_2 (2:1 mol) are combined to form a three-carbon compound (Hanson and Hanson, 1999 and references therein).

2) **RuMP cycle** (Anthony, 1982 for review) needs only three moles of formaldehyde to create a three-carbon intermediate compound. In this pathway, formaldehyde is combined with ribulose monophosphate (via soluble MMO-sMMO) in a process that is specific to type I and X methanotrophs (Hanson and Hanson, 1999 and references therein).

1.2.2.5. Anaerobic methane oxidation

It is now accepted that CH_4 oxidation also occurs in the absence on oxygen (de Lange and Brumsack, 1998), in the anaerobic part of the peat column (e.g. Zehnder and Brock, 1980; Caldwell et al., 2008) and is the main CH_4 oxidation pathway in marine settings (e.g. Blair and Aller, 1995). This process was termed "reverse methanogenesis" (Hoehler et al., 1994) and was studied with the use of ^{13}C depleted archaeal lipids (e.g. Pancost et at., 2000a; Pancost et al., 2001). Archaea (i.e. ANME-1 group) mediates anaerobic CH_4 oxidation although, in some CH_4-rich marine settings, archaeal communities occur along bacteria species (i.e. sulfate reducing bacteria) (Hoehler et al., 1994; Pancost et al., 2001). More recently, the discovery of brGDGTs lipids depleted in ^{13}C, led to the conclusion that anaerobic bacteria (Weijers et al., 2006a) are also capable of oxidizing CH_4 anaerobically (Schouten et al., 2013 and references therein, see chapter 1.8.2.). However, the processes through which CH_4 is oxidized in the absence of O_2 are not completely understood since only a few anaerobic methanotrophs have been cultured (Hinrichs et al., 1999; e.g. Girguis et al., 2003; Vaksmaa et al., 2016).

1.3. Tropical peatlands characteristics (lowland tropical peatlands)

Peatlands record changes in vegetation and in the amount of detrital organic carbon over time. Thus, by studying peat cores we can indirectly assess shifts in temperature, hydrology and biogeochemistry of the soil (Yavitt et al., 1988). Reduced vegetation cover and biomass in ombrotrophic (i.e. rain water fed mires) lowland tropical peat swamps is accelerated by anthropic land use and leads to the migration of water table level down, exposing peat and thus, stored carbon, to the atmosphere and oxic degradation (Page et al., 2011b).

Furthermore, as plant assemblages are a direct consequence of climate (i.e. temperature, hydrology), the occurrence or absence of one taxa through a particular period can provide enough information to assess the hydrological regime. This is also related to the degree of preservation and thickness of the organic content that are a consequence of water table depths and, subsequent aerobic or anaerobic degradation. Drier or wetter seasons influence the depth of the water table, the degree and type for organic matter decay. This has further implications in the overall functioning of peatlands as carbon sinks or sources (Page et al., 2011b). Thus, the ***water table*** divides the peatland into two main layers: the acrotelm and catotelm (Figures 7 and 10). The ***acrotelm*** is the layer above water table that is in contact with the atmosphere and where aerobic decay of organic matter to CO_2 and CH_4 consumption take place. The ***catotelm*** is the layer below water table, where anaerobic processes take place and organic matter is overall stored. However, even in waterlogged soils, degradation takes place anaerobically, with the breakdown of organic matter and subsequent release of CH_4 (Charman, 2002).

The fluctuations in water table depths lead to varying thicknesses of the two layers, governing thus organic matter accumulation and degradation processes (Charman, 2002). Although δD and $\delta^{18}O$ can provide further information on the sources of water (i.e. meteoric, fluvial) and evaporation rates, $\delta^{13}C$ provides vital information on carbon (i.e. CH_4 and CO_2) pathways and recycling within the peatlands. From here on, the concentrations of recalcitrant lipids (i.e. biomarkers) specific to various microbial communities at certain depths, as well as their carbon isotopic signatures, can provide estimates of the microbes community sizes and characteristics (i.e. methanotrophs/ methanogens), activity and rates of CH_4 and CO_2 production and consumption at a certain time (McClymont et al., 2010; Pancost et al., 2000). These principles will be further explored in this thesis in an attempt to provide a first estimate

of CH_4 efflux variations with time in newly discovered Amazonain peatlands (Lähteenoja et al., 2009a, b).

Moreover, several studies done in tropical peatlands and forests (Arai et al., 2014; van Lent et al., 2018), indicated through incubation experiments the importance of ***water-filled pore spaces*** (WFPS) and ***litter availability and quality*** (Updegraff et al., 1995) in driving CH_4 production and oxidation processes. Thus, even under flooded conditions, more CH_4 is oxidize than produced during periods of little to no litter availability and more CH_4 is produced when WFPS has a higher percentage. This indicates the importance of vegetation type and availability of substrates from litter sources compared to woody material for methanogenesis (Arai et al., 2014a).

1.4. South-East Asia peatlands – a tropical comparison

Although the importance, area, effects and variables of boreal and temperate peatlands are starting to be better-understood (Page et al., 2011b), the total area covered by and our understanding of tropical peatlands functioning, are still missing important components. Peat is located at the tropics in humid forests of Central America, Amazonia and (sub)equatorial Africa, covering an area estimated in 2011 at almost 440, 000 km^2 (i.e. between 384, 776-656,430 km^2) with an estimated carbon pool of 81.5-91.8 Gt and a volume of 1,756 Gm^3 (Page et al., 2011b). Although Peruvian extent estimates were included in the 2011 review (Page et al. 2011b; total area provided by Ruokolainen et al., 2001; thickness by Lähteenoja et al., 2009a), extensive research in this area (see subchapter 1.6.; table 1) as well as in tropical Africa (Dargie et al., 2017), indicates that the global tropical proposed area is potentially underestimated.

The focus of recent research from tropical peatlands was mainly on South-East Asia, which cover more than half of peatlands found in the tropics (i.e. 57%, Page et al., 2011b). Furthermore, they were extensively used as an example for the degree of human degradation and for the immediate and long term consequences that followed the decay of these ecosystems (Roucoux et al., 2017; Page et al. 2011b; Arai et al., 2017; Dommain et al., 2014; Koh et al., 2009; Wahyunto et al., 2003, 2004). In SE Asia, degraded peats are due to population growth and excessive use of land for agriculture (e.g. Mega Rice Project) and infrastructure. This meant that lowland peatlands were destroyed through fire and drainage and incorporated into human-used land over the last 3 decades. In the last 25 years (i.e.

starting 1990), half of the peat swamp forests from Malaysia Peninsula, Borneo and Sumatra (i.e. approximatively 7.85 Mha) were transformed into managed land through deforestation, leading to reduced biomass, diversity, habitat loss and water table drawdown (Miettinen and Liew, 2010; IPCC 2014-Field et al., 2014; Jauhiainen et al, 2016). Agriculture practices altered natural drainage systems through the implementation of anthropic drainage systems. They were used to keep the water table levels low and seasonal flooding occurrences reduced as root species (i.e. palm oil, Acacia pulp, and vegetables) do not tolerate anoxic conditions present in lowland peatlands. Nowadays, as a consequence of repeated natural disasters and anthropogenic pressures, SE Asian peatlands act as a major global carbon source (Page et al., 2011b and references therein) and conservation practices are only limited to small projects that aim to conserve the remaining intact, yet restricted areas (Page et al., 2006; 2011b; Roucoux et al., 2017).

SE Asia counterparts on the South American and African continents are mainly unaffected by large scale anthropogenic pressures and their hydrology can be considered "intact" (Roucoux et al., 2017). However, if unprotected, they risk large-scale agriculture expansion projects (legal or illegal), transport infrastructure development with routes that cut through unaffected carbon-rich forests, smallholder activities like cultivation, unsustainable hunting and harvesting, hydropower projects, mining (Roucoux et al., 2017), oil and gas extraction (Yusta-Garcia et al., 2017; Roucoux et al., 2017; Rosell-Mele et al., 2018). Although most of these risks can be prevented and mitigated through conservation (Roucoux et al., 2017) and restoration practices (Page et al., 2006), we need to understand their palaeohydrology and palaeovegetation shifts, environmental pressures in both the absence and presence of human impact, superimposed on global warming and climate change trends, in order to assure their ecological integrity.

1.5. Characteristics of tropical peatlands

In the tropics, anoxia is mainly generated by intense precipitation regimes and waterlogged conditions, abundant vegetation, high growth rates and low rates of oxygen solubility in water due to high temperatures, that lead to high microbial biomasses and demand for oxygen (Junk et al., 2010 and references therein).

1.5.1. Methane emission pathways

The concept of CH_4 and CO_2 production in the anoxic layer of peatlands has been discussed since the beginning of the 19th century (Dalton, 1802; Websky, 1864). Once produced in the anaerobic parts of the peatland, CH_4 can be transported to the surface, and eventually, to the atmosphere, via three possible ways: 1) diffusion through peat; 2) as bubbles (ebullition) and 3) through plants (Figure 10).

Diffusion of CH_4 through peat is the slowest and less effective process over short periods of time of the three pathways; however, it is the main pathway to provide substrate in the aerobic part of the peatland (Whalen, 2005) and thus, the main way of reducing CH_4 effluxes from a peatland. Clymo and Williams (2012) demonstrated that on time scales of 1000s years, diffusion is responsible of around 95% removal of the total CH_4 and CO_2 from the peat column.

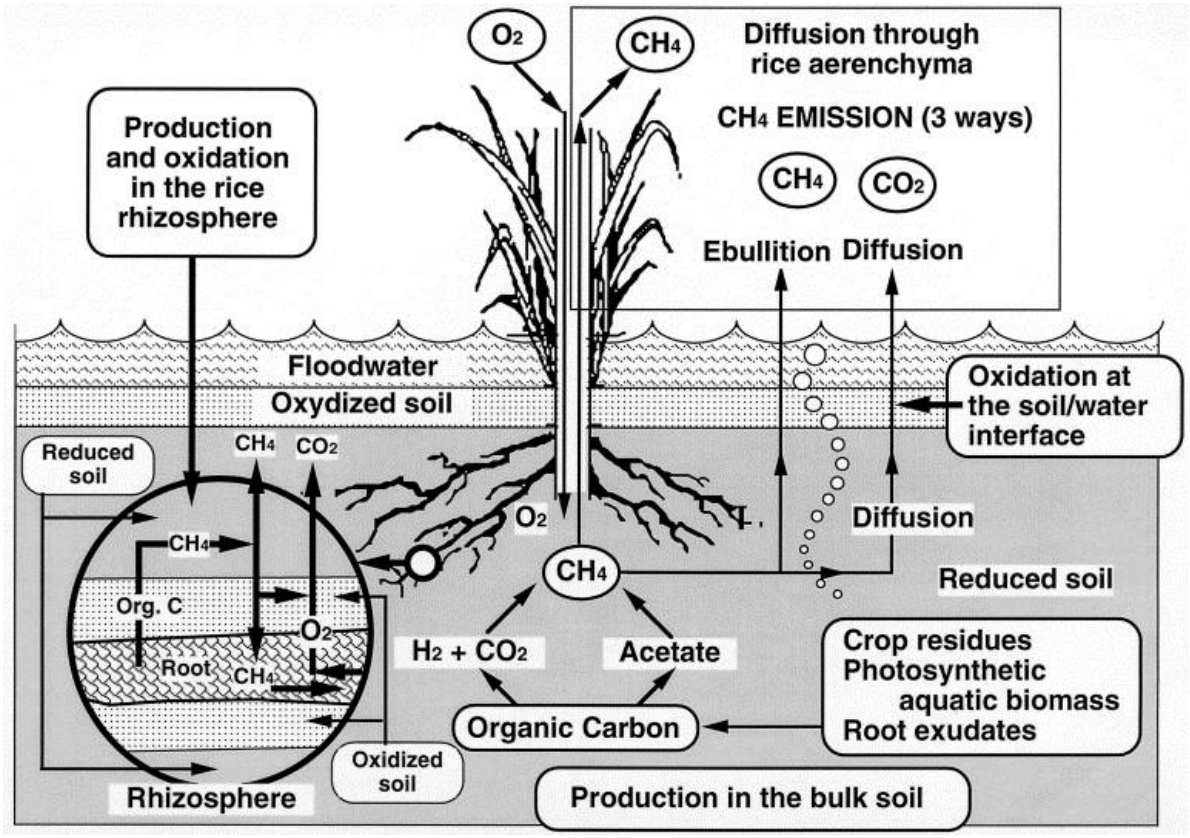

Figure 10 Physical and chemical processes within a peatland. Notice the two main pathways for CH_4 production, thewaythat plans adapt to anoxic conditions and the three pathways of CH_4 emission. The rhizosphere, the area orlayer with active root systems, is an important component of a peatland as it rich in substrate for methanogenesis and potentially rich in oxygen for methanotrophy. Figure from Le Mer and Roger, 2001.

CH_4 transport via bubbles is due to the low solubility of the gas (Clymo and Pearce, 1995). This means that the gas will not enter the aquatic phase readily. Ebullition (Martens and Klump, 1980) is the fasted route through which CH_4 is transported through the oxic layer to the atmosphere. However, during this process, CH_4 bubbles are only partially oxidized, if at all (Laing et al., 2011). Ebullition can be due to several factors such as changes in atmospheric pressure (e.g. Kellner et al., 2005; Comas et al., 2008), changes in water table depth (Strack et al., 2005) and/or temperature (Beckmann et al., 2004) and it is further, shaped by the quality of the peat and its components.

Finally, transport via vegetation is related to adaptations of plant tissues to waterlogged conditions (see for example Chanton et al., 1992; Takahashi et al., 2014). Vegetation living in waterlogged soils adapted to anoxic conditions by developing systems to cope with oxygen scarcity around roots, such as aerenchymous tissues, lenticels (i.e. small pores), and aerating pneumatophores (Figure 10; see subchapter 1.5.2.), all which are further discussed below.

1.5.2. Vegetation adaptation to waterlogging and implications to the CH_4 cycle

Several studies indicated high photosynthetic rates even during periods of high flooding, with new leaves and fruits produced during that time (Junk et al., 2010 and references therein). Thus, vegetation living in waterlogged soils (mangroves, forested peatlands), adapted to anoxic conditions by developing systems to cope with oxygen scarcity around roots, such as aerenchymous tissues, lenticels (i.e. small pores) and aerating pneumatophores (Figure 11; de Graneville, 1974). Aerating roots (pneumatophores) are common in wetlands and were shown to have effect on greenhouse gas emissions from soils (e.g. Purvaja et al., 2004). In Pastaza-Marañón foreland basin (PMFB), their density was positively correlated to in-situ CH_4 fluxes and negatively correlated to the degree of palm forest degradation (van Lent et al., 2018).

M. flexuosa palms are known to possess root pneumatophores for gas exchange (de Granville, 1969). Such structures allow the transport of dissolved O_2 to anoxic depths but can also lead to CH_4 intake from deeper anoxic sections within the peat and its release directly into the atmosphere, by-passing thus the oxidizing surface layer (Pihlatie et al., 2005; van Lent et al., 2018 and references therein).

In the case of species with aerenchymous tissues, gases are transported within the plant via diffusion or humidity-generated pressure fluxes (Takahashi et al., 2014 and references therein). When O_2 is exchanged between shoots and the root system, aerobic methanotrophs can consume CH_4 at the root end (Chanton et al., 1992; Askaer et al., 2011b). These adaptations allow gas movements at rates higher than diffusion (Couwenberg and Fritz, 2012. Furthermore, the presence of aerenchyma structures (Figure 11; i.e. in *Carex* sp.) allows the transfer of CH_4 directly form the anoxic part to the atmosphere, by-passing again methanotrophy (Chanton, 2005; Drew et al., 2000; Van Lent et al., 2018 and references therein).

Cyperaceae species found at both QT and SJO, contain ethylene hormone, known to lead to the formation of aerenchyma, hollow plan tissues that transport oxygen from the atmosphere to roots during anoxic conditions (Mitsch and Gosselink, 1993). Furthermore, this hormone is closely tied to the "rhizosphere oxygenation" that leads to oxic microspaces formation via radial oxygen loss (Naiman et al., 2010; Smith and Luna, 2013) and "aerobic" methanotrophy. However, the presence of aerenchyma can also act in reverse, transporting GHG formed in the catotelm directly to the atmosphere, bypassing bacteria-mediated consumption (i.e. "chimney effect"; Koelbener et al., 2010; Figure 11).

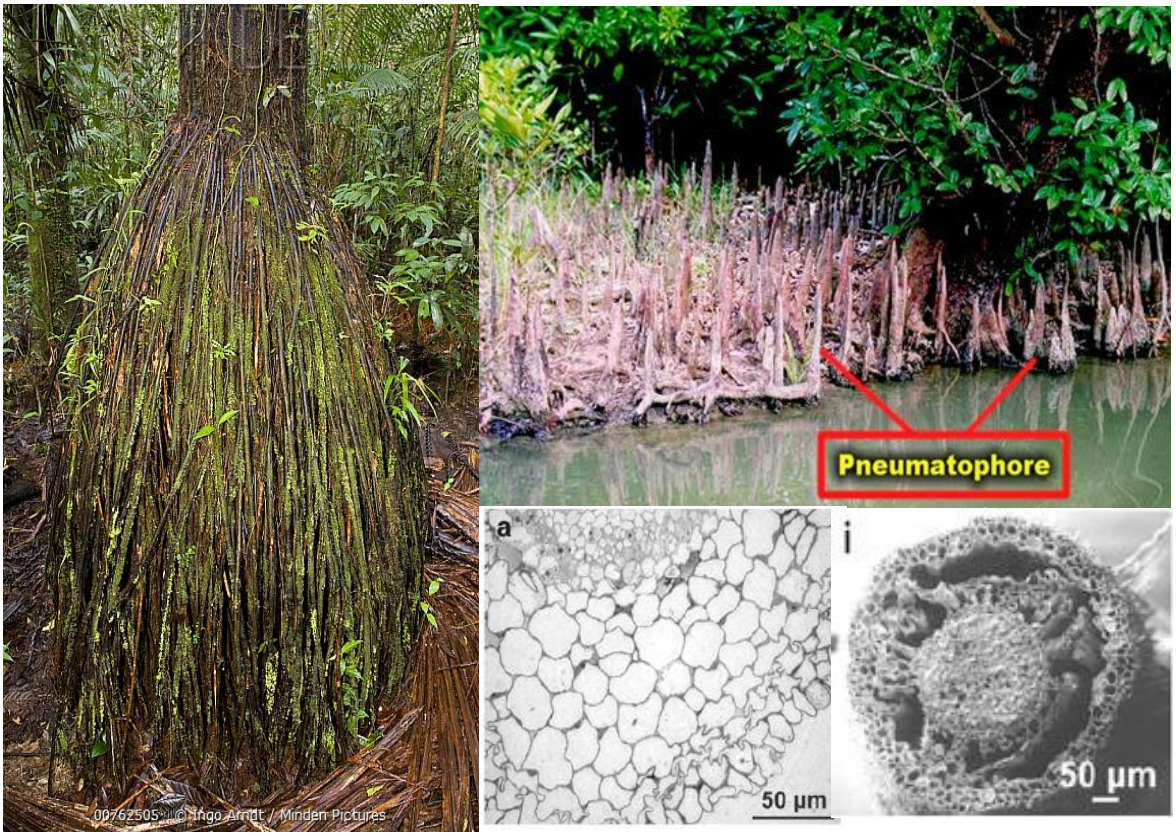

Figure 11 Vegetation adaptations to waterlogging. Left figure (website 2), aerial roots in M. flexuosa; top-right, pneumatophores (website 3) and bottom-right (a, i) aerenchyma tissues (edited from Junk et al., 2010).

1.6. Amazonian peatlands

Lowland tropical peatlands represent more than 8% (33-49 Mha) of peatlands worldwide (386-409 Mha) and store more than 70 Gt of carbon, representing almost 20% of the carbon contained in peat soils worldwide and 2% of the global soil carbon (McClymont et al., 2010 and references therein; Arai et al., 2014). In terms of greenhouse gas (GHG) emissions, peatlands in the Amazon basin have been grouped in past studies with non-peat forming areas (Wilson et al., 2016; Teh et al., 2017) which makes emission rates difficult to discern on a regional scale (Teh et al., 2017 and references therein). Nonetheless, the Amazon basin was approximate to represent 7% of global CH_4 atmospheric contributions (Wilson et al., 2016).

Compared to their SE Asia (i.e. Indonesian and Malaysian) correspondents, tropical peatlands from Amazonia, New Guinea and Central Africa, are regarded as "intact" given the mild anthropic activities (i.e. agriculture, transport networks, deforestation, artificial drainage networks, unsustainable practices), reduced population density (i.e. 2.4 people/hm^2 for PMFB) and conservation attempts (Roucoux et al., 2017; e.g. 1984 touristic reservation Resolucion Suprema No 223-84 ITI/tur at QT site, Van Lent et al., 2018). However, due to demands on local markets for products of *M. flexuosa* palms, unsustainable practices are employed for harvesting, trees being usually cut. These practices were shown to have immediate impacts on CH_4 and CO_2 on-site emissions and vegetation decomposition rates (Virapongse et al., 2017; van Lent et al., 2018).

The existence of extensive peat deposits in Amazonia lowlands was confirmed by field studies taken in 2006 in northern Peru and subsequent publications (i.e. Lähteenoja et al., 2009a, b, 2012; Draper et al., 2014). Carbon accumulating rates have been calculated at 26-195 g C/m^2 /yr (Lähteenoja et al, 2009a) when based on peat radiocarbon dating or between 39±10 and 85±30 gC/m^2/yr (Lähteenoja et al., 2009b) when based on apparent peat accumulation rate. The wide range in accumulation rates is due to different study areas and highlights the overall dynamic nature of hydrology and vegetation in the carbon cycle. Furthermore, they represent a high resolution Holocene palaeohydrologic and palynologic record which was lacking in the Amazon basin during Holocene (Lähteenoja and Page, 2011) as overall palaeoenvironmental records were so far restricted only to speleothems in the region (e.g. Kanner et al., 2013; Bernal et al., 2016), lake sediments (Abbott et al., 1997; 2003) and ice cores (Kanner et al., 2013 and references therein). However, these data sets

are comparable in terms of $\delta^{18}O$ signatures on centennial timescales, allowing interpretation on climate variability and influences on vegetation and peat development.

They have been divided into ombrotrophic and minerotrophic based on the horizontal distribution of nutrients (i.e. Ca, Mg, K, N, Na, Fe; Lähteenoja et al., 2009b; Lawson et al., 2014), showing all characteristics of dynamic peatlands that are known in other tropical areas such as SE Asia and equatorial Africa.

Previous studies in the region focused on the extent of wetlands and water bodies in South America (Eva et al., 2004), with a total area of 940,900 km^2, with the recognition of swamp forests within the PMFB. A few studies focused on local peat deposits from Brazil (Suszczynski, 1984; Lappalainen, 1996), on soil analysis in the Amazonian basin (Dubroeucq and Volkoff, 1998), on vegetation types and ecology (Junk, 1983; Kahn and Mejia, 1990; Kahn and Granville, 1992) or on regional carbon pool approximates from soil (Batjes and Dijkshoorn, 1999) however all have failed to recognize peat formations in their areas of research. The general view was that, although there are vast wetland areas in Amazonia, peatlands cover a very limited area (Ruokolainen et al., 2001 and references therein; Räsänen et al., 1991). Räsänen et al. (1991) holds one of the first published records of peat formation in Northern Peru that also coincide with the location of one of the peat cores in this study, at Lake Quistococha. Their early observations of abundant *M. flexuosa* taxa surrounding Lake Quistococha "with thick peats undergrowth" was confirmed recently by more in-depth studies (see Chapter 3). Furthermore, one of the few attempts to define the soil ecology on a large scale was done by Ruokolainen et al. (2001) in a paper that pointed out the lack of information from these peatlands in terms of peat extent, volumes and characteristics and the need of further research in the area. During their ground vegetation research, the authors have noted that at least *Mauritia* swamps are subject to poor drainage and waterlogged conditions, hold peat accumulation and cover large areas within Amazonia Peru (Ruokolainen et al., 2001 and references therein). They made first observations on the existence of organic matter rich soils, depths and nutrient profiles in this region (i.e. nutrient poor or rich based on hydrological regimes).

Peat accumulations in Amazonia were first compared to the already confirmed Indonesian peatlands and were proven to show similar accumulation rates (Lähteenoja et al., 2009b). Since then, carbon budges estimates based on area, peat's thickness, quality and density started to emerge and considered of global importance (see Chapter 3).

1.6.1. Pastaza-Marañón Foreland Basin – Study area

In this study, we focus on peatlands from Pastaza-Marañón Foreland Basin (PMFB) in Amazonian Peru (i.e. Northern Peru), a lowland wetland region (Lähteenoja et al., 2009b). Peatlands forming here are regarded as massive carbon-storage areas (Draper et al., 2014) but there are still gaps in the knowledge when it comes to regional GHG of particular ecosystems, the way they add up to the global atmospheric budges (Huang et al., 2008; Saikawa et al., 2014; Saikawa et al., 2013, cited by Teh et al., 2017; Lawson et al., 2015) and their contributions to palaeoclimate. Furthermore, studies done in different locations within the basin (Lähteenoja and Page, 2011; Lawson et al., 2014) showed that there are multiple peatland ecosystem types across the region, with peat varying in terms of accumulation rates, physical and chemical proprieties (Lähteenoja and Page, 2011), offering thus a complicated spatial view over the potential variability in terms of CH_4 production and consumption.

1.6.1.1. Geology and topography

From a geological point of view, PMFB in NW Peru is a low-topography, subsided foreland basin of approximatively 100 000 km^2 (reported as 120 000 km^2 in Räsänen et al.,1990; 1992) that has formed due to Cenozoic uplift of Andes (Draper et al., 2014 and references therein). Of its total area, approximatively 44,000 km^2 are covered with peatlands (i.e. 35,600 ± 2,133 km, Draper et al., 2014), making it the largest continuous peatlands discovered to present, with an estimated carbon pool of 3.14 Pg C (above- and below-ground; Draper et al., 2014). The geological setting permits wetland-type environments development (Lähteenoja and Page, 2011). Tropical lowlands in this region are characterized by complicated fluvial dynamics, with anastomosing and braided rivers that eroded into the underlying Miocene-Pliocene strata or adjacent Quaternary deposits. Thus the rivers formed terraces (Räsänen et al., 1991; Roucoux et al., 2013) or deposited quartz- and clay-rich alluvium from the Andean region, Amazon shields or Piedmont basins (Guyot et al., 2007) as dictated by tectonic processes and climatic oscillation (Räsänen et al.,1991).

PMFB is located between Marañón and Pastaza rivers (Figure 12), with the later draining into Marañón River, (part of the Marañón basin) which later drains into the Amazon, forming the largest basin on Earth (Goulding et al., 2003). Marañón river discharge is of 4975 m^3/s (Moquet et al., 2011) (or 16,200 m^3 /s^{-1}/yr, Espinoza-Villar et al., 2012) and it is one of the

three principal rivers that deliver the highest part of sediments to Amazon collected from an area of 350,000 km^2 from the north and central Peruvian Andes (Quintana-Cobo et al., 2018 and references therein). Pastaza river's discharge was reported between 704 m^3/s and 913 m^3/s (Moquet et al., 2011 and Yusta-Garcia et al., 2017, respectively). Moreover, the chemistry of Marañón river was found to influence the overall Amazon water chemistry due to high percentages of minerals transported from salt and carbonate rocks in upper reaches (Moquet et al., 2011), implying thus the importance of the two tributaries in the development and geochemistry of minerotrophic (i.e. high Ca/Mg ratios) peatlands within the PMFB.

Present day mean annual temperature for the areas of Lähteenoja et al. (2009a, b), Lähteenoja and Page (2011) and Teh et al. (2017) studies was reported at 26˚C with precipitations at 3100 mm/year and humidity levels as high as 80-90% (Marengo, 1998). Precipitation regime is of high importance in such settings as rain water, apart from affecting the depth of the water table, can also introduce electron acceptors (i.e. NO_3^-; SO_4^-) that influence the rates of microbial processes in the oxic and anoxic sections of the peat column (Dise and Verry, 2001; Gauci et al., 2002, 2004). Evaporation rates were reported at 1500 mm/yr and thus the climatic and topographic parameters provide a perfect site for waterlogging and anoxic conditions for peat formation and accumulation. The wet season is recorded between November and May with higher river discharges between March and May, when most flood pulses and highest water table depths are known to occur (Espinoza Villar et al., 2009b; Teh et al., 2017). Rain events are less frequent between June and August during the dry season and more predominantly between August and October-when low water table depths occur (Quintana-Cobo et al., 2018).

Studies done by Householder et al. (2012) and Lähteenoja et al., (2009a) have showed that up to 90% of the peatlands in the PMFB are flooded for most time of the year with peat dominating along river floodplains (i.e. variable peat thicknesses in minerotrophic peatlands; between 3.9 m and 12.9 m, Householder et al., 2012; most reported value 7.5 m maxim depth for PMFB, Lähteenoja et al., 2011). Furthermore, they have a high-nutrient content (Householder et al., 2012; Lähteenoja et al., 2009a; Lawson et al., 2014) with high inorganic Ca as the main component (Lähteenoja et al., 2009b) and are affected by annual water table fluctuations due to pulses in Amazonian water budget. The remaining 10% form the ombrotrophic (dome, raised bogs) part of the peatlands (Draper et al., 2014), are not affected by river discharge, receive nutrient-poor waters from rainfall, with lower Ca concentrations (Lähteenoja et al., 2009b) and have been assigned to the "pole forest'' vegetation type. Carbon density of the "pole forest" (i.e. 1391 710 Mg C/ha), although considered

ombrotrophic, is higher than that of nearby peatlands along rivers. This is due to the existence of carbon-rich forests (Draper et al., 2014; Teh et al., 2017), continuous growth of vegetation (i.e. high amount of precipitations and temperatures) and high water table depth during dry season (Kelly et al., 2014 and references therein).

Figure 12 Main Amazon effluents and marked location of Maranon and Pastza rivers (arrows), within the Amazon Basin (Website 4).

1.6.1.2. Factors affecting climate, hydrology and vegetation formation in PMFB

Horizontal migration of Amazonian river channels is the general preferred explanation for peat initiation in this area (Lähteenoja et al., 2009b). Even though samples for this study are associated with pollen zones and are not at resolution that can allow detailed discussions on changes in climate on a decadal and centennial time scale, with the aid of biomarkers, understanding climate forcing mechanisms in South America and looking at an array of data

from different proxies will allow a better understanding of palaeoenvironment changes, peat initiation and formation and vegetation changes seen on broader time scales (see subchapter 6.2.1). Furthermore, data available from this study, as well as biomarker-calibrated pH and temperatures are tested against mid and late Holocene palaeorecords available for the South American continent in order to understand for the first their potential in these newly discovered peatlands (see subchapter 6.2.1).

The great spatial extent of Amazonia allows it to be influenced my numerous climatic factors on time scales that range from several years to thousands. Furthermore, it has been observed that different parts within the region respond differently to climatic factors (Cheng et al., 2013). A few of the factors are discussed below.

External forcing/Orbital scale (from Little Ice Age to Holocene timescale)

Changes at orbital scale (i.e. Milankovitch cycles) have been linked to changes in the spatial distribution of precipitations, with differences seen between the southern and northern parts of the same region (i.e. Brazil, Cheng et al., 2013). However, differences in precipitation between the South of Brazil and West of Amazonia have been attributed to changes in intensity in the South American Monsoon (SAMS), which is caused by differences in insolation budgets linked to precession cycles (Cruz et al., 2005). The SAMS is responsible for high rainfall budgets over South America (Bernal et al., 2016 and references therein), with high intensity monsoons leading to abundant precipitations and relatively wetter periods. Furthermore, differences in precipitations have also been noticed in $\delta^{18}O$ excursions for the eastern and western regions on the South America (i.e. South America Precipitation Dipole, Cheng et al., 2013) continent driven by higher summer insolation budgets that intensify atmospheric convection and precipitations. Coupling between SAMS and low-SST in the North Atlantic was observed during Holocene, during which the South American Convergence Zone extended over most S America, with solar-radiation mediated shifts between the South and North of South America (Bernal et al., 2016 and references therein).

High $\delta^{18}O$ excursions (Figure 13) seen in the isotopic signatures in NE Brazil and E Amazonia during early-mid Holocene (transition from Last Glacial Minimum to Early-Mid Holocene, 10-5k BP) have been attributed to the reduction in intensity of the South America Monsoon (SAM). As Amazonia was receiving lower insolation due to precession

movements, a higher input of moisture from the Atlantic Ocean reached parts of the continent, also decreasing the intensity of the SAM (Aniceto et al., 2014 and references therein). They record a drier period in the first part of Holocene that is followed by sharp decrease in $\delta^{18}O$ values as the climate became significantly wetter (Cheng et al., 2013; Figure 13). During the same period, western Amazonia was experiencing a dry period, with the rain amount reduced by 15-30% compared to normal day (Cheng et al., 2013).

El Nino-Southern Oscillation (El Nino and La Nina)

Occurrence of El-Nino events on a decennial timescale has been linked to lower average precipitation amounts in Amazonia and NE Brazil (Cheng et al., 2013), however it is not yet clear how ENSO is influenced by precession movements and how they are recorded in $\delta^{18}O$ isotopic signatures.

1.6.1.3. Climate influences in PMFB

In terms of climate oscillations in the PMFB region, ^{14}C dates from lake cores published and reviewed by Räsänen et al. (1991) show contradicting ages when coupled with pollen records. Drier periods were first suggested starting with 4000 BP, at 2100 BP and after, at 700 BP for central Amazonia (Absy et al., 1979; 1982) while other studies found evidence of drier climate between 4200-3150 BP (Räsänen et al., 1991 and references therein). However, in Räsänen et al., (1991) study, only 2 out of 6 ^{14}C basal lake depths from Peruvian Amazonia were considered reliable, with the other 4 (and possible previously published dates) affected by allochthonous water-recirculated and deposited older organic matter. A study done by Bush et al. (2007) on lake sediments within the same regions shows that between 4100 and 2540 cal yr BP precipitations increased in the area of study (i.e. after a relatively drier Mid-Holocene period). This coincides with the age of basal organic matter in two of the peat cores (i.e. Quistococha and San Jorge) and could have created the ideal settings that led to first peat accumulations. A relative humid period is also recorded between 3500 and 2800 cal yr BP in a speleotherm recovered from a cave in central Peruvian Andes (Kanner et al., 2013). One study done in Quistococha Lake (Aniceto et al., 2014) depicted two distinctive sedimentation rates, separated by a break in sedimentation. The bottom of the core which was dated between 6100-4900 cal yr BP showed high sedimentation rates (i.e. 0.5cm/yr) and strong inorganic content, being under the influence of Amazon. The break in sedimentation was related to drier conditions during mid-Holocene while the reinitiation of sedimentation

starting 2600 cal yr BP was due to wetter conditions during late Holocene (Aniceto et al., 2014). However, for the same lake, Kelly et al. (2018) found no evidence of hiatus and

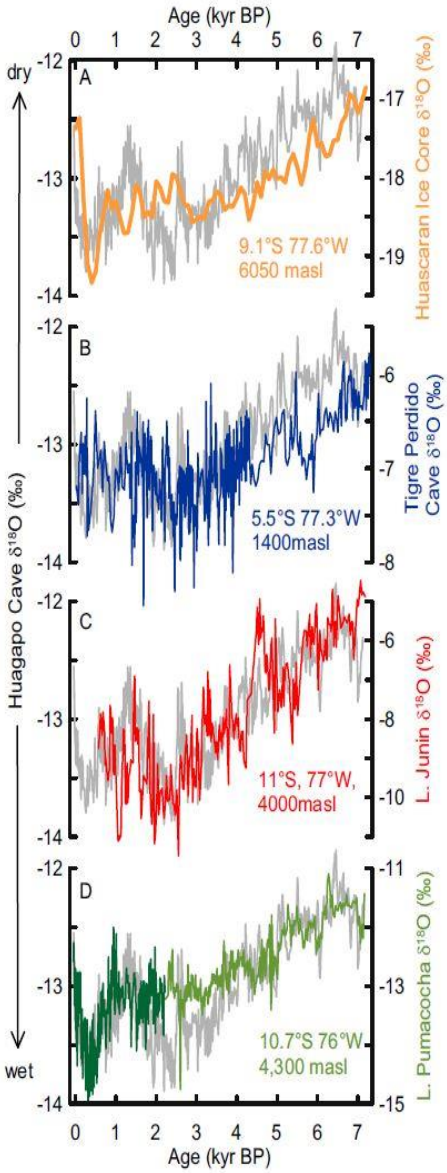

Figure 13 Isotopic records across multiple proxies across South America compared to Huagpo Cave (Peru, grey-left axis) (Kanner et al., 2013).

assigned previous results on detrital old carbon that changed radiocarbon ages. Furthermore, the most recent study done in the Peruvian Andes, analyzed a sedimentary core from the floodplain of Lake Lagarto, situated in the floodplain of Marañón River. However, the core was only 98 cm long with a basal age of 640 Cal yr BP (Quintana-Cobo et al., 2018). The biostratigraphy of the core denotes weaker hydrodynamics, finer and lower density sediment input with a high accumulation rate possible due to the surrounding *M. flexuosa* vegetation and contributions from in-situ primary production (algae production; Quintana-Cobo et al.,

2018). The sedimentation rate decreased from 630-500 cal yr BP to 400 cal yr BP that was linked to decrease precipitation in Andes and thus, decreased discharge.

However, as previously stated fluvial system may deposit reworked sediments and disturbed organic matter from high reaches in lakes and across river banks. It may also lead to age inversions or unreliable biostratigraphic records. This would also have implications in the type and nature of biomarkers present in river banks and lake deposits as a considerable percentage is likely to be allohthonous (Quintana-Cobo et al., 2018 and references therein).

While it is possible to determine climate oscillations (and from here on to describe environmental and vegetation shifts) based on lake/river bank sediment type and rate of deposition (Quintana-Cobo et al., 2018), studying biogeochemical cycles with regards to CH_4 formation and oxidation requires a more in-depth assessment of site-specific conditions.

1.6.2. Studied peatlands

Since their discovery, numerous peatlands within the PMFB have been investigated and some described in terms of physical and chemical parameters. A list of sites that were studied and included in detailed or overall reports and references can be found in Table 1:

Table 1 Studied peatlands in PMFB and reference in which further details can be found.

Peatland name	Reference
Buena Vista	Lähteenoja et al.,2009a, b; Teh et al., 2017; Kelly et al., 2014
San Jorge	Lähteenoja et al., 2009a, b; Teh et al., 2017; Kelly et al. 2014, 2017;
Quistococha	Lähteenoja et al., 2009b; Teh et al., 2017; Roucoux et al., 2013, 2017; Kelly et al., 2014; Lawson et al., 2014; Van Lent et al., 2018; Kelly et al., 2018
Charo	Lähteenoja et al.,2009a, b; Teh et al., 2017
Riñón	Lähteenoja et al., 2009a, b;
Miraflores	Lähteenoja and Page, 2011; Teh et al., 2017
Nueva York	Lähteenoja and Page, 2011

Maquia **Roca Fuerte** **Aucayacu** **Nueva Alianza** **Tacshacocha** **San Roque** **Buena Vista del Maquia**	
Chino **Ex Petroleros** **Fundo Junior** **Itaya 1,2,3** **Pebas** **Primavera** **San Nicolas** **Santa Rosa** **Tarapoto**	Lähteenoja et al., 2009a

1.7. Biomarkers and their use as proxies

The term of ***"geolipid"*** is commonly used to describe decay-resistant biomarkers in sediments and soils. Lipids, former components of cell membranes, are typically recalcitrant in nature compared to other biochemical components of organic matter, and insoluble in water, making them more long-lived in the sedimentary records (e.g. Meyers, 1997; Briggs and Summons, 2014; Luo et al., 2018).

Biomarkers (i.e. biological markers or geolipids) are here defined as decay-resisting molecular compounds originating from past-living organisms and vegetation, that are now found as fossil molecules across a wide range of environments (Peters et al., 2005). They are former geolipids that have undergone chemical transformations (i.e. oxidation, cyclization), maintaining however they chemical structure (i.e. backbone structure) (Briggs and Summons, 2014). They are highly useful in attempts of quantifying past environmental changes (Eglinton et al., 1964; Eglinton and Calvin, 1967) as they record conditions in the environment at the time of their formation and organism's death, acting thus as proxies in the absence of direct evidence. If a link is demonstrated between the biological component and present recalcitrant-lipid, they are regarded as proxies in describing the initial

composition and sources of organic matter, palaeoenvironment characteristics, level and processes of biodegradation (Gonzales-Vila, 1995). The first convincing linkage made between geolipids and living organisms was made by Treibs (1934), when a correlation was made between chlorophyll *a* in photosynthetic organisms and porphyrins in petroleum. Furthermore, they can be used as tools in understanding former-living communities, vegetation-type successions at one point in the geological record and the thermal record that led to the formation of oils and rocks. They are known to characterize all three domains of life (Gaines et al., 2009; Figure 14) and, as they are resistant to decomposition and diagenesis, biomarkers are ubiquitous in nature and can be found in rocks, crude oils, sediments and soils that formerly sustained life (Meyers, 2003; Hunt et al., 1996; Peters et al., 2005; Gaines et al., 2009).

The main geolipids employed in this research include hydrocarbons (**alkanes, hopanoids**), **fatty acids**, and **glycerol dialkyl glycerol tetraethers** (GDGTs) and are discussed below with their main applications for this study. Alkanes and n-alkanes are used to depict changes in vegetation at a site and between the three peatlands while hopanoids, fatty acids and GDGTs provided information on variation in concentrations of archaea and bacterial masses with respect to past water table depths, pH, temperatures, vegetation and levels of anoxicity. Furthermore, isoGDGTs are employed in discussions on variations in CH_4 cycle as they occur in the anoxic part of the peatland, with isoGDGT-0 indicating anaerobic methanogen mass, while isoGDGTs 1-4, are known for their anaerobic methanotrophic processes. BrGDGTs, on the other hand, since they are related to anaerobic bacteria (Acidobateria) are employed to understand competition processes in the catotelm, however, based on recent articles (see subchapter 1.7.2.2.), the potential for an aerobic source is also discussed.

1.7.1. Alkanes and n-alkanes

Leaf waxes act as a barrier against many factors within the ecosystem. At a molecular level, they are composed of n-alkanes with an odd over even preference, n-alkanols and fatty acids (with an even over odd preference), aldehydes and esters (Jenks and Ashworth, 1999; Figure 15). Their molecular fossils have various degrees of resistance to degradation (i.e. recalcitrance) and their concentrations can aid palaeoenvironmental reconstructions (Eglington and Hamilton, 1967; Eglinton and Calvin, 1967; Poynter et al., 1989; Pu et al., 2011). This is due to the fact that different plant species that characterise certain environments (i.e. arid, submerged), will biosynthesize specific lipids that, if preserved, can

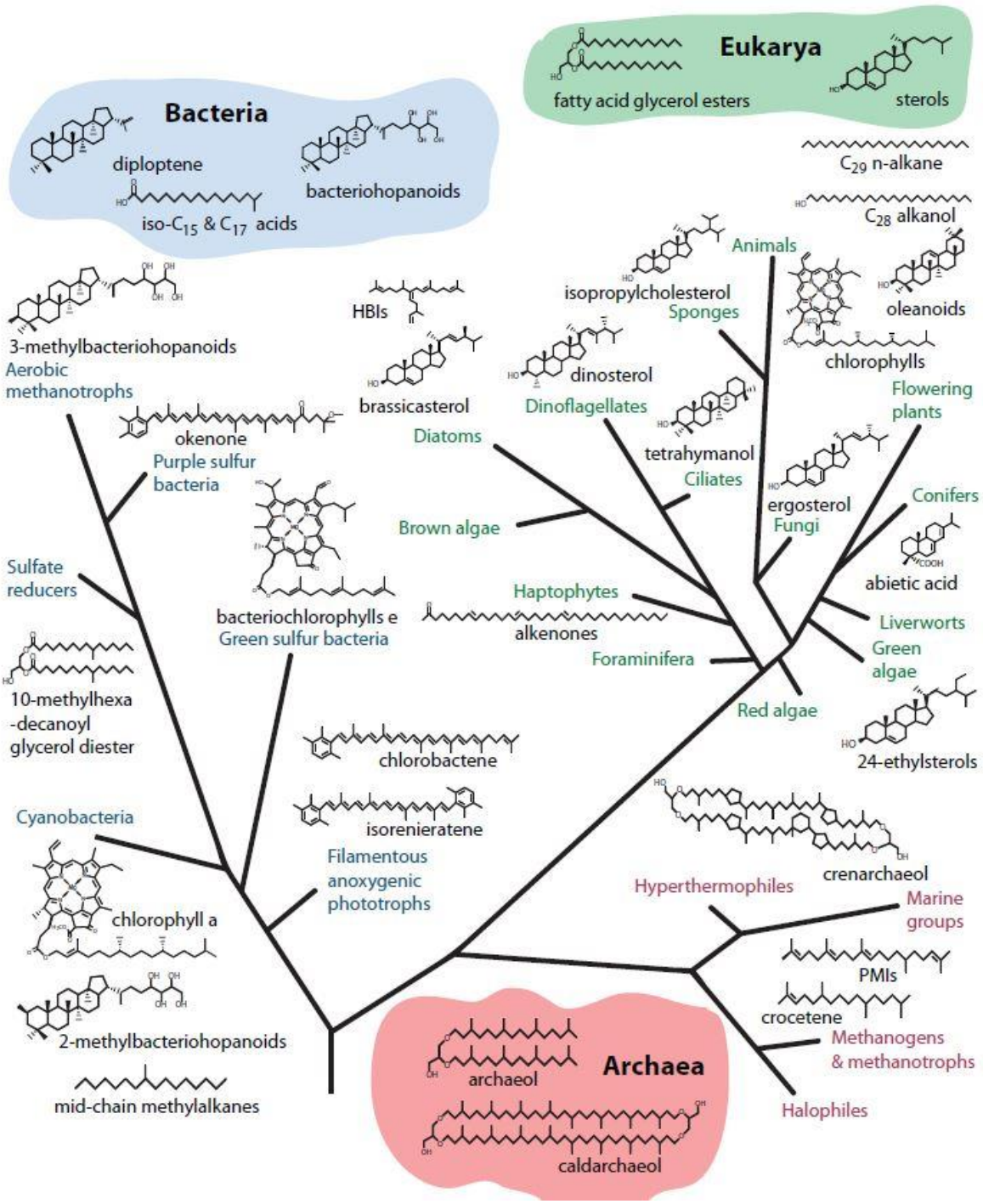

Figure 14 Biomarkers characterizing all three domains of life and their subdivisions (Briggs and Simmons, 2014). Notice corespondents of flowering plants, bacteria and archaea.

be analyses as biomarkers. One of the most important and highly used biomarkers are **n-alkanes** (Figures 15 and 16), mainly due to their high potential for preservation across a wide range of temperatures (Meyers, 1997) which makes them ubiquitous in nature. They are found in the N1 fraction extracted via Hexane (see Chapter 2), as part of the aliphatic hydrocarbon fraction, along with hopanes.

N-alkanes are divided into three groups based on their chain lengths: short-chain (<C_{21}), middle-chain (C_{21}-C_{24}) and long-chain n-alkanes (>C_{25}). This division is primary based on the primary source that biosynthesize them. The general assumption is that odd short-chain n-alkanes are produced by microbial organisms (Dinel et al., 1990) while odd long-chain n-alkanes with peaks in n-C_{27}, n-C_{29} and n-C_{31} (Figure 16), by vascular plants (Eglington and Hamilton, 1967). Eglinton et al. (1962) and Eglington and Hamilton (1967) demonstrated that the odd long-chain n-alkanes are biosynthesized by terrestrial higher plants and, more precisely, they are components of leaves' epicuticular waxes (Figure 15). Moreover, one study showed that bacteria is able to biosynthesized n-alkanes across all three chain lengths (i.e. C_{15}-C_{28}, e.g. Li et al., 2018), algae contribution is inferred from a peak in the n-C_{17} n-alkane with no odd/even preferred distribution (Gonzales-Vila, 1995 and references therein;) while non-emergent and emergent aquatic plants have peaks in concentrations at n-C_{21}, n-C_{23} or n-C_{25} (Ficken et al., 2000; Crenwell, 1984). In this study, shorter-chains (<n-C_{15}) were not identified on chromatograms, which can be due to their volatile or easily dissolvable nature in water and subsequent loss (Brown, 1987). Furthermore, the length of the n-alkane chains and degree of branching has an impact on the degradation process and speed at which microbes can degrade them (e.g. Singh et al., 2011 and references therein). For example, longer chain alkanes, alkanes with cyclopropyl moieties and branching structures have the effect of reducing their biodegradation potential, making them more resistant to biological-mediated breakdown (e.g. Atlas, 1981).

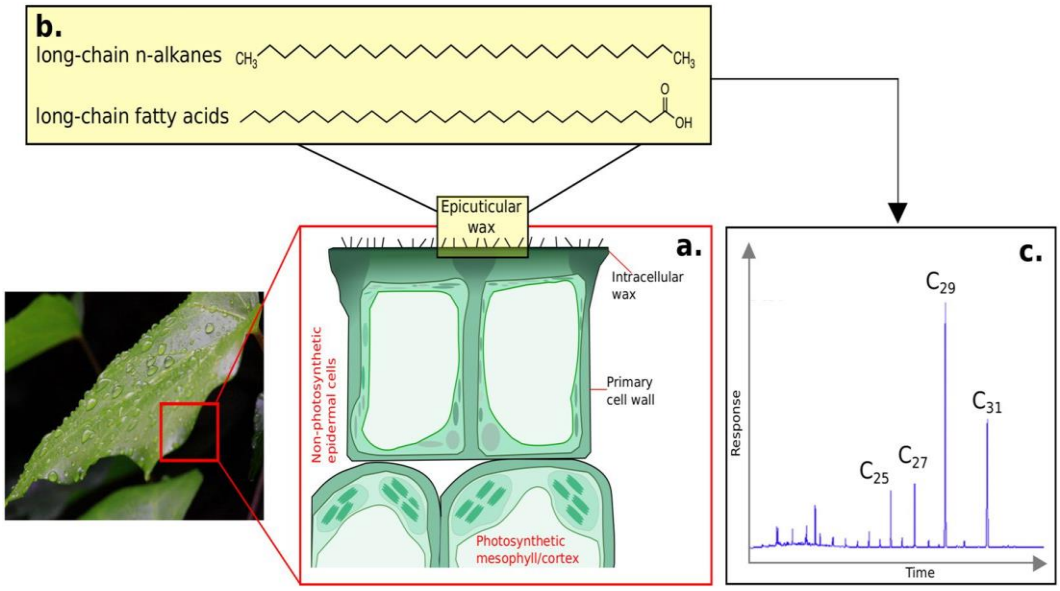

Figure 15 N-alkane and fatty acids provenience from epicuticular leaf wax and characteristic n-alkane chromatogram (taken from Eley and Hren, 2018). Notice that both biomarker groups originate from the surface of a leaf (a) and the signature of n-alkane in figure c is dominated by long-chain n-alkanes with an odd over even predominance.

However, recent studies have showed that these provenience generalizations should be used with care as they might lead to misinterpretations of the organic matter source, palaeonvironmental events and vegetation successions. For example, Kuhn et al., (2010) showed that even over odd (E/O) short-chain n-alkanes preference (i.e. n-C_{16} and n-C_{18}) can indicate an input from tissues of higher plants (i.e. leaves and roots) and thus should not be attributed to thermal breakdown (i.e. fires, diagenetic) as previously thought. Eckmeier and Wiesenberg (2009) argued the contrary, suggesting that this n-alkane distribution can prove useful in archaeological studies of land use, as it can be used as indicators for biomass burning. Several of the proxies available in literature and relevant for this study are based on general accepted n-alkanes signatures.

Nonetheless, they have been employed over a wide range of environments and sample types with their potential already demonstrated in peatbogs and wetlands (e.g. Nichols et al., 2006; 2009; 2014; Baker et al., 2016; Pancost et al., 2002) and, due to existing palynological records that led to palaeoenvironmental reconstruction at QT and BVA sites (Roucoux et al., 2013; Kelly et al., 2017), these proxies have been verified and applied accordingly in BVA samples and the rest of the PMFB peatlands.

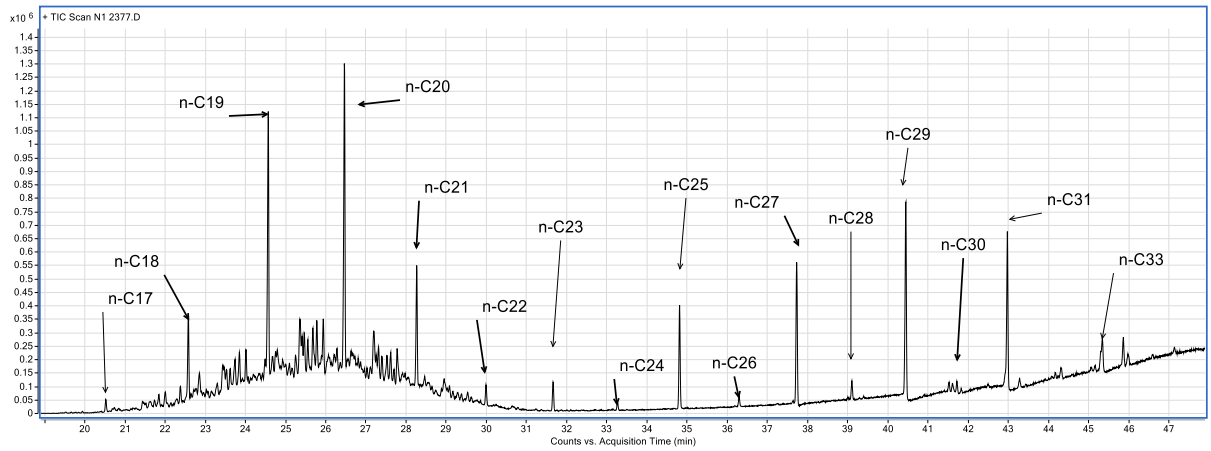

Figure 16 N-alkane distribution as seen on GC-FID in a sample from the surface of QT peatland.

1.7.1.1. Carbon preference index (CPI)

The carbon preference index (CPI) is employed in petroleum studies in order to assess the maturity or source of organic matter. CPI values for n-alkanes provides a relative distribution between the odd and even n-alkanes' concentration within the sample. For example, in fresh higher plant OM, n-alkanes will show a preference of odd over even (O/E) carbon number (i.e. higher concentrations of C_{odd} than C_{even}) and thus, the CPI will have higher values than

in samples containing older, microbial-reworked OM (Andersson and Meyers, 2012). If the samples contain a higher input of algae or bacterial reworked material, the CPI will have lower values, as there will be a higher concentration of shorter-chain n-alkanes, causing thus a shift in distribution. Thus, relatively higher values in CPI will indicate better preserved terrestrial organic matter, while relative lower values, will indicate a higher degree of microbial reworking or more labile OM sources (Baker et al., 2016). Studies employing the CPI proxy in peat-forming environments (Baker et al., 2016; Andersson and Meyers, 2012) reported high values (i.e. up to 12), suggesting the high preservation degree of OM in these settings and highlighting the effect of penetrating roots on CPI at depth.

Due to the fact that different formulas have been proposed and discussed throughout literature (e.g. Bray and Evans, 1961; Allan and Douglas, 1977; Rieley et al., 1991; Marzi et al., 1993; Andersson and Meyers, 2012), this study employs the CPI proxy proposed by Bray and Evans (1961) due to its wider use in literature and range of n-alkane that the formula covers (n-C_{24} to n-C_{32}). However, other CPI formulas provide the same information as other similar proxies (see for example Marzi et al., 1993), that of biodegradation and overall organic matter source(s).

Bray and Evans: $$CPI = \frac{1}{2}\left(\frac{C_{25}+C_{27}+C_{29}+C_{31}}{C_{24}+C_{26}+C_{28}+C_{30}} + \frac{C_{25}+C_{27}+C_{29}+C_{31}}{C_{26}+C_{28}+C_{30}+C_{32}}\right)$$

1.7.1.2. Paquatic (P_{aq})

$P_{aquatic}$ (P_{aq}) is a proxy ratio that can be employed to understand changes in vegetation types as it is used to determine the input of aquatic plants (i.e. submerged and floating) that produce mid-chain n-alkanes (i.e. C_{23} and C_{25}) relative to long-chain n-alkanes (i.e. >C_{29}) found in the leaf wax of higher plants (Ficken et al., 2000). This proxy has been first used to describe the relative input in lake settings, yet has been employed in peatlands studies, especially in intertropical and tropical setting (e.g. Baker et al., 2016) due to fluctuating nature of the water table, characteristic hydraulic conductivity and frequency of flooding events that can cause shifts in vegetation.

$$P_{aq} = \frac{C_{23} + C_{25}}{C_{23} + C_{25} + C_{29} + C_{31}}$$

Thus, the first study that employed P_{aq} (Ficken et al., 2000), proposed that for P_{aq}<0.1, the main vegetation input comes from terrestrial higher plants; values between 0.1 and 0.4 are characteristic of emergent macrophytes or a mix between the two ends, while values between 0.4 and 1 are characteristic of submerged or floating vegetation. The latter can either indicate increased precipitations (Pu et al., 2011) and/or an increase in flooding frequency and duration.

1.7.1.3. P_{wax}

P_{wax} is a proxy ratio that allows distinctions between different higher plant species input. For example, palaeoenvironmental conditions could have been favourable for predominantly vascular plant, yet changes in diversity due to competition factors, could have led to certain species to prevail, and consequently, have a higher input to bulk OM (Baker et al., 2016 and references therein). A relatively low P_{wax} value will also indicate increase in precipitations and thus a more humid period as homologues C_{23} and C_{25} would increase in concentrations. Alternatively, a relatively high P_{wax} could indicate a decrease in precipitations and increase in temperature, thus a drier climate with less input from the C_{23} and C_{25} homologues (Pu et al., 2011).

$$P_{wax} = \frac{C_{27}+C_{29}+C_{31}}{C_{23}+C_{25}+C_{27}+C_{29}+C_{31}}$$

1.7.1.4. Average chain length (ACL)

One previous use of the ACL was based on the assumption that n-alkane lipids derived from grass have longer chain lengths that those derived from woody vegetation (Cranwell, 1973), thus having the potential of identifying changes between grass and woodland vegetation, and in a peatland, between drier and wetter intervals. However, more recent studies and literature reviews (e.g. Buch and McInerney, 2013) showed that there is little correlation between the vegetation type and ACL, with ACL values being higher in woody plants in only some studied sites and it is, in turn, an unreliable proxy (i.e. only 7 out of 26 reviewed sites showed

differences between different vegetation types, Wang et al., 2015). The use of ACL should be thus site specific and not employed between different locations (Wang et al., 2015).

Poynter et al., (1989) proposed that the distribution of n-alkanes in samples of aeolian dust varies with **latitude**, and thus, with climate and temperature, with long-chain odd-carbon-numbered n-alkanes being produces in greater concentration in warm and dry climates (Calvo et al., 2004). This correlation between the average chain length of n-alkanes and temperature can be used as a relative palaeothermometer proxy and offer best results when employed over a wider time range comprising glacial and interglacial cycles or between samples from different latitudes. Studies thus attributed a relatively higher value in ACL to relatively drier and/or warmer periods (Peltzer and Gagosian, 1989).

Furthermore, ACL has been shown to differ significantly between individuals within the same genus (i.e. values ranging between 26.87 and 28.99; Hoffmann et al. 2013) and multiple environmental parameters (i.e. temperature, precipitation, and hydrology) have been shown to cause changes in ACL values.

For this study, samples are characteristic of a tropical lowland environment, with high humidity and precipitations all year round due to latitudinal positioning. Due to all of the above-discussed issues with this ratio, values of ACL will only be discussed in relationship to vegetation and environmental changes depicted through other proxies or biomarkers, as supplementary evidence and no interpretations will be made solely on its values. Both $ACL_{23\text{-}33}$ and $ACL_{23\text{-}39}$ have been calculated and compared (i.e. numbers refer to length of n-alkanes within the covered range), however little to no variation has been observed between the two, and $ACL_{23\text{-}33}$ is further depicted in graphs.

$$ACL_{23-33} = \frac{23 * C_{23} + 25 * C_{25} + 27 * C_{27} + 29 * C_{29} + 31 * C_{31} + 33 * C_{33}}{C_{23} + C_{25} + C_{27} + C_{29} + C_{31} + C_{33}}$$

$$ACL_{23-39} = \frac{23 * C_{23} + 25 * C_{25} + \cdots + 39 * C_{39}}{C_{23} + C_{25} + \cdots + C_{39}}$$

1.7.1.5. Pristane vs Phytane (Pr/Ph) ratio

Pristane and phytane are isoprenoid hydrocarbons whose ratio (i.e. Pr/Ph ; Figure 18) is usually employed in petroleum research (e.g. Goossens et al., 1988; Van Graas et al., 1981; Moustafa and Morsi, 2012; Nwadinigwe and Alumona, 2018), as a detector of oil spill contamination (McIntyre et al., 2007), in marine environmental studies (Rontani and Bonin, 2011) or as a tool to understand palaeoenvironments of deposition (e.g. Didyk et al., 1978; Peters et al., 2005; Zulkifley et al., 2015). In the marine environment, prokaryotes are contributing to the formation of pristane (i.e. during feeding; oxidation end products of α-tocopherol) and phytane (i.e. degradation of chlorophyll phytyl side-chain). Furthermore, methanogens residing in lakes below the bioturbated layer are another important phytane producer (Risatti et al., 1984).

In wetland environments, they are formed via processed of biodegradation. Pristane is formed via oxidation of chlorophyll phytyl side-chain (i.e. decarboxylation), phytol, in aerobic environments while phytane through reduction of phytol (i.e. dehydration), in anoxic environments (Blumer et al., 1963; Blumer and Thomas, 1965). As they both have the same predecessor molecule (chlorophyll phytyl side-chain), their ratio (i.e. Pr/Ph) was used in many studies to gain an insight into the oxygen levels in their environment of formation (Brooks et al., 1969; Didyk et al., 1978). However, chlorophyll is not the only precursor phytane and pristine (i.e. can also form from tovophernols, see Peters et al., 2005) yet the ratios can indicate plant input in environment with different levels of oxygen (Gola et al., 2013 and references therein) thus above-discussed ratios are used with caution when assessing redox conditions in the environment.

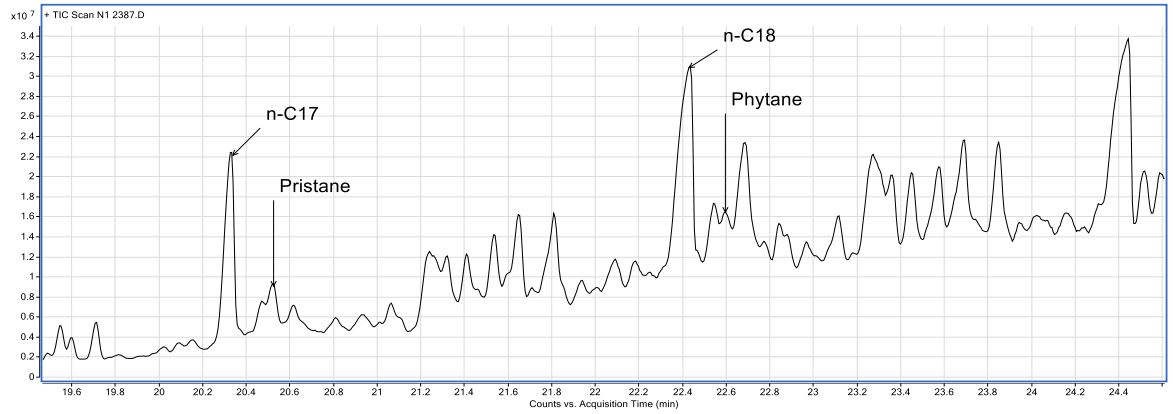

Figure 17 Pristane and phytane retention times relative to n-C_{17} and n-C_{18} in analysed samples on a GC-MS chromatogram. Notice that they both appear one compound away from the main n-alkane.

Phytane in the GC-MS sample chromatograms was identified based on the retention time of a phytane standard (Figure 17). Pristane was identified using its characteristic ions m/z 113, 183 and molecular ion (M^+ 268) and by compering its mass spectra with the NIST library. In the studied samples, both elute a compound away from n-C_{17} and n-C_{18}, respectively (Figure 17).

The Pr/Ph ratio was proposed as an indicator of the environment of deposition, and more specific, as an oxic-anoxic proxy for palaeoenvironment (Brooks er al., 1969; Didyk et al., 1978). For example, Lijmback (1975) proposed an aquatic depositional setting for ratio values less than 2 (Pr/Ph<2), fluvio-marine and coastal swamp settings for values between 2 and 4, and peat swamp settings for values up to 10 (Nwadinigwe and Alumona, 2018 and references therein).

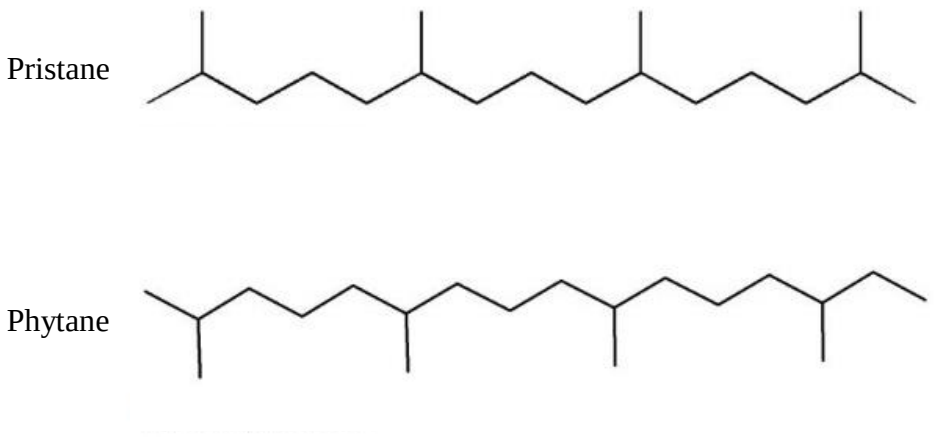

Figure 18 Chemical structure of pristine (top) and phytane (bottom).Edited from website 5 and 6.

Zulkifley et al. (2015) analysed the geochemical characteristics of a lowland tropical peatland in Malaysia (Kota Samarahan-Asajaya area) and found very similar values to those depicted in QT, SJO and BVA in PMFB peatlands, which indicated an oscillation in the environment between anoxic and suboxic conditions given by the fluctuating nature of the water table in both locations. Mohialdeen et al., 2015, in a study on Kurdistan oilfields, observed low ratios of Pr/Ph (i.e. 0.72-0.91), pristine/n-C_{17} (i.e. 0.25-0.39) and phytane/n-C_{18} (i.e. 0.35-0.45) and concluded that the biomarkers were formed from OM deposited under anoxic conditions in a marine setting.

1.7.2. GDGTs

Glycerol dialkyl glycerol tetraethers (GDGTs) are membrane lipids found in both bacteria and archaea. Although they were initially thought to be limited only to the latter phylum, since their discovery in bacteria cultures (Langworthy et al., 1983; Sinninghe Damsté et al., 2007), GDGTs are more widely recognized in both groups.

They occur in a wide range of environments such as lakes, oceans, soils and peat bogs (Weijers et al., 2006a, b, 2007; Zheng et al., 2015; Naafs et al., 2017a) and have a high preservation potential, being found in sediments as old as 140 Ma (Schouten et al., 2013 and references therein), with their diagenic products (i.e. biphytanes) found in much older sediments. They can be analysed in their intact form (i.e. containing the polar head, Figure 20) or as core lipids (i.e. without the polar head) through various methods (see Schouten et al., 2013 for method review), however this study focuses on and refers to core lipid distribution within the three peat cores from Pastaza-Marañón foreland basin.

Due to their recalcitrant nature, they can be used as biomarkers and, moreover, due to their specific distribution in some environments, they are used as palaeoenvironmental proxies in order to infer past OM sources, sea surface and air temperatures (Schouten et al., 2002; Weijers et al., 2007a), soil and peat pH and temperature (Weijers et al., 2007a; Zheng et al., 2015; Naafs et al., 2017a).

Archaea, although a prokaryote as bacteria, synthetize a monolayer membrane (Figure 21) where the GDGT isoprenoidal lipid spans the full membrane (Weijers et al., 2006b), and these lipids (i.e. biphytane structures) are bounded to a glycerol moiety via an ether link (Figures 21 and 23) (i.e. whereas phospholipids that characterize bacteria consist of two straight fatty acids with an even number of carbon that are linked to a glycerol-3-phosphate compound via **ester bonds;** Figure 22). The branched (i.e. methylated) isoprenoidal chains of archaea are based on two main lipid configurations (i.e. core structures) that are at the base of diether lipids: **archaeol (C_{20}**; see subchapter 1.4.2.4.**)** or **caldarchaeol (C_{40})** (Caforio and Driessen, 2017 and reference therein). A higher variation in chemical structures is found in archaea lipids that contain caldarchaeol back-bone as it contains 4 ether bonds (i.e. tetraethers; Figure 20). These morphological differences were seen as adaptations to extreme environments (i.e. highly acidic, anoxic and/or high growth temperatures) in which archaea are known to dominate, particularly because ether bounds are more resistant than ester ones. However, subsequent studies (Michaelis and Albrecht, 1979; Chappe et al., 1979;

1980) have discovered GDGTs in numerous non-extreme environments (i.e. lakes, marine sediments).

Bacteria – dialkyl glycerol diester lipids

As only a few studies on cultures of archaea exist, biological GDGT sources are yet to be further discovered (Auguet et al., 2009 and references therein). However, their ubiquitous occurrence in nature together with cultures of the few strains, allow delimitations of their environmental conditions in which they occur (see Schouten et al. 2013 for biological sources of GDGTs in Euryaarchaeota, Crenarchaeota and Thaumarchaeota)

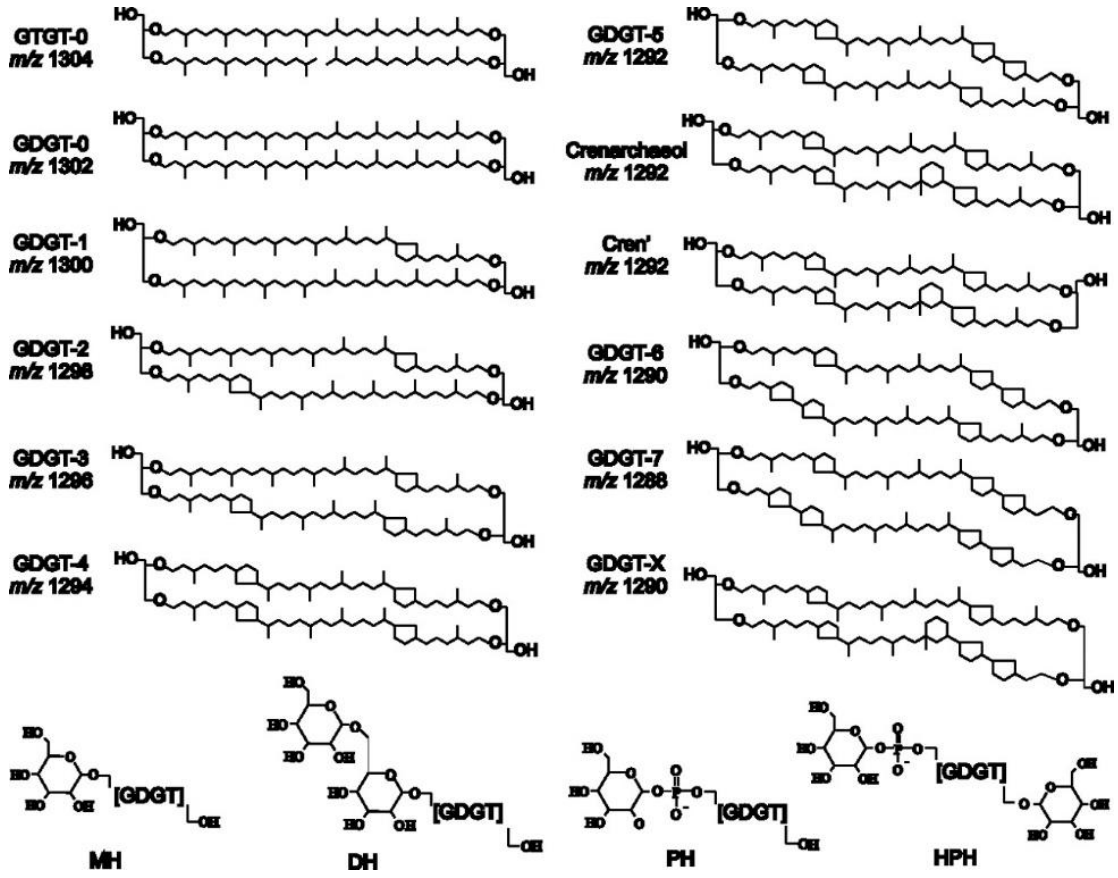

Figure 19 Core isoGDGTs' chemical formulas, common name and characteristic m/z ion. Notice below structures of intact GDGTs (taken from Pitcher et al., 2011).

17.2.1. Isoprenoid GDGT

Isoprenoid GDGTs are known to be produced by a wide range of archaea (Zheng et al., 2015 and references therein; Weijers et al., 2006a, b; Schouten et al., 2007b). Their notation

GDGTx (with x ranging from 0 to 8), refers to the number of cyclopentane moieties within their formula (Figure 19).

GDGT-0 (m/z/=1304; also known as **caldarchaeol**) is found in almost all groups of archaea (apart from the halophilic group) however, due to its occurrence in CH_4 oxidizing environments (Pancost et al., 2001; Elvert etal., 2005; Blaga et al., 2009), higher abundance in anoxic peat sections than in oxic ones and the ^{13}C depleted signature of its biodegradation products, it was linked to **methanogenic euryarchaea (**e.g. Zheng et al.,2015; Schouten et al., 2013 and references therein). For example, high concentrations of GDGT-0 occur during wet and warm intervals in a peat core from Zoigê-Hongyuan, East of Tibetan Plateau, suggest that it can be produced by methanogenic archaea (Zheng et al., 2015).

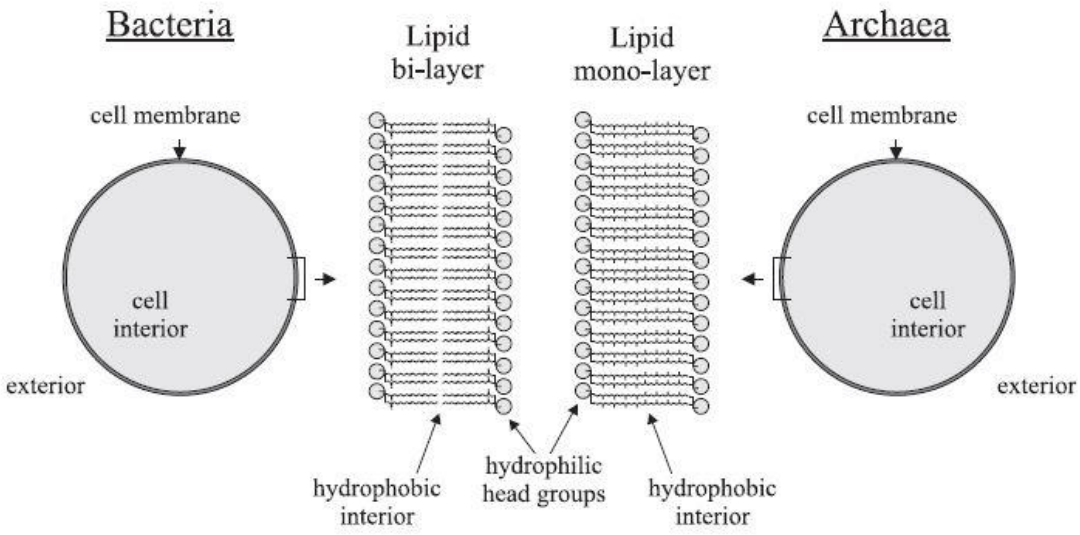

Figure 20 Differences at lipid level between the membrane structure of bacteria and archaea (Weijers, 2007, PhD thesis). Noticed the bi-layer lipid membrane and ordering in bacteria and mono-layer in archaea.

Crenarchaeol (m/z=1292) is the only isoGDGT to contains a cyclohexane structure and was assigned mainly to Thaumarchaeota (Schouten et al., 2013 and references therein). It was found to dominate during drier periods in a peat core from Eastern Tibetan Plateau and it was associated with increased **archaea-mediated oxidation** of ammonia (Zheng et al., 2015). Furthermore, in the same study, crenarchaeol was found in higher concentrations during proposed drier periods with higher oxygenated (and pH) sediments (also known to favour development of Thaumarchaeota; Figure 22) that could possible lead to higher effluxes of N_2O and thus was assigned to the oxic part in sediments or peatlands (Zheng et al., 2015).

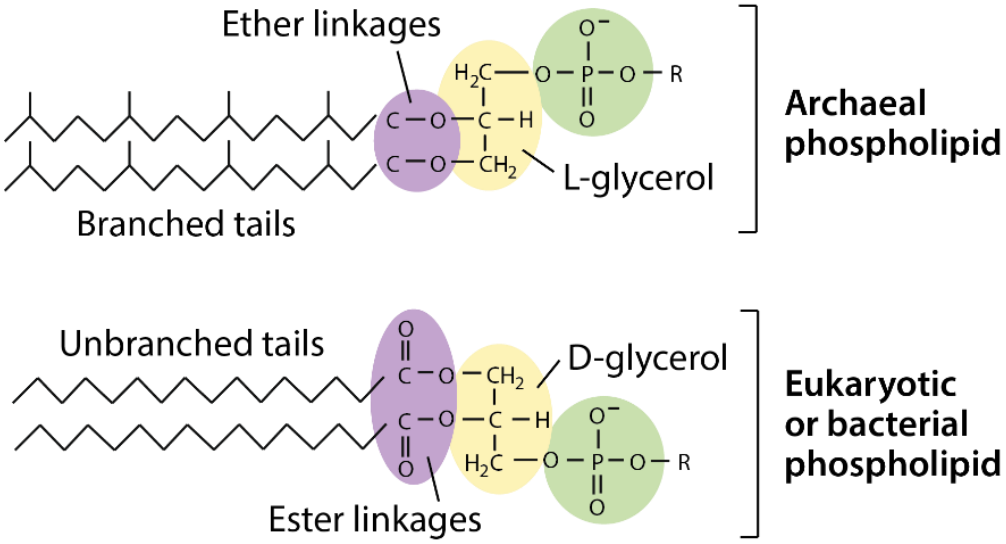

Figure 21 Differencess between archaea and bacteria phospholipids (website 7). Notice the branched trails (isoprenoids) and unbranched trails in bacteria (straight fatty acids).

GDGTs 1-4 (m/z=1300, 1298, 1296, 1294) are present in Crenarchaeota, Thaumarchaeota and in some groups of Euryarchaeota (Figure 22) and were not shown to be produced by a wide range cultured methanogenic archaea, however they were found in anaerobic CH_4 oxidizing environments suggesting a possible **methanotrophic archaea** source (i.e. ANME-1) when they have higher concentrations than crenarchaeol. Furthermore, their degradation products (i.e. biphytanes) had ^{13}C-depleated isotopic signatures, especially for GDGT-1 (Schouten et al., 2000; Schouten et al., 2013 and references therein).

GDGTs 5-8, were previously only associated with environments with extreme temperatures (i.e. hot springs) and no link was made with CH_4-producing or –oxidizing environments (Schouten et al., 2013 and references therein). However, they were recently discovered (i.e. GDGTs 5-7) in tropical ombrotrophic peatlands and seem to be restricted by pH< 5.1 and temperatures>19.5°C. Furthermore, relative increases in isoGDGTs 5-7 concentration might be correlated with increasing temperature on the background of constant pH, making them a potential proxy for assessing palaeotemperature increases (Naafs et al., 2018 b).

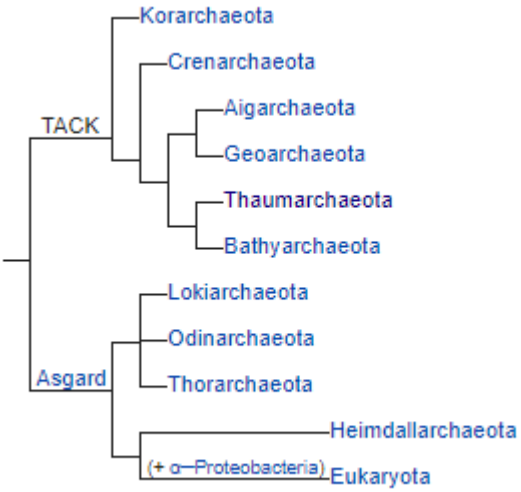

Figure 22 Main divisions of proteroarchaeota (website 8)

1.7.2.2. Branched GDGTs

Branched GDGTs were not reported until recently as major components of any microbes, however they possess features that are found in both bacteria and archaea. Weijers et al. (2006a) attributed these lipids to a **bacteria** source in a study that showed the presence of cyclopentyl moieties and membrane spanning character (Figure 23) which were thought to be characteristic only to archaea and suggested that membrane adaptations can be due to the highly acidic environments in which they live.

In high latitude peatlands, temperatures are expected to hinder bacteria growth during the cold season, thus, in those settings the GDGTs' distribution most likely reflects summer-active communities (Naafs et al., 2017a and references therein). However, due to their latitudinal positioning (i.e. tropics), peatlands in PMFB experience temperatures of 26°C (Marengo, 1998) all year round, thus it is expected that: i) surface samples to record GDGTs values of the season in which they were collected, bearing values that also indicate the position of the water table (i.e. wet vs dry season); ii) core section to be at equilibrium with mean average annual temperature (MAAT) (Naafs et al., 2017a and references therein).

They were first identified in peat bogs (Schouten et al., 2000; Pancost and Sinninghe Damsté, 2003; Weijers et al., 2006b) and assigned to bacteria with the identification of "GDGT-8" chemical structure (i.e. 1,2-di-*O*-alkyl-*sn*-glycerol; Weijers et al., 2006b).

They differ from isoprenoid GDGTs due to the branched and cyclopentyl structures in their n-alkyl moieties (Figure 24), which sets them apart from archaea's stereoconfiguration which is opposite (Weijers et al., 2006b). Furthermore, their basic structure (i.e. 13,16-dimethyloctacosane) is found in and ascribed to bacteria. Several lines of evidence assigned brGDGTs to bacteria sources, and more precisely, to bacteria that live in **anaerobic environments**, however, organisms that produce them are not known with confidence (Naafs et al., 2017a). Firstly, brGDGTs were found in higher abundance in the anoxic part of sediments and peat columns (Weijers et al., 2006b; Zheng et al., 2015; Naafs et al., 2017a). Secondly, their carbon isotopic signature suggests that the producer(s) grow(s) on heterotrophic substrates (Pancost et al., 2000; Pancost and Sinninghe Damsté, 2003). Finally, due to several occurrences in culture-based (Sanninghe Damsté et al., 2011) and natural sediments (De Rosa et al., 1988; Pancost et al., 2000; Weijers et al., 2006; Peterse et al.,2010), in which they were also reported to decrease in concentration with decreasing pH, they were attributed to **anaerobic mesophilic bacteria** with one confirmed source in the *Acidobacteria* phylum (Weijers et al., 2009a; which is also positively correlated to pH values, Jones et al., 2009).

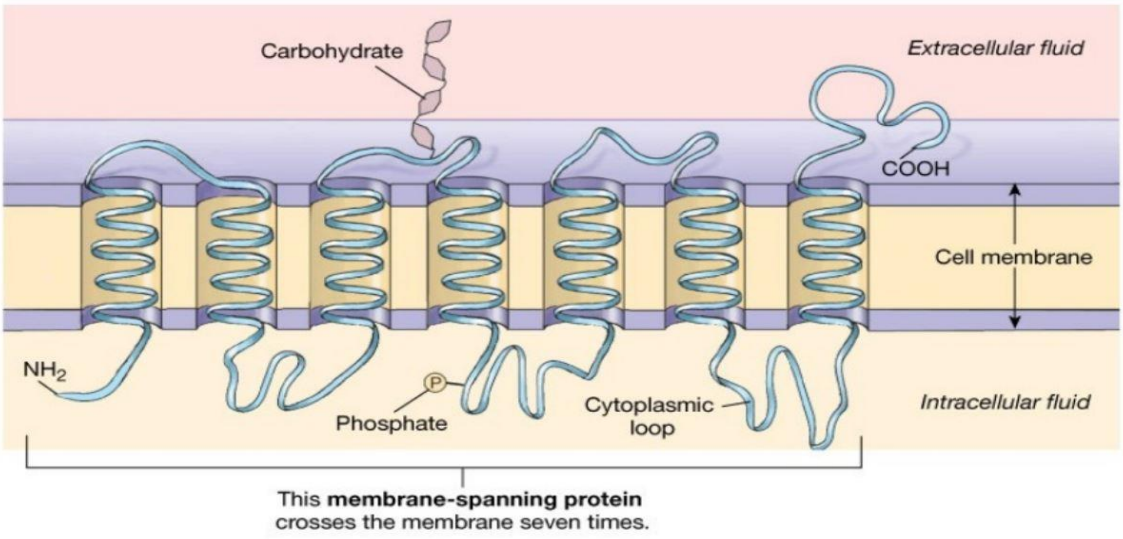

Figure 23 Visual representation of membrane -panning character of branched GDGTs (Website 9).

In Schouten et al., (2013), **aerobic bacteria sources for brGDGTs** were not dismissed and a study done by Sinninghe Damsté et al. (2011), found two *Acidobacteria* that produced brGDGT-I under aerobic conditions. Although mainly thought to be indicative of anaerobic microbes, they can also be produced by aerobic or facultative aerobes (Weijers et al., 2006a; Loomis et al., 2014).

Further publications adapted the generalized view that brGDGTs indicate bacteria communities, while isoGDGTs, CH_4-producing or consuming archaea communities. Proposed biosynthetic pathways for both br- and isoGDGTs can be found in Weijers et al., (2006). In terms of general occurrence, the ternary diagram below (Figure 25; Schouten et al., 2013), indicates the fact that brGDGTs occur predominately in terrestrial environments while Crenarchaeol and GDGT-0 (i.e. Caldarchaeol), are found in marine or lacustrine environments.

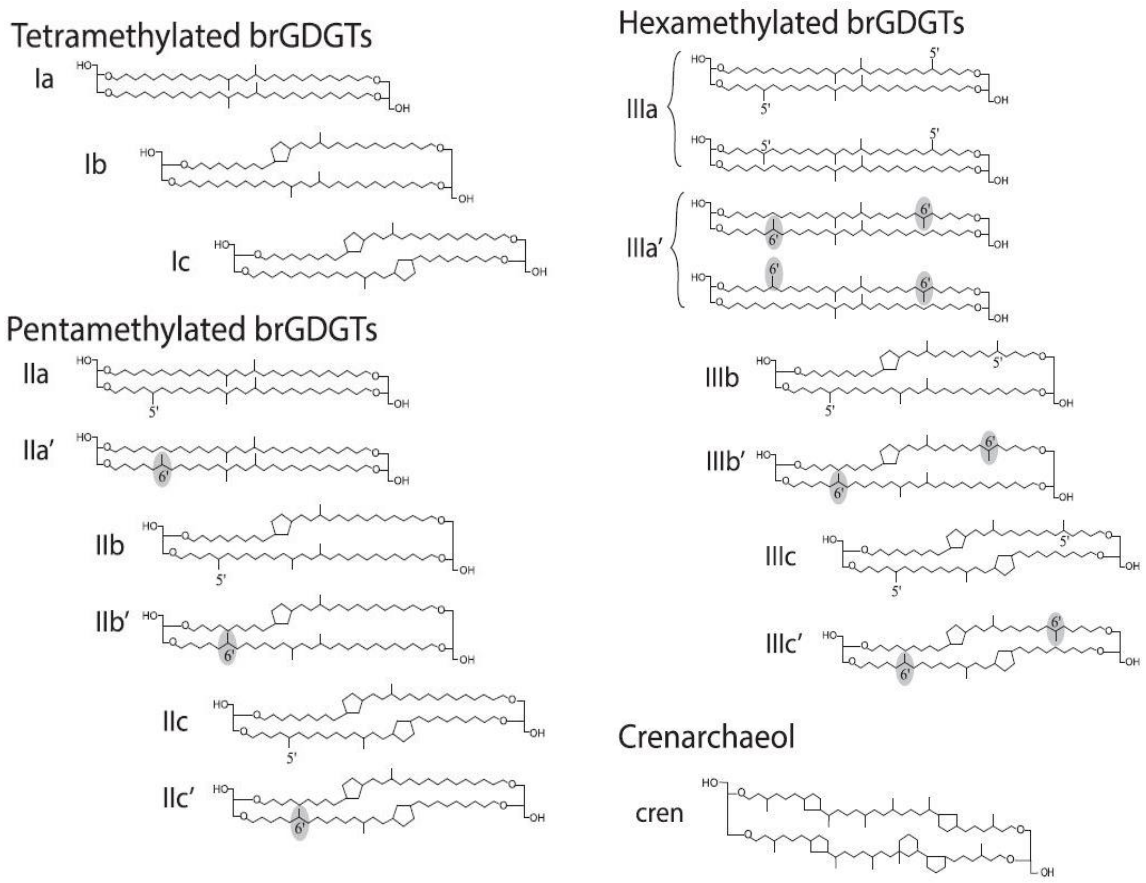

Figure 24 Core brGDGTs chemical formula representation and names. Notice the hexane moiety in Crenarchaeol and the highlighted methyl radicals where the addition occurs at the α and/or ω-6 position (edited from Naafs et al., 2017).

The presence of both iso- and brGDGTs within peatlands of PMFB has numerous implications and values when describing variations in water table depth and the impact of anoxia on CH_4 effluxes. Thus, while isoGDGTs can indicate either anaerobic CH_4 production and/or consumption, implying high water tables and waterlogged conditions, brGDGTs have the potential to indicate both the anaerobic component of bacteria and, coupled with concentration of aerobic bacteria producers, the existence of a constant acrotelm or the fluctuating nature of the water table depth. Varying concentration between

the two groups (i.e. methanogens and methanotrophs) can also indicate competitive relationships or the input (or lack) of suitable substrate for methanogenesis. Furthermore, due to a high temperature regime at tropics, microbes, and consequently, GDGT production at surface and potentially at depth takes place all year round. Thus, it can be possible that if large and unexplained concentrations are seen in core samples relative to surface ones, that they may be the result of continuous accumulation under anoxic conditions. Due to the recalcitrant nature of GDGTs, crenarchaeol and/or brGDGT-Ia (i.e. if aerobic Acidobacteria main source) they need to be assessed against present day conditions in order to determine their potential as biomarkers within these environments.

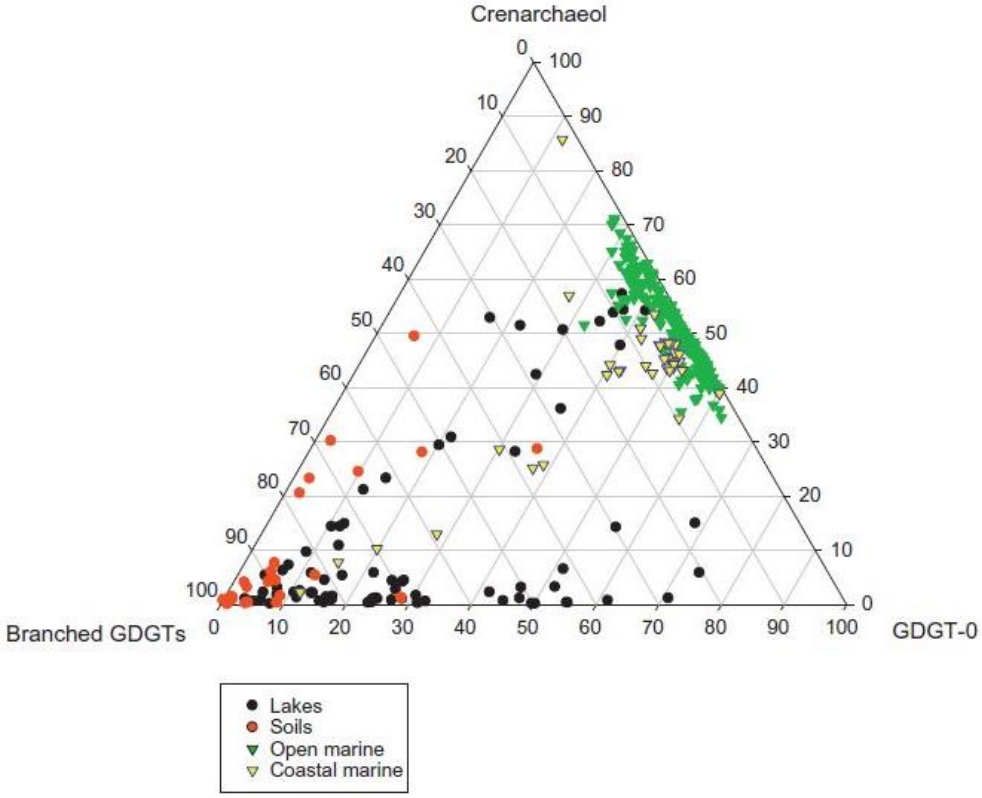

Figure 25 Ternary diagram indicating relative composition of samples from different aquatic and marine environemnts in terms of brGDGTs, GDGT-0 and Crenarchaeol concentrations (Schouten et al., 2013).

1.7.2.3. Proxies

MBT'5me and CBT'peat indexes for MAAT and pH calibrations in peat

MBT'$_{5me}$ index is an indicator of the degree of methylation of the brGDGTs, which is positively correlated with temperature; while CBT'$_{peat}$ index is an indicator of isoGDGTs

cyclisation and is positively correlated with peat pH (Naafs et al., 2017a). The MBT'$_{5me}$ reported here does not contain the methyl radical at the C_6 position (De Jonge et al., 2014) and it is based on the fact that brGDGT-Ia concertation has a positive correlation with MAAT, while brGDGT-IIa and brGDGT-IIIa bear a negative correlation with MAAT (Naafs et al., 2017a). The database used for calibration is dominated by high latitude peatlands, however it contains samples from PMFB and the main peatlands, also investigated in this study. The error (RMSE) for temperature calibration was of 4.7°C and for pH calibration of 0.8 units (Naafs et al., 2017a).

$$MBT'_{5me} = \frac{[Ia + Ib + Ic]}{[Ia + Ib + Ic + IIa + IIb + IIc + IIIa]}$$

$$CBT'_{peat} = log\frac{Ia + IIa' + IIb + IIb' + IIIa'}{Ia + IIa + IIIa}$$

$$pH = 2.49 \times CBT_{peat} + 8.07$$

$$MAAT_{peat}(℃) = 52.18 \times MBT'_{5me} - 23.05$$

MBT and CBT proxies for MAAT and pH calibrations in soils

In soils, different calibrations are used based on the concentrations of branched and isoprenoidal GDGTs (Weijers et al., 2007b).

$$MBT = \frac{[Ia + Ib + Ic]}{[Ia + Ib + Ic] + [II + IIb + IIc] + [IIIa + IIIb + IIIc]}$$

$$CBT = -\log\left(\frac{[Ib + IIb]}{[Ia + IIa]}\right) \ (CBT \pm 0.3)$$

$$MBT = 0.122 + 0.187 \times CBT + 0.020 * MAT$$

$$CBT = 3.33 - 0.38 \times pH$$

The pH error was calculated to ±0.1 pH units, while the CBT error was of ±0.3 (Weijers et al., 2007b). These proxies are used for determining pHs and temperature calibrations in the clay-rich, inorganic layers, underlying both QT and BVA peatlands.

Methane index and Cald/Cren

Methane index (MI) was developed (Zhang et al., 2011) to track marine gas hydrate destabilization due to the fact that it takes into account the relative contribution of isoGDGTs-1, -2 and -3 that are known to be synthesized, although not exclusively, by methanotrophic archaea (Zhang et al., 2011) and associated with CH_4-producing euryarchaea (Dirghangi et al., 2013 and references therein). Furthermore, the $\delta^{13}C$ trend of these lipids, matched the trend of MI, indicating light carbon incorporation, which is specific to large amount of CH_4 releases. Crenarchaeol and its isomer were attributed to planktonic (and benthic) crenarchaeota (Sinnighe Damsté et al., 2002), allowing them to distinguish the relative input of biomass of non-methanotrophs in marine environments from that of archaea. Although MI was developed for marine environments, a study by Dirghangi et al. (2013) applied the index in terrestrial environments, on soil samples from two distinct climates (i.e. wet and dry), with different levels of soil moisture. The study showed a good correlation between the index caldarchaeol/crenarchaeol (Cald/Cren) and MI, proving its further use on land.

$$MI = \frac{[GDGT-1] + [GDGT-2] + [GDGT-3]}{[GDGT-1] + [GDGT-2] + [GDGT-3] + [Cren] + [Cren_{iso}]}$$

Cald/Cren index is used in terrestrial settings to assess relative contribution from methanogenic euryarchaea that are known to syntetisise caldarchaeol (i.e. isoGDGT-0), and thaumarchaea, the only known, up-to-date, producer of crenarchaeol (Dirghangi et al., 2013 and references therein), suggesting values of MI<0.5 to be indicative of CH_4 oxidation while Cald/Cren>20 as input from methanogenic archaea-correlating thus terrestrial environments with anoxic conditions (Dirghangi et al. (2013). MI can thus be used to an extent in waterlogged conditions where caldarchaeol measurements are not available. MI values were multiplied by 100 to show comparable trends with Cald/Cren, thus we will interpret values of MI<50 as indicators of CH_4 oxidation.

1.7.3. Archaeol

Archaeol (i.e. bis-O-phytanylglycerolether; 2,3-di-O-isopranyl sn-glycerol diether; Figure 26) is a ubiquitous archaeal diether lipid diagnostic for methanogens and methanotrophic archaea since it is a component of their membranes (Koga et al., 1998b; Niemann and Elvert, 2008). Due to its recalcitrant nature (Navale, 1994; Pease et al., 1998), it has been employed in multiple studies regarding wetlands and peatlands (Pancost et al., 2011; Zheng et al., 2014), permafrost (Lupascu et al., 2014), cold seeps (e.g. Hinrichs et al., 1999; 2000; Pancost et al., 2000 a, b; 2005), stratified marine columns (Berndmeyer et al., 2014, unquantified); hypersaline environments (Pease et al., 1992) to characterize microbial communities (esp. Euryarchaeota). The oldest sediments, in which archaeol was found, date back to Eocene (van Dongen et al., 2006). Its successor, sn-2-hydroxyarchaeol has a low recalcitrant nature (Pancost et al., 2011), and was not identified in samples available for this study. Archaeol was used in the past to understand redox conditions within peatlands and more specifically, the influences of water table positions on CH_4 production. Archaeol was only found below water table depth (i.e. catotelm) in the 4 ombrotrophic peatlands studied by Pancost et al. (2011) across Europe; however, their concentration was highest at the interface between the oxic and anoxic layers within the peat. In temperate ombrotrophic bogs, this is due to the fact that methanogenesis relies on substrate availability, which is highest at the interface.

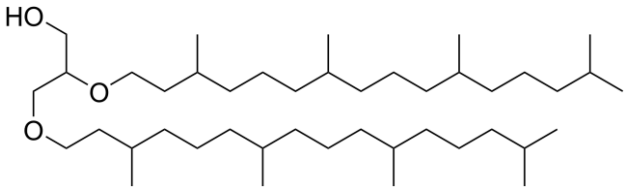

Figure 26 Archaeol chemical structure (website 10).

Studies employing archaeol as a biomarker in the CH_4 cycle, found concentrations of 2-8 μg/g in cold seeps carbonate rocks (Pancost et al., 2005) and between 1.5 and 35 μg/g in NE Tibetan Plateau peats (Zheng et al., 2014) during Holocene. In several studies, due to its depleted isotopic signature, archaeol was linked in origin to methanogens and consequently, used as an indicator of CH_4 production (Lim et al., 2013; Koga et al., 1998; Pancost et al., 2005).

In PMFB, since archaeol is found in higher abundance in core samples (i.e. up to 6 μg/g) and only as a trace biomarker in surface samples at all three locations (i.e. 0.048-0.23 μg/g), we

can speculate that its abundance is related to the position of the water table and occurrence of anoxic conditions, indicating a relationship with the anaerobic methanogen community (Pancost et al., 2011). Furthermore, water table at these sites has high positions all year round (Teh et al., 2017), allowing anoxic conditions to prevail in microsites even during the dry season at shallow depths, explaining in part the occurrence or archaeol in smaller concentrations in surface samples (e.g. Lim et at., 2013). Furthermore, methanogenesis is not restricted in these settings by decreasing temperatures or substrate availability (i.e. limited bioproduction). Surface peat temperature was recorded between 24.8 and 26.1°C (Teh et al., 2017), while the presence of trees and diverse vegetation types at all three sites could provide root exudate substrates for methanogenesis (see subchapter 1.2.; Pancost et al., 2011 and references therein).

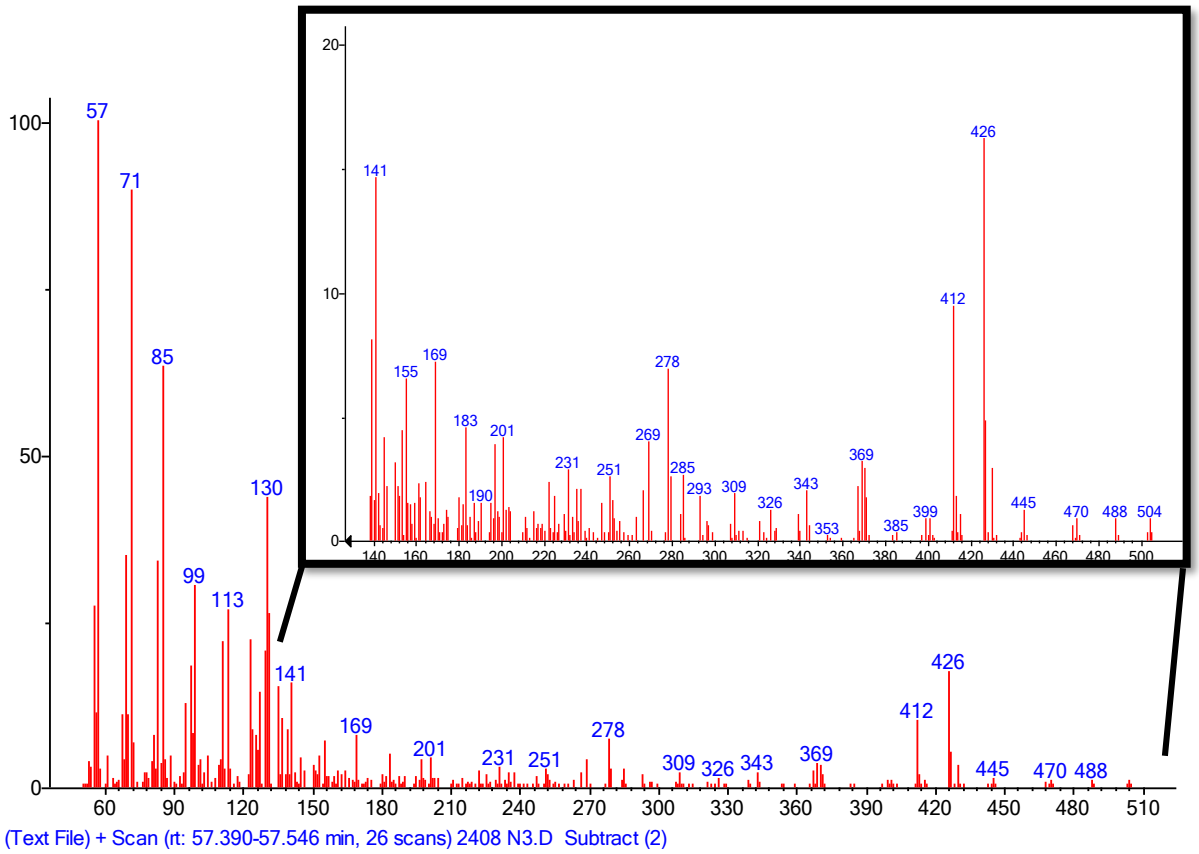

Figure 27 Mass spectra of the compound identified as archaeol. The background noise was removed.

Here, we only analyze archaeol (i.e. core lipid) and do not investigate the distribution and concentrations of phospholipid archaeol that was proposed as an indicator for living methanogen community or glycolipid-bound archaeol that characterizes fossilized and living communities (Lim et al., 2013). Archaeol was identified in GC-MS after its characteristic signature m/z=130 alongside a few other signatures (i.e. m/z=57, 169, 197, 278, 341, 369,

412, 426), after the mass spectra provided in Teixidor and Grimalt (1992). Its mass spectra after background noise subtraction is provided in Figure 27.

Several studies linked methanogenesis to shallow depths within peatland (i.e. depths between 20 and 50 cm, Zheng et al., 2014 and references therein). This, together with high rates of peat accumulation in these tropical sites allow the assumption that archaeol concentrations down-core are palaeosignals and do not represent present day active communities (i.e. ruling out continuous accumulation). However, as mentioned studies are restricted to temperate or boreal sites, where temperature, depth of roots, vegetation type and root exudates availability differs, cautions was exerted when interpreting results.

1.7.3. Hopanes

Hopanoids found in OM are mainly indicative of prokaryotes, and more exactly, they were confirmed in proterobacteria (α-, β-, ϒ-; Figure 28) and planctomycetales (Talbot et al., 2008a and references therein). Rohmer et al. (1984) reported hopanes in most cyanobacteria and obligate methylotrophs studied, in many chemoheterotrophs of gram-positive and -negative bacteria and in all purple non-sulphur bacteria. However, they were absent in purple and green sulphur bacteria and, at that time, they are reported absent from archaea (Rohmer et al., 1984; Fischer et al., 2005). They were compared in terms of function, structure and biosynthesis to sterols (i.e. steroids, such as cholesterol), characteristic to eukaryotes (Rohmer et al., 1979; Rohmer et al., 1984; Kannenberg and Poralla, 1999). However, more recent work demonstrated the presence of sterols in prokaryotes (Volkman, 2003; Pearson et al., 2003) and of both sterols and C_{30}-hopanoids in higher organisms such as ferns, lichens fungi (Ageta and Arai, 1983; Rohmer et al., 1992; Volkman, 2005 and references therein) and tropical tree resin (Ourisson et al., 1987), instructing for greater care when assigning biomarker sources.

Although the simplest hopanoid, diploptene, can be biosynthesized in the absence of oxygen, within the prokaryote division, it is mainly characteristic of aerobic bacteria (Rohmer et al., 1984; Ourisson et al., 1987; Rohmer et al., 1992; Kannenberg and Poralla, 1999). However, this assumption is not entirely true at present, as several studies reported the presence of hopanoids in anaerobic bacteria (i.e. Härtner et al., 2005; Sinninghe Damsté et al., 2004; Kool et al., 2014). Furthermore, others reported the presence of hopanoids in anaerobic and CH_4 producing and consuming environments (Elvert et al., 2000; Pancost et al., 2000) and

their presence was proven through cultures of facultative and obligate anaerobic bacteria (Sinninghe Damsté et al., 2004; Fischer et al., 2005; Rush et al., 2014; Kool et al., 2014). More recently, Kool et al. (2014) described the occurrence of bacteriohopanepolyols (BHP) in Candidatus "*Methylomirabilis oxyfera*", an anaerobic methanotroph with the genomic potential of producing 3Me-hopanoids. As hopanoids are also produced via diagenetic alteration of BHPs (Kool et al., 2014 and references therein; Ries-Kautt and Albrecht et al., 1989; Pancost et al., 2003), the hopanes present within sediments could come from diverse aerobic and anaerobic bacteria, with methylation of C_2 or C_3 not being restricted to aerobic methanotrophs, or even aerobic bacteria (Kool et al., 2014 and references therein).

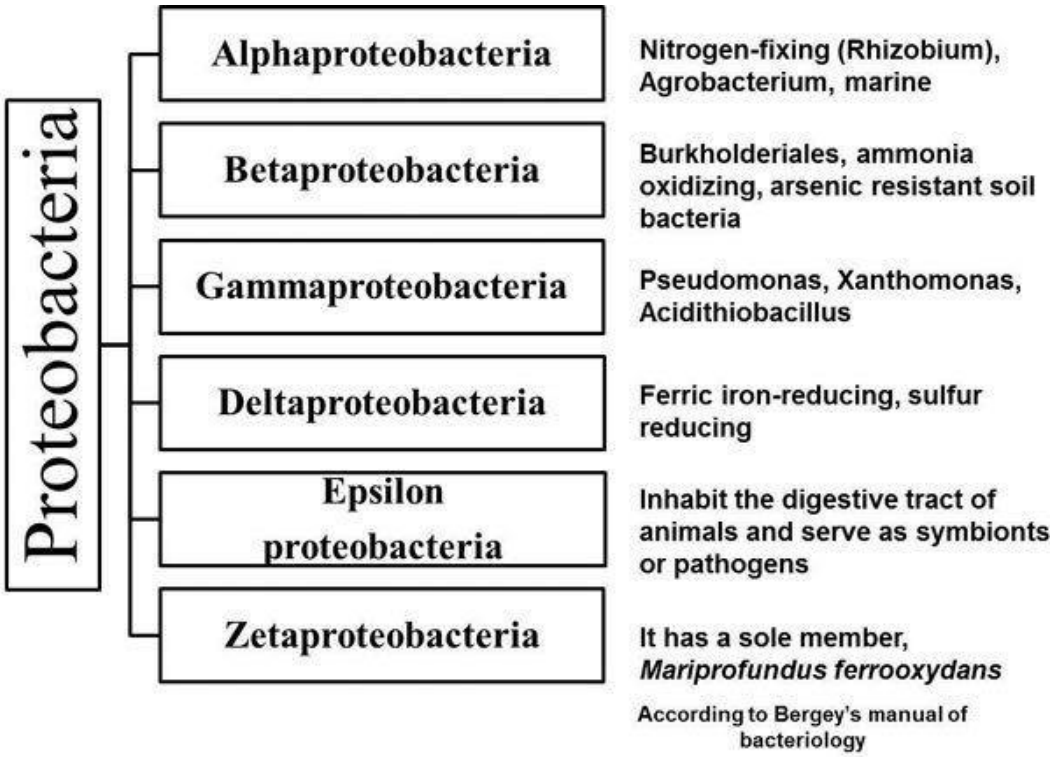

Figure 28 Subdivisions of Proterobacteria (Website 11).

In bacteria cell's membrane, hopanoids are hydrophobic and contained between phospholipids (Kannenberg and Poralla, 1999; Figure 29). Although their roles within divisions of bacteria are not completely understood (Saenz et al., 2015), they are known to be involved in membrane strengthening, organisation and fluidity, crucial for cell growth and functioning (Kannenberg and Poralla, 1999). One of their most researched function is that in membrane ordering. Hopanoids, like sterols, act as outer membrane regulators in bacteria, aiding its flexibility and stability among other functions. It has been demonstrated that in *Methylobacterium extorquens*, the main hopanoids' (diplopterol, 2-methyl-

diplopterol and BHPs) ordering function is proportional to their number or "loading" in the outer membrane (Saenz et al., 2015). This means that hopanoids have a regulating and ordering function dictated by their density in the outer membrane. Although research still needs to assess their wide range of roles across members of bacteria domain, considering parallels between sterols and hopanoids could be a first step in overcoming this knowledge gap.

Biological bacterial membranes have a bilayered structure created by the alignment of hydrophobic and hydrophilic ends of the phospholipids or glycolipids (Figure 29). The hydrophobic end of a phospholipid is orientated towards the interior of the cell's membrane while the hydrophilic polar heads, towards the exterior (i.e. extracellular space and cytosol-intracellular space) – in direct contact with the water phase, leading to low membrane permeability and forming a matrix for proteins arrangement within the membrane's walls (Caforio and Driessen, 2017). Furthermore, bacteria and eukarya kingdoms are characterized by phospholipids that contain straight fatty acids (i.e. saturated or unsaturated) that are bonded to a glycerophosphate structure (i.e. glycerol-3-phosphate, Figures 20 andf 29).

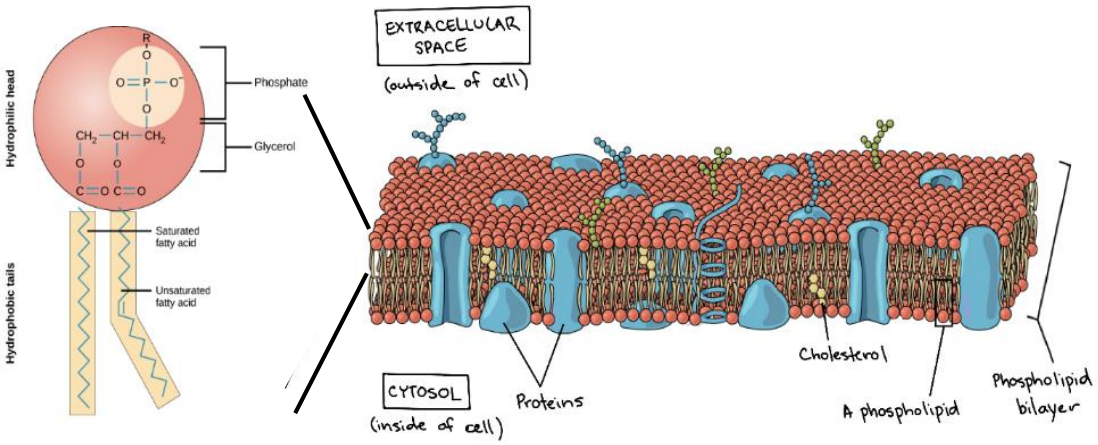

Figure 29 Simplified model of a phospholipid (left) and bilayer membrane structure (right). The "head" of the lipid is facing outward and is composed of hydrophilic polar end containing phosphate or glycerol radicals (i.e. phospolipids or glycerolipids) while the "tails"-is made of two hydrophobic non-polar ends which are saturated or unsaturated fatty acids. (Figure edited from Khan Academy, website 12). Notice the role and location of Cholesterol in membrane ordering in eukaryotes that is very similar to that of hopanoids in prokaryotes.

1.7.3.1. Nomenclature and stereochemistry

Hopanoids belong to the diverse group of isoprenoids, from where they get their structurally characterizing name, triterpenic isoprenoids or pentacyclic triterpenoids, a name indicating that they have 30 carbons and 5 rings in their backbone structure (Figures 30 and 31).

However, the overall chemical structure of a hopane can have anywhere between 27 and 35 carbons, yet it maintains its specific backbone configuration (Kannenberg and Poralla, 1999; Volkman, 2005 and references therein).

The biological-specific hopanoid stereochemistry is usually lost during diagenetic processes that lead to the generation of isomers, with different chemical geometries (Peters and Moldowan, 1991). Changes in the stereochemistry of hopanoid skeleton occur at C_{17}, C_{21} and C_{22}, the latter being involved in the R and S configurations (Peters et al., 2005; Figure 31). Numbers in front of carbon denote the location of the atom within the hopanoid structure. The α(H) and β(H) notations are related to the spatial geometry of the covalent bond between the carbon (i.e. in this case, at C_{17}, C_{21} and/or C_{22}, chirality centres) and hydrogen. The **α** geometry indicates that the bond between the C and H is orientated below the plane of the paper or the plane defined by the 3D projection of the molecule (i.e Figure 30) while the **β** geometry indicated the bond is orientated above the plane (Peters et al., 2005).

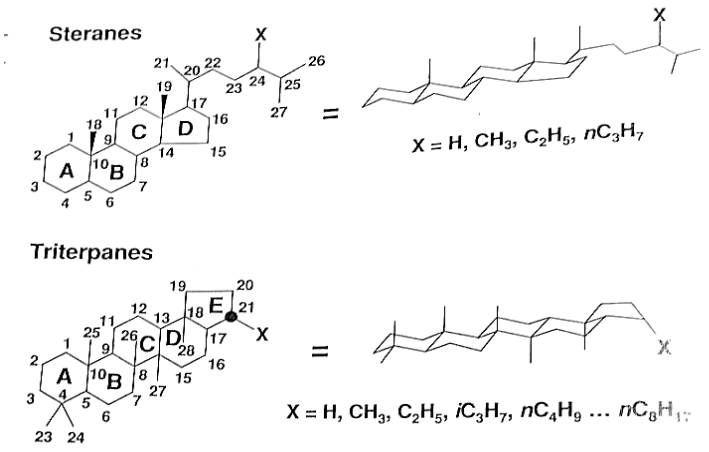

Figure 30 Sterane and triterpene condifuration (edited from Peters et al., 2005.)

Thus, for example, the abbreviation ββ in hopanoids will refer to the fact that the molecule has the hydrogen at location carbon-17 and carbon-21 above the plane of the paper. The αβ abbreviation refers to the fact that the first bonds at C_{17} is orientated below and the second bond at C_{21} above the paper plane.

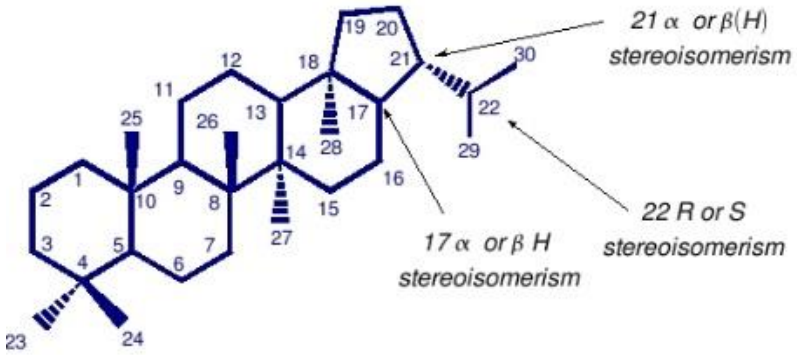

Figure 31 Carbon numbering in hopanes and positions of stereoisomerism (Website 13).

The R and S geometries refer to the geometry of the asymmetric C_{22} (Peters et al., 2005). The C_{22} epimerization with R and S spatial geometries can be established by ordering the substituents of C_{22}, an asymmetric carbon, in the order of their atomic masses, with the lowest one (i.e. a hydrogen atoms) away from the viewing point. The remaining constituents will be numbered, starting with the highest. An arrow from the 1st substituent (i.e. the one with the highest atomic mass) to the 2nd substituent, will indicated a R (i.e. clockwise) or S-geometry (i.e. counterclockwise).

The biological configuration corresponds to the ββ (i.e. 17β, 21β-hopanoid) stereoisomer of a hopane. In petroleum-forming settings/sedimentary rocks, with increase maturation, the ββ stereoisomer will be transformed into the thermally stable αβ configuration, with the highest concentrations in most samples or/and in the βα (Peters and Moldowan, 1991). In terrestrial and especially in peat-forming environments, the isomerisation was attributed to pH, hydrology or temperatures (Huang et al., 2015; Inglis et al., 2018). Due to the fact that the stereoisomers of a hopanoid will have the same chemical formula and characterizing ions, they can be distinguished on chromatograms based on their elution times and relative

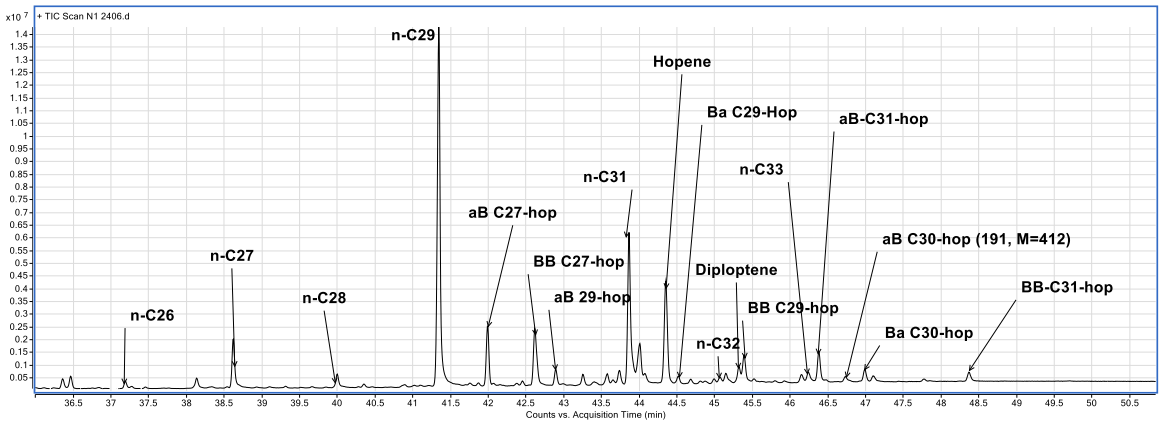

Figure 32 Identified hopanes and elution order in a peat sample from BVA. Notice elution time after n-C_{29} alkane.

concentrations. The αβ-S geometry will elute first, followed by the αβ-R (Huang et al., 2015). The βα (S, R) and ββ (S, R) will elute next, in this order (Figure 32).

1.7.3.2. Hopanoid biochemical formation

Hopanoids form through bacteria mediated cyclization of squalene via squalene-hopene cyclase (SHC) (Figure 33), a process similar to the cyclization of oxidosqualene that leads to the formation on sterols (see Kannenberg and Poralla, 1999 review for steps in squalene formation). Cyclization of squalene takes place in a single step with the disappearances of the 6 double bonds, closing of the 5 rings and formation of 9 stereo centres (Kannenberg and Poralla, 1999). The simplest hopanoids are **diploptene** (17α(H), 21β(H)-hop-22(29)-ene; or simply, hopane) and **diplopterol** (22-hydroxyhopane) that contain 30 carbons in their molecular structure. The complex or elongated hopanoids, known as bacteriohopanepolyols (BHPs) contain an extra side chain starting at C-30 (Figure 31). The geometry and structure of the side chain (i.e. Spencer-Jones et al., 2016) and the fact that the whole BHP molecule is recalcitrant in nature, allows them to be employed in phylogenetic identifications alongside diploptane and diplopterol, characterizing methanotrophs together with a wide diversity of bacteria (Rohmer et al., 1984; Talbot et al., 2008).

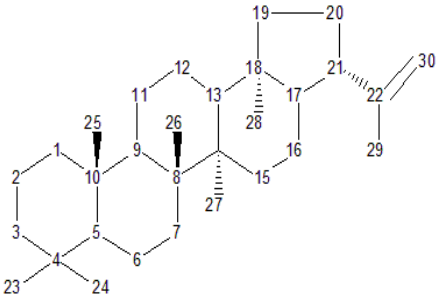

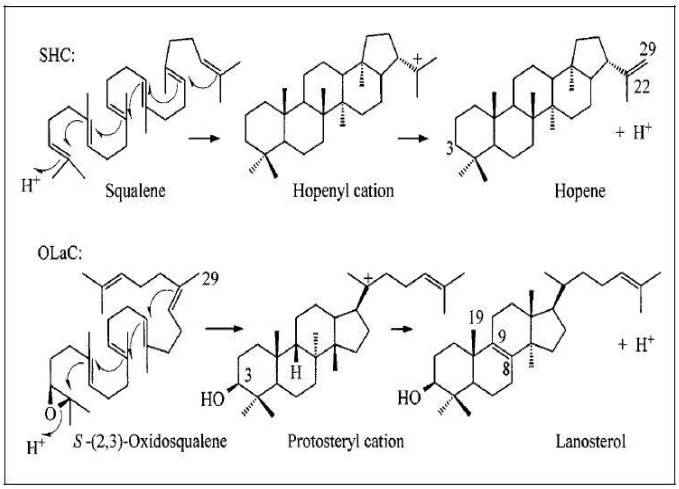

Figure 33 Squalene and oxidosqualene cyclization processes (Kannenberg and Poralla, 1999).

1.7.3.3. Diagenesis and stereochemical transformations

During early stage transformations, biological hopanoids (i.e. ββ structures) and BHPs can be modified via a series of chemical processes into shorter BHPs, hopanols or hopanes with 2 or 3 hydroxyl radicals, hopanes, hopenes or hopanoic acids (Figure 34; Peters and

Moldowan, 1991; Huang et al., 2015 and references therein). Their degradation products are used in palaeoenvironmental reconstructions (i.e geohopanoids) as they go expected stereochemical transformations (e.g. Huang et al., 2015; Inglis et al., 2018). Commonly, with increasing thermal maturation, the biological, ββ-hopanoid structures is transformed into αβ or βα more stable stereoisomers while hopanoids with more than 30 Carbons in their chemical structure, also experience stereochemical changes at C-22 (i.e. S or R; MacKenzie et al., 1980; Peters and Moldowan, 1991;).

Thermal maturation can be thus assessed via two main indices: a decrease in the $\frac{\alpha\beta+\beta\beta}{\beta\beta}$ ratio and an increase in the $\frac{22S}{22R+22S}$ ratio (MacKenzie et al., 1980; Inglis et al., 2018 and references therein).

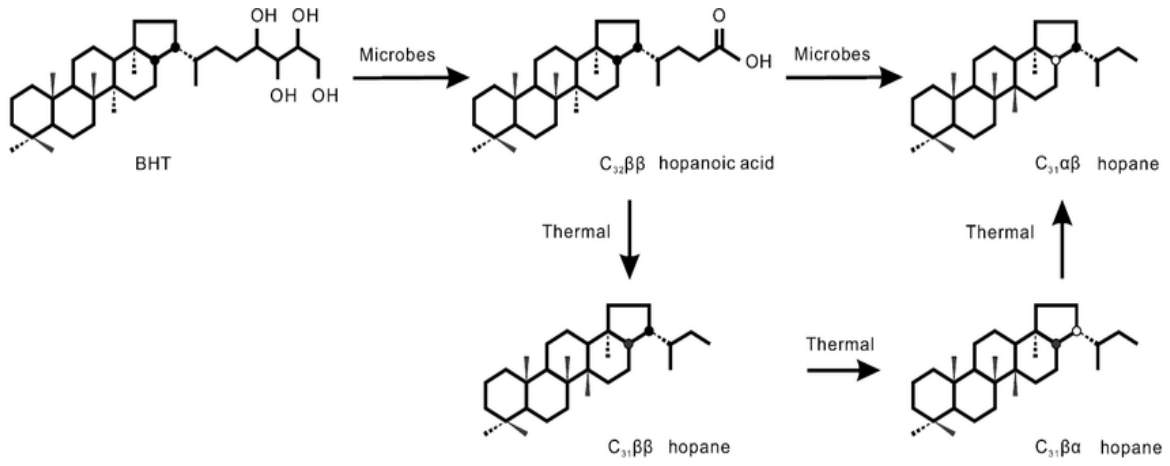

Figure 34 Proposed pathway of BHP degradation and hopane formation (Xie et al., 2014).

1.7.3.4. Hopanes – pH proxies

However, the dominant presence of αβ-22R-C_{31} hopanoid (i.e. homohopane) instead of ββ configuration in modern peat deposits (i.e. thermally imature), implies either that αβ-C_{31} hopane is produced in-situ by bacteria or that its precursors are highly sensible to environmental conditions (Pancost et al., 2003; Inglis et al., 2018). One of the main precursors of αβ-C_{31} hopane could be C_{32} hopanoic acid that undergoes decarboxylation (Inglis et al., 2018 for full-proposed pathway). Huang et al. (2015) proposed that pH, temperature and redox conditions can have a strong influence on the low-temperature isomerization of C_{31}-hopane in acidic peat deposits, however, at a global scale, Inglis et al.

(2018) confirmed only the strong correlation between $\frac{\alpha\beta+\beta\beta}{\beta\beta}$ ratio and pH and that low-temperature acid-catalysed isomerisation takes place in early stages of peat formation. Based on this relationship the following hopane pH-based proxy was proposed:

$$pH = 5.22 \times \left(C_{31}\ hopane\ \frac{\beta\beta}{\alpha\beta + \beta\beta}\right) + 3.11;$$

with a r^2=0.64 and RMSE=1.4, for n=94 (Inglis et al., 2018).

1.7.3.5. Diploptene

One of the first studies done on the chemical provenience and structure of **diploptene**, dates back to 1970 when it was named compound X by Gelpi et al (1970). Its molecular ion (i.e. molecular mass, m/z 410; Figure 35) and base peak (i.e. ion fragment with the highest intensity; m/z 191) were recorded probably for the first times on a mass spectrometer and found in three cyanophycean algae, *Chroococcus turgidus, Nostoc sp. and Lyngbya aestuarii*.

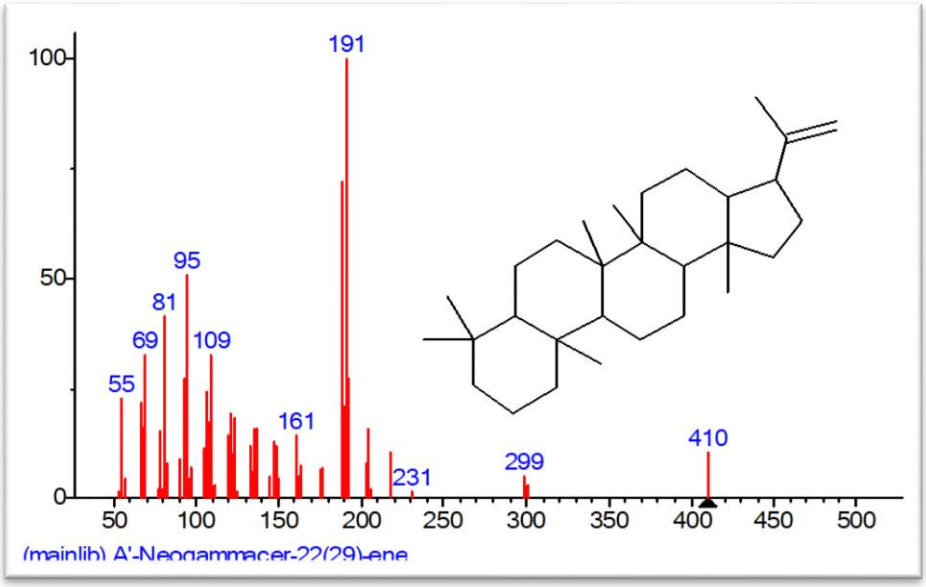

Figure 35 Mass spectra of diploptene as provided by NIST library.

As its base peak was specific to pentacyclic triterpenes, an attempt to define its chemical structure was made. In 1971, two other studies identified the same compound in two other bacteria: *Methylococcus capsulatus* (Bird et al., 1971) and *Bacillus acidocaldarius* (De Rosa

et al., 1971) and since, independent studies have reported the existence of diploptene in other bacteria classes (Rohmer et al., 1984).

Simple hopanoids (i.e. diploptene and diplopterol) can thus be major indicators of bacteria within the environment (Elvert et al., 2001 and references therein). Diploptene was detected in diverse environments (Figure 36), such as soils (Putkinen et al., 2009), lacustrine and lake sediments (Elvert et al., 2001; Davies et al., 2016), microbial mats, oceanic sediments and coastal environments (Prahl et al., 1992).

Table 1
$\delta^{13}C$-values of diploptene and diplopterol from the literature; numbers refer to Fig. 2.

	Diplopterol (‰)	Diploptene (‰)	Environmental setting	Approx. age	References
1.		−73	Cold seep sed.	Modern	Elvert et al. (2000)
2.		−66	Marine sed.	Late glacial	Yamada and Ishiwatari (1999)
3.	−68	−70 to −75	Surface sed.	Modern	Elvert and Niemann (2008)
4.	−70 to −60		Marine sed.	Modern to 45 kyr	Hinrichs et al. (2003)
5.	−40 to −30	−42 to −39	Water column	Modern	Schubert et al. (2006)
6.		−40 to −25	Marine sed.	Modern to 35 kyr	Uchida et al. (2004)
7.		−25 to −45	Marine sed.	Modern	Freeman et al. (1994)
8.		−48 to −39	River sed.	Modern	Prahl et al., 1992
9.		−26 to −32	Marine sed.	Modern	Yamada et al. (1997), Naraoka et al. (2000)

Figure 36 Isotopic signature of diploptene and diplopterol and environments in which they were found (Ménot and Bard, 2010).

1.7.3.6. Diplopterol

Diplopterol is made of a C_{30} hopanoid skeleton, with an additional hydroxyl radical at C_{22} (see Figure 31 for numbering). In several studies, diplopterol was reported alongside diploptene to trace aerobic CH_4 oxidation within different environments and samples (Figure 36) yet, as they are not exclusively synthesized by CH_4 oxidising bacteria (MOB, Pancost and Damsté, 2003), further proxies should be taken into consideration when assessing their provenience. Thus, the majority of studies proved this correlation (i.e. diploptene/diplopterol – MOB) by analysing their carbon isotopic signature; under the premise that if in CH_4-producing environments they are indicators of MOB, their $\delta^{13}C$ signature should be strongly negative, indicating thus CH_4 as the main or only carbon source (Ménot and Bard, 2010).

The process of squalene cyclization to form diplopterol lipids is characteristic to a wide variety of bacteria (Ourisson et al., 1987). Several studies have used diplopterol alongside diploptene as biomarkers to track aerobic CH_4 oxidation in aquatic setting (e.g. Hinrichs et al. 2003, Uchida et al., 2004; Ménot and Bard, 2010). A study conducted by Summons et al.

(1994) showed that in terms of ^{13}C depletion, squalene showed the least depleted signature, followed by diploptene and diplopterol.

Diplopterol was identified based on the base peak m/z=131 that corresponds to BSTFA silylate sidechain, and supplementary m/z=189, 191 that indicate the pentacyclic triterpenoid structure together with m/z=95, 149, 395 (Sessions et al., 2013; Elvert and Niemann, 2008). The mass chromatogram is provided below. As N3 fraction in which diplopterol eluted was derivitised using BSTFA compound (see Methods-Chapter 2), the SiC_3H_9 compound (mass=73.1891) attached to the –OH radical, with the m/z=501 indicating the whole mass of the compound (Figure 37).

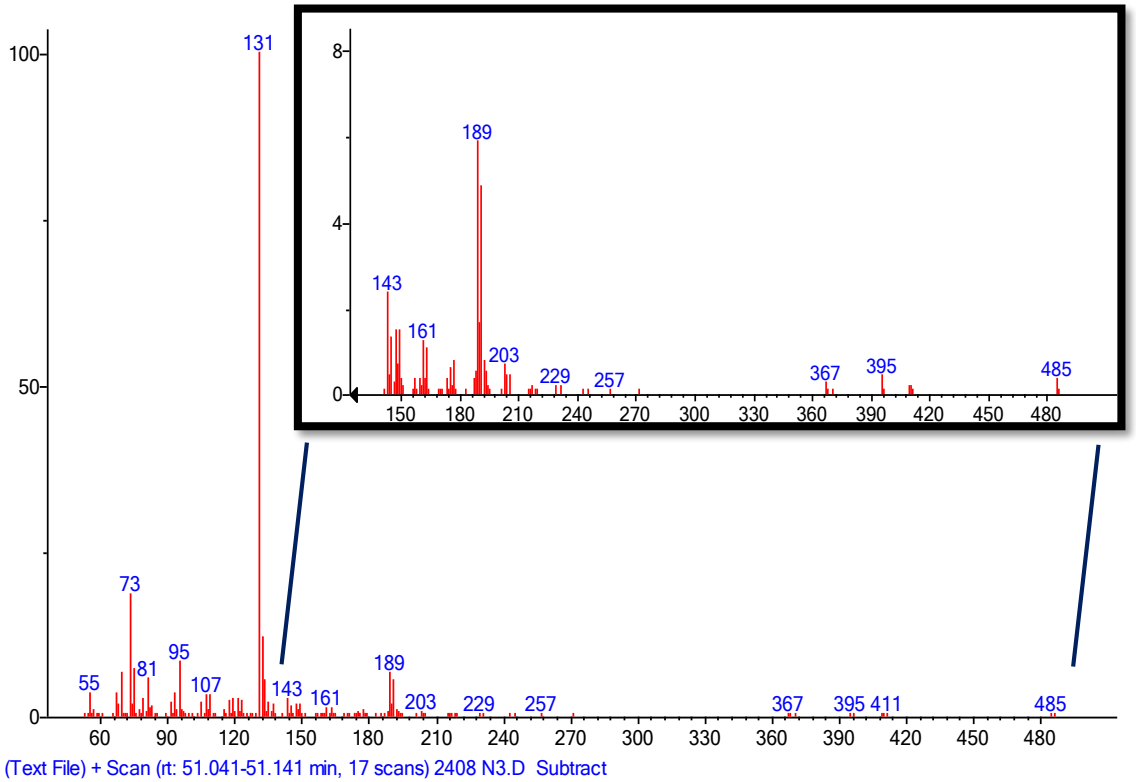

Figure 37 Mass spectrum of Diplopterol in analysed samples. Notice zoom-in box and relative intensities of m/z fragments taken on NIST library software.

1.7.3.7. Diploptene and diplopterol: biomarkers for methanotroph bacteria

Diploptene and diplopterol negative $\delta^{13}C$ values indicate CH_4 oxidation, and thus, bacterial CH_4 consumption (Ménot and Bard, 2010). In this context, more depleted $\delta^{13}C$ values suggest higher CH_4 oxidation and hence, higher CH_4 supply. As CH_4 is depleted in ^{13}C, similarly negative signatures will be showed by organism that incorporate CH_4 or consume MOBs, thus CH_4 can be traced through the food web (Pancost et al., 2000; Davies et al., 2016). In peatlands, diploptene's characteristic $\delta^{13}C$ signature, was recorded between −30‰

and −40‰ PDB, relatively enriched when associated to values of biogenic CH_4 (-60‰). However, other studies done in lacustrine environments (Naeher et al., 2014) have recorded values of $\delta^{13}C$ as low as -60‰, indicating biogenic CH_4 as the only carbon source (Figure 38).

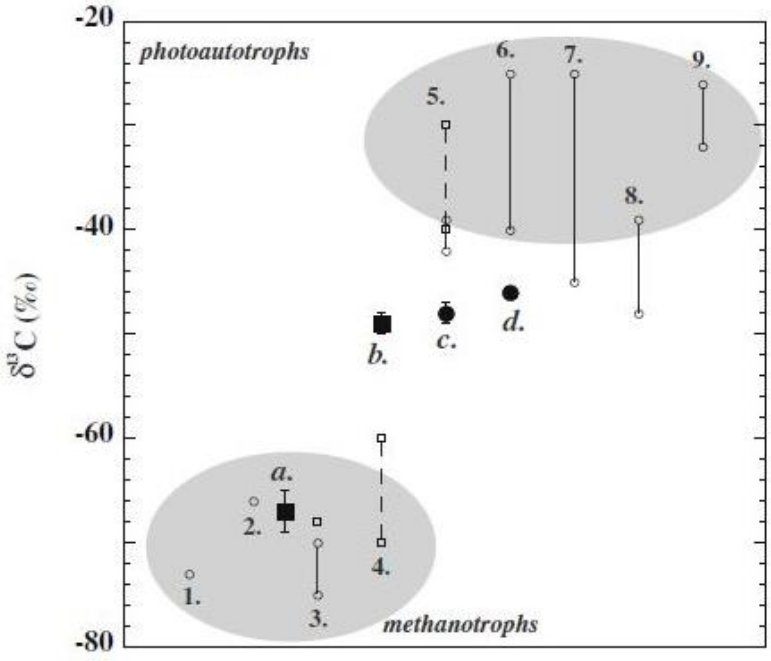

Figure 38 Carbon isotopic signaturess of diploptene and diploopterol (circles and squares, respectively) taken from Menot and Bard, 2001.

1.7.4. Fatty acids

Eukaryotes and bacteria membranes contains phospholipids that aid in their overall impermeability and functionality (Boschker and Middelburg, 2002). Phospholipids fatty acids (PLFA) contain a hydrophilic head, composed out of a phosphate or glycerol compounds (i.e. phospholipids or glycolipids, Zelles, 1999; Figure 30), orientated towards the water-phase (i.e. towards the extracellular space and cell space) and hydrophobic tails, composed of two fatty acids (FA i.e. acyl constituents; Kaneda, 1991) linked via ester bounds to the larger phospholipid. The structural differences in FA have implications on membrane fluidity and growth such that microbes with only straight FA in their membranes require monosaturated FA to regulate fluidity and growth, whereas membranes that contain branched FA are already suited for these functions (Kaneda et al., 1991 and references therein). Moreover, soil PLFAs with a chain length between 14 and 20 carbon atoms are typically considered to be of predominantly bacterial and fungal origin (Zelles, 1999) and

for certain bacteria groups, the use of FA can allow taxonomic identifications to genus level (Boschker and Middelburg, 2002).

Here, the main focus is on monosaturated FA, several of which were proposed and investigated in multiple studies regarding methanotroph populations across a wide range of environments (see short review Table 2). Although methods that analyse intact phospholipid exist (Sturt et al., 2004), only FA chains are analyzed in this study, reflecting thus the microbial community at the time of deposition. Moreover, although FA were methylated for GC analysis (i.e. obtaining Fatty Acids Methyl Esters, FAMEs, see Methods-Chapter 2), compounds discussed in this section were converted to FA, reflecting their true molecular carbon number. Furthermore, unsaturated FA nomenclature will follow the one proposed by Frostegård et al. (1993), where the unsaturation is counted from the methyl end (aliphatic or ω end). The structure of C19:1ω9 FA in both trans- and cis- configurations (Figure 39) is provided for reference. For saturated FA, iso- indicates the position of a methyl branch at the 2nd last C from the aliphatic end while anteiso- indicated the position of a methyl branch at the 3rd last C. Saturated FA have the notation Cx:Y, implying a straight chain (i.e. x-number of carbons and Y-number of double bonds) with varying number of carbons.

Saturated and polyunsaturated FA are also included in this study however, their distribution is only used to infer relative changes in the environment and microbial structure (e.g. White et al., 1979; Nichols et al., 1985) since they are known to be subject to environmental shifts and stress (Guckert et al., 1986; Kieft et al., 1994). In terms of palaeoenvironment reconstructions, long-chain FA with and even/odd preference indicate input from epicuticular leaf waxes (Eglington and Hamilton, 1967; Volkman, 2006) and can be transformed through hydrogenation to n-alkanes with and even/odd preference in reducing environments (Welte and Ebhardt, 1968; Welte and Waples, 1973). Even carbon numbered FA with 12 to 18 carbons are important constituents in aquatic plants (Peters et al., 2005) and microbial FA have typically between 12-24 carbons, with the most common ones between 14-20 carbons (Denich et al., 2003).

More specific FA (Table 2) such as C15:0 has been used in studies of sulphate reducing bacteria that is also involved in anaerobic CH_4 oxidation, iC15:0 and iC17:0 are indicators of gram-positive bacteria while C18:0 and C17:0 do not occur in any specific bacteria. Other studies showed that saturated (i.e. C16:0, C17:0, C18:0 and C19:0; see review Trotsenko and Khmelenina, 2005) and polyunsaturated (C18:2ω7c,12c and C18:2ω6c,12c; Bodelier et al., 2009) FA were suggested to represent methylotroph bacteria (e.g. Nichols et al., 1985) and their distribution and variations can be used together with biomarkers used for

palaeoenvironmental assessments and GDGTs to discuss changes in CO_2 and CH_4 production and consumption. Higher levels of unsaturation are found in green algae (i.e. C18:3ω3), diatoms (i.e. C16:2ω4, C20:5ω3, C22:6ω3) (Boschker and Middelburg, 2002) and thus, in eukaryotes.

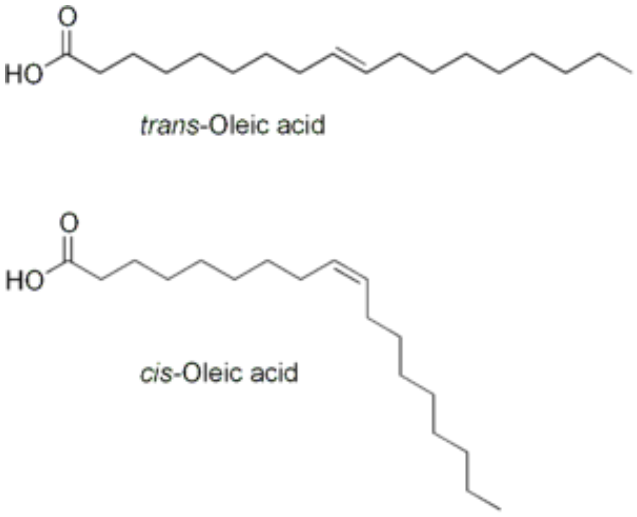

Figure 39 Trans- and cis- structures in a fatty acid. Notice bend in the FA chain in cis- structure (Website 14).

In lake environments, unsaturated FA have been noticed to drastically decrease after the first 8 cm of sediments, due to their relatively less stable configuration that makes them susceptible to microbial reworking (Meyer et al., 2003 and references therein; Cranwell, 1981 and references therein).

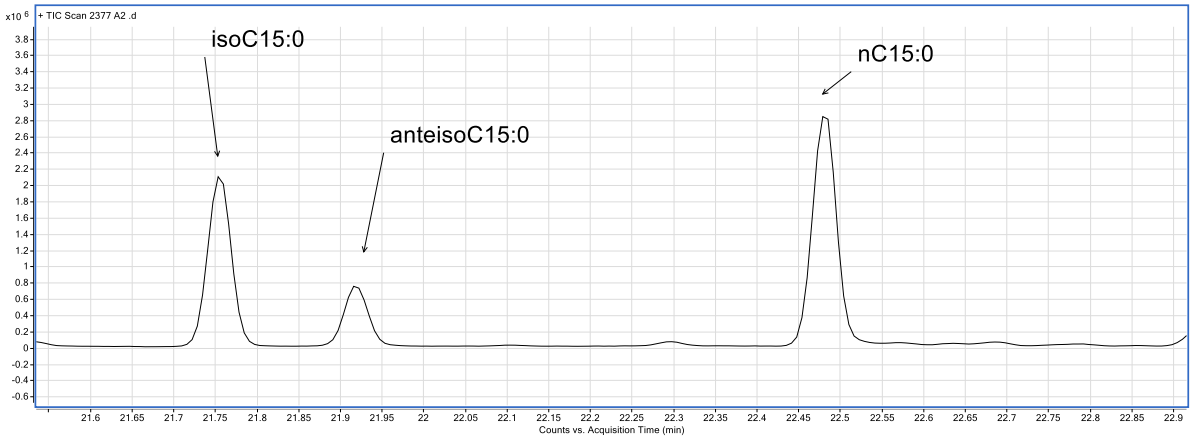

Figure 40 Elution order of iso- and anteiso C15:0 in a surface peat sample from QT.

FA with even-carbon number predominated in terms of concentrations. Identification of FA was made based on mass (M+) in GC-MS and identification of iso- and anteiso- based on characteristic m/z: m/z specific for M+ -43 dominated for iso- whereas m/z specific for M+-57 dominated in anteiso-. Elution order was: iso-, anteiso-, saturated FA as in other studies

investigating FA (e.g. Heindel et al., 2012; Figure 40). As one of the objectives of this project is to provide information on the methane cycle, monosaturated fatty acids with 16 and 18 carbons were investigated in all three peatlands.

1.7.5. Summary of used biomarkers and proxies

A summary is provided below (Table 2) for the quick identification of biomarkers, proxies and their applications in this research. However, as they are employed in a tropical wetland setting, their applications might differ for other environments or research questions.

Table 2 containing a summary of the biomarkers and proxies used in this study, together with their functions and references,

Proxy	Equation	Indications	References
	n-alkanes		
Carbon preference index (CPI)	$\frac{1}{2}(\frac{C_{25}+C_{27}+C_{29}+C_{31}}{C_{24}+C_{26}+C_{28}+C_{30}}+\frac{C_{25}+C_{27}+C_{29}+C_{31}}{C_{26}+C_{28}+C_{30}+C_{32}})$	CPI ↑ → better preserved terrestrial OM CPI ↓ → microbial reworking or more labile OM sources	Bray and Evans, 1961; Baker et al., 2016; Andersson and Meyers, 2012
Paquatic (P_{aq})	$\frac{C_{23}+C_{25}}{C_{23}+C_{25}+C_{29}+C_{31}}$	Aquatic (mid-chain n-alkanes) vs terrestrial OM input (long-chain n-alkanes). Paq<0.1 → terrestrial OM; Paq= 0.1 – 0.4 →emergent macrophytes; Paq>0.4 → submerged and floating vegetation.	Ficken et al., 2000; Baker et al., 2016 and references therein
Pwax	$\frac{C_{27}+C_{29}+C_{31}}{C_{23}+C_{25}+C_{27}+C_{29}+C_{31}}$	Proxy to distinguish between higher plant species input; relatively low Pwax-humid period; relatively higher Pwax-drier period;	Pu et al., 2011; Baker et al., 2016 and references therein
Average chain length	$(\Sigma[C_n]\times n)/\Sigma[C_n]$ *[C_n]-concentration of the n-alkanes with n atoms, n=23 – 33*	Grass vs woody vegetation; Latitude (climate) proxy; Relative T°C proxy; Used in relation with other biomarkers and proxies.	Cranwell, 1973; Peltzer and Gagosian, 1989; Poynter et al., 1989; Calvo et al., 2004
Pristane – Phytane ratio	*[Pr]/[Ph]*	oxygen levels in their environment of formation; Pr/Ph > 1 suboxic to oxic; Pr/Ph<1 anoxic.	Brooks et al., 1969; Didyk et al., 1978;Gola et al., 2013
	isoGDGTs		
Caldarchaeol GDGT-0	*[GDGT-0]*	methanogenic euryarchaea	Zheng et al.,2015; Schouten et al., 2013 and references therein
Crenarchaeol	*[Crenarchaeol]*	archaea-mediated oxidation of ammonia	Zheng et al., 2015
GDGTs 1-4	*[isoGDGTn]* *Concentrations of GDGTn, n=1 – 4*	methanotrophic archaea	Schouten et al., 2000; Schouten et al., 2013 and references therein
GDGTs 5-7	*[isoGDGTn]* *Concentrations of GDGTn, n=5 – 7*	in tropical ombrotrophic peatlands: restricted by pH< 5.1 temperatures>19.5°C; ↑ when constant pH and increasing T°C	Naafs et al., 2018 b

Methane index (MI)	$\frac{[GDGT1]+[GDGT2]+[GDGT3]}{[GDGT1]+[GDGT2]+[GDGT3]+[Cren]+[Cren_{iso}]}$	MI<0.5 → CH_4 oxidation	Zhang et al., 2011; Dirghangi et al. (2013)
Cald/Cren	*[Caldarchaeol]/[Crenarchaeol]*	Cald/Cren>20 input from methanogenic archaea in terrestrial and anoxic environments	Dirghangi et al., 2013 and references therein
	brGDGTs		
brGDGTs	*[brGDGTn]* *Concentrations of GDGTn, with n= Ia, Ib, Ic, IIa, IIIa etc.*	anaerobic mesophilic bacteria(Acidobacteria); lake and soil environments; competing with archaea in anaerobic settings	Schouten et al., 2013
MBT'_{5me}	$\frac{[Ia+Ib+Ic]}{[Ia+Ib+Ic+IIa+IIb+IIc+IIIa]}$	Degree of methylation; MBT'$_{5me}$ positively correlated with T°C	Naafs et al., 2017a
CBT'_{peat}	$log\frac{Ia+IIa'+IIb+IIb'+IIIa'}{Ia+IIa+IIIa}$	Degree of cyclisation; CBT'$_{peat}$ positively correlated with pH	Naafs et al., 2017a
pH_{peat}	$2.49\times CBT_{peat}+8.07$ *RMSE=0.8*	pH proxy in peatlands	Naafs et al., 2017a
$MAAT_{peat}$(℃)	$=52.18\times MBT'_{5me}-23.05$ *RMSE=4.7℃*	T°C proxy in peatlands	Naafs et al., 2017a
MBT_{soil}	$\frac{[Ia+Ib+Ic]}{[Ia+Ib+Ic]+[II+IIb+IIc]+[IIIa+IIIb+IIIc}$		Weijers et al., 2007b
CBT_{soil}	$-log\left(\frac{[Ib+IIb]}{[Ia+IIa]}\right)\ (CBT\pm 0.3)$		Weijers et al., 2007b
MBT_{soil}	$0.122+0.187\times CBT+0.020*MAT$	MAT=mean annual T°C proxy for soil	Weijers et al., 2007b
CBT_{soil}	$3.33-0.38\times pH$ *RMSE pH=0.1*	pH proxy for soil	Weijers et al., 2007b
Archaeol	*[Archaeol]*	Component of methanogens and methanotrophic archaea membranes	Koga et al., 1998b; Niemann and Elvert, 2008; Pancost et al., 2011; Zheng et al., 2014
	Hopanes		
Diploptene **Diplopterol**	*[Diploptene]* *[Diplopterol]*	30-carbon hopanoid found in the membranes of bacteria; aerobic settings	Ourisson et al., 1987; Rohmer et al., 1992; Kannenberg and Poralla, 1999 Rohmer et al. 1984; Fischer et al., 2005;
pH$_{(hop)}$	$5.22\times\left(C_{31}\ hopane\ \frac{\beta\beta}{\alpha\beta+\beta\beta}\right)+3.11$ *RMSE=1.4*	pH proxy based on C_{31} hopane	Inglis et al., 2018
	Fatty acids and strains		
	Potential type I methanotrophs		
C16:1ω5 (t)		-	Bodelier et al., 2009
C16:1ω8c		-	Bodelier et al., 2009; Bowman et al., 1993
C16:1ω7c		Methylocella silvestris	Zigah et al., 2015 (and ref therein)
C16:1ω6c		Methylomonas	Taipale et al., 2009
C18:1ω8c		Methylocystis strain	Dedysh et al., 2007
C14:0, C16:0		ubiquitous	Bodelier et al., 2009; Mills et al., 2013; Bowman et al., 1991;1993

C16:1ω5c		(also found in fungi, Olsson, 1999)	Nichols et al., 1987
	Potential type II methanotrophs		
C16:1ω8c			Bowman et al., 1991
C16:1ω7c			Bowman et al., 1993
C18:1ω8c			Bodelier et al., 2009; Bowman et al., 1991
C18:1ω7c			Bodelier et al., 2009, Zigah et al., 2015; Maxfield et al., 2006
C18:1ω9			Maxfield et al., 2006
C18:1ω9c			Bowman et al., 1991
Ammonia-oxidising bacteria			
C16:1ω7c C16:1			Bedard and Knowles, 1989
Gram positive bacteria			
iC14:0, aC15:0,iC15:0, aC17:0 iC17:0		Micrococcus sp. Tetraspaera sp. Actinobacterium sp.	Taipale et al., 2009
iC16:0,iC18:0			Frostegard et al., 1993b Morgan and Winstanley, 1997
brC14:0, brC15:0, brC16:0			
Gram negative bacteria			
18:1ω7c			Taipale et al., 2009
Other			
10Me16:0		Desulfobacter (bacteria) Actinomycetale	Rajendran et al., 1993 and ref therein; Frostegard et al., 1993b

1.8. Importance, aims and previous research

The importance of understanding peatlands in Pastaza-Marañón foreland basin (PMFB), northern Peru, can be discussed at different geographical levels and time scales. Thus, on a local and regional scale, peat here forms under different hydrological regimes and vegetation types (Lähteenoja et al., 2009a, b; Lähteenoja and Page, 2011; Roucoux et al., 2013; Kelly et al., 2017). The samples available for this study were collected from three different vegetation types, from both the surface and depth, allowing us not only to understand how CH_4 effluxes varied in the past, but also how they might vary in the future under different climate change scenarios.

At a latitudinal scale, these peatlands form in a tropical climate, which means in permanently humid and warm conditions with high water tables. Part of the organic matter that forms in these settings is not oxidized as it is stored in the anoxic layer. Thus, these peatlands act as an important carbon sinks that need to be conserved.

Finally, on the global scale we are interested in atmospheric CO_2 and CH_4 budgets. Peru has the 4th largest area of peatlands in the tropics (Hergoualc'h et al., 2018) and furthermore, PMFB within Peru was linked to high tropospheric CH_4 concentrations (del Aguila-Pasquel, 2017 and references therein). The high potential of CH_4 effluxes from waterlogged peatlands and the frequency of these conditions in PMFB (Lähteenoja and Page, 2011; Lähteenoja et al., 2012), led to the hypothesis that PMFB represents an important potential source of greenhouse gases globally.

A first rough approximate of the CH_4 emissions from the Neotropics is between 4.9 and 8.6% of the present 645 Tg CH_4/year global total (Winton et al., 2017 and references therein). From the IPCC's 5th Assessment Report (IPCC, 2014) we know that CH_4 has a global warming potential 28 times higher than that of CO_2 over a period of 100 years. Since these peatlands are new components on the CH_4 map, it means that present day CH_4 budgets are underestimated and that there is an immediate need to understand processes that led to CH_4 (and CO_2) production and potential for consumption in the past. Furthermore, the PMFB peatlands are regarded as one of the largest intact tropical peatlands (Roucoux et al., 2017), however, a recently published study (Hergoualc'h et al., 2018) showed that modern land-use practices can have immediate impacts on carbon sequestration in these vulnerable ecosystems. For example, in areas of degraded *M. flexuosa* swamps, one of the most common peatland types in PMFB, there was a shift from palm swamp vegetation to forests

(i.e. woody-vegetation; Hergoualc'h et al., 2018) that caused a reduction in carbon sequestration between 11% and 17%, depending on whether the area was characterized as medium or severely degraded, respectively (Hergoualc'h et al., 2018). Thus, by understanding how these peatlands cope with present day anthropogenic stresses and how they functioned in the past, we can provide data for their future successful conservation.

Since their discovery (Lähteenoja et al., 2009a), there have been numerous studies in the area. We now have a good approximation of the area covered by peatlands through remote sensing, their carbon pool size (Draper et al., 2014) and local past changes in vegetation and hydrology from pollen analysis (Roucoux et al., 2013; Kelly et al., 2017). Radiocarbon dates provided information on when peat started to accumulate at various sites in the region (Lähteenoja et al., 2009a, b; Roucoux et al., 2013; Kelly et al., 2017), and from that time onward, peat accumulation rates were calculated and breaks in deposition assessed (see for example Kelly et al., 2017). Further studies included nutrient and geochemical analysis (Lähteenoja et al., 2009a; Lähteenoja and Page, 2011; Lawson et al., 2014), hydraulic conductivity of peat at various locations and depths (Kelly et al., 2014), present day and past water table variations (Teh et al., 2017; Swindles et al., 2014), ecohydrology of peatlands (Swindles et al., 2014) and pore water dissolved organic carbon (DOC) (del Aguila-Pasquel, 2017). Studies published during this research also produced degradation maps via remote sensing (Hergoualc'h et al., 2018), looked at the ecology, harvesting practices, economy management and spatial distribution of *M. flexuosa* (Virapongse et al., 2017 and references therein), at the floristic diversity within PMFB (Draper et al., 2018) and at the lacustrine records and human settelments in the area (Kelly et al., 2018). Most importantly, there are also recently published studies on quantifications of the CH_4 efflux during the dry and wet seasons (Teh et al., 2017; del Aguila-Pasquel, 2017; Winton et al., 2017) in peatlands characterized by different vegetation types, on pneumatophore density, their effect on CH_4 fluxes within PMFB, on the relationship between degradation (del Aguila-Pasquel, 2017; van Lent et al., 2018), pH and carbon quality (Winton et al., 2017) and CH_4 effluxes from the basin. All of the latest studies confirm the importance of peatlands in these region as important and dynamic ecosystems that store vast amounts of carbon.

It is important to realize that since the confirmation of peat in PMFB (less than 10 years ago from the first published research; Lähteenoja et al., 2009a, b), although only restricted areas have been investigated, a vast suite of physical and qualitative parameters are now known. Furthermore, with regards to the CH_4 cycle, Lawson et al. (2014) highlighted the importance of the hydrological regime, water table depth fluctuations and high, year-round temperatures

in understanding the role of the microbial community and its potential impact on carbon storage and organic matter accumulation within PMFB. Del Aguila-Pasquel (2017) provided a rough annual CH_4 estimate and commented on the importance of identification of CH_4 sources and pathways within the basin and Winton et al. (2017) argued on the "especially urgent" nature of research regarding the CH_4 cycle. However, little to no research has been conducted on the CH_4 variations through time as a major component of the past and present carbon cycle and only a few comments have been made on the microbial communities from the aerobic and anaerobic parts of a peatland and how they (might) react to local and climatic changes (see however Naafs et al., 2017a, 2018; Inglis et al., 2018).

The main objectives of our study are to assess the employability of a suite of biomarkers in tracking vegetation and hydrology changes, as well as CH_4 production and efflux in PMFB over time, as a function of various environmental parameters (i.e. water table depth, temperature, vegetation, nutrient content, dissolved oxygen, pH etc.). Given this important gap in knowledge, the successful conservation of the remaining tropical peatlands, in the light of long-term consequences arising from the degradation of SE Asia peatlands, is crucial and an improved understanding of the processes that govern organic matter accumulation and decomposition at a microbial scale is needed. Based on these, further aims and proposed methods that arise from the main objectives are as follows:

1) Evaluate the potential of a suite of biomarkers present in surface and core samples to accurately depict present-day and past environmental and climate changes assessed primarily through pollen-records and geochemical analysis in order to test the large scale applicability of biomarkers within these environments;
2) Understand and describe changes in biomarkers ascribed to methanogen (i.e. archaeol, isoGDGT-0) and methanotroph (i.e. hopanes, fatty acids, isoGDGT) communities with depth and relate them to various changes in the palaeoenvironment;
3) Observe any correlations between climate, vegetation types, inferred CH_4 production and consumption potential and changes in the concentrations of biomarkers indicative of methanotrophs;
4) Assess the changes in concentration and potential of diploptene, a bacteria biosynthesised biomarker, to inferred fluctuations in CH_4;
5) Recommend further biomarker-related steps for additional research and formulate questions that still need to be answered.

2. Methods

This chapter describes the methods, instruments, chemical techniques and software used to extract and analyse 33 samples available for this Master by Research project. References are provided where the complete process is not described. All glassware used was soaked in Decon solution, cleaned, dried and combusted in the furnace for 6h at 450°C to prevent any contamination. A summary of the complete process is found below (Figure 41).

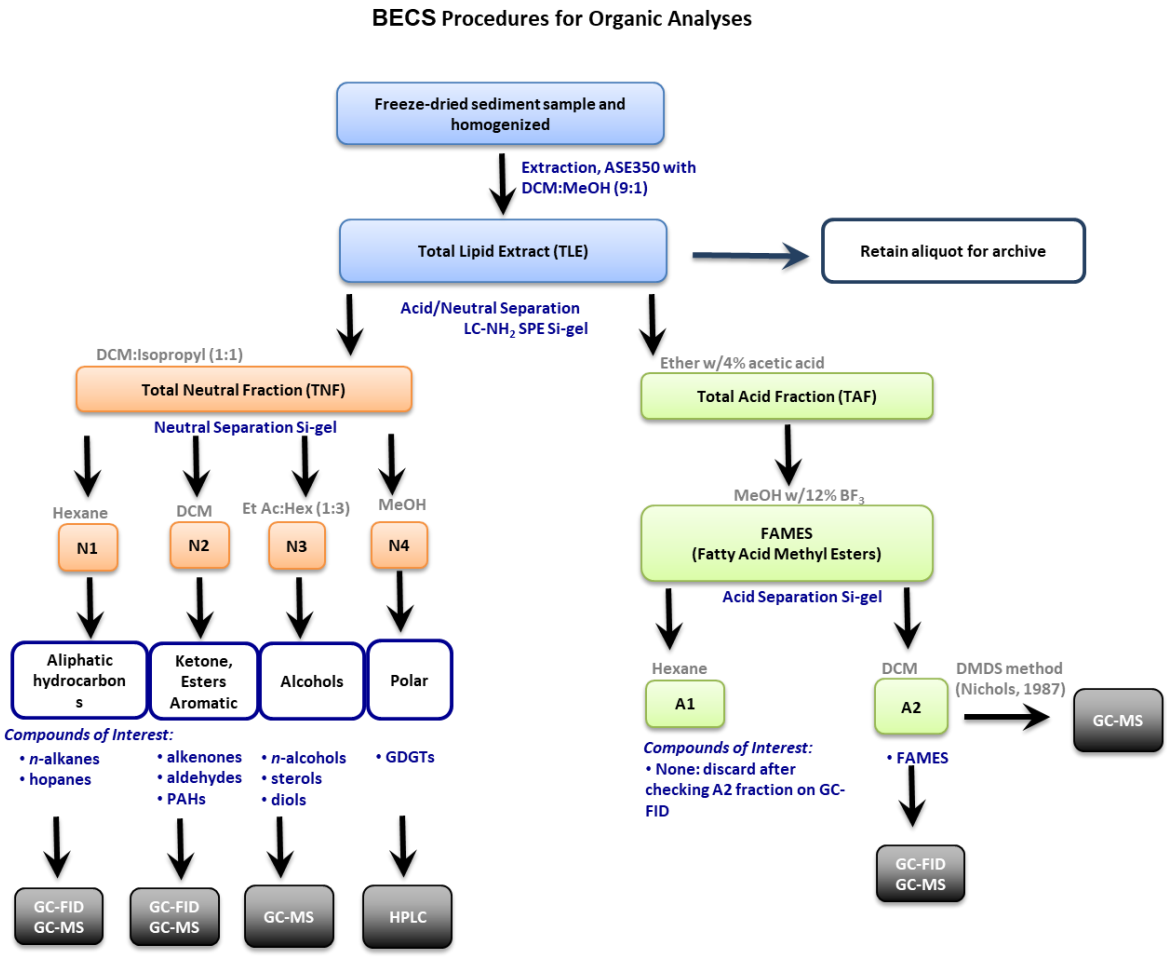

Figure 41 BECS Procedures for Organic Analyses extraction and processing. Steps are further explained in the following sections. Black squares have been added to the original diagram to indicate final analysis processes and GC instruments used for data acquisition. Although N2 fractions and part of the N3 components have not been included in the report, they have been analysed for further processing. Black boxes represent the final analysis method.

2.1. Peat sample collection and core collection

Peat core and surface samples were collected in the summer of 2010 by a research group, Dr Katherine Roucoux included, from the University of St Andrews. The three available cores (Quistococha, Buena Vista, San Jorge; Figure 43) were acquired using a stainless-steel Russian-type corer and were shipped under a temperature of 4°C (see Lawson et al., 2014) to limit vegetation and microbial further development.

Half-hectare forest census plots in each peatland were divided into 10 (20m x 20m) squares (A type) and 5 rectangles of (10m x 20m - B type) (i.e. in order to cover the remaining area). The corners of each A type squares and the centre part (5 sample points in total/square) were sampled at the surface and the material combined (as illustrated in Figure 42). For this research project, surface samples belonged to type A squares 1, 3, 5, 7 and 9 (i.e. in Figure 42, sample 2377-square 1; sample 2379-square 5 and sample 2381-square 9). The cores at each site were collected between squares type A 3 and 8 (slightly more in subplot 3 in SJO; see exact grid location in Figure 43) (Dr Katherine Roucoux; private correspondence). The cores were divided into samples at a resolution of 8 cm and 33 samples were wrapped in plastic foil, transferred to plastic bags and sent to University of Glasgow, where they were stored into a freezer at a temperature below 0°C.

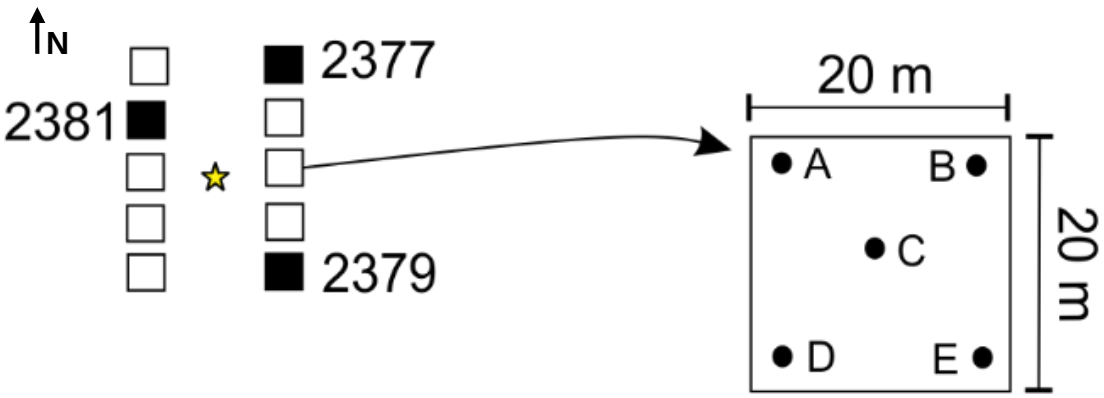

Figure 42 Sampling strategy for surface sample collection illustrating only type A squares at QT (not to scale). For this research, samples 1, 3, 5, 7 and 9 were provided. Their corresponded on the above figure is as follows: sample 2377-square 1; sample 2379-square 5 and sample 2381-square 9. Notice the sampling strategy in a 20m x 20m square. The corners of the square and centre were sampled and combined, making one analysed sample in this study representative of a 400 m^2 area. The star represents the location of the core, that can be correlated with Figure 43.

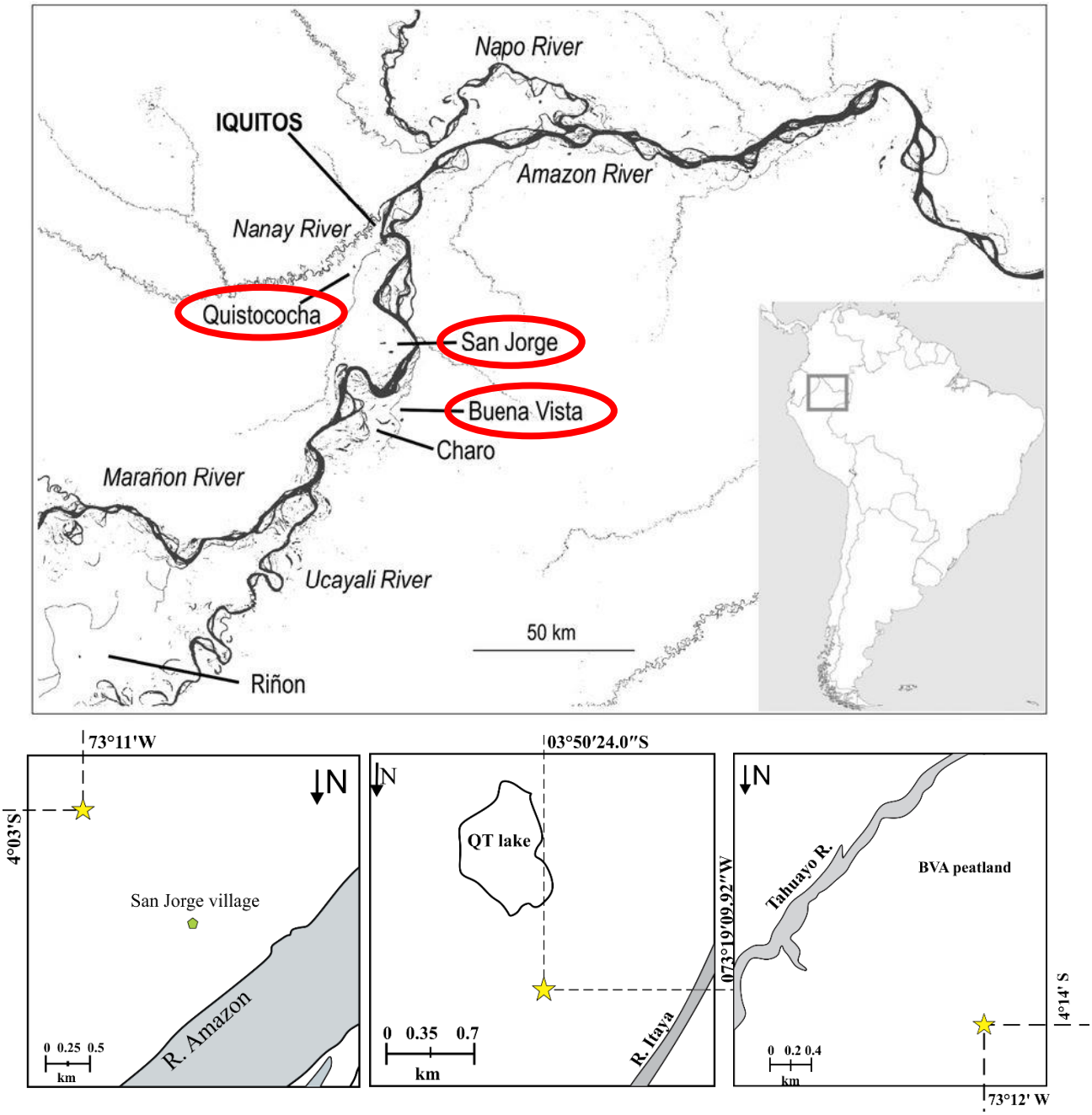

Figure 43 Overview over Pastaza-Marañón Foreland Basin. Top figure represents the location of the three peatlands in relationship with the Amazon river and each other (Lähteenoja, 2009b). The bottom figures represent zoom-ins on areas from which the cores were collected (i.e. yellow star). Notice the exact grid location marked on margins for SJO, QT and BVA peatlands (left to right) and major geomorphologic features in the area. Maps have been digitized from aerial field maps used in during field work by Dr Outi Lahteenoja and Dr Katherine Roucoux.

2.2. Freeze-drying and homogenization

Rubber gloves were used to unwrap the samples. Gloves were cleaned between each sample and changed between surface and cores samples from each location to limit contamination.

A freeze-drying technique was used to remove the water content from the frozen samples via sublimation. Samples were transferred from a freezer into an Alpha 1-2 LD-Christ freeze-drier. The opening of the plastic bags was previously covered with tissue held in place with rubber bands to prevent material from escaping under vacuum. The base temperature was -50°C and pressure dropped to 0.070 mbars to allow water removal via sublimation. Samples were kept in the freeze-drier between 36h and 48h.

Dried samples where then homogenized using a pestle and mortar. Twigs and thick, woody plant roots that could not be broken down were removed at this point to a plastic labelled vial. The pestle and mortar were rinsed with DCM after each sample.

2.3. Accelerate Solvent Extraction (ASE)

The ASE 350 (Agilent) was used to extract the organic content from each of the samples. For each sample, two ASE caps and one body were used. The cell's caps were lined with pre-combusted glass fibre filters that prevented sample material to block the cell or pass through into collection vials. One cap and a body were hand tightened, their weight measured, and samples were loaded via a metallic funnel into pre-cleaned ASE cells. Approximatively 0.5 g of each sample was added into a pre-cleaned ASE cell via a metallic funnel and the exact mass determined via subtraction (i.e. masses ASEcap+ASEbody+Sample – ASEcap+ ASEbody) and recorded. The remaining space in the ASE body was filled with combusted sand and the 2nd cap was attached. Two (or three) cells containing only combusted sand (i.e. blanks) were loaded at the beginning, (middle) and end of each run to assure that no contamination from the ASE occurred. Blanks were treated as normal samples and transferred as TLE in GC-2ml-vials and analysed on GC-FID. The ASE cells containing samples where then loaded into the ASE tray with 60 ml vials lined with aluminium foil for collection in corresponding places and the "rinse" function was performed in triplicate.

2.4. Total Lipid Extract (TLE)

TLE was collected in 60 ml vials and gently dried under N_2 in a Turbo Evaporator. The 60ml vials where removed before completely drying and the TLE was transferred in pre-weighted 8 ml vials, dried and weighted, in order for TLE mass to be determined.

Following BECS laboratory procedure, when the mass of the TLE was greater than 10 mg, it was split into two aliquots, one with a mass of 10 mg that was later processed and analysed and the remaining part archived. Exceptions were made for a few samples when the mass was close to 10 mg.

2.4.1. Acid and Neutral separation

A small piece of quartz wool was transferred using tweezers to the top of the capillary tube in a borosilicate Pasteur pipet to prevent Si-gel reaching the collection vials and superclean LC-NH3 Si-gel was loaded into the pipet (approx. 4 cm) using a funnel, creating a "column" (Figure 44). A small quantity of combusted sand was added to the top of the LC-NH3 Si-gel to prevent drying and the column is pre-conditioned with 2-3 ml 1:1 DCM:ISO, which was collected in a "waste" 8 ml vial and discarded.

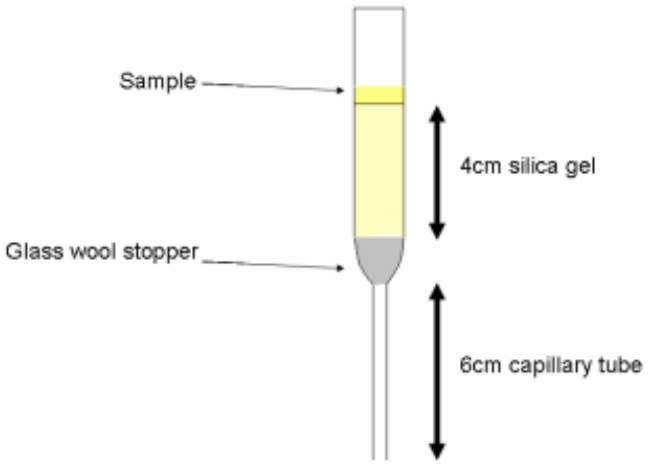

Figure 44 Column diagram showing the make-up of a separation column.

The TLE was further separated into Neutral and Acid fractions (TNF and TAF, respectively) which was done by transferring 10 mg of TLE dissolved in approximately 0.5 ml of 1:1 DCM:ISO into a pre-condition borosilicate Pasteur pipet. The TLE vial was washed 2 times with small quantities of 1:1 DCM:ISO and sonicated 5-15 seconds to allow full transfer of the sample into the column. Approximatively 4 ml of 1:1 DCM:ISO were passed through the column and the TNF was collected into a pre-weighted and labelled 8ml vial. TAF was collected in a similar fashion by eluting 4ml ether with 4% acetic acid onto the same column. Both TNF and TAF were gently dried under N_2 with a hot plate set at 38°C and their dry mass calculated.

2.4.1.1. TNF separation

The TNF fraction was further separated into N1, N2, N3 and N4 fraction to allow easier compound identification and minimize coelution during final steps of analysis.

A new column was created in the same manner as previously described (Figure 44) however it was loaded with approx. 3-4 cm of 230-400 mesh/35-70 micron silica powder. The columns were preconditioned by eluting 2-3 ml Hexane that was collected in an 8 ml waste vial and discarded.

TNF was dissolved in a small quantity of Hexane and transferred into the column. The TNF vials were further washed with small volumes of Hexane and sonicated to ensure that all organic material was transferred. N1 fraction was collected into a pre-weighted 8 ml vials by eluting 4 ml of Hexane through the column. Notice at this point that Hexane was used to pre-condition the Silica powder, to dissolve and transfer the sample and to collect N1 fraction as it allows non-polar compounds (i.e. n-alkanes and hopanes) to elute. The polarity of the following solvents is increased in order for more polar compounds to elute. N2 fraction was thus further collected by eluting 4 ml of DCM through the same column, followed by N3, which was collected by eluting 4 ml of 25:75 Ethyl Acetate:Hexane and lastly, N4 fraction was collected by eluting 4 ml of Methanol through the column. The column was left to dry and discarded. 8 ml vials were dried under N2. A summary of the process can be found below (Table 3).

Table 3 Fraction, solvent and amount used for their extraction, and collected final fraction.

Fraction	Solvent	Volume ml (solvent)	Organic Content
N1	Hexane	4	Aliphatic hydrocarbons
N2	DCM	4	Ketone/Ester/Aromatics
N3	Ethyl acetate:hexane (25:75)	4	Alcohols
N4	Methanol	4	Polar

The N1 fraction eluted through the column and collated in a 8 ml vial was completely transparent, and the colour of subsequent fraction shifted from light yellow (N2), to light green (N3) and light brown (N4) for the analysed peat samples.

Once dried, N1 and N2 fractions were transferred into an insert in 2 ml GC vials. The insert was lifted using a spring to allow easier GC syringe injection. N3 and N4 fractions were further processed.

2.4.1.2. N3 BSTFA derivitisation

Derivitisation reactions are used to transform certain compounds in order to increase their volatility using the same GC temperature conditions, detectability and elution times during GC analysis. Highly polar compounds are thus chemically altered to allow them to elute at lower temperatures than they would normally would during GC (Knapp, 1979). Of interest here are compounds that contain hydrogen bonds (i.e.-OH, -COOH) that lower their volatility when passed through the column. In reactions used during this project, the analyte's mass was increased by chemically attaching radicals with known masses to certain chemical elements (i.e. polar parts) in its chemical structure (Orata, 2012).

The N3 fraction was further processed by adding 30 µl of BSTFA (i.e. N, N–bis(trimethyl–silyl)trifluoro-acetamide; Figure 45) and 40 µl of pyridine in 8 ml vials containing the fraction. N3 was blown down for a short period of time to replace O_2, the vial was sealed with a Teflon-lined cap and left for 2h at 80°C.

Pyridine was used as a reaction catalyst while BSTFA reacts with alcohols to form trimethylsilyl (TMS, Mass=73) which are volatile and easy to separate (Scott, 2003). However, as the TMSs are less compatible with the Flame Ionization Detector (FID), GC-MS was used to identify and quantify N3 fraction. Samples were transferred and dissolved in DCM and analysed within 48h from derivitisation once pyridine was dried.

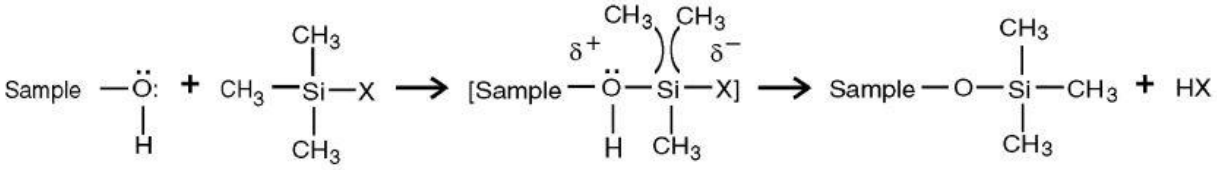

Figure 45 Chemical equation and reaction of TMS derivitisation.

2.4.1.3. N4 filtering

N4 fraction was dried, transported in 8 ml vials and processed at the University of Bristol, Organic Chemistry Unit (OGU). Samples were dissolved in a small volume of 99:1 Hexane:Isopropylic Acid (99:1 Hex:IPA) for transferring using a pipette in a high TOC syringe fitted with a 0.45 μm filter. The syringe was previously cleaned with three consecutive beds of 99:1 Hex:IPA. The sample was then passed through the syringe, 8 ml vial rinsed with 3 small volumes of Hex:IPA (99:1), collected in a 3.5 ml vial and dried. Filtering allowed removal of residual particles larger than 0.45 μm, that is incompatible with the HPLC system.

Samples were transferred in inserts placed in 2 ml GC vials. Approximatively 10 μl of C_{46} (GDGT C_{46}) with a concentration of 24.04 ng/μl was added as an internal standard (i.e. 240.4 ng). The inserts were dried, redissolved in a known volume (100 μl) of Hex:IPA (99:1) and analysed. An external standard with known composition was added to aid the identification process.

2.4.2. Total Acid Fraction (TAF)

The TAF was dried in a pre-weighted 8 ml vial and its mass was calculated. The TAF fractions need to be methylated prior to analysis. 100 μl of Methanol (MeOH) with 12% BF_3 was added into the vial leading to the formation of Fatty Acids Methyl Esters (FAMEs). The vial was sealed with a Teflon-lined cap, placed at 70°C for 1h and dried under N_2 under a hot plate at 38°C. Further separation was required.

A column with regular Si-gel was constructed as described below. Hexane was used for cleaning the column and transferring the TAF samples. TAF 8 ml vials were washed with small volumes of Hexane to ensure complete TAF transfer. 4 ml of Hexane were eluted through the column and collected in a pre-weighted 8 ml vial (A1 fraction). 4 ml of DCM were the eluted to collect the FAME fraction (A2 fraction). A1 fraction was kept until A2 was successfully analysed and discarded. A2 fractions were transferred into inlets in 2 ml GC vials, dried and dissolved in a known DCM volume (i.e. 150μl).

2.4.2.1. DMDS method

Due to particular interest in the location of the double bounds in FAMEs, the method described in more detail in Nichols et al., (1986) was performed first on 6 pilot FAME samples, after their concentrations were determined through GC-FID analysis. The procedure allowed the opening of the double bond to occur through the addition of two – CH_3S radicals. A characteristic mass spectrum is provided in Figure 46.

The A2 fraction was transferred in Hexane in 8 ml vials. 100 µl of Dimethyl Disulphide (DMDS) was added along 1-2 drops of Iodine (6% w:v in diethyl ether). The vial was sealed with a teflon-lined cap and left in the oven for 48h at 50ºC. After 48h the samples were remove from the oven and left to cool at room temperature. 1ml Hexane and 1.2 -1.5 ml Aqueous Sodium thiosulphate (5% w:v in distillated water) were added to remove iodine. The solution was hand shacked until completely transparent and left to segregate in two layers based on densities on a flat surface. The top layer contained the organic part, which was extracted using a pipette (A2 org). 0.5-1 ml of Hexane:Chloroform (4:1, v:v) were added and shacked well. Placed on a flat surface, two layers separated and the top layer extracted again using a pipette (A2 org). A 0.5-1.5 g of Na_2SO_4 and shacked well to remove any water that might have been transferred. A2 org was dried under N_2, dissolved in a small volume of Hexane and transferred using a 500 µl syringe to not allow Na_2SO_4 dried powder to pass into the insert in the 2 ml GC vial. The A2 org vial was washed twice with Hexane and the

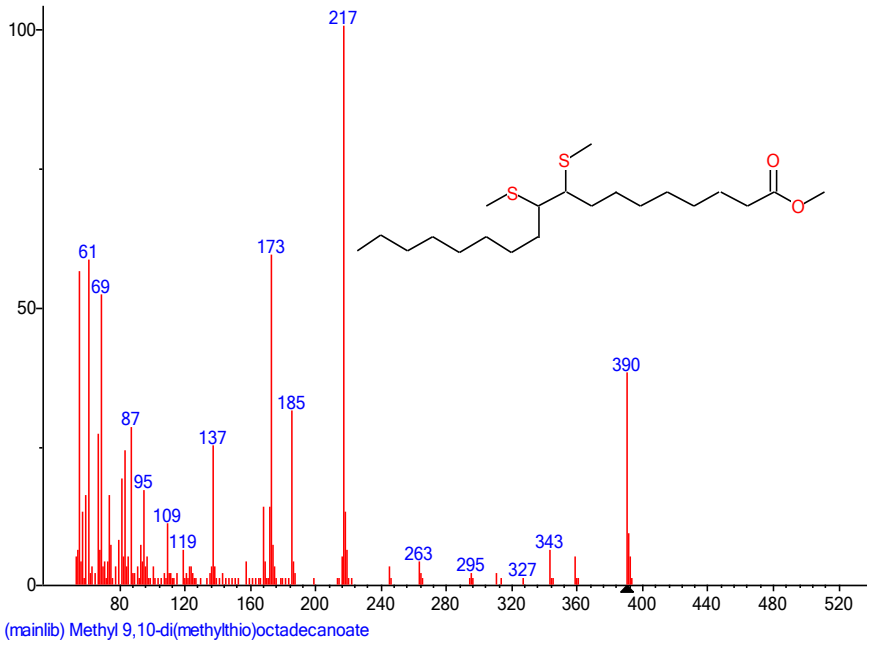

Figure 46 Showing DMDS derived monosaturated FA. Notice the position of CH_3S- radicals where the double bond occurs.

transfer repeated. The samples were dried in the insert and a known amount of Hexane (150 µl) was added.

A full list of specific fragments and their m/z values are provided in Nichols et al., (1986). For the purpose of this study only signatures specific to the location of the double bond in FAMEs with 16 and 18 Carbons were investigates and their specific m/z signatures are provided below (Table 4; Figure 46).

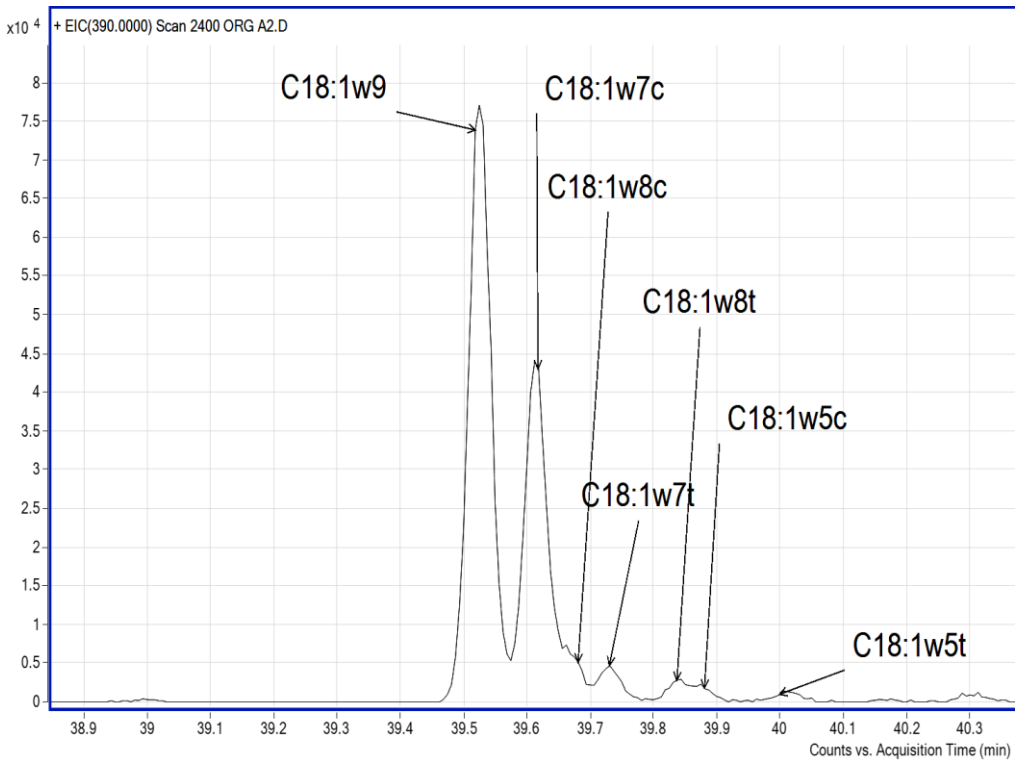

Figure 47 Variety of C18:1 fatty acids as seen at BVA after the DMDS derivitisation. The signal was enhanced by performing the search based on the m/z=390 ion.

2.4.2.2. Nomenclature and characteristic ions

In terms of nomenclature, as an example, for the C16:1ω7, C_{16} represents the number of Carbons in the Fatty Acids that corresponds to the C_{17}-FAME; 1ω7 represents the number of double bounds, in this case, one, and the ω carbon position, C_7. Carbon numbering is performed from the chain end opposite to the carboxylic acid group (i.e. –COOH), present in the fatty acid structure and it is indicated with the ω symbol. The Δ nomenclature refers to position of carbon as numbered from the carboxylic end (Table 4). Notation ***c*** or ***t*** refers to the optical structure of the molecule, cis- or trans- that elutes in this order (Figure 47).

Table 4 Monosaturated FA m/z frangment signatures for BVA identification. Notice mass of compound and the two fragments that cab be identified in the mass spectra of each compound.

Fatty accids	Mass of compound	ω-fragment	Δ-fragment
16:1ω9c	362	173	-
16:1ω8c	362	159	203
16:1ω7c	362	145	217
16:1ω7t	362	145	217
16:1ω6c	362	131	231
16:1ω5c	362	117	245
16:1ω5t	362	117	245
18:1ω9c	390	173	217
18:1ω8c	390	159	231
18:1ω7c	390	145	245
18:1ω7t	390	145	245
18:1ω5c	390	117	273

2.5. Standards and Blanks

Composition of BECS external standard mix (STD) is provided below (Figure 48). For every GC-MS or GC-FID run, the BECS standard was analysed in three different concentrations (1:0 STD:DCM, 1:1 STD:DCM; 1:3 STD:DCM) for compound and concentrations determination.

In order to adjust compound concentrations for changing GC temperatures during analysis (see GC-FID and GC-MS methods), three calibration curves were calculated for each run for STD compounds eluting before the 25-minute mark, between 25-35 minutes and after 35 minutes. Linear regression equations were calculated using Microsoft Excel and expressed as:

Equation 1: $y = ax$

where y=peak area from chromatogram and x=compound concentration; calibration curves were used only if they provided a r^2 value between 0.94 and 0.99.

A quality check test was performed at the end of each run by injecting in the 1:0 STD:DCM vial and comparing the concentrations of several compounds to the initial 1:0 STD:DCM. A

blank GC-vial containing only DCM was added and run after 7-10 samples in order to determine if any contamination from the GC machine occurred.

A set of blanks were used in the ASE run. Two cells were filled with combusted sand and added at the beginning and end of the sequence to test for any contamination that might come from the ASE or prior. The blanks were treated as normal samples and their masses calculated, however, they were not separated further into TNFs and TAFs. The blank TLE was transferred into inserts in 2 ml GC vials and analysed on the GC-FID. The majority of minor GC peaks that appeared had concentrations below 1.5 µg/g, with a single peak having a concentration of approximatively 78 µg/g, however this peak did not interfere with the concentrations of the compounds of interest. The peak was identified as a phthalate, a plastic contaminant.

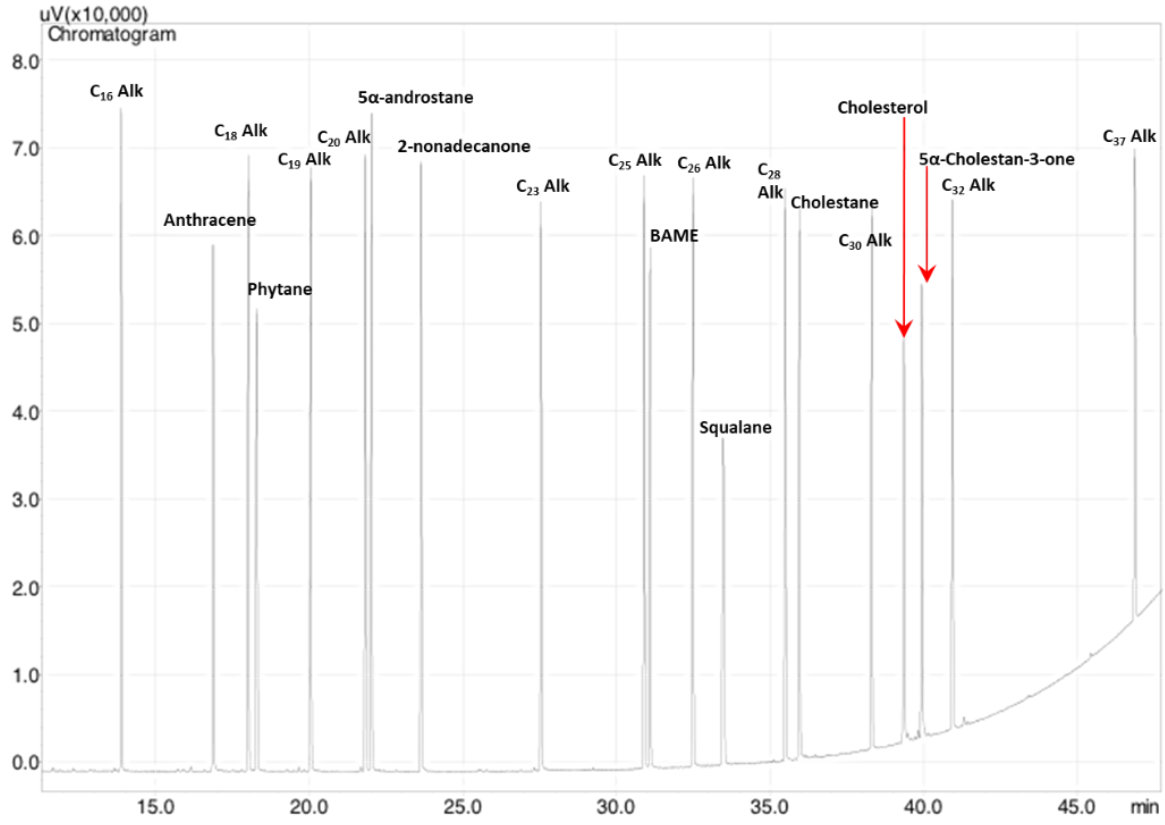

Figure 48 General BECS standard, showing including compounds and relative retention times on a GC-FID.

Compound concentrations

Once identified, the compounds' peak area was extracted and divided by ***a*** (Equation 1). The result was then calibrated to the volume in which the sample was dissolved (i.e. usually 150 µl), to the initial mass of total TLE and to the mass of dried sediment added to ASE cells. Final results represent compound mass per gram of dried peat (µg/g).

2.6. GC-MS

Samples were run on GC-MS Agilent 5977 for identification within the range 50-600 m/z. The column used was a HP-1-MS column, 60m long, with a 0.250 mm internal diameter and 0.25 μm film thickness. The initial oven temperature was 60°C (stabilised for 2 min), and increased with 30°C/min until 120°C and with 5°C/min until 305°. The total run time was 56 minutes with first result at 10 minutes (i.e. gas cut off after 10 minutes). The front inlet temperature was 310°C, interface temperature between MS and source 310°C, while the temperature of the source was 230°C and that of the MS quad 150°C. Purge time was 0.705 minutes and purge flow 50 minutes. The column flow was 1.2 ml/min and flow velocity 28.4 cm/sec. The method used constant flow. The injection volume was 1μl. Helium was used as the carrier gas, with a flow of 25 ml/min.

2.7. GC-FID

Samples were run on GC-FID Agilent 7890 for quantification within the range 50-600m/z. The column was a RTX-1Restek column, with a length of 60m, internal diameter of 0.250mm and film thickness of 0.25μm. The oven temperature program started at 60°C and stabilised for 2 minutes, increased at a rate of 30°C/min until 120°C and then at a rate of 5°C/min until 330°C where it stayed for 15 minutes.

The front inlet used splitless injection at a temperature of 320°C; purge time was 0.705min and purge flow 50 minutes. The run time was 61 minutes. Flow was at 1.2 ml/min, velocity 30.4 cm/s. The method used constant flow, with changing pressure (psi). Hydrogen was used as the carrier gas, with a flow of 40ml/min.

N4 - GDGTs

N4 fraction was re-dissolved in a mixture of Hexane:Isopropanol (99:1, v:v) and samples passed through a 0.45 μm PTFE filter. 10 μl of C_{46} with a concentration of 24.04 ng/μl was added as an internal standard. Samples were then gently dried under N_2 and redissolved in 100 μl.

Analysis of core lipids (GDGTs) was performed on a high performance liquid chromatography/ atmospheric pressure chemical ionisation – mass spectrometry

(HPLC/APCI-MS) using a ThermoFisher Scientific Accela Quantum Access triplequadrupole MS (Naafs et al., 2017a). The method used selective ion monitoring mode with m/z m/z 1302, 1300, 1298, 1296, 1294, 1292, 1050, 1048, 1046, 1036, 1034, 1032, 1022, 1020, 1018, 744, and 653) for increased sensitivity and ease of identification (Naafs et al., 2017a).

3. Quistococha peatland (QT) (core 03°50′24.0″S, 073°19′09.92″W)

3.1. Introduction

At present, peat forms at Quistococha under *M. flexuosa*-dominated palm swamp vegetation, in an acidic peat with intermediate nutrient availability (Teh et al., 2017; Figure 49). Lähteenoja et al. (2009 a) described the peatland as "nutrient-poor minerotrophic peatland", which was later confirmed by van Lent et al. (2018) who classified the site as minerotrophic (i.e. Ca/Mg>6). This indicates a complicated hydrological regime, with a combination of atmospheric, riverine and groundwater sources. At present, this vegetation covers approximatively 78% of the peatlands in Pastaza-Marañón foreland basin (PMFB; Draper et al., 2014). Furthermore, *M. flexuosa* grows here in a relatively constant humid (80-90%) and hot (>25°C) climate with mean annual precipitation of 3097 mm/yr and two weak distinguishable seasons, a drier one between June and September and a wetter one between November and December (Marengo, 1998; Roucoux et al., 2013). The samples available for this study come from the peat core that was used for pollen analysis by Roucoux et al., (2013) and geochemical analysis by Lawson et al. (2014), core QT-2010-1.

3.1.1. Site description, location, geology

Quistococha peatland (QT) is located in the proximity of Itaya River, in the Amazon floodplain, only 10 km away from the Iquitos city, in NE Peru (Roucoux et al., 2013, Figure 49). A lake bearing the same name is located within the peatland, several hundred meters away from the coring site. The lake area is approximatively 1 km^2, with a depth of 3.2−4 m (Räsänen et al., 1991; Aniceto et al., 2014). Sediments from this lake were analysed by Aniceto et al. (2014) and will provide additional data when interpreting environmental change experienced at this location.

Due to the meandering nature of the Amazon river and adjacent alluvial, easily eroded sediments and rock units, higher grounds and terraces bound the present-day floodplain (Figure 49), marking the extent of palaeochannels. At the study site, the Amazon carved terraces (i.e. up to 15 m in height, Aniceto et al., 2014) in the Quaternary and Miocene-Pliocene strata, forming channels. As the QT peatland is bounded by terraces (Figure 49),

water flow is restricted, leading to waterlogged conditions and peat formation. Furthermore, a clay levee is located to the east of the peatland, limiting water flow (Kelly et al., 2014).

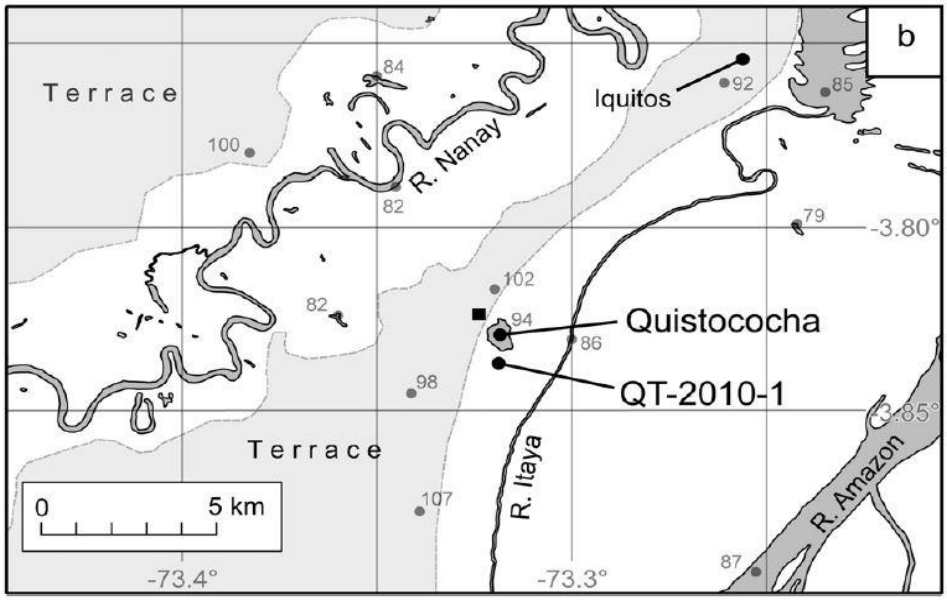

Figure 49 Location of QT peatland and Quistococha Lake. Notice the elevated terrace in the W-NW of QT peatland and theproximity of river Itaya and Amazon. Numbers refer to measured elevations. Edited from Roucoux et al., (2013).

At present, two rivers are located close to QT, Itaya and Nanay, both tributaries of the Amazon River, however, the latter does not influence the geochemistry of QT. The Itaya river was referred to as an important flood water source for adjacent peatlands since it formed in 1761 (Roucoux et al., 2013 and references therein). The QT site is part of the Amazon floodplain, currently in an infilled palaeochannel and part of an area that is permanently waterlogged and periodically flooded during the wet season, known as "varzea" (Roucoux et al., 2013; Aniceto et al., 2014).

3.1.2. Age model and peat accumulation rates

The QT-2010-1 core consists mainly of peat yet it extends below into the underlying silts and clays, reaching a depth of 630 cm (Roucoux et al., 2013). The age model presented in Figure 50 was constrained using 7 samples that were radiocarbon dated. The age model shows that peat started accumulating at the site around 2200 cal yrs BP ago (i.e. calibrated years before present). The peat has an average accumulation rate of 1.43 mm/yr between 0

and 260 cm and 3.30 mm/yr, between 260 and 395 cm (Roucoux et al., 2013), similar to rates reported in other studies within the same peatland (Lähteenoja et al., 2009a).

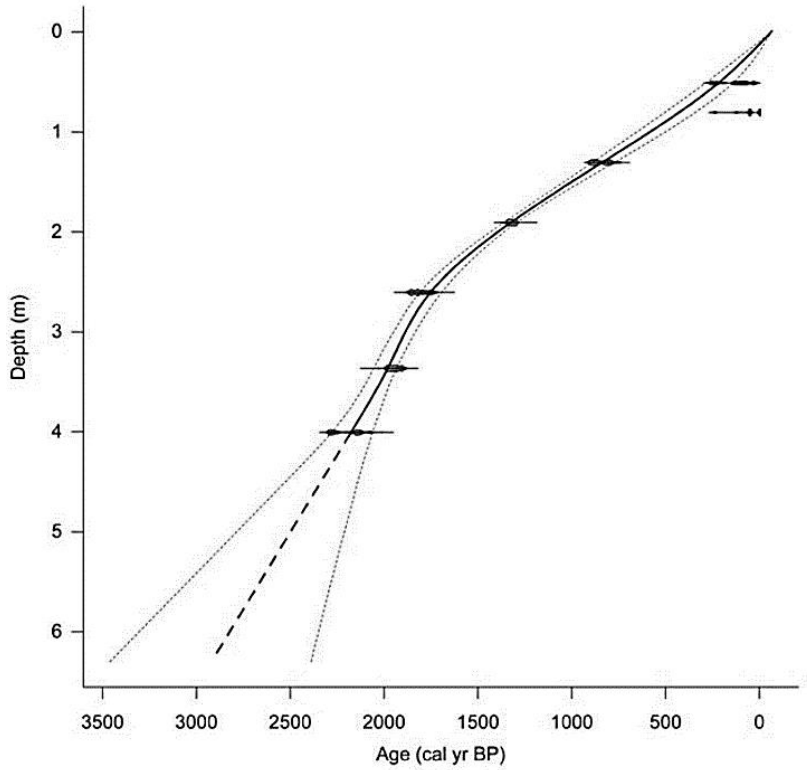

Figure 50 Age model for QT peatland. Notice the 6th sample that is not in stratigraphic sequence, showing a kink in the age model, due to possible younger root material within the sediment (Roucoux et al., 2013).

3.1.3. Vegetation and samples

The present day vegetation is palm swamp (Draper et al., 2014) doiminated by *M. flexuosa*, locally known as aguajal. *M. flexuosa* palm swamp, started to develop around 1000 cal yr BP, but pollen of this species was first recorded around 2100-1990 cal yr BP where the

Vegetation type	Site name	Nutrient status*	Latitude (S)	Longitude (W)	Plots	Flux chambers
Forested	Buena Vista	Rich	4°14'45.60"	73°12'0.20"W	9	74
Forested (short pole)	San Jorge (centre)	Poor	4°03'35.95"S	73°12'01.13"W	3	26
Forested (short pole)	Miraflores	Poor	4°28'16.59"S	74° 4'39.95"W	16	142
M. flexuosa Palm Swamp	Quistococha	Intermediate	3°49'57.61"	73°12'01.13"	119	433
M. flexuosa Palm Swamp	San Jorge (edge)	Intermediate	4°03'18.83"S	73°10'16.80"W	6	81
Mixed palm swamp	Charo	Rich	4°16'21.80"S	73°15'27.80"W	8	56
*After Householder et al. 2012, Lahteenoja et al. 2009a, and Lahteenoja et al. 2009b						

Figure 51 QT peatland nutrient status, geographical location and number of measurements taken by Teh et al. (2017).

species is indicative of decreasing flooding episodes relative to the deeper, seasonal flooding indicated by the pollen in the preceeding interval (Roucoux et al., 2013).

Palynological records show a complicated vegetation history at this location, with abrupt inversions and transitions (see subchapter 3.1.4.; Roucoux et al., 2013), not following a predictable and accepted (i.e. unidirectional) model developed for Asian tropical peatlands (Kelly et al., 2017 and references therein). As a summary (Figure 52), vegetation development started as sedge fen and floating mat vegetation (2200 cal yr BP), evolved into a periodically flooded woodland (i.e. 1800 cal yr BP), oscillated twice between herbaceous and seasonally floaded woodland (1880-1010 cal yr BP) and finally started to establish itself as the current vegetation type from 1000 cal yr BP until 400 cal yr BP. The changes in vegetation types are primarily thought to be caused by changes in the flooding regime and the highly dynamic banks of Amazon River (Roucoux et al., 2013). Thus, peat accumulation at the site is primarily a result of lateral river migration (Lähteenoja and Roucoux, 2010 and references therein) (Roucoux et al., 2013).

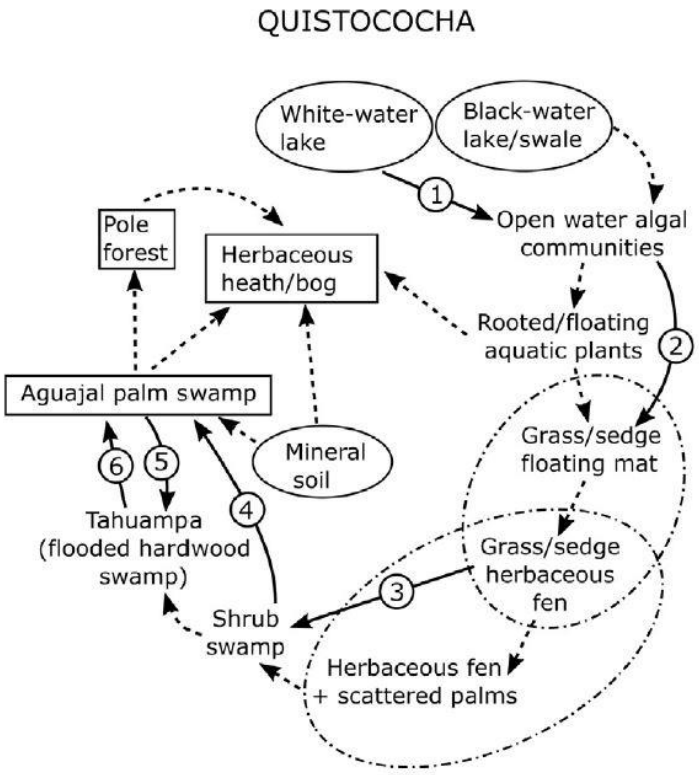

Figure 52 Vegetation development at QT (Kelly et al., 2017).

Pollen data analysis of one of the cores from QT suggests that for at least the past 2280 cal yr BP (i.e. radiocarbon dating), vegetation at this site saw multiple shifts (Figure 52). Starting with the lowermost, sandy part of the record and working upwards towards recent peat deposits, these changes in vegetation and sediment types will allow a more comprehensive

interpretation of how and why biomarker signatures vary in time. Changes in vegetation cannot be attributed only to changes in climate due to presumed stability of temperature expected in this tropical region, but need to be treated as local changes, primarily caused by the dynamic character of the two rivers in the area (i.e. Itaya and Amazon). Overall, in the past 2200 years, conditions favored deposition of peat, although the hydrological regime saw several shifts at the site. One sample from each vegetation or sub-vegetation type was available for biomarker study. Data and interpretation from pollen records (Roucoux et al.,2013) at the site are provide below.

3.1.4. Literature review on vegetation changes based on pollen assemblages (Roucoux et al., 2013)

0. Below the pollen record (630-432 cm) – age greater than 2280 cal yr BP

The section between **630-432 cm** is not covered by the current analysed samples within this project (Figure 53). It was described as a fine sand deposit with a high magnetic susceptibility that contained high inorganic content and from which an approximate age could not be extracted. Although the age is not known, it was **greater than 2280 cal yr BC**, relative to the above section (Roucoux et al., 2013).

Another sedimentary record (i.e. 3 cores) taken from Lake Quistococha (3°49’46.87” S 7°19’05.67” W), located in the proximity of the peat-core indicates drier conditions during mid-Holocene (Aniceto et al., 2014). The influences of the Amazon on the area started to decrease after 5800 cal yr BP and although Aniceto et al. (2014) found evidence of a hiatus and thus a drier period within the QT lake cores, more recent research by Kelly et al. (2018) assigned the inferred hiatus to input of older organic matter from floods that could have offset the radiocarbon ages. The decline in Amazon River influences on the site was set between 4490-2180 cal yr BP and the area was probably outside of Amazon’s sediment-rich floods by 2180-1660 cal yr BP (Kelly et al., 2018).

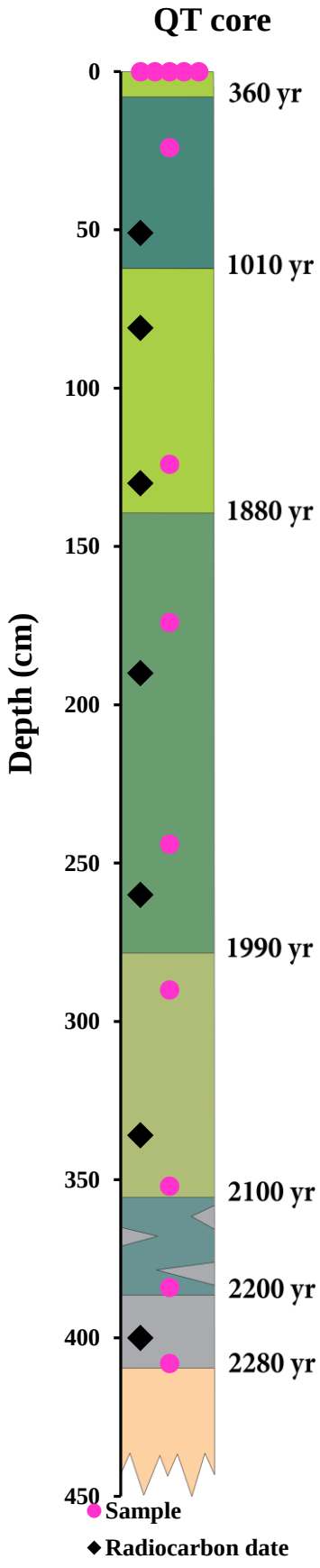

Figure 53 QT peat core graph with sample and radiocarbon depth.

1. Zone QT-1 (432-408 cm) – 2280-2200 cal yr BP

Peat deposits start just above 432 cm and the first pollen assemblage was recorded between **432-408 cm** by Roucoux et al. (2013). The sample available for analysis from this pollen zone available comes from **410 - 420 cm.** This part of the core was dated at ca. **2280-2200 cal yr BP** and pollen was found in inorganic clay, marking a change in the environment from fluvial to a calmer, lake-like setting (Roucoux et al., 2013; i.e. ox-bow lake). The clayey unit creates an impermeable layer (Kelly et al., 2014) with consequences on ground water flow, maintaining waterlogged conditions. Clay deposition rate was calculated for the region at 5 cm/100 yr (Räsänen et al., 1991). Vegetation was composed of species adapted to newly exposed sediments-in environments where light competition is low (i.e. *Cecropia* sp.), including many herbaceous taxa (Roucoux et al., 2013).

2. Zone QT-2 (408-376cm) – 2200-2100 cal yr BP

The following pollen zone occurs between 4.08-3.76 m, matches with the sample between **380 - 388 cm** and was dated to **2200-2100 cal yr BP.** The base of this section has an increase in organic matter content from the previous zone. Organic matter makes up 75% of this section and is interbedded with layers of clay sediments, marking the point when peat started to accumulate at this site. This indicates that the area was still affected by periodic flooding events (i.e. by white-water rivers, high in sediment content). Pollen records provide an indication of two possible types of present flora: marginal fen and/or floating mat vegetation. Other taxa (i.e. *Hevea guianesis*) that can also be found today at the site indicate the development of a vegetation able to adapt to periodic or permanent waterlogged conditions (Roucoux et al., 2013).

3. Zone QT-3 (376-296 cm) 2100-1990 cal yr BP

The next section was delimited between **376-296 cm** and dated between **2100-1990 cal yr BP**. This coincides with the **348 - 356**

cm sample from the same core. The average organic content reaches 90%, and pollen records indicate the existence of flood-adapted species, thus waterlogged conditions continued in this area. The main flood water source switched from the sediment-rich Amazon to sediment-poor waters of Itaya River (Roucoux et al., 2013).

Based on pollen records, vegetation changed from temporal/permanent waterlogged taxa to wet woodland representatives. Higher in this section, pollen of *M. flexuosa* is found, which is the main vegetation present at this site today. This indicates a change in the flooding regime from deep (i.e. 3-5 m) seasonal flooding to a permanent waterlogged environment with episodic shallow flooding events (~1.5 m) (Roucoux et al., 2013 and references therein).

4. Zone QT-4 (296-152cm) 1880-1010 cal yr BP

The section spanning between **296-152 cm** was dated at **1880–1010 cal yr BP** and coincides with samples between **294-286 cm** (i.e. subzone QT-4a), **248-240 cm** (i.e. subzone QT-4b) and **178-170 cm** (i.e. subzone **QT-4c** in Roucoux et al., 2013).

The main change in the environmental conditions at the site is marked by a decrease in *Mauritia* species and an increase in pollen from species characteristic to seasonally flooded forest, adapted to deeper and longer flooding events. The presence of other new taxa in this environment (i.e. **subzone QT-4a**) (i.e. *Acalypha, Ficus, Papilionoideae, Mimosoideae*) and low pollen percentage from *Cyperaceae* and *Poaceae* species indicate that the canopy was closed.

In the following subzone **(QT-4b**), *Cyperaceae* and *Poaceae* are dominating, suggesting an opening of the canopy and herbaceous vegetation. This was caused by two possible events: a decrease in the depth and duration of flooding episodes and/or development of a permanent water body at the site that sustained fen and possibly floating mat vegetation.

Subzone **QT-4c (**together with QT-4d, no sample available), saw the same vegetation repetition as 4a and 4b, with the canopy closing under woodland vegetation (4c) and opening, with input from herbaceous taxa pollen (4d; ~110yr).

5. Zone QT-5 (152-72cm) 1010-360 cal yr BP

The next zone was divided between **152-72 cm**, dated **1010–360 cal yr BP**, coincides with the samples from **120-128 cm** and marks another episode of *M. flexuosa* expansion and appearance of two taxa common in permanent waterlogged regions. The canopy was also closed and peat continued to accumulate with low inorganic sediment input.

6. Zone QT-6 (72-16cm) 360 cal yr BP - Present

The final section spans between **72-16 cm**, was dated at **360 cal yr BP to present** and contains the final sample from this site, **20-28 cm.** The pollen assemblages in this zone indicate (i.e. see Roucoux et al., 2013 for further data) that deep seasonal flooding episodes stopped and that the canopy remained closed (see Roucoux et al., 2013 for further details).

Present day vegetation and environmental data

The main vegetation type, characterized by *M. flexuosa* (Roucoux et al., 2013), is known to possess adaptations to waterlogging and anoxic conditions (Granville, 1969; see subchapter 2.4.1.). Davalliaceae *nephrolepis*, a fern species, also occurs at the site (see subchapter 6.2.).

Data on present day gas emission, air and peat temperature, conductivity, dissolved oxygen, water table levels and pHs were collected from the top 15 cm of the peat column by Teh et al., (2017; Table 5). Between the three peatlands studied here and reported in Teh et al. (2017), QT represents the highest mean flux of CH_4 (36.7± 3.9 mg CH_4-C/m^2/day), alongside the highest mean flux of N_2O (1.11±0.44 μg N_2O/m^2/day). A summary of the parameters is provided below:

Table 5 Present day parameters at QT (Teh et al., 2017).

QT	Peat(T°C)	Air(T°C)	Conductivity (μS/$m^{2)}$	Dissolved O_2 (%)	WT level (m)	pH	CH_4 C/m^2/day
Wet season	25.6 ± 0.6c	26.3 ± 0.1	45.9 ± 2.1	19.4 ± 1.3	37.2 ±1.7	5.04 ±0.03	46.7± 8.4
Dry season	25.3 ± 0.1	26.4 ± 0.1	51.9 ± 1.8	17.3 ± 1.5	6.1 ± 1.3	5.49 ±0.03	28.3± 2.6

Furthermore, van Lent et al. (2018) found that CH_4 fluxes vary within the QT peatland based on levels of degradation experienced by the location. The study (in-vitro incubation experiments, relative fluxes provided) found that sites characterized as intact and medium degraded acted as CH_4 sinks with no shifts to sources for any water-fill pore-space (WFPS) values (i.e. 20% to 100%-mimicking flooding). The peat forming in a highly degraded site acted as a CH_4 source only when WFPS values were higher than 70%. This was further correlated with emissions of N_2O from each site, which was found to have a negative relationship with CH_4 production. N_2O emissions were found to be highest within those sites

when WFPS was at 84% and at 100%. CO_2 production (i.e. incubation experiment) and C mineralization was also found to be higher at highly degraded sites (van Lent et al., 2018).

3.1.5. Geochemistry and peat conductivity (K) at QT site

Magnetic susceptibility decreases abruptly in two steps: before 2800 cal yr BP and after 2600 cal yr BP and is minimum at the base of the peat core (i.e. 413 cm) (Roucoux et al., 2013; Lawson et al., 2014). The grain size increases downward, in the clay-silty unit underlying peat, which is also recorded in the QT Lake (Aniceto et al., 2014). C and N content increase abruptly from the depth of 413 cm (i.e. first peat deposits) with higher N (wt%) values towards present. The C/N ratio is seen to increase gradually at the transition between clay and peat. This was interpreted as an important input from algal sources before peat initiation, which correlates well with the lake-type environment proposed by Roucoux et al., (2013). Fluctuations seen in the ratio within the peat column was interpreted by Lawson et al., (2014) as inputs from different vegetation types. Lignin values fluctuate between 40 and 80 wt% (organic matter fraction), with values around 60% at the base of the peat core, suggesting a high recalcitrant character of the peat and potential for biomarker studies.

Ca, Fe, Mn and Na show similar trends, decreasing upwards while Al, Mg and K are increasing increase upwards, within the peat column. Ca, Mg, Al, K and Fe show very high values in clayey silt unit compared to present day values, indicating the mix origin of weathered material from higher reaches (Lawson et al., 2014). Lower values of Mg and Ca within the peat column indicate lower input from nutrient-rich waters, and thus, lower influence from Amazon River. This was experienced during longer periods of time when precipitation was the main water source along secondary sources of ground water input (Lawson et al., 2014), the latter which gives QT its nutrient-intermediate status.

In the top part of the peat column (0-150 cm), C/N and lignin ratios are seen to decrease towards the top (Figure 54). One suggested explanation was that the input from fresh roots, changes in litter quality and less decayed material towards the top (Lawson et al., 2014). The slight increase seen in K, Ca, Mg and Na relative to the bottom peats (150-413 cm) was attributed to organism uptake of nutrients and thus, higher demands for K and Ca by vegetation (i.e. bioaccumulation). Na relative increase was attributed to its recycling by fungi and animals. A further breakdown of surface nutrient profiles in soils and litter fall is

provided by Van Lent et al. (2018), taking into account variations based on degradation characteristics of sites within the QT peatland.

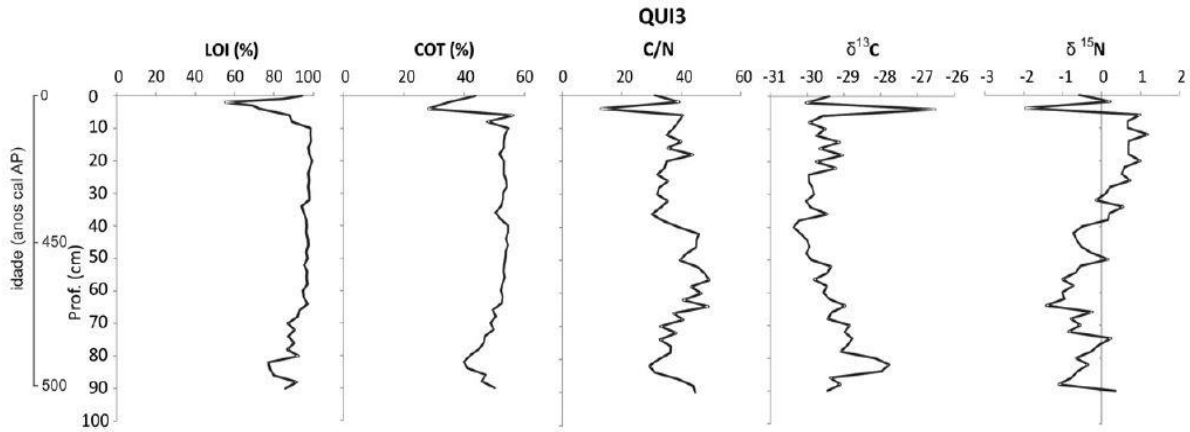

Figure 54 Quistococha lake sediment core parameters (Aniceto et al., 2014).

The relative increase in Fe and Mn in upper peats was attributed to redox conditions (i.e. Fe and Mn soluble under acidic conditions) and to the fact that peat at QT might be periodically exposed to oxic condition down to 30 cm in depth (27 cm below surface during dry season, Kelly et al., 2014). Furthermore, the water can be oxygenated due to root transport (i.e. known to penetrate depths of 1.5 m – Kelly et al., 2014; see subchapter 1.5.2.) or increased water intake by vegetation (Lawson et al., 2014) which would have high implications in the CH_4 cycle.

3.1.6. Hydraulic conductivity (K)

Hydraulic conductivity is a major physical parameter that influences the position of water table within a peatland (Table 6). It was related to the type of plant material and its degree of decomposition. Thus, in terms of its values, a relatively high K indicates high potential for water flow (i.e. high peat permeability), while low values will restrict water flow within the peatland (Kelly et al., 2014). This would relate to the Fe and Mn profiles seen by Lawson et al. (2014) and proposed redox conditions, to the degree of peat aeration and microbial development.

K differs at QT within the same peat core and within the same peatland (and vegetation type), (Table 6; Kelly et al., 2016). Across the peatland, K was also an order of magnitude higher at a depth of 50 cm compared to 90 cm depth, indicating that depth has an important impact on the behaviour of water flow within this peatland (i.e. whereas depth did not have a significant impact on K within BVA and SJO). K median value for the three plots (i.e. A, B,

C-moving away from Quistococha Lake towards C), are summarized in the table below for the two depths:

Table 6 Hydraulic conductivity parameters with distance from QT lake at two different depths (Kelly et al., 2016)

	A	**B**	**C**
50 cm	0.00369 cm/s	0.01606 cm/s	0.00387
90 cm	0.00167 cm/s	0.00627 cm/s	0.00164

3.1.7. Published isotopic data

Bulk carbon isotopic measurements are available in Roucoux et al., (2013; Figure 55) for depths that correspond to radiocarbon dating. The lightest value is recorded at a depth of 80-81cm (i.e. $\delta^{13}C$=-37.6‰ while the heaviest, at the depth of 130-131cm (i.e. $\delta^{13}C$=-29.3‰).

Code	Depth (m)	^{14}C age	Calibrated age range yr BP (2σ)
UBA-20048	0.50–0.52	117	269 to 12
UBA-18437	0.80–0.81	–	252 to −7
UBA-18438	1.30–1.31	911	915 to 745
UBA-18440	1.90–1.91	1411	1353 to 1287
UBA-18441	2.60–2.61	1867	1872 to 1727
UBA-18439	3.36–3.37	1997	1999 to 1882
UBA-18442	4.00–4.01	2161	2308 to 2056

Figure 55 Radiocarbon and calibrated ages at QT, edittted from Roucoux et al., 2013.

3.2. Results

3.2.1. N-alkanes

The summed masses of n-alkanes in the 5 surface samples is almost equal to the sum of n-alkanes in the 8 core samples, with values of 2284.5 µg/g and 2266.9 µg/g, respectively. Short chain n-alkanes in the range of nC_{16}-nC_{20} have the highest masses in surface samples, followed by medium length n-alkanes and finally, long-chain n-alkanes. The same situation is true for most core samples, however, unlike surface ones, the length of the n-alkanes extends up to 38-39 carbons, whereas surface samples' maximum chain length is 31 carbons. Short and medium-length n-alkane individual concentrations spike at surface and at depths of 348-356 cm and 286-294 cm. Long-chain n-alkanes (C_{26}-C_{36}) have their maximum concentrations and smaller peaks at different depths. Overall, in the long n-alkane range, odd numbered chains dominate in most samples (Figure 56).

CPI peaks at 120-128 cm and 20-28 cm, when it reaches values of 12.03 (Figure 57.1.). The lowest CPI value is recorded in the clay, inorganic unit, and, in peat containing samples, at the depth of 240-248 cm, where a local disturbance in vegetation was depicted in pollen records by Roucoux et al. (2013).

P_{aq} varies between 0.07 and 0.28, crossing the threshold for emergent macrophytes between 380-388 cm and 348-356 cm and once more, at the depth of 120-128 cm (Figure 57.2).

ACL and P_{wax} show mainly the same trends, with the lowest values recorded between 380-388 cm and 348-356 cm, however they peak at different point within this range. Furthermore, ACL decreases in surface samples, while P_{wax} shows an increase at surface (Figures 57.3. and 55.4).

For the QT site, values of the Pr/Ph ratio are mainly below 1, varying between 0.24 and 1.27, with Pr/n-C_{17} and Ph/n-C_{18} ranging between 0.11-0.59 and 0.09-0.61, respectively (Figure 57.5).

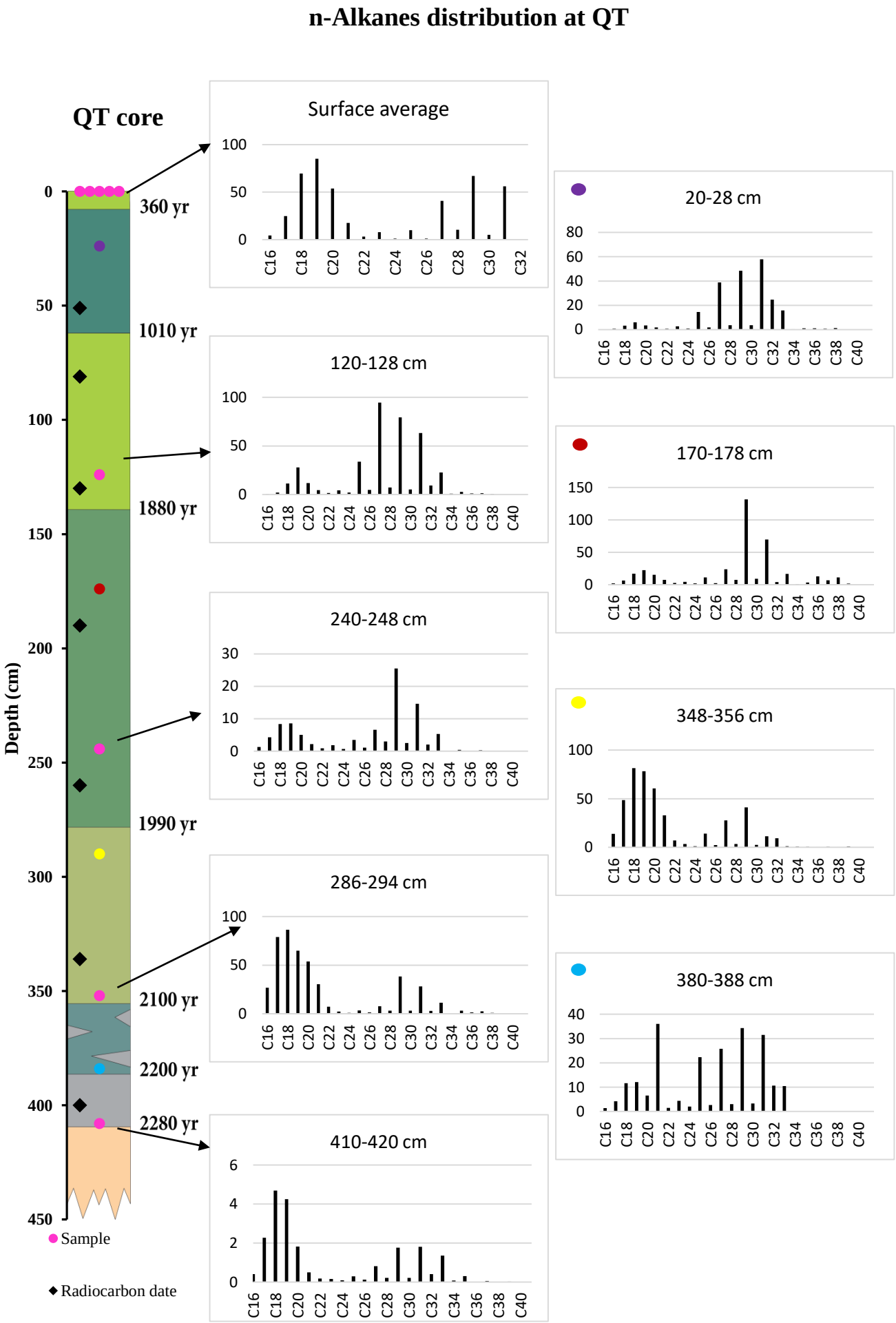

Figure 56 N-alkane concentration distribution with depth at QT. For each plot, the x axis represents number of carbons in each n-alkane while y axis is in μg/g, indicating concentration. Notice coloured circles in the peat-log representing samples maching up with graphs on the right-hand side.

n-Alkane proxies and hopanes

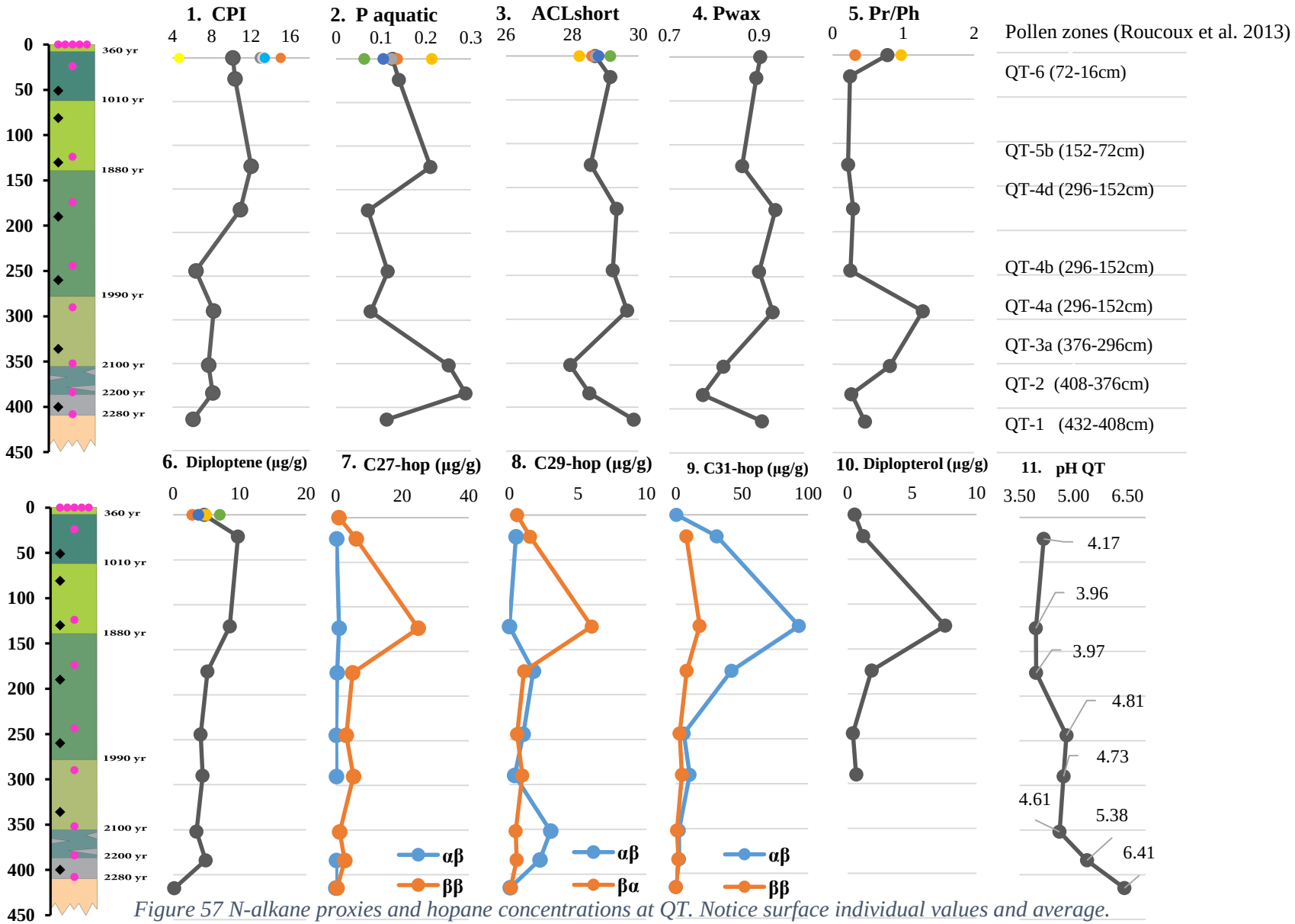

Figure 57 N-alkane proxies and hopane concentrations at QT. Notice surface individual values and average.

iso- and br-GDGTs

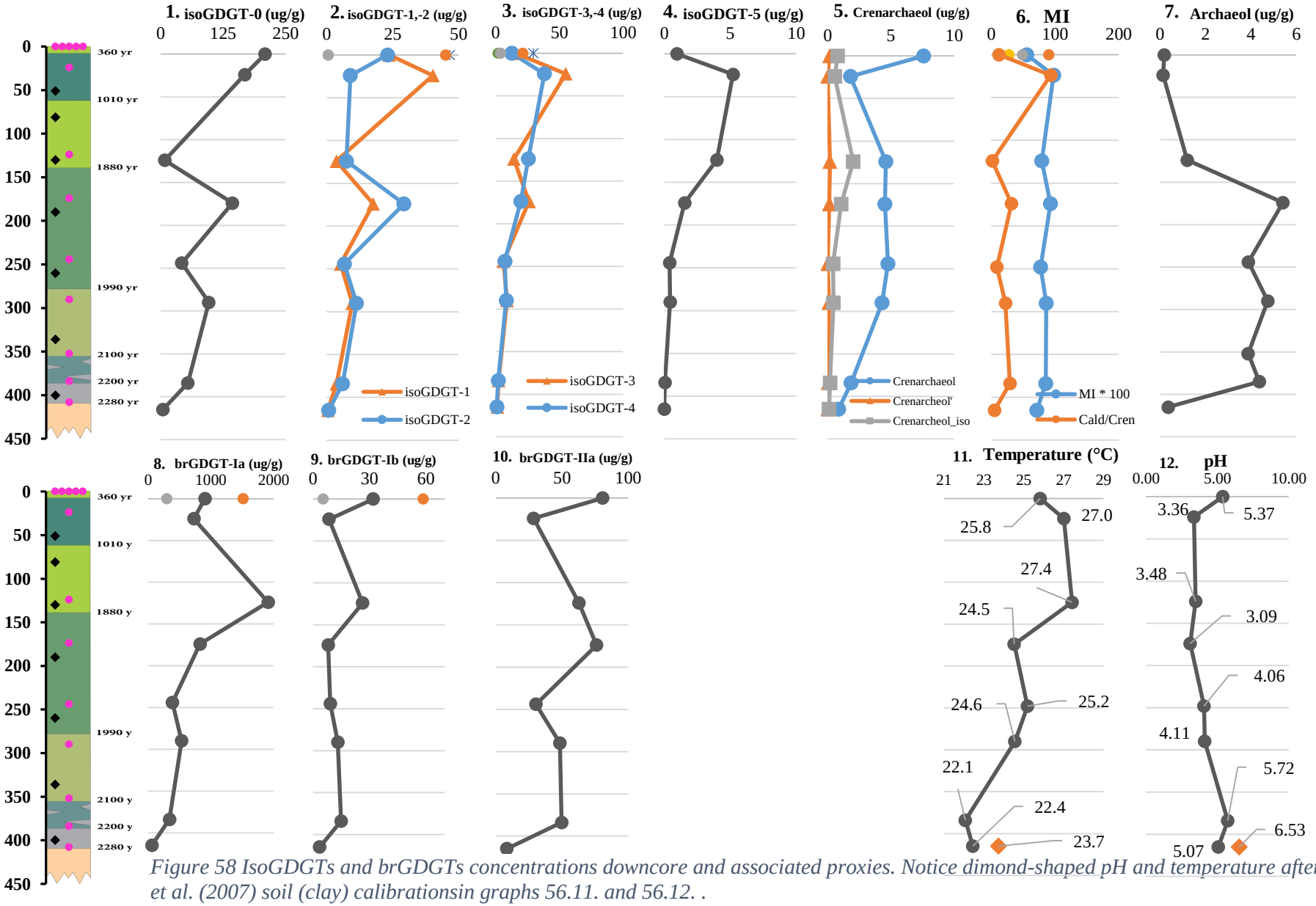

Figure 58 IsoGDGTs and brGDGTs concentrations downcore and associated proxies. Notice dimond-shaped pH and temperature after Weijers et al. (2007) soil (clay) calibrationsin graphs 56.11. and 56.12. .

Fatty acids

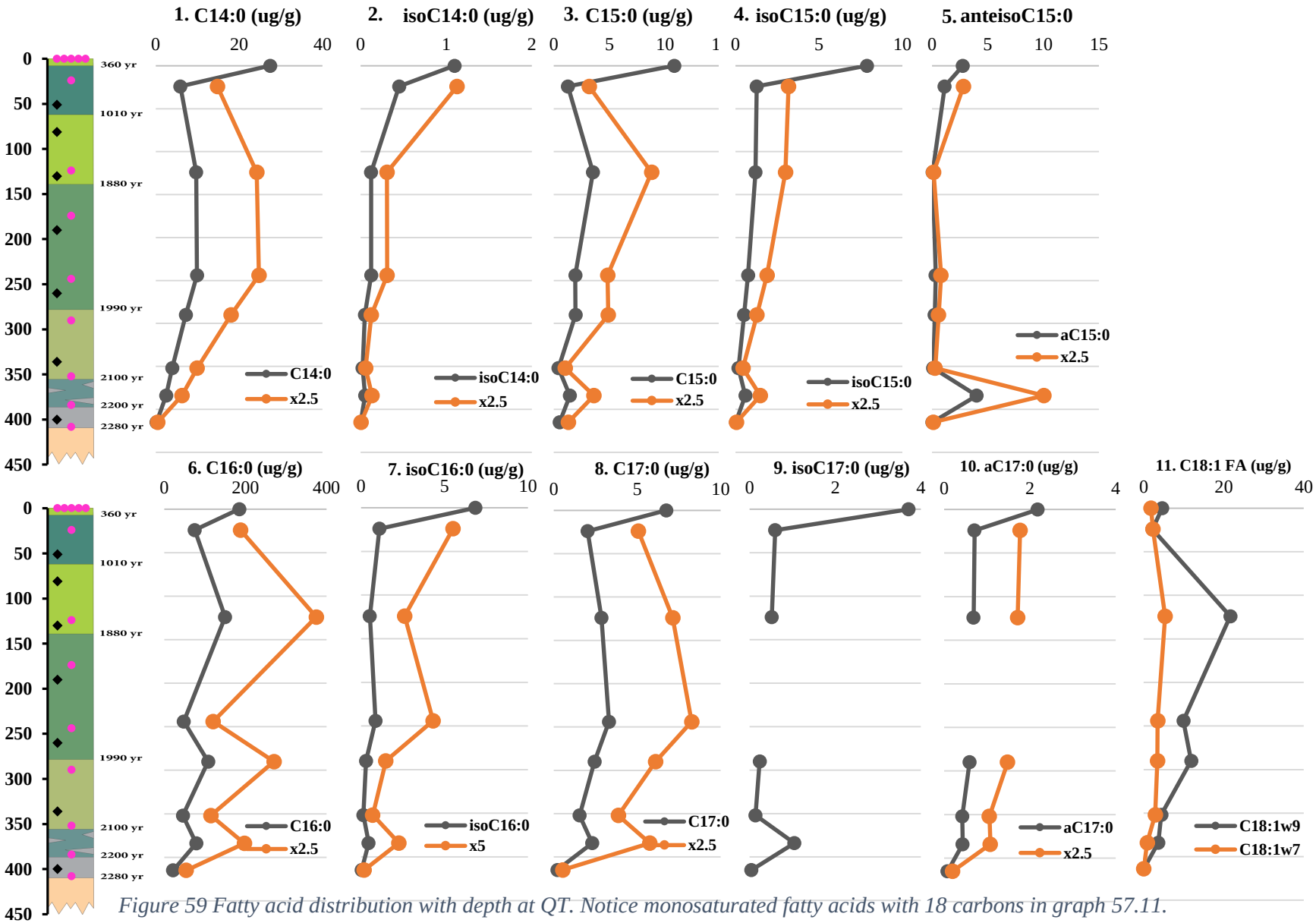

Figure 59 Fatty acid distribution with depth at QT. Notice monosaturated fatty acids with 18 carbons in graph 57.11.

3.2.2. GDGTs

At QT, brGDGTs dominate with 80% the total distribution of GDGTs, with the remaining 20% made out by isoGDGTs (Figure 60). Even in the three measured surface samples, brGDGTs varied between 70% and 95%, with the remaining fraction representing relative isoGDGT input.

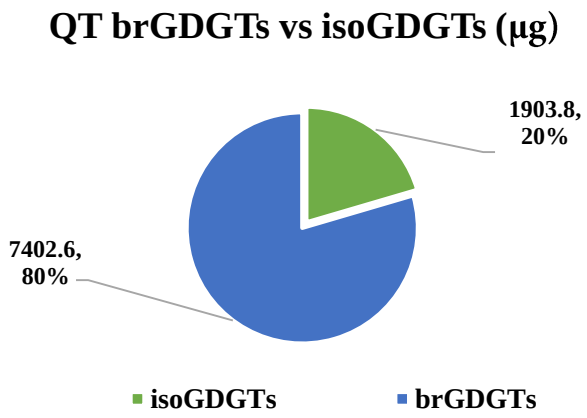

Figure 60 Iso- and brGDGT (green and blue, respectively) distribution at QT in surface and core samples.

In the brGDGTs fraction, brGDGT-Ia (Figure 58.8.) has the overall highest concentrations, representing 89.05% (i.e. 6592.14 µg/g) of the total brGDGTs. Its concentrations increase steady from 57.93 µg/g recorded in the clay samples to 120-128 cm where it peaks, reaching 1909.9 µg/g.

BrGDGTs –Ib and –IIa (Figures 58.9. and 58.10.) have the next highest concentrations, both peaking in surface samples with average concentrations of 151.34 µg/g and 469.75 µg/g, respectively. Although not shown in this section, brGDGT-Ic, -IIc, and –IIIa, also occur in all sample, with their summed concentrations of 78.09 µg/g, 5.08 µg/g and 28.06 µg/g, respectively.

Peat temperature calibrated through brGDGTs indicates the lowest value for the depth of 380-388 cm when it reached 22.08°C (±4.7°C). It increases slightly upwards and peaks at 27.43°C (±4.7°C) at 120-128 cm (Figure 58.11). Surface calibrated temperature is at 27.02°C (±4.7°C) whereas instrumental temperature was reported at 26.4°C (Teh et al., 2017).

Calibrated pHs and temperatures using brGDGT proxy proposed by Naafs et al. (2017a; see subchapter 1.7.2.3.). The GDGT-calibrated pH for the 410-420 cm sample has a value of 6.53 compared to 6.41 for the same depth given by the hopane-calibrated pH. The GDGT-calibrated pH continues to decrease to a value of 3.09 for a depth of 170-178 cm (Figure 54.12), and reaches 5.37 in the surface samples.

In terms of isoGDGTs, the highest concentrations are recorded for isoGDGT-0 (caldarchaeol), which represents 49.14% of the total isoGDGTs at QT. Its lowest values are recorded in the 410-420 cm samples and in the 120-128 cm sample, with concentrations of 4.6 µg/g and 8.08 µg/g, respectively. IsoGDGT-0 peaks in surface samples, reaching a concentration of 208.89 µg/g.

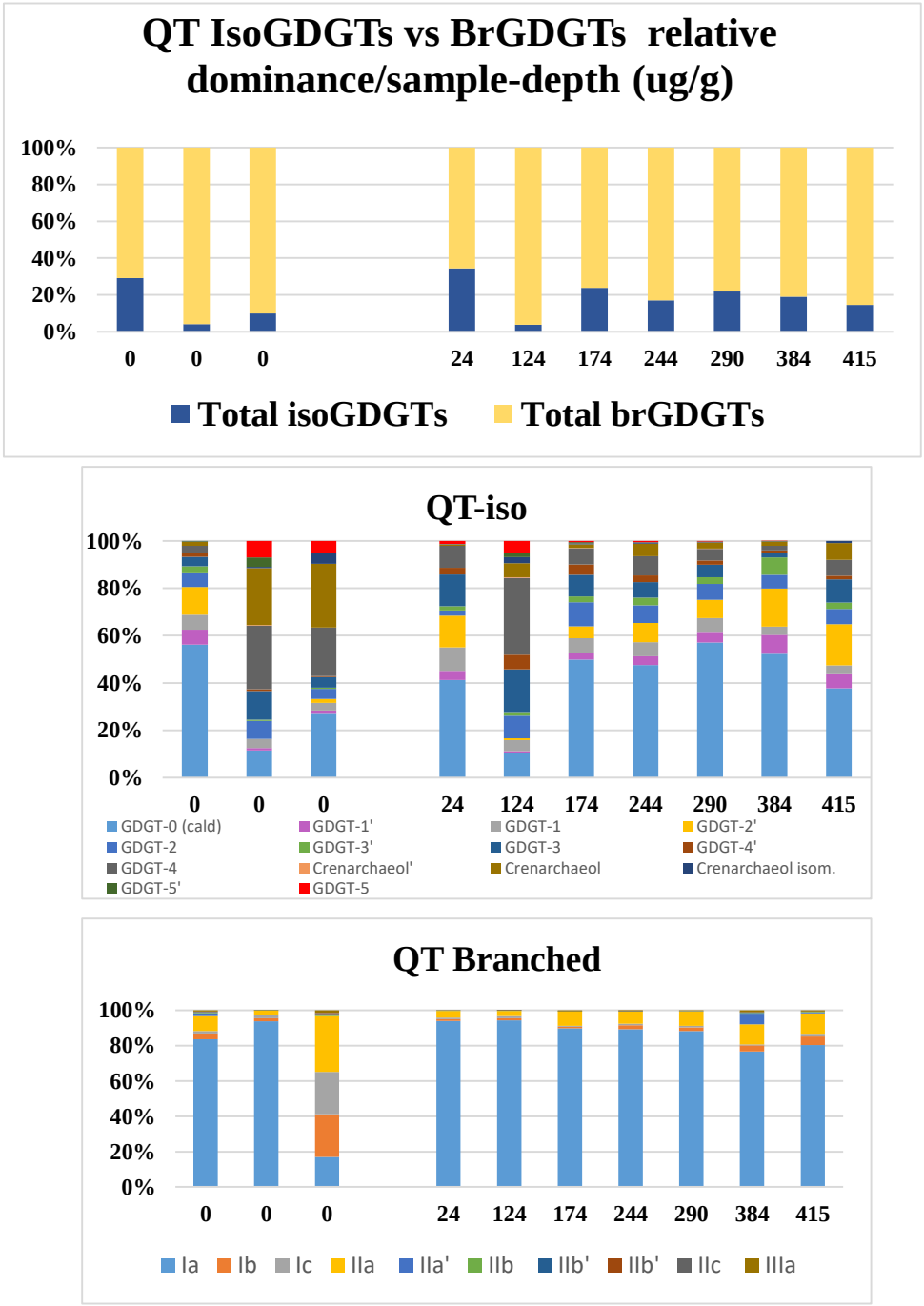

Figure 61 Relative isoGDGT and brGDGT input of GDGTs at QT with respect to each sample. Notice x axis corresponding to depth of sample in cm.

IsoGDGTs-1, -2, -3 and -4 have similar concentrations, mostly limited between 0 and 50 µg/g (Figure 58.1.-58.3.). IsoGDGT-1 and -2 appear to be coupled until the depth of 120-128 cm, peaking together at170-178 cm with values of 17.61 µg/g and 29.26 µg/g. After the depth of 120-128 cm, a decoupling

takes place, with isoGDGT-2 remaining fairly constant and increasing in the surface samples, while isoGDGT-1 initially increases at 20-28 cm then decreases, bearing the same average concentrations in the surface samples of 23 µg/g. IsoGDGT-4 reflects less changes depicted in isoGDGT-1 and -2 at depth, showing only a slight increase from the bottom of the core until the depth of 20-28 cm where it reaches its highest concentration of 38.13 µg/g (Figure 58.3.). IsoGDGT-3 shows the same concentration shifts as isoGDGT-1 and -2, however, at the depth of 20-28 cm it reaches a concentration of 54.89 µg/g, the highest between the four (Figure 58.3.).

IsoGDGT-5 is seen at all depths, apart from the organic-poor, clay-rich sample. Its concentrations are seen to increase steady towards surface, and range between 0.051 µg/g and 5.21 µg/g reached between 20-28 cm (Figure 58.4).

Crenarchaeol and its two isomers increase slightly from the bottom of the core, with the greatest concentration increase seen in crenarchaeol. Its concentration peak at the surface, at a value of 7.58 µg/g (Figure 58.5.).

Caldarchaeol/Crenarchaeol (Cald/Cren) fluctuates between high and low values, with the troughs recorded for depths of 410-420 cm, 240-248 cm and 120-128 cm (i.e. 5.29, 8.86 and 1.75, respectively). The ratio peaks at 20-28 cm with a value of 93.51. The methane index (MI) was multiplied by a factor of 100 in order to be plotted on the same graph as Cald/Cren. The lowest value is recorded in the surface samples, at 55.59 while the highest value for the same depth as Cald/Cren, 20-28 cm, where it peaks at 97.78 (Figure 58.6).

3.2.3. Hopanes

The main hopanes reported here are C_{27}-hop, C_{29}-hop and C_{31}-hop with their stereoisomers. Furthermore, diploptene is found in both surface and core samples, while hopanes αβ stereoisomers were not identified in surface samples (Figure 57).

For C_{27}-hop, ββ stereoisomers was found in all samples, and peaked at the depth of 120-128 cm, while for C_{29}-hop, the βα isomer and for C_{31}-hop, the αβ isomer peaked at that depth, displaying concentrations of 24.8 µg/g, 5.99 µg/g and 93.01 µg/g, respectively (Figure 57).

Diploptene is seen to increase steady towards the surface, peaking at a depth of 20-28 cm, at a value of only 9.75 µg/g, and showing a lower average value in surface samples, of 4.66 µg/g. However, at surface, values ranged between 2.89 and 7.01 µg/g (Figure 57.6.).

The calibrated pH based on the hopane-proxy proposed by Inglis et al. (2018), indicates a bottom core pH of 6.41 that is recorded in the organic-poor, clay unit and decreases upwards, towards more acidic conditions, reaching 3.95 at the depth of 120-128 cm. There is a slight increase at 20-28 cm to a pH of 4.175 (Figure 57.11.). Since the C_{31}-hop ββ isomer was not identified in surface samples, the depth of 20-28 cm represents most recent calibrated pH measurement for this core.

3.2.4. Fatty acids

Fatty acids (FA) were investigated in order to determine microbial community shifts, thus only short chain saturated, unsaturated and branched FA were analysed for QT (Figure 59). Their variations in concentration with depth are presented in Figure 59, and for most, due to higher concentrations in surface samples that hindered changes at depth, their concentrations were multiplied by a factor of 2.5 and plotted on the same graph (i.e. orange plot). There appears to be a decoupling between the saturated and branched FA correspondents. For example, C16:0 shows multiple shifts in concentration at depth and its trough are mirrored by peaks in the branched FA. Similarly, C14:0 is seen to decrease in concentration between 120-128 cm and 20-28 cm while isoC14:0 is seen to increase between these depths.

Between C14 and C17, even numbered FA dominated the fraction. The highest concentration in this range is recorded by the C16:0, that peaks in the surface samples with a value of 184.9 µg/g (Figure 59.6.), followed by C14:0, with the highest concentration of 27.43 µg/g at surface.

Between the monosaturated FA, C18:1ω9 shows changes in concentrations with depth, peaking with 21.58 µg/g at 120-128 cm, while C18:1ω7 does not vary greatly in concentration, ranging only between 0.02 and 5.38 µg/g (Figure 59.11).

Table 7 Summary of QT results and observations.

Palaeoenvironment	Interpretations and observations
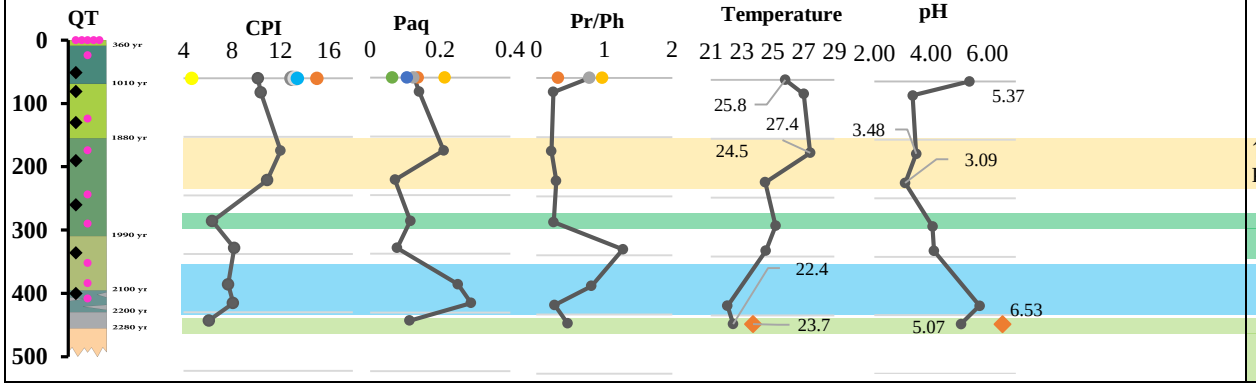	↑ CPI (high conservation) Paq~0.2; Pr/Ph<1 (anoxic) ↓↓ CPI (low conservation) Paq<0.2(terrestrial); Pr/Ph<1 (anoxic) → herbaceous taxa Lake-like environment; ↑Paq Non-peat forming environment (soil); notice sharp ↑ in CPI, ↓in Pr/Ph and pH (diamond)
Aerobic bacteria vs archaea (concentrations in μg/g)	
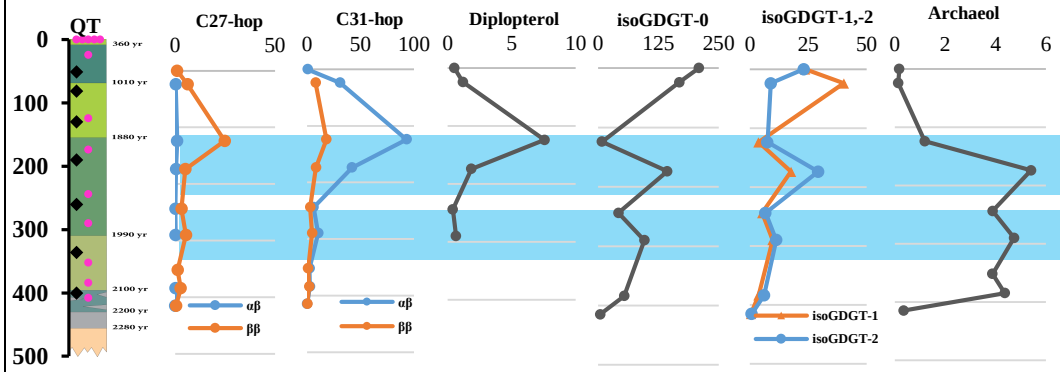	↑ aerobic bacteria; ↓methanogens ↓methanogens
Methane efflux potential (source/sink)	
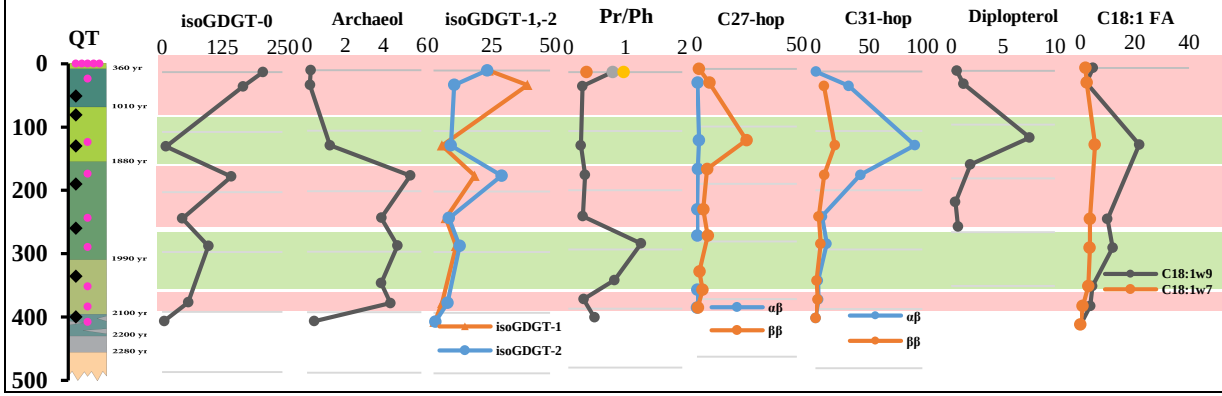	Potential CH_4 source Potential CH_4 sink Potential CH_4 source Pr/Ph↑ oxic; ↑hopanes and C18:1 FA; Potential CH_4 sink Potential CH_4 source

3.3. Interpretation

Zone QT-1 (410-420 cm) – 2280- 2200 cal yr BP

- **n-Alkanes**

The bottom of QT core has a P_{aq} that records lacustrine palaeoenvironmental conditions (P_{aq}>0.12), supporting the pollen record (Roucoux et al., 2013). The organic matter input was probably, in part, from emergent macrophytes that grew at the site (Ficken et al., 2000; see subchapter 1.6.1.2.). CPI has a relative low value indicating more labile, easily degradable organic matter sources (Andersson and Meyers, 2012), with ACL peaking at this point together with P_{wax} and given the different palaeoenvironment and composition of this sample, the peaks can be interpreted as different environmental conditions than in further pollen zones. The Pr/Ph ratio shows lower values than up-core, below 0.5, indicating anoxic conditions (Zulkifley et al., 2015). Individual n-alkane concentrations are low, dominated by short chain n-alkanes (i.e. n-C_{17}, n-C_{18}, n-C_{19}, n-C_{20}) however, extending up to n-C_{39}, indicating allochthonous input, suggesting that although the palaeoenvironment was a lake-like setting, higher plants were present in the area, and provided organic matter to the lake. The bottom of the lake was probably anoxic, however, microbes are expected to survive closer to the surface.

- **GDGTs**

In terms of GDGTs concentrations, we see very low values in the silty-clay sample that indicates that both brGDGTs and isoGDGTs may be autochthonous in nature (i.e. not carried-in by floodwaters). Because the palaeoenvironment for this depth was most likely a lake-like setting (P_{aq}), with open and well-oxygenated waters at the surface (Zheng et al., 2015 and references therein), there was minor production of both br- and isoGDGTs. Crenarchaeol and the two isomers have also a small input, suggesting no contribution from ammonia-oxidizing Thaumarchaeota (Schouten et al., 2013 and references therein). However, in a different study in the area, part of the offset in MBT and CBT-based temperatures recorded by Amazon's deep-sea fan was attributed to in-situ river production of br-GDGTs rather than to soil erosion (Zell et al., 2013a; Zell et al., 2014 and references therein), thus, Amazon floodwaters may deliver a small quantity of brGDGTs to these peatlands. The GDGT-calibrated pH (Naafs et al., 2017a) for this depth is slightly too acidic than expected, with a value of 5.06 (±0.8), indicating a mix between atmospheric precipitations and river floodwater, with a higher input from the former. GDGT-calibrated

temperature (Naafs et al., 2017a) is again lower than expected, at 22.45°C (±4.7°C). However, the calibrations used here are peat-specific, thus for this clay-rich sample, a lake- or soil-based GDGT calibration would probably yield more accurate results. For example, the soil CBT and MBT calibrations proposed by Weijers et al., (2007a) result in a 23.74°C temperature while the pH is again, slightly higher, at 6.53 that are more characteristic of the assigned palaeoenvironment (diamond-shaped plots in Figures 58.11. and 58.12.).

- **Hopanes**

The oxygenated surface waters could have allowed aerobic bacteria to develop yet there is also a high possibility of allochthonous hopane input-this distinction is probably best seen in the co-occurrence of αβ, ββ and βα isomers for the same depth, that indicate a mix between mature and immature organic matter. However, the hopane-calibrated pH has the highest value, of 6.4 (±1.4), indicating different environmental conditions than the one that influenced and sustained the formation of peat up-core. This also correlated to the GDGT calibration of Weijers et al. (2007a), a value of 6.53 and indicating the presence of microbes in the water column.

- **FA**

Similarly to previous biomarkers, most short-chain FA have low concentrations in QT-1 pollen zone (Figure 59). Saturated FA seem however to dominate compared to unsaturated and branched, indicating well preserved organic matter and the lack of degradation after this point. BrGDGDs are also found in reduced concentrations at this depth and thus, saturated FA can represent components of the anaerobic bacteria community.

Zone QT-2 (380-388cm) – 2200-2100 cal yr BP

- **n-Alkanes**

The increase in CPI from the previous sample indicates the onset of peat accumulation, low decomposition rates and thus, high water tables and anoxia. This only in part supports the palynological interpretation that the the peatland periodically flooded (Roucoux et al., 2013), with the possibility of a marginal lacustrine environment formation. P_{aq} ratio peaks in QT-2, indicating higher input from aquatic plants, with values of 0.28 (Figure 57.2), strongly indicating emergent macrophytes and a pool formation at the site. The organic matter of mainly aquatic sources accumulated at the bottom of the lake, leading to oxygen depletion and lack of decay. Roucoux et al. (2013) identified pollen of plant species of floating mat

vegetation or marginal fen, with floodwater delivered to the site from the Amazon, confirming this biomarker signal. ACL and P_{wax} values decrease, indicating higher humidity and precipitations that in this case correlate with P_{aq} and a pool development scenario. Overall, mid-chain n-alkanes have high concentrations at this depth, dominated by n-C_{21}. Long-chain n-alkanes with an odd distribution also show an increase, indicating as in the previous sample the presence of higher plants at the site, now with a relatively higher input. Pr/Ph ratio (Figure 57.5) indicates highly anoxic conditions at the bottom of the pool where organic matter accumulated, conditions that occur in fen and *Cyperaceae* habitats (e.g. Lawrence and Zedler, 2011; Roucoux et al., 2013).

- **GDGTs**

All plotted brGDGTs and isoGDGTs show a 4 to 6-fold increase in concentrations at this depth, indicating again waterlogged and anoxic condition (Figure 58). At QT, this indicates the conditions recorded by the organic matter that accumulated at the bottom of a lake-like setting, with a high possibility of well-oxygenated surface waters (Roucoux et al., 2013).

IsoGDGTs

There is an increase in the Cald/Cren ratio and MI that reach values of 29.35 and 85.4, respectively (Figure 58.6). This is due to the relative higher increase in Caldarcheol (i.e. isoGDGT-0) that is a potential biomarker for methanogenic archaea (Schouten et al., 2013 and references therein). Together with the high MI value (i.e. 85), they indicate the onset of CH_4 production and, consequently, the potential for CH_4 consumption (Zhang et al., 2011). Indeed, we see an overall increase in isoGDGTs 1-4 that could suggest development of CH_4-consuming archaea (i.e. ANME-1 phylogenetic group), an increase in isoGDGT-0, a methanogen biomarker (caldarchaeol), that is again correlated to the potential presence of methanotrophic Archaea but only a small increase in crenarchaeaol despite favorable occurring conditions (i.e. warm temperatures, Scouten et al., 2000; Zhang et al., 2006). The relatively low concentration of crenarchaeol, which was found in other peatlands (Pancost and Sinninghe Damsté, 2003; Zheng et al., 2015), suggests that there was little input from other archaea sources and that the site was mainly anoxic, with little potential for oxygen-demanding archaea (i.e. oxidising Thaumarchaeota) to develop. Thus, lake waters were poorly oxygenated or unable to support crenarchaeol-producers development.

Moreover, the presence of abundant biomarkers of potential CH_4-consuming microbes (i.e. isoGDGT 1-4), indicate CH_4 production was likely in the environment at this time. Archaeol concentrations (Figure 58.7) also increase at this depth (i.e. from 0.36 to 4.36 µg/g)

supporting the interpretation of an increase in or establishment of a methanogen community. The increase in archaeol is comparable to brGDGT and isoGDGT increases, with values that are 12-times higher than recorded in the clay unit below.

The presence of isoGDGT-5 in this pollen zone is characteristic of a pH acidic, ombrotrophic peatland (i.e. pH < 5.1) (Naafs et al., 2018b). Indeed, the GDGT-calibrated pH for this depth was calculated at 5.7 (±0.8) for the inferred lake-like setting, indicating possible allochtochonus isoGDGT-5 input from flood waters (Zell et al., 2014) or a calibrated pH that should take into account the lower error (-0.8, pH~4.9). Furthermore, given that these values are recorded in a peat sample that represents a period of approximatively 264 years (i.e. peat accumulation rate between 260-395 cm was calculated at 3.30 mm/yr and the sample spans 8 cm), it is expected to see fluctuations in dominant water sourcce between river and atmospheric precipitation over this time frame, even within a lake-like setting. Thus, floods might not have been so frequent or floodwater might have been shed faster than today (i.e. higher peat permeability, higher hydraulic conductivity surrounding the lake).

BrGDGTs

BrGDGTs at this location show a relative increase from the previous sample, which should be expected between a clay-rich sample (QT-1) and an organic-rich one (i.e. peat). Plotted brGDGT-Ia,-Ib,-IIa show increasing concentrations, thus higher input from anaerobic bacteria (Schouten et al., 2013) in these anoxic and warm settings (Figure 58.8.-58.10.; Zheng et al., 2015).

Also, for this depth we see input from brGDGT-IIa', -IIb' (i.e. with an additional methyl radical at the 6th C position, see De Jonge et al., 2013) which would suggest again relatively higher pH than in the rest of the peat column (Naafs et al., 2017a and references therein, Zheng et al., 2018). This is also supported by geochemical and pollen evidence, which suggest input from sediment-laden Amazon river occurred at this time (Roucoux et al., 2013; see subchapter 3.1.1.).

- **Hopanes**

The first increase in hopanes is seen most predominantly in diploptene, ββ C_{27}-hop and αβ C_{29}-hop and can be due to the establishment of the first bacteria community. The fact that at a depth of 384 cm (i.e. QT-1) the ββ biological form of the C_{27}-hop stereoisomer is still found, can either imply that organic matter did not undergo complete thermal maturation (i.e. that the ββ configuration is stable for the physio-chemical conditions at depth for QT) or that ββ C_{27}-hop might be produced in-situ, after anoxic conditions were established (i.e. potential

archaea source). As previous stated, hopanes can also be produced by facultative and obligate anaerobs (e.g. Fischer et al., 2015) and this correlates with evidence from br-GDGT data that also increases at this depth and led to an inferred increase in the anaerobic bacteria component (see subchapter 1.7. 2.2.). No ββ isomer of the C_{29}-hopane was identified; however, both stable configuration αβ and βα of C_{29}-hop were identified for this depth which could possible suggest a higher degree of microbial-mediated "maturation" and chemical stability recorded through the C_{29}-hop (i.e. rather than through C_{27}-hop) within this acidic environment (Huang et al., 2015 and references therein). C_{31}-hop shows lower concentrations relatively to up-core values, however, it shows an increase from the previous depth, and both ββ and, the thermally mature αβ stereoisomers are found, leading to a pH value of 5.37 (±1.4). Overall, the bacteria community (either aerobic and/or anaerobic) seems to increase in size at this point and, as the palaeoenvironment was characterised by seasonal floods (Roucoux et al., 2013). The existence of an aerobic peat layer at the surface during the dry season could have allowed (facultative) aerobic bacteria to develop over the course of 20-25 years, even in aerobic microsites around roots during the wet season (Naiman et al., 2010; Smith and Luna, 2013).

- **FA**

At this depth, all represented FA increase in concentrations with the onset of peat deposition. The peak in aC15:0 indicates an increase in gram positive bacteria and more specifically, in aerobic bacteria (Table 2). However, interpreted in the same context with GDGTs, pollen record and up core changes, the increase in concentrations can be a consequence of flooding, higher inorganic sediment input at this depth (i.e. the increase in organic matter was only up to 75% with white water input from Amazon, Roucoux et al., 2013) and thus, higher nutrient input compared to periods of waterlogging. Both proposed biomarkers for type II methanotroph are seen to increase, indicating the potential for CH_4 oxidation even at early stages of QT peatland development. Crenarchaeol also increases in concentrations, thus the water table could sustain a relative stable bacteria community between flood events. Compound specific isotope analysis for this depth would be a good indicator of the early bacteria communities and CH_4 oxidation potential as it is also advantaged by a thin peat deposit with potential little available substrate for methanogenesis.

Zone QT-3 (348-356 cm) 2100-1990 cal yr BP

- **n-Alkanes**

A spike in short-chain n-alkanes indicating continuous input of aquatic plants characterizes this pollen zone. The CPI value decreases implying a vegetation change with input from both terrestrial and aquatic species (also increase in P_{aq} and P_{wax}). The site was probably still dominated by the presence of a pool (i.e. P_{aq} of 0.25). The increase seen in Pr/Ph ratio indicates subanoxic conditions (>1) that contradicts the pollen record interpretation (QT-3) of a permanently waterlogged forest (Roucoux et al., 2013). As P_{aq} implies the existence of a pool at the site, the water could have had a higher percentage of dissolved oxygen (subanoxic). If the peatland was waterlogged and mainly anoxic, the signal can however be due to the aerenchyma adaptations of plants, possible allowing the oxidation of phytol (Blumer et al., 1963) and apparition of *M. flexuosa* at the site (Roucoux et al., 2013; see subchapter 1.5.2.). The ACL ratio has the lowest ratio, indicating vegetation adapted to increased precipitation thus in this case, to permanent waterlogged conditions.

Short-chain n-alkanes dominate at this depth, with n-C_{18} and n-C_{19} reaching concentrations of 81 and 78 µg/g respectively. This suggests the recalcitrant potential of biomarkers, as short chain n-alkanes can be easily degraded (e.g. Singh et al., 2011), and the overall low maturity of peat.

- **Hopanes**

In QT-3 zone, all hopanes apart from βα C_{29}-hop show decreasing concentrations. This can be related to the shift in the hydrological regime that changed from seasonal floods to permanent waterlogged conditions (Roucoux et al., 2013). The relative decrease can be attributed to the overall lack of oxygen that could have restricted the aerobic bacteria community only around root networks. Furthermore, the presence of hopanes during predominant anoxic conditions with concentrations higher than present day when the water table is above surface all year round (Teh et al., 2017), can support the possibility of hopane input from anaerobic bacteria (e.g. Härtner et al., 2005; Sinninghe-Damsté et al., 2004). However, as the brGDGT sample could not be analysed for this depth, less can be inferred about the anaerobic bacteria community. The increase in βα C_{29}-hop, which is not the most stable configuration can either suggests that the ββ C_{29}-hop stereoisomer was chemically altered to the βα configuration and/or that the βα C_{29}-hop also acts as the precursor of chemically altered extended hopanes (>C_{30} from BHPs, Inglis et al., 2018 and references therein) although this assumption needs further investigation in these settings. The hopane-

calibrated pH for this depth is 4.61 (±1.4), slightly lower than at the previous depth, indicating a higher input from atmospheric precipitations that also probably supported the permanently waterlogged conditions.

- **FA**

The decrease seen in FA at this depth can be again related to an increase in flooding frequency, sediment input and waterlogged conditions, with less available oxygen. The presence of an anoxic pool indicated through a high P_{aq} (i.e. 0.25) probably restricted the producers of short chain FA, as at this location medium and long-chain FA that indicate vegetation input increased in concentrations (data not displayed).

Zone QT-4a (294-286 cm)

- **n-Alkanes**

Between the depths of 294 and 286 cm (i.e. approx. 35 years), the organic matter input was a combination between aquatic, with evidence of lipids from microbes (i.e. n-C_{16} to n-C_{21}; Dinel et al., 1990), and vascular plants which are detected through the dominant odd over even long-chains n-alkane signal (Figure 56). There is also a decrease in the CPI ratio, suggesting a higher input from non-vascular species however, at this depth P_{aq} decreases below 0.1, bearing a strong terrestrial signal, indicating the retreat of the open pool from the site towards the end of the 8 cm sample span (see subchapter 6.2.1. for extrapolated ages). Pr/Ph ratio increases towards subanoxic values (i.e. >1) indicating either a dynamic water table or/and a constant acrotelm. An increase is also seen in ACL and P_{wax} values that suggests hot and drier conditions however, given the tropical setting with constant temperatures and precipitations regimes, this can also be related to higher plants expansion at the site, seen as an increase in the concentration of n-C_{31} from the previous depth. As it was depicted through pollen analysis (Roucoux et al., 2013), these proxies indicate a flooded forest, however biomarker data indicate that the flooding regime was most likely seasonal as seen through the increase in the Pr/Ph ratio to subanoxic values and ACL and P_{wax} that could indicate a higher frequency of dry events.

- **GDGTs**

Overall, there was relatively higher input of isoGDGTs (Figure 58) than in the previous discussed sample, indicating a larger and more active methanogenic archaea community supported by periods of higher water tables and anoxia.

isoGDGTs

The steady increase in isoGDGT-0 (caldarchaeol) can indicate either higher or consistent input with time from methanogenic archaea at this depth (Kates et al., 1993; Pancost and Sinninghe Damsté, 2003) or input from non-methanogenic crenarchaeota (Schouten et al., 2000). Crenarchaeol concentrations also increase from previous depth, suggesting that crenarchaeota is a possible contributor to isoGDGT-0 concentrations. However, within the same sample, archaeol indicates the same slight increase, confirming methanogen origin or a higher methanogenic community than in the previous samples (Zheng et al., 2015; Pancost and Sinninghe Damsté, 2003; Naeher et al., 2014).

A similar increase, however, relatively more pronounced, is seen in isoGDGTs 1-4, which indicates an equal development in the anaerobic methanotroph euryarchaea, which is associated with the occurrence of methanogenic euryarchaea (Weijers et al., 2004).

The MI value is similar to the previous sample, indicating a sustain level of CH_4 production, while the Cald/Cren ratio decreases due to a relatively higher input of crenarchaeol supraimposed on the slowly increasing background of caldarchaeol (isoGDGT-0).

brGDGTs

Only brGDGD-Ia shows a slight increase, while the next most abundant isoprenoidal GDGTs (-Ib and –IIa) show a slight decrease in concentrations. This could indicate minor shifts in the active anaerobic bacterial community as the increase in isoGDGT-Ia still suggests anoxic conditions (i.e. waterlogging). This slight decrease in the less abundant isoGDGTs also highlights the relative small accumulation overtime of brGDGTs (i.e. palaeosignal) as they are less prone to oxic degradation than isoGDGTs (Schouten et al., 2013 and references therein).

The calibrated pH value is 5.72 (±0.8), which is consistent with periodic flooding of the area, however, it also the highest value in this area, suggesting a shift in the environmet after this point. The calibrated temperature is at 22.08°C (±4.7 °C).

- **Hopanes** (discussed for depths 290, 244 and 174 cm)

Between 290 cm and 174 cm, which covers 3 samples (i.e. depths 286-294 cm, 240-248 cm and 170-178 cm; QT-3, QT-4a, QT-4b) not much variation is seen in the concentration of hopanes at QT, apart from a sudden increase in the αβ C_{31}-hop at the depth of 174 cm. During this time, based on pollen records (Roucoux et al., 2013), the environment oscillated from flooded woodland to waterlogged conditions with herbaceous taxa and again to a seasonally

flooded forest. However, these changes were not depicted in the hopane record, leading to the possibility that the presence of floods and waterlogged conditions restricted the development of an aerobic bacteria at the site. The anaerobic bacteria community, as seen from brGDGTs shows a decrease at a depth of 244 cm that is also depicted in ββ C_{27}-hop, βα C_{29}-hop and αβ C_{31}-hop implying again anaerobic bacteria as a possible source for hopanes (e.g. Härtner et al., 2005; Sinninghe-Damsté et al., 2004), a signal that is again seen at shallower depths within the same peat core. In addition to this, the increase seen only in αβ C_{31}-hop mirrors the increase seen in the brGDGT-Ia. The calibrated hopane-based pH for this section was between 3.9 and 4.8 (±1.4), confirmed by the overall acidic character of QT at present.

- **FA**

With the shift in hydrology towards a flooded regime, there is again an increase in most short-chain biomarkers, however, at this depth, floodwater was described as sediment poor (i.e. black water, Roucoux et al., 2013) from Itaya river. Water replenishment within the peatland could also have had an impact due to input of oxygen-rich river water compared to the former standing water under waterlogged conditions (e.g. Venterink et al., 2003; Morales-Olmedo et al., 2015). Furthermore, a flooded regime implies periods of higher and lower water tables, allowing acrotelm development during the dry season.

Zone QT-4b (240-248 cm)

- **n-Alkanes**

This depth sees a decrease in short chain n-alkanes concentration while the long-chain n-alkanes only decrease slightly. CPI decreases at this depth showing relatively higher input from even n-alkanes compared to the long-chain odd n-alkanes and, based on overall lower concentrations, less well-preserved organic matter. Pr/Ph ratio decrease below 0.5 indicating highly anoxic conditions which, correlated with the decrease in non-vascular and aquatic plant input (i.e. P_{aq}=0.11), lead to the interpretation of permanent waterlogged conditions. The ACL and P_{wax} also show relatively lower values suggest wetter conditions.

Roucoux et al. (2013) proposed two scenarios for this depth and shifts in vegetation: i) either a reduction in flood frequency and depth that led to a tree mortality and herbaceous dominant vegetation or ii) the previous woodland vegetation replacement by fen or floating mat vegetation with the development of a pool. Biomarker data seems to indicate that the first

scenarios is more likely due to: a decrease in n-alkanes and the P_{aq} ratio; no n-alkane signal from higher plants; biomarker and pollen evidence decoupling compared to the previous depth of 380-388 cm aquatic setting; aerobic setting expressed through a relatively high Pr/Ph ratio, which was not seen during the previous pool development, indicating oxic condition and an increase in Crenarchaeol indicating a periodic occurrence of an acrotelm, discussed below.

- **GDGTs**

All plotted GDGTs, apart from crenarchaeol show decreasing trends, suggesting lower water table depths, a thicker acrotelm and anaerobic activity restricted to possible anoxic microsites. Indeed, microbial communities seemed to have reacted to pollen-inferred environmental changes as expected as this sample comes from a section that is here interpreted as characterized by decreased flood depths and frequencies, tree mortality and replacemnet by herbaceous taxa (Roucoux et al., 2013).

IsoGDGTs

IsoGDGT-0, which indicates methanogenic archaea input (Pancost and Sinninghe Damsté, 2003), shows a significant 2-fold decrease suggesting that CH_4 production was reduced. This can be due to a lowering in water table depth that restricted the methanogen community to horizonts already depleted in substrate (Zheng et al., 2014 and references therein). This interpretation is also supported by a relative increase in crenarchaeol, which is representative of mainly archaea communities living in oxygen-rich settings and thus indicates a drier period (Zheng et al., 2015 and references therein). Finally, archaeol is also seen to decrease in concentrations (i.e. from 4.74 to 3.89 µg/g), supporting this argument. IsoGDGTs 1-4 show similar decreasing trends suggesting that methanotroph archaea community also decreased in size since there was less CH_4 available for consumption.

MI values also indicate lower values, under 80, but these values suggest that CH_4 was still produced at lower depths and some consumed at surface.

BrGDGTs

BrGDGTs indicate that anaerobic bacteria responded to less anoxic conditions and then decreased as seen in brGDGT -Ia, -Ib and -IIb, which mirror that of isoGDGTs. It is interesting that biomarkers specific to the aerobic bacteria community (i.e. hopanes, diploptene, diplopterol) did not increase in concentration in this sample (Figure 57). As there is no major geochemical shift at this time (Lawson et al., 2014), this may be due to a limited

community of aerobic bacteria in the area given the previous waterlogged conditions or to competition between anaerobic and aerobic methanotrophs over lower CH_4 and poor substrate availability (i.e. provided by herbaceous taxa). As part of the CH_4 is also consumed in the anaerobic part, this period and consequently, biomarker concentration, might be specific to lower CH_4 effluxes. $\delta^{13}C$ signatures of methanotroph related biomarkers are expected to be enriched (less negative) than at the previous depth if less CH_4 was available, and if microbes consumed other substrates at this time.

The GDGT-calibrated pH value (Naafs et al., 2017a) is lower than expected for such an environmental shift, at 4.05 (±0.8) as drier surface conditions would result in less organic acid production (e.g. Clymo, 1984). The pH calibration made using hopanes (Inglis et al., 2018) bears a higher value of 4.8 (±1.4), the highest within the peat column for this calibration and the two values are within error of each other. However, both pH values indicate atmospheric precipitation input was probably constant and no drier period was reported around 1800 cal yr BP (see subchapter 1.6.1.3.).

Temperature calibration holds a value of 25.19°C (±4.7°C), the highest until 170-178 cm, which can explain the correlations between a lower water table, low pH and lack of evidence for a dryer period. Thus, a higher temperature would imply higher rates of evaporation during the wet period which would allow the pH to remain acidic. The presence of herbaceous vegetation and thus lack of penetrating roots (i.e. decrease in n-alkanes across all ranges) at this depth also implies less root exudates for methanogenesis. Several studies discussed the importance of root systems in soil and peats (Huguet et al., 2013; Ayari et al., 2013) in enhancing brGDGT production. As roots extend in the toposoil (i.e. below surface), they create the microbial active (and frequently anoxic) rhizosphere (Huguet et al., 2013 and references therein), enriched in substrate. Thus, herbaceous vegetation could not provide required substrate for both anaerobic and aerobic communities, hence the reduce signal from hopanes. One further implications is that, although trees did not grow at this stage, forested and palm swamp vegetation types that occurred upcore (see subchapter 3.1.4.) were expected to have root systems extending down to this depth and lead to further increase in substare and methanogenesis (i.e. increase in isoGDGT-0) however, this is less visible in the biomarker data and thus serves as a proof for the ability of biomarkers to depict palaeoenvironmental signals in these settings (i.e. ruling out continuous accumulation).

- **FA**

At this depth, short chain FA do not provide significant information on environmental changes, with only C14:0, isoC16:0 and C17:0 increasing slightly in concentrations. However, no iso- and anteisoC17:0 were identified for this depth, possible supporting the interpretation of a lack of substrate for bacteria and a restructuring of the microcommunity. Furthermore, only C18:1ω9 biomarker mirrors concentrations changes seen in other FA while C18:1ω7 remain almost constant until the surface.

Zone QT-4c (170-178cm)

- **n-Alkanes**

In terms of n-alkanes, this depth is characterized by a high input from higher plants (i.e. vascular), with an odd over even predominance of long-chain n-alkanes. This indicates the re-establishment of the forested vegetation which is also supported by increases in CPI, ACL and P_{wax} proxies. The low Pr/Ph ratio and decrease in P_{aq} indicate anoxic conditions, probably waterlogging or periodic flooding also implying the adaptation of current vegetation to the lack of dissolved oxygen and high water tables. There is also an increase in the relative input of n-alkanes $>C_{33}$, however, n-C_{36} and n-C_{38} dominate in this range (Figure 56). Since longer n-alkanes are more resistant to microbial degradation (Singh et al., 2011), it can indicate the development of new vegetation species (i.e. high ACL; see subchapter 1.7.1.4.) under the already developed canopy.

- **GDGTs**

The recovery in all GDGTs concentrations at this depth again supports the re-establishment of previous wet, waterlogged and anoxic conditions. Most microbe-related biomarkers indicate relative fast increases, suggesting microbial community recovery. These trends support the pollen interpretation of a seasonlly flooded woodland with closed canopy and flood waters delivered by the Itaya River (Roucoux et al., 2013).

IsoGDGTs

All isoGDGTs have higher concentrations than in the previously flooded environment (i.e. depth 294-286 cm), seen as a first peak in the data (Figure 58). It is most possible that the spike seen in isoGDGTs is a palaeosignal, indicating the highest methanogenic (isoGDGT-0) and anaerobic methanotrophic (isoGDGT 1-4) community at this location up to this point.

The higher relative increase in isoGDGT-1, -2 and -3 compared to -4 that had not occurred until this point could be due to responses in different producers (i.e. if different sources) as dictated by competition. Archaeol peaks at this depth, suggesting a well-established methanogenic community and high CH_4 production. Crenarchaeol maintains its previous high values, signifying that thaumarchaeota managed to cope with shifts in the environment, however it might be restricted to peat's (palaeo)surface. Water table oscillations at this depth (and in the above peat sections) were probably limited to a shallow depth below surface since isoGDGT are more prone to degradation in the presence of oxygen (Zheng et al., 2015 and references therein).

MI values increase again to 92.8 representative of overall high CH_4 production and incorporation.

BrGDGT

Although brGDGTs decay slower than isoGDGTs, their concentrations show a less proeminent increase, suggesting that the recovery of the anaerobic bacteria community did not matched the increase in anaerobic archaeal community. Furthermore, there is a decrease in brGDGT-Ib relative concentration, possible indicating competitive relationships. The calibrated pH is the lowest for this peatland, at 3.08 (±0.8), suggesting an increase in precipitation in the area. The calibrated temperature is at 24.5°C (±4.7°C) and this slightly lower value could have been influenced by vegetation type that provides shading (i.e. closed canopy).

- **FA**

The FA sample for this depth was not available for the final analysis.

Zone QT-5 (120-128 cm) 1010-360 cal yr BP

- **n-Alkanes**

At this depth, there is an increase in the input of shorter chain n-alkanes with n-C_{19} dominating in this range and a slight decrease in the long-chain n-alkanes. The Pr/Ph ratio indicates overall anoxic conditions while the P_{aq} increases above 0.2 implying emergent macrophyte input and a lake-like setting development. However, due to the strong odd to even dominance of long-chain n-alkanes the main vegetation was probably forested and under waterlogged conditions, allowing macrophyte development in short-lived, localized

pools. The CPI peaks at this depth suggesting sustained input from terrestrial vegetation while the decrease in ACL and P_{wax} might be due to apparition of different vascular vegetation species.

- **GDGTs**

During this period, there is a relatively very low input from isoGDGTs (less than 5% of the total GDGTs in this sample) which could potentially suggest the lack of substrate for methanogenesis (i.e. humified herbaceous taxa) or that there was a substantial re-arrangement in the microbial community during the previous drier event (i.e. grass development; no sample available; see Roucoux et al., 2013). As in the previously available sample, it follows a drier period during which the canopy was opened and the woodland vegetation (represented by the sample at 170-178 cm) was replaced by herbaceous taxa (similar to sample depth 240-248 cm; Roucoux et al., 2013).

IsoGDGTs

All isoGDGTs apart from crenarchaeol show decreasing concentrations. The most abrupt decrease is recorded in isoGDGT-0 (caldarchaeol) from previous values of 143 µg/g to 8.08 µg/g. This indicates a considerable decrease in methanogen community that caused a possible collapse in the immediate levels on the food chain (i.e. decrease in isoGDGT-1, -2 and -3 – anaerobic methanotrophs). This interpretation is also supported by low concentrations of archaeol of 1.19 µg/g. Although pollen analysis indicates vegetation adapted to permanent waterlogged conditions, the water table might have fluctuated, frequently oxygenating deeper horizons, not allowing a stable and continuous anaerobic microbial community to develop. This is to some extent also indicated through a constant concentration of crenarchaeol that is synthesized by thaumarchaeota living in oxic environments. IsoGDGT-4 shows increasing concentrations, however, without compound specific isotopic analysis and without having further samples from the same or adjacent depths, it is difficult to decide between the possible scenarios: i) either only certain anaerobic methanotrophs existed at the time with disappearance of previous species, leading to available niches (i.e. increase in isoGDGT-4); ii) isoGDGT-4 producer(s) might be facultative, growing on other carbon substrates than CH_4; iii) vegetation type influences (discussed below); iv) localized disturbance. There is also an increase in the concentration of isoGDGT-5, which was only found in peatlands with pH<5.1 and, although not much about the occurrence of this biomarker is known in peatlands so far (Naafs et al., 2018),

simultaneous increase in isoGDGT-4 and isoGDGT-5 (which continues in the above sample) might be due to either the existence of the same produces or to favorable conditions for both.

The MI reflects changes in CH_4 production, with a value close to the threshold of CH_4 oxidation (Zhang et al., 2011). It is possible that during this period the environment acted as a CH_4 sink, with further evidence coming from peaks in concentrations of C18:1ω7 and C18:1ω9 fatty acids, hopanes and diplopterol.

BrGDGTs

BrGDGT-Ia and brGDGT-Ib reach peak values at this depth – which supports the permanently waterlogged environment and anaerobic conditions (Sinninghe Damsté et al., 2000). This suggests that lower CH_4 production was the primary driver of isoGDGT -1 to -3 decrease and that methanogenesis decrease (i.e. isoGDGT-0 decrease) was possible a consequence of low substrate availability. Calibrate pH has a value of 3.47 (±0.8) while calibrated temperature is at 27.4°C (±4.7°C).

Another correlation can be made between vegetation succession at the site and fluctuations in overall GDGT concentrations. The previous decrease in isoGDGT (i.e. 240-248 cm) was noticed after the first appearance of *M. flexuosa* vegetation at QT while the current discussed decrease during the re-establishment of *M. flexuosa* at the site. *M. flexuosa* contains special adaptations to waterlogged conditions such as a thickened exodermis tissues that allow oxygen exchange between plant and environment (de Granville, 1969; see subchapter 1.5.2.) implying also oxygen leakage from roots into the anoxic environment (van Noordwijk et al., 1998). From 260 cm upwards, peat accumulation rates also started decreasing from 3.30mm/yr to 1.43 mm/yr and this depth yields concurrent increase in aerobic bacteria (i.e. hopanes, diplopterol, fatty acids). It is thus possible that the presence of *M. flexuosa* vegetation, although restricted to waterlogged environments, to provide enough oxygen through root diffusion in the anaerobic part of the peat to allow micro-oxic site formation (also crenarchaeol increases), and simultaneous aerobic and anaerobic bacteria decomposition (i.e. hopane and brGDGTs increase).

- **Hopanes**

All hopanes peak in concentration at this depth suggesting conditions favourable for the bacteria community. The palaeoenvironment was assessed as permanently waterlogged (Roucoux et al., 2013), thus it is hard to imagine a thicker anoxic layer to support aerobic activity. Furthermore, the concentrations are higher than at previous depths when water table oscillated during the wet and dry season, thus palaeohydrology cannot be considered the

main (or only) driver. As discussed above, due to prevailing waterlogged conditions, many plants could have developed aerenchyma tissues and in terms of vegetation, at this depth there was also an expansion in *M. flexuosa*, a palm species known to possess root pneumatophores for gas exchange (de Granville, 1969). The presence of these adaptations could explain the increase in aerobic hopane producers as oxygen could have travelled from the surface to the roots and create oxic microsites for in-situ CH_4 consumption (see subchapters 1.2.2. and 1.5.2.). Furthermore, anaerobic bacteria biomarkers (brGDGTs) also peak at this point, showing a positive relationship with hopane concentrations as seen before, suggesting that anaerobic bacteria can also be a source of hopanes. Another possibility for this overall increase is correlated to the peak seen in αβ C_{31}-hop. As the αβ C_{31}-hop is overall the most abundant hopane at this location, several studies argued that it can also come from BHPs biological hopanoids, after oxidation and decarboxlation reactions catalysed by the acidic environment (Ries-Kautt and Albrecht, 1989; Huang et al., 2015 and references therein). BHPs were not included in this study; however, this relationship can be explored further in these environments.

Finally, the hopane calibrated pH also shows the lowest value at this depth of 3.95 (±1.4), indicating high atmospheric input and waterlogging.

- **FA**

The peak seen in C18:1ω9 is also depicted in hopanes and brGDGTs implying a well-developed (aerobic and/or anaerobic) bacteria community. Again, it would be interesting to analyse the carbon isotope signatures for this depth as it is expected that the majority of hopanes will indicate a mixed signal or ^{13}C enriched while monosaturated FA could bear a less enriched signal, allowing thus the confirmation of monosaturated FA as biomarkers for type II methanotrophs in these environments. As type II methanotrophs are facultative, they could also consume CO_2, and ^{13}C incorporation could indicate the relative degree of CH_4 production.

Zone QT-6 (20-28 cm) 360 cal yr BP

- **n-Alkanes**

This depth is characterized by relative low input from short chain n-alkanes, and a dominant input from odd long-chain n-alkanes indicating terrestrial vegetation. The increase however in n-C_{32} from the previous depth (i.e. 24.6 µg/g compared to 9.32 µg/g) was correlated to

the increase in pollen from Davalliaceae *Nephrolepis* fern species, as this relationship was also seen at San Jorge peatland. The CPI decrease at this depth is due to the increase in the n-C_{32} concentration and subsequent decrease in n-C_{33} and can also indicate higher biodegradation. Pr/Ph ratio indicates anoxic, thus waterlogged conditions while P_{aq} suggests the presence of macrophyte vegetation due to an increase in n-C_{25}.

- **GDGTs**

At this horizon, isoGDGTs have the highest relative dominance, with almost 35% of the total GDGTs indicating a greater input from archaea.

IsoGDGTs

All isoGDGTs show an increased in concentrations (i.e. isoGDGT 0-5) with the exception of isoGDGT-2 and crenarchaeol. The increase in isoGDGT-0 indicated that methanogenesis resumed together with the re-establishment of anaerobic methanotrophy (i.e. isoGDGT-1,-3,-4), however archaeol concentrations remained low until the surface. The decrease in crenarchaeol indicates dominant anaerobic conditions-thus, the water table rarely decreased below surface. This is also supported by the fact that isoGDGTs-3 and -4 show decreasing concentrations in adjacent samples – suggesting that peaks seen in isoGDGTs at this depth are palaeosignals as isoGDGTs degrade faster under oxic conditions (Schouten et al., 2003 and references therein). Indeed, this sample comes from a period that did not experience any deep seasonal flooding, with the canopy closing under *M. flexuosa* (Roucoux et al., 2013). The cessation of deep seasonal flooding indicates that the site was mainly fed by rainwater.

MI peaks at this depth as crenarchaeol concentrations decrease – indicating strong CH_4 production and incorporation.

BrGDGTs

BrGDGTs show decreasing concentrations from previous depths, indicating a decreasing anaerobic bacteria community, possible due to competitive relationships with archaea.

Calibrated pH yields a value of 3.35 (±0.8) while calibrated temperature has a value of 27°C (±4.7°C).

- **Hopanes**

Apart from diploptene, which shows a slight increase in concentration, all hopanes decrease in concentrations indicating anaerobic conditions. Most values return to previous down core concentrations, suggesting that conditions that supported the previous increase in hopane

concentration at 170-178 cm and 120-128 cm and, consequently, in bacteria community, were unusual and require further investigation at those depths.

Diploptene initial increase is possible due to the persistence of *M. flexuosa* species at present that can reach depths of 24-30 cm (van Lent et al., 2018) potentially providing oxygen at depth. Furthermore, the present-day waterlogged conditions had a positive influence on the size of the anaerobic bacteria community as depicted through brGDGTs concentrations yet, at least at the surface, this is not reflected in concentrations of identified hopanes making the link between anaerobic bacteria and hopane distribution somewhat complicated.

The hopane calibrated-pH for this depth is 4.17 (±1.4), within the error range of GDGT-calibrated pH.

- **FA**

The decrease just before the surface in some FA can be explained through the simultaneous decrease in brGDGs and hopanes, as they return to previous values found downcore. The decrease is only experienced in short chain straight FA which are considered ubiquitous indicators of microbial biomass (Finean and Mitchell, 1981; Morgan and Winstanley, 1997). It is however not clear why the proposed methanotroph FA biomarker also decreases at this point. This suggests that CH_4 effluxes could have been higher during this period since the potential for CH_4 consumption was reduced.

Given the proximity to the surface and the relatively young age of peat deposits, biodegradation at FA level is probably reduced, and the decrease in concentrations can be seen as an environment and/or vegetation induced change. Furthermore, the lack of seasonal flooding (Roucoux et al., 2013) could also had an impact in terms of nutrient or dissolved oxygen input of various microbes on which methanogens and methanotrophs rely for substrate production, and thus cause a restructuring in their community as we see biomarkers indicative of gram-positive bacteria (i.e. iC14:0, aC15:0; Table 2) to increase at this depth

Surface

- **n-Alkanes**

Surface biomarkers can be correlated with present day conditions and vegetation. At present, vegetation at QT is dominated by *M. flexuosa, M. armata* and *Tabebuia insignis* palm trees that lead to the formation of woody peat (Roucoux et al., 2013). There are no reports of pools that could contain aquatic vegetation (i.e. n-C_{19} dominant concentration), however we see an overall higher input from short chain n-alkanes compared to odd long-chain n-alkanes.

This could suggest that input of short-chain n-alkane can be a common occurrence down core, however they are preferentially removed by microbial activity and degradation under oxic conditions (Singh et al., 2011). As the surface part of the peat is freshly deposited, the occurrence of undecomposed leaves fragments, rich in n-alkanes and FA, was incorporated into the analysed samples. The aquatic signal depicted in QT-1, -2 and -3, indicates well preserved vegetation at the bottom of a lake, compared to further terrestrial samples in which decay can take place. The CPI for the surface of QT, is at 10.15, relatively lower than the immediate down-core values, however this is due to incorporation of n-alkanes that were preferentially removed in downcore samples.

- **GDGTs**

BrGDGT-Ia, the most abundant GDGT in surface samples, is discussed in more details at BVA as having a potentially aerobic producer, *Acidobacteria* (Sinninghe Damsté et al., 2014). While a relationship is seen at BVA, this is not clear at QT (nor SJO). Here we see that the biomarker increases in concentration at surface, compared to the previous depth. Although a link can be made with the potentially oscillating nature of the water table at depth and relative easier degraded character of brGDGTs in the presence of oxygen, Teh et al. (2017) reported a positive (i.e. above surface) water table depth and smaller dissolved oxygen levels for the dry season, compared to the wet one (Taable 5). While this can be due to root oxygen intake or higher microbial community and oxygen consumption during the dry season and can affect the degree of brGDGT-Ia production from an aerobic source, the increase experienced in the concentration of this biomarker contrary to the oxygen-poor environment argues that an aerobic source for brGDGT-Ia is less possible and subjective to further investigation before applied downcore.

- **Hopanes**

The fact that diploptene does not reach trace concentrations at the surface while the ββ isomers are either very low in concentrations or unidentified can be due to varying competition relationships and various adaptations of hopane producers, implying multiple sources for this biomarker.

As only αβ C_{31}-hop was identified in the surface samples, pH values could not be calculated, however, for the dry season when samples were collected, Teh et al. (2017) reported a pH value of 5.49, within the error range of the pH value calibrated at 20-28 cm (i.e. 4.17).

- **FA**

All short chain FA increase in concentration at the surface indicating alteration downcore at least for the iso- and anteiso-isomers. The increase is greater for all saturated and branched biomarkers, however, the increase in C18:1ω9 is less than the peaks seen at approximatively 124 cm and 290 cm down-core. This should however take into account the fact that downcore samples consist of homogenised 8 cm of peat in depth, which represent approximatively 56 years between 0-260 cm and 24-25 years of deposition between 260-395 cm (Roucoux et al., 2013). However, since at the site the water table was reported above ground during the wet and dry season (Teh et al., 2017), the presence of bacteria- and methanotroph-proposed biomarkers during the dry season when dissolved oxygen (%) is also slightly lower (Teh et al., 2017), suggests adaptations of bacteria to low oxygen levels and high water tables (i.e. oxic microsites).

Implications of type II methanotroph biomarkers at QT

Compared to the following two peatlands, SJO and BVA, the diversity of monosaturated FA depicted through the DMDS method is limited. Thus, at surface we only found evidence of C18:1ω9t, c and C18:1ω7, while at depth no distinction could be further made, thus it is expected that only trans- isomers of the C18:1ω9 and C18:1ω7 were present, characteristic of type II methanotrophs (Table 2). Type I methanotrophs were only found in pollen zone QT-5b, where it is possible that a higher pH was recorded for a short period of time, or that type I could have developed in a pool-like setting. However, the lack of diversity in monosaturated FA does not necessary implies a lower methanotroph biomass, but it can be an indicator of a less diversified community able to grow on both CH_4 and CO_2 (Hanson and Hanson, 1996). As type II methanotrophs grow in acidic environments with CH_4 concentrations higher than atmospheric ones, it indicates active consumption of the CH_4 produced at QT.

3.3.1. QT peatland synthesis

One of the main characteristics of QT peatland is its anoxic character as depicted through values mainly below 1 for the Pr/Ph ratio (Figure 57.5), which is characteristic of wet tropical lowland peatlands (Zulkifley et al., 2015). This indicates that the site experienced high water tables and anoxic conditions that allowed peat to form and accumulate. Even in QT-1 pollen zone that is made up of lake-deposited clays, the Pr/Ph value is below 1, indicating that the lake at the time has anoxic bottom waters, which allowed organic matter accumulation. The anoxic character is maintained until pollen zone QT-4a, recorded between 296-152 cm, where we see a peak in Pr/Ph above 1 that indicate subanoxic conditions prevailed. The biomarker data suggests that the water table was more dynamic at this time, likely due to a seasonal flooding regime. However, above this depth, pollen zones show the same anoxic levels recorded in the lower part of the peat core, indicating the return of waterlogged conditions.

Further n-alkane based proxies indicate the presence of a lake-like setting for pollen zones QT-2 and QT-3a, confirming thus the pollen record, however, the aquatic signal seen in zone QT-5b was recorded during a period when the canopy was closed, and individual n-alkane profiles show an odd/even predominance, indicating the presence of higher plants at the site. Thus, this bimodal n-alkane distribution can be due to permanent waterlogged conditions or pool development at the site that could have allowed aquatic specific vegetation to develop in the proximity of terrestrial vegetation. This is also confirmed by the P_{wax} index that shows a relatively high value at this depth (120-128 cm), compared to pollen zones QT-2 and QT-3a, where a lake-like setting was inferred.

At depth in QT, the brGDGTs are dominated by brGDGT-Ia that indicates overall anaerobic conditions (Zheng et al., 2015), confirming previously discussed proxies. BrGDGT-Ia has a decreasing trend after pollen zone QT-5b, with a relative increase in brGDGT-IIa, which could be due to changes in the active microbial community with depth as vegetation changed, caused by slight changes in temperature, available substrate or pH. Most isoGDGTs show a step-like increase towards the surface, oscillating as a consequence of shifts in the hydrological regime.

Hopanes are indicative of aerobic bacteria and show low overall concentrations at depth, until pollen zone QT-5b, where they peak in concentrations. This was attributed to vegetation adaptations under waterlogged conditions that prevailed upcore. Thus, the presence of *M.*

flexuosa and other species adapted to waterlogging, could have oxygenated parts of the anoxic peatland around root systems, and allowed a larger bacteria community to develop. However, this is recorded during a time when methanogenesis was low as depicted through the collapse in isoGDGT-0 producers (methanogens) and isoGDGTs 1-4 (anaerobic methanotrophs). Thus, the increase in hopanes can be also due to competitive relationships between facultative consumers or to secondary microbial producers, as depicted through the peak in brGDGT-Ia (possibly Acidobacteria-see subchapter 1.7.2.).

The quantifiable presence of FA biomarkers indicative of type II methanotrophs confirms the site's description in terms of environmental preferences and competitive relationships between type I and type II (see subchapter 1.2.2.3.). Since C18:1ω7 and C18:1ω9 (c, t) biomarkers are found both at surface and at depth another way to ascribe them to a producer, apart from carbon specific isotope analysis (CSIA) and peat incubation experiments, is to assess the environment conditions and its potential of harbouring one type over the other. Thus, type II methanotrophs are facultative, having the potential of consuming both CO_2 and CH_4. They also prefer low levels of O_2, with high CH_4 effluxes and reside at the interface between the oxic and anoxic layers. They also occur in acidic and nutrient-restricted environments (see subchapters 1.2.2.2. and 1.2.2.3.). All these conditions describe QT at present day, however the ability of type II to switch between CO_2 and CH_4 consumption (Hanson and Hanson, 1996) might indicate that CH_4 is not efficiently oxidised in this environment.

Through DMDS method (see subchapter 2.4.2.1.) both cis- and trans- stereoisomers of C18:1ω9 were identified, and only the cis isomers for C18:1ω7. Thus, Figure 59.11. (C18:1ω9) probably indicates their combined concentrations. In some samples (e.g. 120-128 cm), evidence of type I biomarkers was also found, for example C16:1ω7, however, due to low concentrations, compounds could not be identified through the DMDS method or accurately quantified through GC-MS and GC-FID. It is possible that at depths where C16:1 monosaturated FA occur, the environment was less acidic and had water input from secondary sources.

Finally, new data generatedin this study shows pH and temperature changes in this peat core and indicate that the peat started to accumulate in a pH neutral setting, and that the pH slowly decreased towards present, towards more acidic values. This is recorded through both hopane and GDGTs calibrated proxies, with a subacidic pH values of 6.41 and 6.53, respectively. Surface pH was calibrated only with the use of GDGTs, and presented an average value of 5.37 (±0.8), recorded during the dry season when the surface samples were

collected. This correlates well with the instrumental data recorded by Teh et al. (2017), who reported a value of 5.49 during the dry season. Calibrated temperatures show a step-like increase, from a lowermost value of 23.74°C(±4.7°C) to a maximum of 27.43°C (±4.7°C) recorded in pollen zone QT-5b. After this point, calibrated temperatures show a slight decrease, reaching 25.82°C (±4.7°C) in the surface samples. Again, this correlates well with instrumental data, as during the dry season, surface temperatures were reported at 25.6°C (Teh et al., 2017).

4. San Jorge (4°03'S, 73°11'W)

4.1. Introduction

Peat at San Jorge accumulates at present under short pole forest vegetation, in the center of the peatland, in an acidic soil with poor nutrient availability (Lähteenoja et al., 2009b; Teh et al., 2017). This vegetation type characterizes the most carbon-dense area in Amazonia, estimated at 1391±710 Mg-C/ha (11% of the peatland area at PMFB), when carbon stored below ground is considered (Draper et al., 2014). The maximum extent of the peat core collected by Lähteenoja et al. (2009b) reached down to 590 cm (Lähteenoja et al., 2009b) and the core collected by Kelly et al. (2017), down to 238 cm as the domed shaped of the peatland allows thicker peat accumulations within the center. The samples discussed in this chapter are from the same core used by Kelly et al. (2017) and pollen interpretations are available for comparison with biomarker data.

4.1.1. Site description, location and geology

Located in the Loreto region of N Peru and, in the NE of PMFB, near the Amazon River, San Jorge peatland is 35 km away from Iquitos (Figure 62) and receives its name from a nearby village (Kelly et al., 2017).

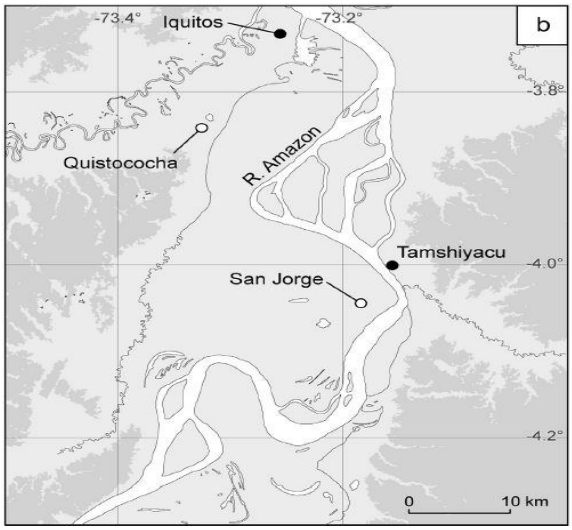

Figure 62 Geographical location of San Jorge peatland (SJO). Notice the proximity of Amazon River, and its relative distance from Quistococha peatlanad (Kelly et al.,2017).

4.1.2. Age model and peat accumulation rates

For this peatland, two distinct sets of radiocarbon dates (Lähteenoja et al., 2009a, Kelly et al., 2017) and one of ^{210}Pb are available in literature, the later extending down to 50 cm. The average peat accumulation rate for the peat column extracted by Lähteenoja et al. (2009a) was calculated at **1.92 mm/yr** (Figure 63).

Study site, core code, and sample depth (cm)	Radiocarbon age	Cal yr BP (1950)	LOI (%)	C content (%)	Dry bulk density (g cm^{-3})	Interval for which the accumulation rates were calculated (cm)	Peat accumulation rate (mm yr^{-1})	C accumulation rate (g m^{-2} yr^{-1})
San Jorge							**1.92 ± 0.05**	**85 ± 30**
SV24, 70–80 cm	*110 ± 30*	*145 ± 115*	94.8	50.9	0.094	–	–	–
SV24, 170–180 cm	1250 ± 35	1205 ± 65	98.6	55.9	0.077	0–175	1.45 ± 0.10	62 ± 8
SV24, 270–280 cm	2020 ± 35	1952.5 ± 52.5	98.1	55.1	0.078	175–275	1.34 ± 0.18	57 ± 10
SV24, 360–370 cm	2325 ± 35	2337.5 ± 22.5	45.1	23.2	0.154	275–365	2.34 ± 0.39	84 ± 17
SV24, 460–470 cm	2600 ± 35	2740 ± 20	62.3	32.9	0.156	365–465	2.48 ± 0.26	128 ± 19
SV24, 560–570 cm	2850 ± 35	2945 ± 65	64.4	36.7	0.109	465–565	4.88 ± 1.65	195 ± 70

Figure 63 Depths, ages and physical characteristic of peat at SJO (Lähteenoja et al., 2009a).

The peat started accumulating at the core-site between 2160 and 2370 cal yr BP (Figure 63; Kelly et al., 2017), ages that are slightly higher than those calculated by Lähteenoja et al. (2009a, above table). Based on the age model provided by Kelly et al., (2017), the accumulation rate (i.e. apparent peat accumulation rate) in the section between 240 cm and 112 cm was 1.4 mm/yr. A lower accumulation rate was noticed between 112 cm and 90 cm

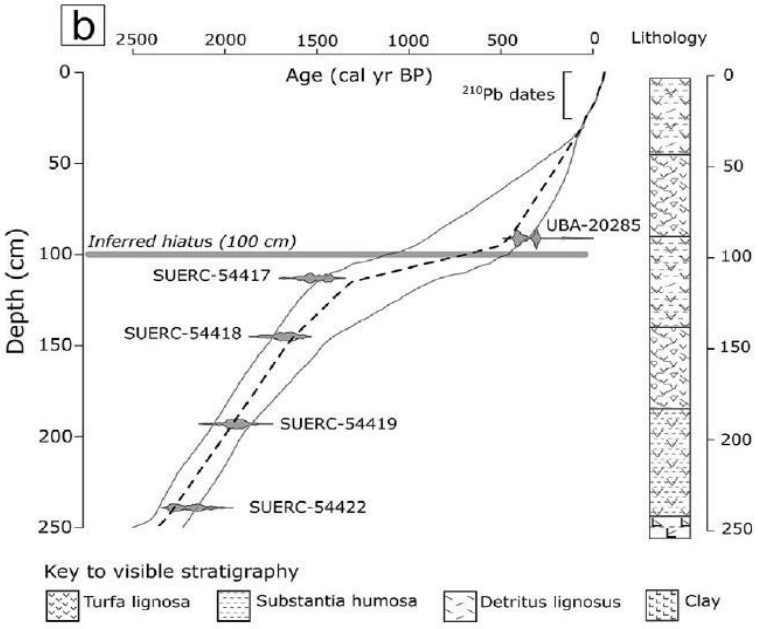

Figure 64 Age model of SJO peatland (Kelly et al., 2017). Notice inferred hiatus in accumulation at the depth of 100cm.

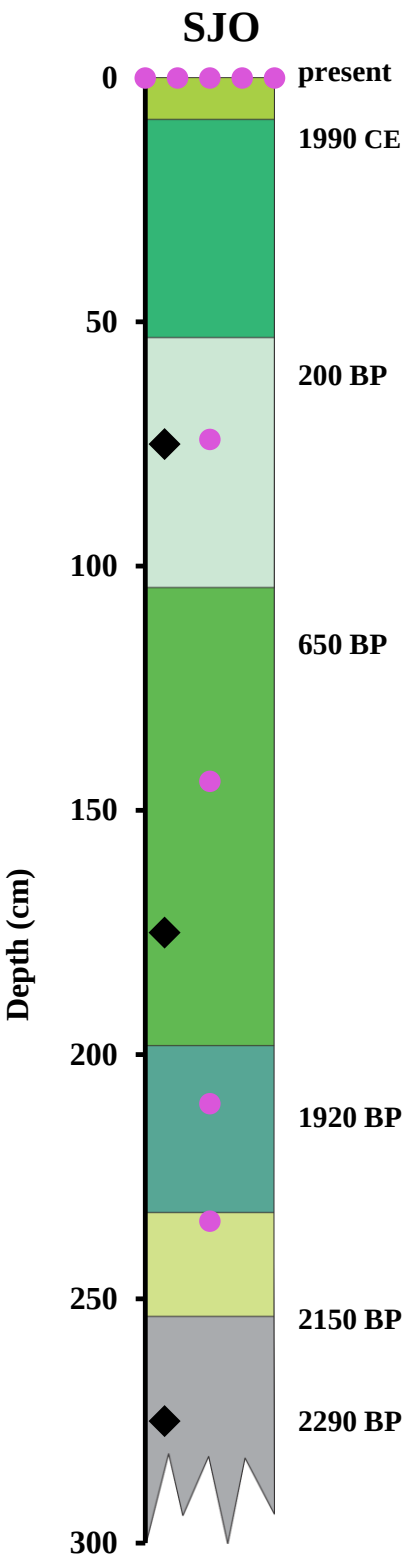

Figure 65 SJO core with depth of available samples (pink circles) and location of radiocarbon ages (black diamonds). Ages provided are in calibrated years

(i.e. 0.4 mm/yr) and a hiatus was inferred for this period (Figure 64). From the depth of 112 cm to present, the accumulation rate was 2.0 mm/yr.

4.1.3. Literature review on vegetation, core, pollen zones and samples (Kelly et al., 2017)

The vegetation at SJO was described as short-pole forested (Teh et al., 2017), with a low diversity, dominated by closely spaced slim trees (Kelly et al., 2017). Only ten species of trees were identified within the area studied by Kelly et al. (i.e. 0.5 ha), three of which made up 83% of the individuals in the surveyed area (Kelly et al., 2017).

0. SJO-0: (640-240 cm) Age greater than 2290 cal yr BP

The core extracted by Kelly et al. (2017) extends downwards into the underlying sediments composed of sandy silts and clays (640-560 cm), with high magnetic (i.e. not on Figure 65. The above section (i.e. 560-240 cm) sees an increase in the organic matter content, with wood-fragments and leaves mixed with clays.

This inorganic sediment succession at the bottom of the core (640-240 cm) reflect changes in Amazon river's energy, from medium-high, that was transporting and depositing sand material, to progressive decreasing energy, when silts and clays were deposited. This indicates a progressive retreat of the Amazon River from the area (i.e. braided system), continuous/permanent flooding, silt-clay deposition and a lake-like environment forming at the site due to the existence of intact leaves found within the sediment (Kelly et al., 2017).

1. SJO-1 (240-220 cm) 2290-2150 cal yr BP

The first peat deposits are recorded at **240 cm** and the peat has the general aspect as in other PMFB peatlands, fibrous with thin roots

and unidentifiable plant material (Lähteenoja et al., 2009a). The lowermost sample from SJO for this study comes from the depth of **230-238 cm**.

Similar to QT peatland development, first pollen records within the peat material indicate a dominance of *Cecropia sp*., a light demanding specie that colonises newly exposed land (Roucoux et al., 2013; Kelly et al., 2017; and references therein). The water table was expected to remain high during this period, leading probably to anoxic conditions and waterlogging, which allowed peat accumulation.

2. SJO-2 (220-188 cm) 2150-1920 cal yr BP

The next pollen zone is recorded between **188-220 cm**, which coincides with the sample **206-214 cm.** Higher Ca/Mg values than recorded in the previous section (>60) indicate water sources alongside precipitations.

Pollen records indicate the presence of herbaceous and early shrub colonizers. Pollen of marginal-lake and floating mat vegetation is seen and towards the top of this section, pollen of *Mauritia-t.* is present. The presence of *Mauritia sp*. indicates, similarly as in QT peatland, frequent and deep flooding (i.e. 1.2 m, Nicolson, 1997) events or permanent waterlogged conditions (Kelly et al., 2017).

3. SJO-3 (188-100 cm) 1920-650 cal yr BP

The next sample (i.e. **140-148 cm**) comes from the section between **100-188 cm**. During this period of deposition, pollen indicates a vegetation reversal, the site changing from *Mauritia t.* vegetation back to *Cyperacea* and *Poaceae* species that make up a marginal/floating mat vegetation, that dominated in the sample from 220-240 cm. Pollen from other species that characterise an aquatic setting (i.e. freshwater algae, lake-like environment) is recorded in high abundance. As their development requires high-nutrient input and as Ca/Mg ratio spikes at this point, nutrient-rich water sources were inferred alongside the presence of a lake-like environment with well-oxygenated waters, similar to the present day Quistococha Lake environment (Kelly et al., 2017).

The pollen from the top of this section is dominated by *Mauritia* and *Mauritiella* species and indicates a return to previous terrestrial and waterlogged conditions, however, the transition between the two vegetation types is also associated with a hiatus or a slow peat accumulation rate (Kelly et al., 2017).

4. SJO-4 (100-52 cm) 650-200 cal yr BP

The following section (100-52 cm) is characterized by palm swamp vegetation, similar to present day QT, with possible seasonal flooding. The sample available from this peat section comes from a depth of **70-78 cm**.

5. SJO-5 (52-8 cm) CE 1750-CE 1990

Finally, the section between **52-8 cm** (no sample available), contains pollen of a pioneer specie (i.e. *Alchornea*) which is interpreted as the development of a secondary forest. Present day vegetation establishment is probably marked by the apparition of species (i.e. *M. flexuosa, Malvaceae*) that indicate shallow flooding depths, and by a decrease in the Ca/Mg ratio, which suggests ombrotrophic conditions. Based on the age model, the present-day vegetation establishment was inferred at 200-150 cal yr BP (Kelly et al., 2017). A summary of vegetation shifts is indicated in Figure 66.

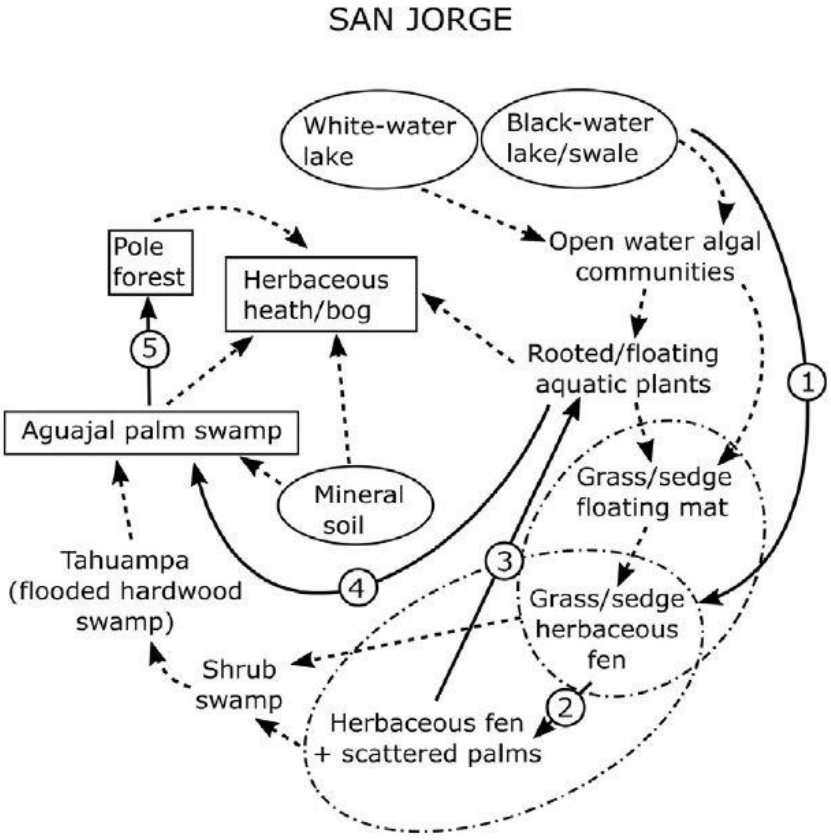

Figure 66 Vegetation successions at SJO (taken from Kelly et al., 2017). Uncertain vegetation and environments are represented by dashed lines while high certainty environments in rectangles. Dashed and solid arrows represent proposed and certain evolution pathways.

Surface samples

Surface samples and present-day environmental parameters, collected by Teh et al. (2017), indicate acidic conditions and confirm the ombrotrophic status of SJO (Lähteenoja et al., 2009b). Methane efflux is higher during the wet season, when peat temperatures and pH are also relatively higher (Table 7). Air temperature is constant during the two seasons. A summary of present-day parameters is provided in the table below (Teh et al., 2017).

Table 8 Physical parameters at SJO (edited from Teh et al., 2017).

Forested-short pole vegetation (centre)	Peat(T°C)	Air(T°C)	Conductivity ($\mu S/m^{2)}$	Dissolved O_2 (%)	WT level (cm)	pH	CH_4 $C/m^2/day$
Wet season	25.2 ±0.0	27.6±0.1	21.0 ± 0.0	4.4 ± 0.0	26.9 ±0.5	4.88	60.4±9.1
Dry season	24.8± 0.1	27.5	48.5 ±4.8	33.1 ±2.6	-4.7±0.4	3.8	18.8±2.6

4.1.4. Geochemistry and hydraulic conductivity (K)

Overall, SJO is characterized by a low Ca/Mg ratio (Lähteenoja et al., 2009b), which gives its acidic and nutrient-poor status (Teh et al., 2017).

The hydraulic conductivity models ran by Kelly et al. (2014) show that within the SJO domed peatland, lack of precipitation for 30 days would cause water table decrease for 30-50 m into the peatland, with water probably exiting the system around the margins. During a longer dry period, the affected area would extend more into the peatland. Groundwater flow would not affect substantially the water table depth in the centre of the peatland; however overland flow and evapotranspiration were not incorporated into the model and can have a significant impact on water levels (Kelly et al., 2014; Table 8).

Table 9 Hydraulic conductivity at SJO at two different depths (Kelly et al., 2014).

Depth within peat column	**San Jorge (K estimates)**
50 cm	0.00464 cm/s
90 cm	0.00414 cm/s

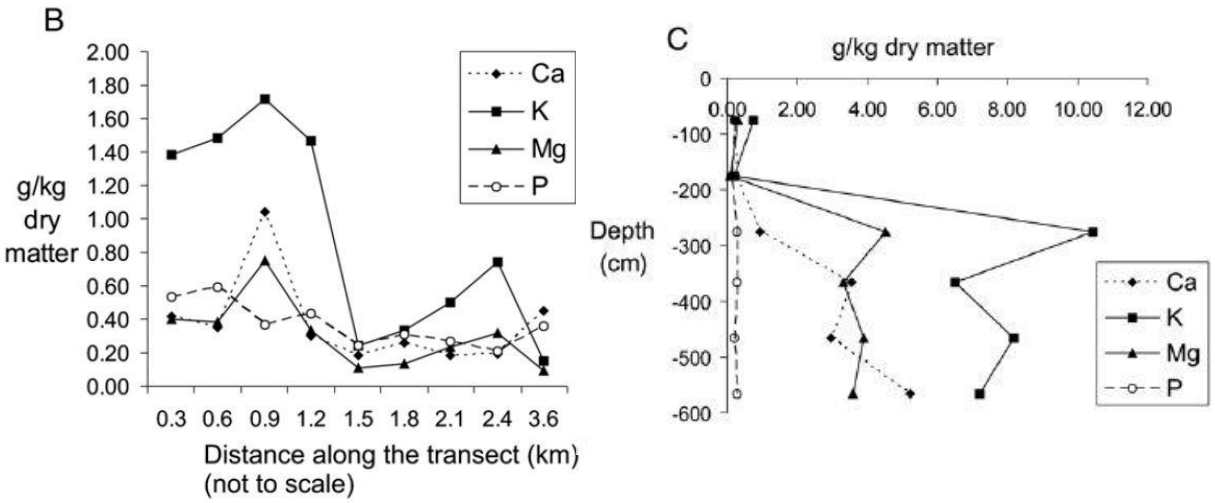

Figure 67 Nutrient content in the surface peat (B) and at depth (C) along a 3.3 km transect (edited from Lähteenoja et al., 2009b).

The sharp decrease of nutrients showed in Figure 67 (B), which takes place between 1.3 and 1.5 km along the transect, implies that this part of the mire is fed by low nutrient water from precipitations. Comparisons between nutrient content between the three locations suggests however that margins are rarely washed in nutrient-rich flood waters as although noticeable here, nutrient levels in marginal peat is still low (Lähteenoja et al., 2009b). The nutrient increase at depth (i.e. sharply seen in K, Mg and Ca; Figures 67 and 68) marks the limit between the ombrotrophic and minerotrophic conditions within the mire (Lähteenoja et al., 2009b).

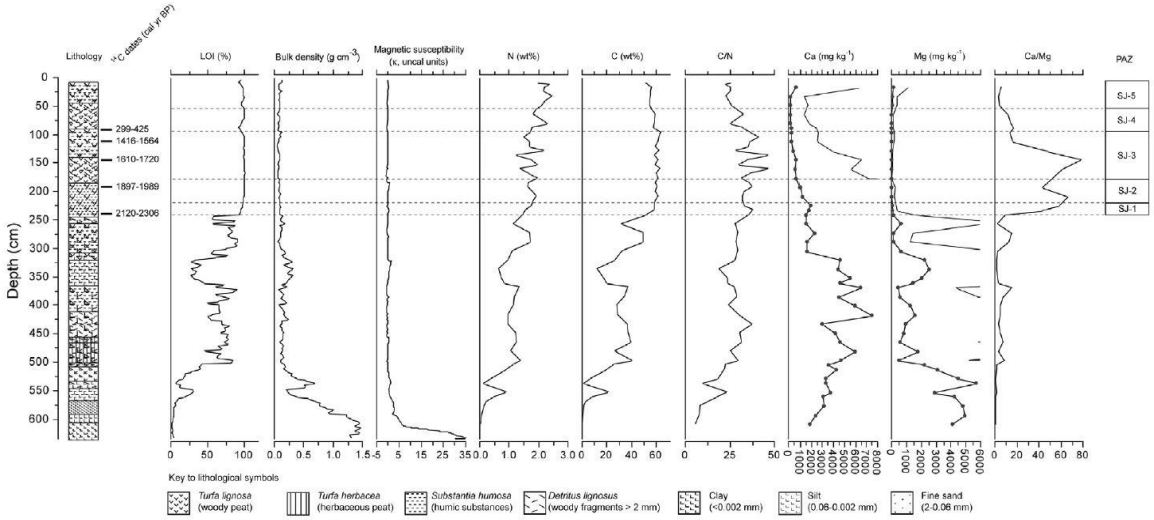

Figure 68 Geochemical parameters at SJO (Kelly et al., 2017). Notice pollen zones only in the top part of graph and overall low LOI below 250 cm at this site. From left to right: LOI, Bulk density (g/cm^3), magnetic susceptibility, N (wt%), C (wt%), C/N, Ca (mg/kg), Ca/Mg.

4.2. Results

4.2.1. N-alkanes

At SJO, n-alkanes in 4 surface samples (Figure 69) and the available 4 core samples sum up to 3831.73 µg (i.e. 3.821 mg/g). N-alkanes in the surface samples make up 76.8% of this total, with n-alkanes in core samples, making up only 23.2% of the total at SJO.

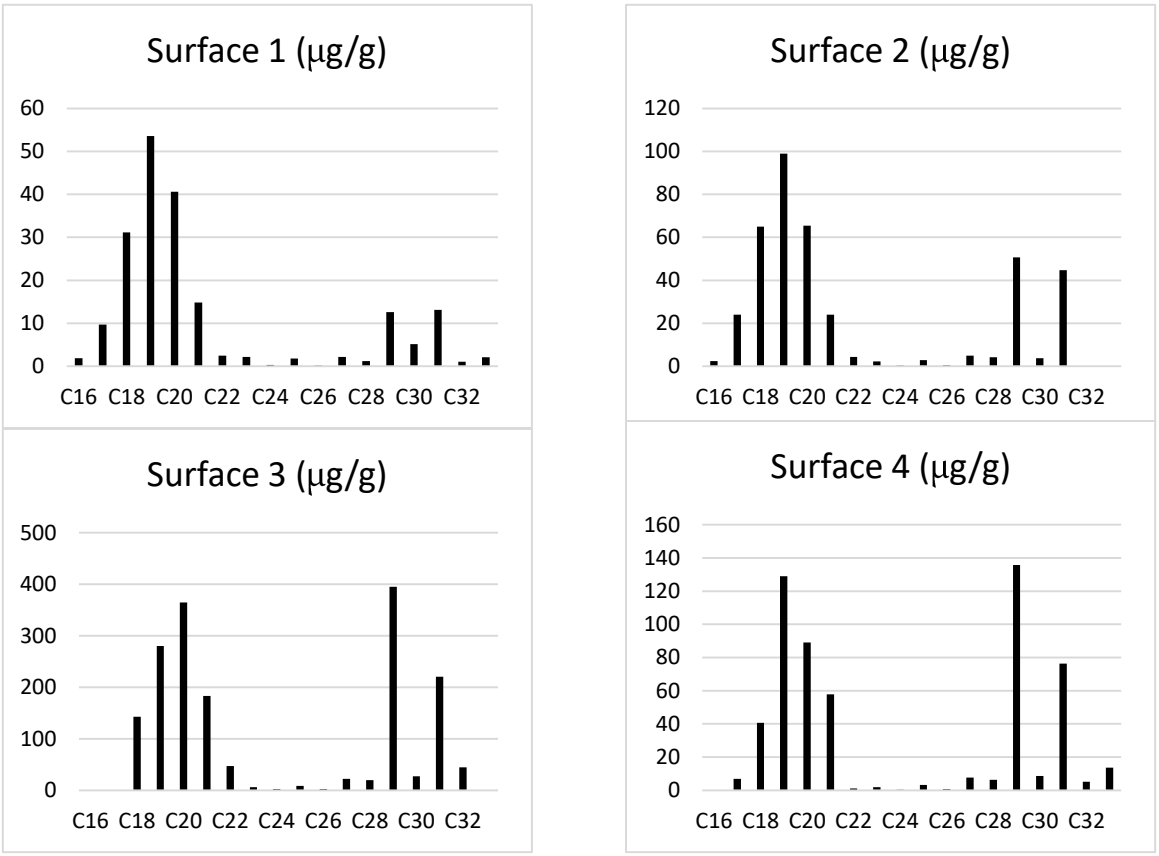

Figure 69 Surface sample n-alkane composition at SJO. Notice differences in long-chain n-alkanes in terms of concentrations and overall increase input from short chain n-alkanes, with no prefer distribution.

N-alkanes in the surface samples are dominated by short-chain n-alkanes (i.e. $<C_{21}$) with no preferred distribution (Figure 69). They make up almost half of the total concentration of n-alkanes at surface (i.e. 49.1%) and represent more than a third of the total n-alkanes at SJO (i.e. 37.7% of both surface and core). Their concentrations dominate over medium and long-chain n-alkanes only at the depth of 230-238 cm where n-C_{18} and n-C_{19} peak at 33.67 µg/g and 27.6 µg/g, respectively, and at surface.

Long-chain n-alkanes ($>C_{25}$) have the next highest concentration in surface samples. They represent 38.99% of the surface fraction, and 29.95% of the total n-alkane fraction at SJO.

At surface, they show a strong odd/even predominance and only in 2 of the 4 surface samples (i.e. Surface 3 and Surface 4), the concentration of n-C_{29} and n-C_{31} is comparable to that of short chain n-alkanes. At depth, long-chain n-alkanes dominate, showing again a strong odd/even preference, apart from the depth of 206-214 cm where, n-C_{32} has comparable concentrations (Figure 70).

The CPI proxy has a value of 9.53 in the bottom peat sample (238-230 cm), depicts a minimum value of 4.31 at the depth of 206-214 cm and peaks in the surface samples, with a value of 12.19 (Figure 73.1.). P_{aq} has values lower than 0.05 for all samples apart from the one at 140-148 cm, where it peaks at 0.17 (Figure 73.2.). The ACL, Pwax and Pr/Ph ratios have similar trends, depicting a minimum at the depth of 206-214 cm (Figure 73.3.-73.5.).

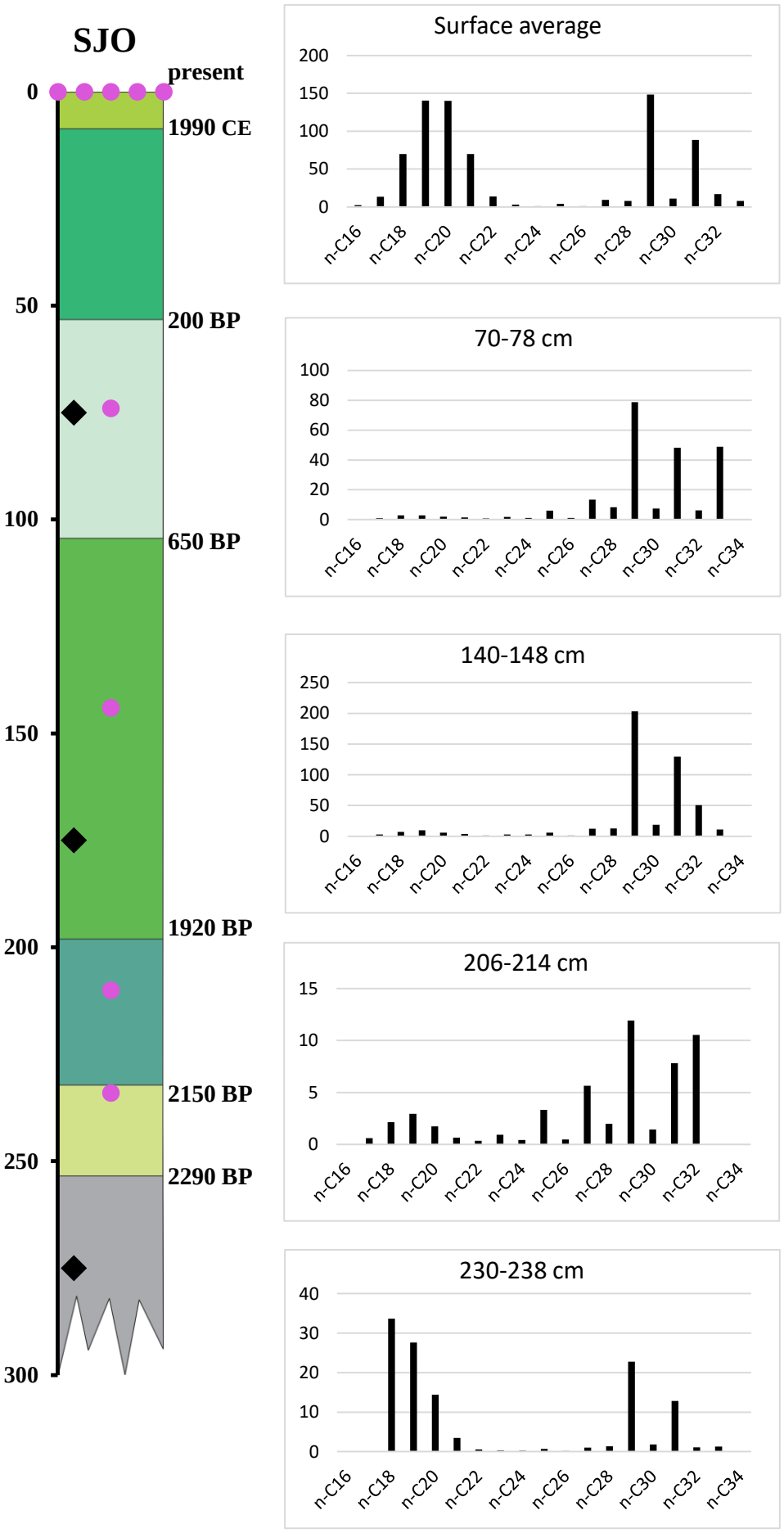

Figure 70 N-alkane concentration distribution with depth at SJO. X axis represents carbon number while y axis represents concentration in µg/g.

4.2.2. GDGTs

At SJO, GDGTs concentration is of 5339.9 µg/g, of which 13% is represented by isoGDGTs and the remaining 87% is made up of brGDGTs (Figure 71).

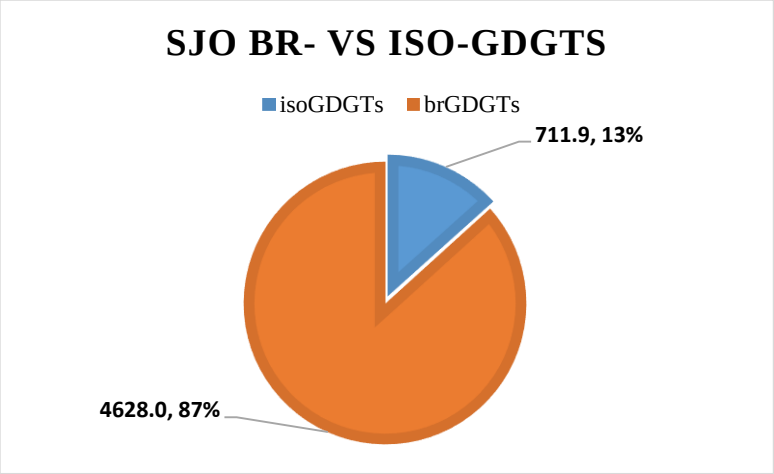

Figure 71 GDGT distribution at SJO. IsoGDGTs make up only 13% of the total, corresponding to 711.8 µg/g while brGDGTs represent the remaining 87%, or 4628 µg/g.

In terms of isoGDGTs, the highest concentrations are recorded isoGDGT-0 that peaks with 116.25 µg/g at 140-148 cm. IsoGDGTs-1,-2,-3,-4 and Crenarchaeol, also record peaks at that depth, with concentration of 37.8 µg/g, 52.1 µg/g, 72.9 µg/g, 58.8 µg/g and 29.1 µg/g, respectively. IsoGDGT-5 peaks at the same depth, however only with a maximum concentration of 9.5 µg/g. IsoGDGTs then decrease to trace concentrations in surface samples (Figures 74.1. – 74.4.).

BrGDGTs are dominated by brGDGT-Ia, which is seen to decrease from 385 µg/g recorded at 280-288 cm to 319 µg/g at 206-214 cm. The following increases in concentrations take place at 140-148 cm to a value of 1581 µg/g and then it peaks at 70-78 cm to a value of 1730 µg/g. In surface sediments, brGDGT-Ia is found in trace amounts. The following highest concentration is recorded in brGDGT-IIa, with a maximum of 104.9 µg/g recorded at the depth of 140-148 cm, followed by both brGDGTs-Ib and –Ic that peak at different depth, however with similar concentrations of 32.9 µg/g and 34.9 µg/g, respectively (Figures 74.8.-74.10.).

The methane index (MI *100) varies between 41, the lowest value recorded at the surface and 94, recorded at 206-214 cm depth. At the same depth, Cald/Cren ratio also peaks 20.9 (Figure 74.7.). Calibrated pHs values are between 3.1 and 4.66 (±0.4) that occur at 206-214

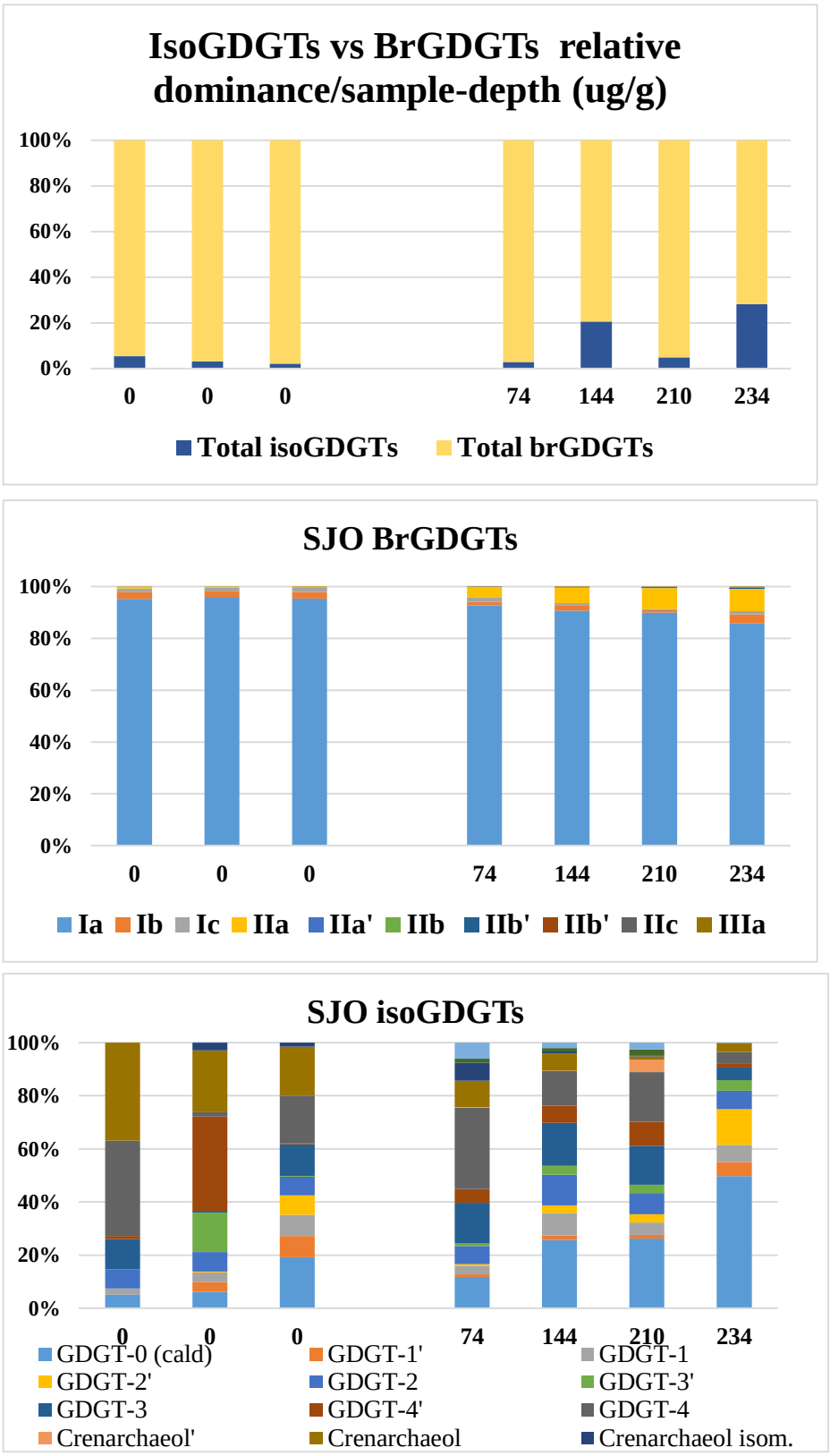

Figure 72 GDGTs relative distribution at SJO. Notice that x axis represents depth in cm.

cm and at 230-238 cm, respectively. Surface calibrated pH is at 4.04 (±0.4), while the reported instrumental pH at present is of 3.8 (Teh et al., 2017) Calibrated temperatures increase from 24.23°C (±4.7℃) recorded at 230-238 cm towards the surface where their reach 28.9°C (±4.7°C). Present day instrumental temperatures during the dry season were reported at 27.5°C (Teh et al., 2017), within the error range.

4.2.3. Hopanes

Hopanes' summed concentrations in surface samples is only 10.16 µg/g as several hopanes could have not been identified. However, the sum of their core concentration is of 371.4 µg/g. The highest concentration is seen in hopane (i.e. $C_{30}H_{52;}$ C_{30}-hop), that peaks at the depth of 140-148 cm, reaching 130.9 µg/g, and then decreasing towards surface, to a value of 0.62 µg/g (Figure 73.8.). The next highest concentrations are recorded for the αβ isomers of C_{27}-hop and C_{31}-hop, that peak at the same depth with hopane (C_{30}-hop), with values of 19.4 µg/g and 28 µg/g, respectively (Figures 73.6. and 73.9.).

Diploptene, although a hopene, does not depict the same trends recorded in hopanes, as it decreases slightly from 280-288 cm and increases after towards recent, reaching values between 2.9 µg/g and 40.7 µg/g at surface, with an average of 16.2 µg/g (Figure 73.10.).

The hopane-calibrated pH (Inglis et al., 2018) indicates that the pH at 280-288 cm was of 3.64, increases to 4.2 and then decreases again to 3.57 at 70-78 cm, all within an error of ±1.4 (Figure 73.12.).

4.2.4. Fatty acids

Unlike QT peatland, SJO has less branched FA within the range of C14 and C18 (Figure 73). Saturated FA from C16-18 show decreasing concentrations upward, while C14 and C15 are constant. FA C17 has both isomers present, and both show increasing concentrations upward, peaking in surface samples, however their concentrations vary between 0.1 µg/g and 0.7 µg/g. The highest concentrations are recorded by saturated FA, with peaks in C16 and C18 of 71.1 µg/g and 77.5 µg/g at the depth of 230-238 cm. Monosaturated FA have the same concentration shifts, peaking at a depth pf 70-78 cm, where C18:1ω7 has a concentration of 5 µg/g and C18:1ω9, 7.6 µg/g (Figure 73.8.).

n-Alkane proxies and hopanes

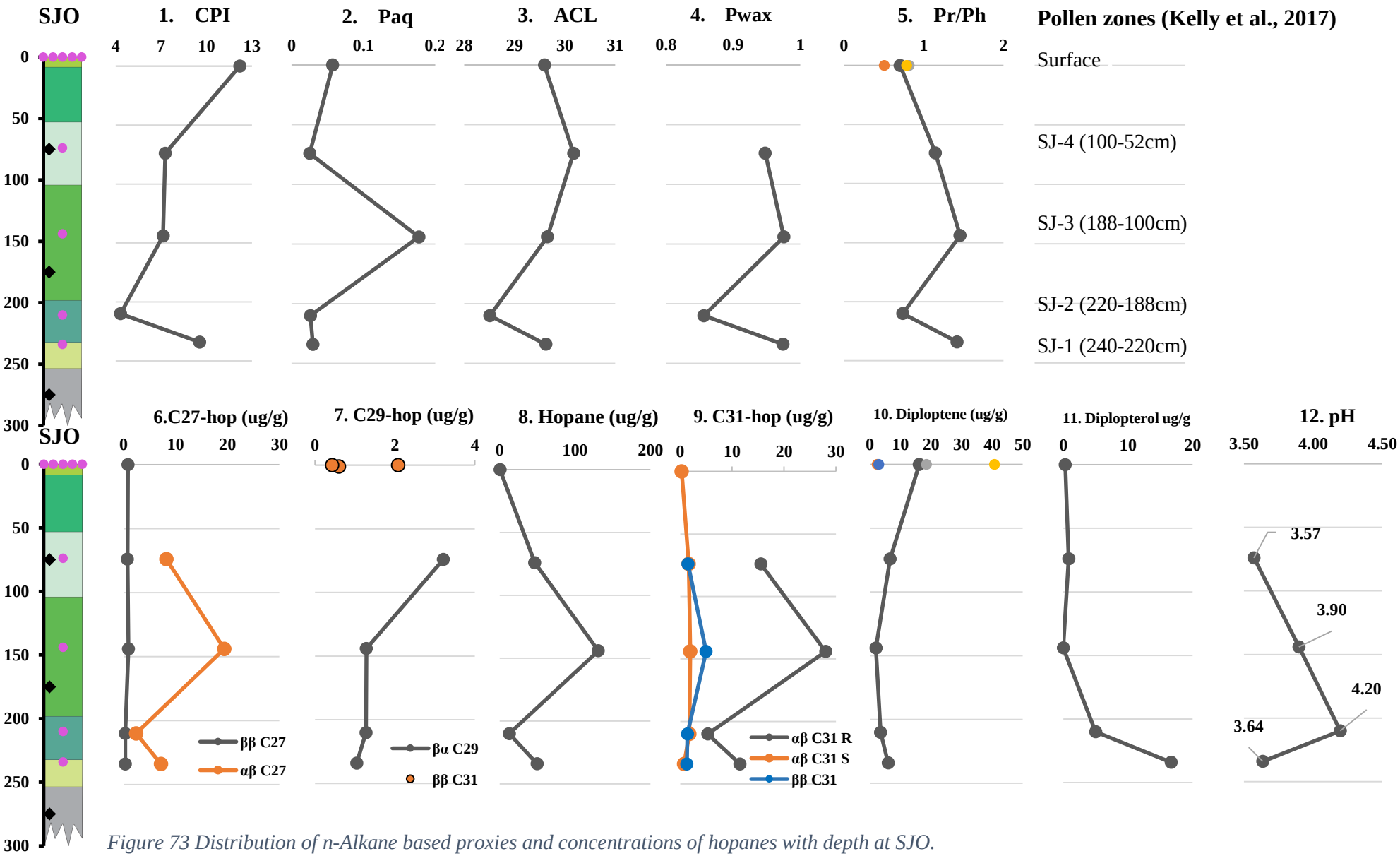

Figure 73 Distribution of n-Alkane based proxies and concentrations of hopanes with depth at SJO.

iso- and br-GDGTs

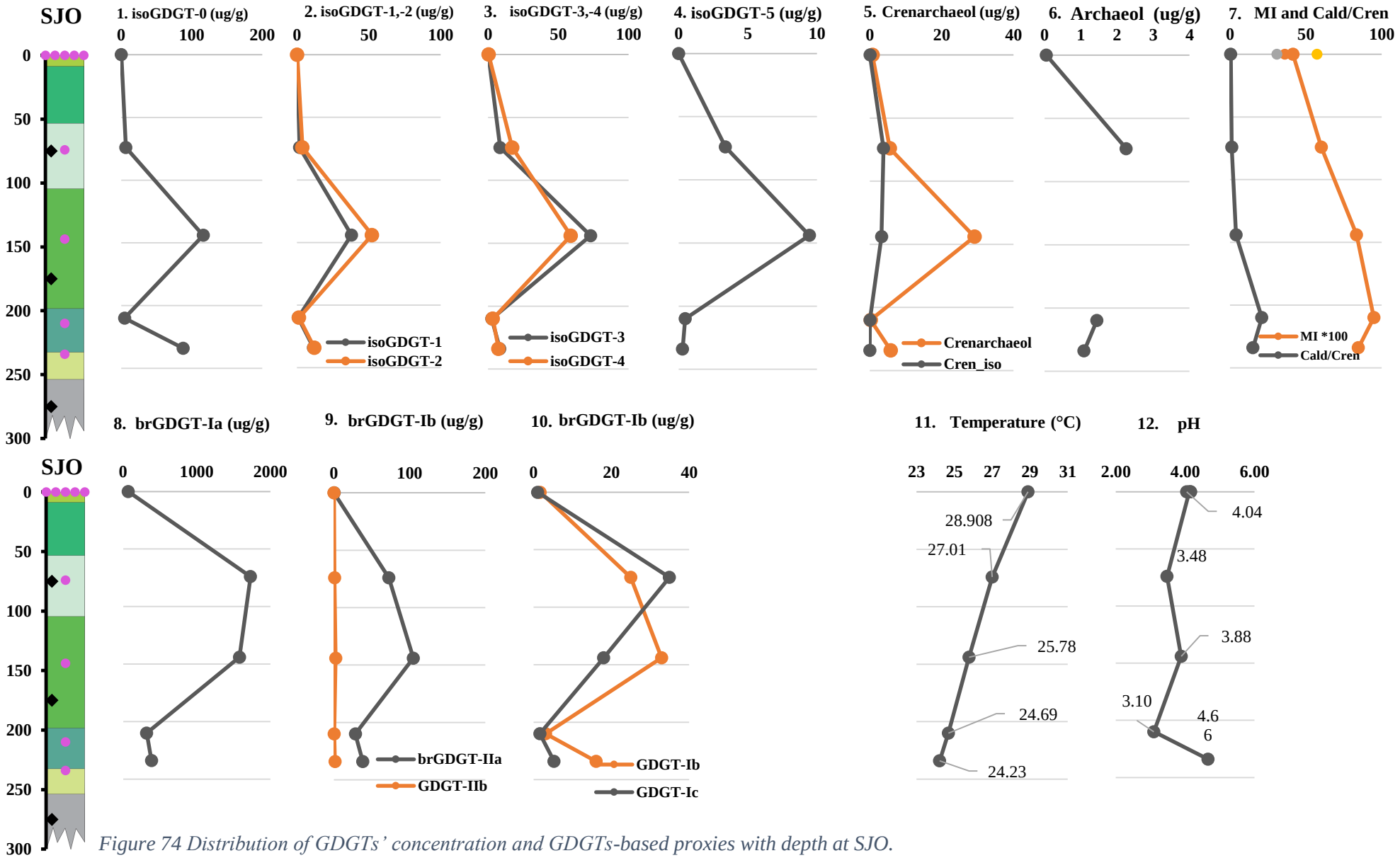

Figure 74 Distribution of GDGTs' concentration and GDGTs-based proxies with depth at SJO.

Fatty acids

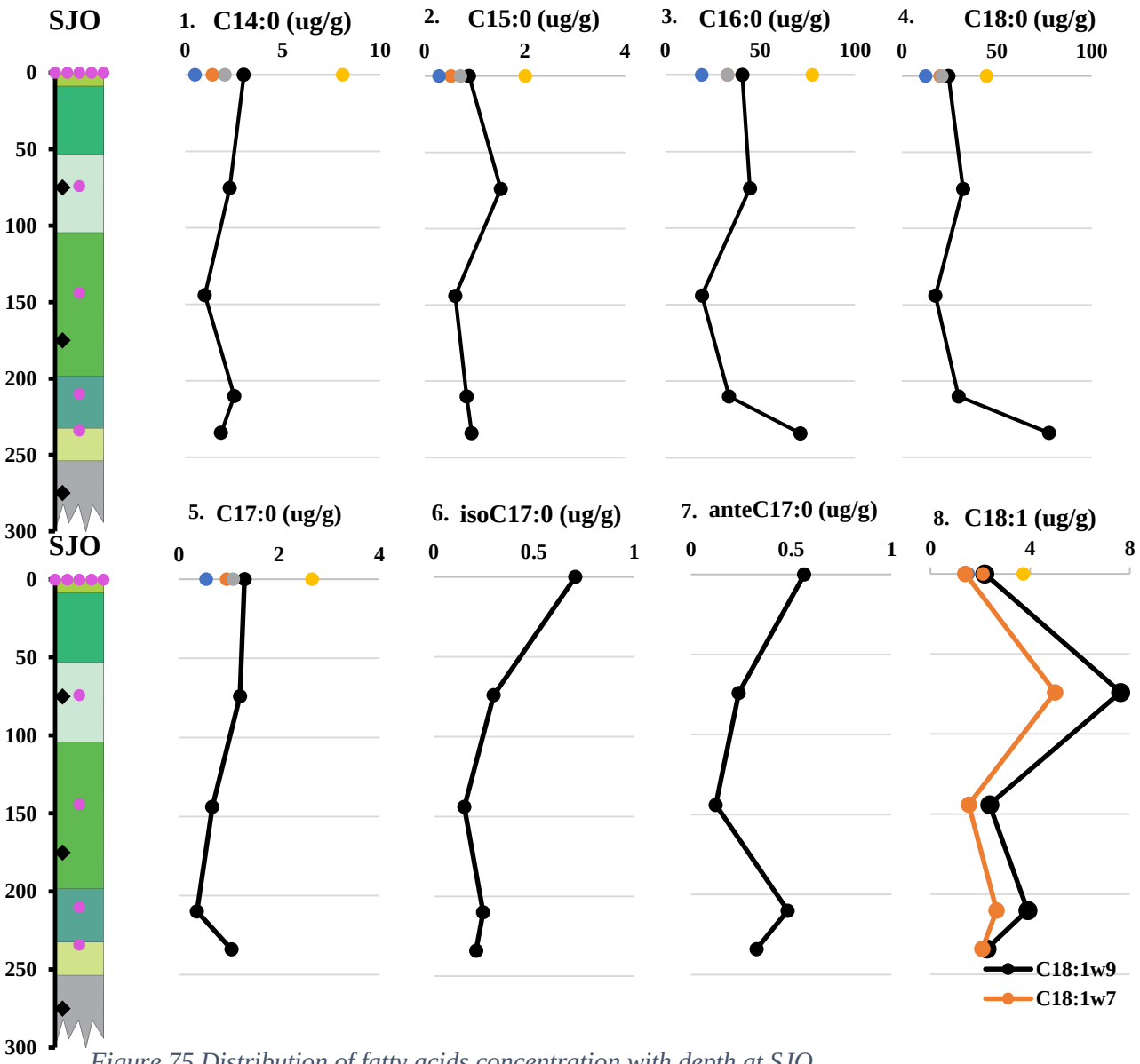

Figure 75 Distribution of fatty acids concentration with depth at SJO.

Table 9 SJO summary of results and observations.

Palaeoenvironment	Interpretation and observations
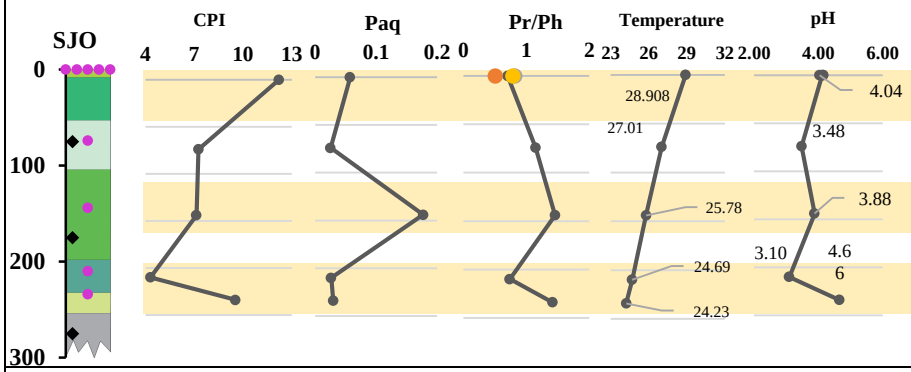	**↑T°C towards recent; Paq<0.1 → terrestrial, highest CPI → undecomposed OM** **Paq~0.2 → lake-like environment** **↑CPI, ↓Pr/Ph and pH acidic → peat deposit; initially better preservation of OM then CPI↓↓**
Aerobic bacteria vs archaea (concentrations in μg/g) 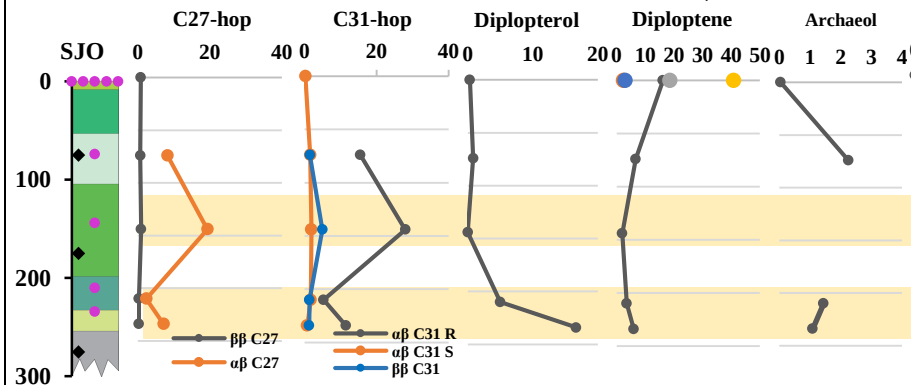	**Highest [hopanoids] and [isoGDGT] in lake-like setting → stratificated waters?** **Highest [diplopterol], high αβ C31R and C27 → mature peat; high methanogen community**
Methane efflux potential (source/sink) 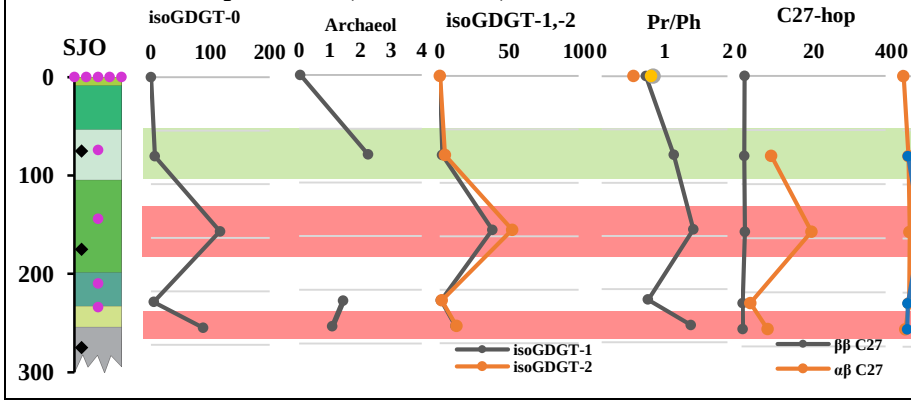	**Highest [C18:1 FA] and low [isoGDGT]→ potential for CH_4 sink** **Low [C18:1 FA] and [hopanoids] and high [isoGDGT]→ potential for CH_4 source → ebullition?** **Low [C18:1 FA] and high [isoGDGT]→ potential for CH_4 source**

4.3. Interpretation

230-238 cm

- **n-Alkanes**

The sample from SJO-1 is rich in organic matter, comes from just above the clayey unit and indicates the onset of peat accumulation at the site. This is characterized by a strong input from short chain n-alkanes (n-C_{18} to n-C_{21}) and a lower input from n-C_{29} and n-C_{31}. This indicates i) input of terrestrial organic matter alongside non-vascular plants and ii) low decomposition and/or restricted diagenesis at depth since short chain n-alkanes are more prone to be removed by microbes (i.e. immature peat) (Singh et al., 2011). The Pr/Ph ratio indicate suboxic conditions thus suggesting a periodically flooded or waterlogged terrestrial (i.e. P_{aq}<0.03) environment.

- **GDGTs**

At this depth we see the highest relative input from isoGDGTs (i.e. 28%) mainly due to a relatively smaller contribution from brGDGTs, possible indicating initiation of waterlogged conditions.

IsoGDGTs

Relative high concentrations in isoGDGT-0 (87.9 µg/g) indicate contributions form methanogenic Archaea (Pancost and Sinninghe Damsté, 2003) and that the environment was already acting as a CH_4 source, with high MI values of 84. Relatively high values in isoGDGT-1, -2, -3 and -4 suggest that part of CH_4 was also oxidized anaerobically (Schouten et al., 2013), however, the presence of crenarchaeol, which is indicative of thaumarchaeota, suggests the existence of oxic or suboxic microsites or fluctuating water table depths. This is also supported by a high Pr/Ph ratio that suggests a suboxic environment. As the peat at this point was just starting to accumulate, it is possible that it also had a high hydraulic conductivity, allowing faster water shedding (e.g. Winton et al., 2017 and references therein).

BrGDGTs

Anaerobic bacteria have a reduced input compared to up-core samples however, brGDGDT-Ia has concentrations of 385 µg/g. Calibrated pH for this depth is 4.65 (±0.8), the highest value at this location, indicating secondary (river) water sources and possible interaction of groundwater with the clayey unit beneath, a process that was proposed within PMFB

(Winton et al., 2017). The calibrated temperature is 24.2°C (±4.7°C), which correlates with present day instrumental peat temperatures recorded during the dry season (Teh et al., 2017; Table 7).

- **Hopanes**

Unlike QT and BVA, the first sample at SJO (i.e. 230-238 cm) comes from an organic-rich, peat horizon, that underlies a clay deposit. At this depth, the dominant hopanes are C_{30}-hop (hopane or hop-17, 21-ene; 49.7 μg/g) and αβ C_{31} R-hop (i.e. 11.5 μg/g), which is well above the αβ C_{31} S -hop isomer and the ββ stereoisomer. This is unusual given that 22R isomer is preferentially removed by degradation (e.g. Bost et al., 2001), indicating thus the immature nature of peat. In order to have a better understanding of the degree of peat maturation, the overall percentage of PAH fraction from total biomarkers (i.e. polyaromatic hydrocarbon) could be traced within this peatland, as polyaromatic structures are thermodynamically stable and resist degradation (Chambers et al., 2011 and references therein). This could correlate to the degree of peat humification and with the position of water table and hydrological conditions. Thus, for this depth, waterlogged conditions prevailed, with short periods when the water table was below surface, allowing the development of an aerobic bacteria community.

Diplopterol peaks at this horizon and it is seen to decrease upwards, while diploptene shows a decrease towards surface (Figures 73.10. and 73.11.). It is possible that diploptene increase is caused by the dehydration of diplopterol towards surface also suggested by the presence of C_{30}-hop however, this relationship between C_{30}-hop and diplopterol is not seen in upper samples, indicating that C_{30}-hop is produced in-situ and that diplopterol producers also decreased in concentrations.

The hopane-calibrate pH is at 3.64 (±1.4) implying a constant and high amount of atmospheric precipitations.

- **FA**

Compared to the bottom of QT and BVA core (i.e. clay-rich), the first sample from the SJO core represents peat's composition, with C16:0, C17:0 and C18:0 showing higher concentrations than in the above sections. As indicated in the Pr/Ph ratio, the environment at the time was suboxic, which probably allowed the development of bacteria community, however, the lack of diagenesis depicted through hopanes is also supported by the occurrence of higher FA concentrations at this depth.

Biomakers specific to type II methanotrophs have relatively low concentrations and since no evidence of degradation is seen in other short chain biomarkers, the low concentrations of C18:1ω9 and C18:1ω7 are probably due to a less active aerobic methanotroph community in the (palaeo)environemnt, however CH_4 could have still been oxidised anaerobically.

206-214 cm

- **n-Alkanes**

At this depth there is a reduction in the overall n-alkane content (Figure 70), with a relatively high input and further increase of n-C_{32} from the previous depth that, based on correlations seen at QT, could be due to an expansion of a fern specie (Kelly et al., 2017), *Davaliaceae Nephrolepis*. P_{aq} has a low value, below 0.1 indicating a terrestrial environment. The Pr/Ph ratio decreases below 1 indicating anoxic conditions, suggesting that the site experienced waterlogging or long flood events. The CPI has the lowest value, suggesting a shift in the environment and less input from vascular plants, which was also noted by Kelly et al. (2017) who indicated a predominance of herbaceous vegetation (Figure 70). It is thus possible, that the input from aquatic plants was reduced at this point, thus the signal is not yet being picked by P_{aq}.

- **GDGTs**

In terms of GDGTs, there is a decrease in their overall input, with declining concentrations in both iso- and brGDGTs, suggesting a possible overturn in the microbial community. At this point, herbaceous and shrub taxa were dominating and there was an increase in the Ca/Mg ratio (Kelly et al., 2017). Kelly et al., (2017) argued that this indicates secondary water sources and furthermore, proposed the formation of a marginal lake-type palaeoenvironment at this depth, however this is not recorded through the P_{aq} proxy.

isoGDGTs

All isoGDGTs show very low concentrations (i.e. tending to 0 µg/g). Furthermore, crenarchaeol, which is associated with oxic conditions, also has very low concentrations (i.e. below 1 µg/g) and does not allow an interpretation based solely on water table values. MI values peak at this depth, however, since both crenarchaeol and isoGDGT-0 also have low concentrations, the MI value cannot be used as an indicator for high CH_4 effluxes at this depth. Archaeol biomarker only shows a small increase in concentration form the previous depth. Furthermore, since pollen records (Kelly et al., 2017) indicate the formation of a

marginal lake, and peat continued to accumulate at this depth, it is likely that the main drives of GDGTs decrease were vegetation type and available substrate.

The shift from *Cecropia* tree sp. (230-238 cm) to herbaceous and shrub vegetation most probably caused a restructuring of the rhizosphere with less substrate for methanogenesis, (Huguet et al., 2013 and references therein; Hanson and Hanson, 1996). The methanogen community could be limited in occurrence only to one or two groups and thus, restricted in the type of substrate that they can consume for methanogenesis (Hanson and Hanson, 1996). The decrease in the methanogen community could have also caused a collapse in archaeal anaerobic methanotrophs, which might be a line of evidence in supporting their obligate nature (i.e. depleted carbon isotopic signatures expected for isoGDGTs 1-4 at this site).

brGDGTs

The depicted collapse in the anaerobic bacteria is less pronounced than in the case of anaerobic archaea. BrGDGT-Ia only slightly decreases in concentration from the previous depth (i.e. from 385 µg/g to 319 µg/g), however other brGDGTs show a 2 to 10-fold decrease in concentrations. Since brGDGTs are synthesized by heterogenic anaerobic bacteria (Sinninghe Damsté et al., 2000; Oppermann et al., 2010), they are not necessarily associated with the decrease in methanogenesis that could explain isoGDGT-producers collapse. Thus, their slight decrease supports the interpretation that the change in vegetation and available substrate are possible the main drivers.

Furthermore, in the above section (Figure 64), a hiatus or decrease in organic matter accumulation rates was inferred (Kelly et al., 2017), before the apparition of *M. Flexuosa* palms. This decrease in fresh organic matter input correlates with the decrease in methanogen community, as acetate pathway for CH_4 production was demonstrated in boreal peatlands to be the main process at the surface part of peatlands during periods of high input of fresh organic matter (e.g. Avery et al., 1999; Bellisario et al. 1999, Chasar et al., 2000). Even the fact that at the top of this section individuals of *M. Flexuosa* were found through pollen analysis (Kelly et al., 2017), which would allow thicker roots to extend downwards possibly to this depth (20-30 cm, van Lent et al., 2018) did not provide sufficient or the required substrate for methanogenesis. During this period, the peat at SJO acted as a CH_4 sink, which is also supported by a relative increase in the concentrations of C18:1ω7 and in C18:1ω9 fatty acids, thought to be indicators of methanotrophic bacteria (see subchapter 1.7.4.).

Calibrated pH value for this depth is 3.09 (±0.8), the most acidic for this peatland while temperature is similar to the calibrated value for the below section, at 24.7°C (±4.7°C).

- **Hopanes**

Concentrations decrease for all hopanes apart from a minor increase in βα C_{29}-hop. This indicates a restricted aerobic layer, periodic flooding and waterlogged conditions that did not allow the development of an aerobic bacteria community. A decrease in concentration is also seen in brGDGTs, indicating the fact that a small fraction of the hopanes may not come from the palaeo-acrotelm, but may postdate surface peat accumulation as they can also be biosynthesized by anaerobs, for example from anammox bacteria or can be degraded from other hopanes. However, diploptene, a major constituent lipid in bacteria, does not follow this trend (Sinninghe Damsté et al., 2005; van Winden et al., 2012). The hopane calibrated pH peaks at this depth, with a value of 4.2 (±1.4) yet it is within the error range of GDGT calibrated pH and present day value (Table 7).

- **FA**

Most short chain FA decrease while concentrations of the two monosaturated are relatively higher, arguing again against biodegradation. It is thus possible that CH_4 emissions increased at this depth due to higher water table levels and anoxic conditions (i.e. low Pr/Ph ratio). The potential presence of type II methanotrophs can again support the overall CH_4-sink behaviour of the peatland at this location.

140-148 cm

- **n-alkanes**

This depth is characterized by a high increase in long-chain n-alkanes, with n-C_{29} and n-C_{31} dominating (Figure 70). There is also a further increase in n-C_{32}. N-C_{32} can enter the composition of marine algae (Bianchi and Canuel, 2011), however here it correlates with the pollen record by Kelly et al. (2017) as it occurs at the same time across both SJO and QT with the increase in pollen from *Davalliaceae* Nephrolepis, a fern species. The CPI increases from the previous depth, indicating a higher input from higher plants and P_{aq} peaks at this depth, which correlates with the pollen record (Kelly et al., 2017) that indicates the presence of a marginal or floating mat vegetation in an aquatic setting. Pr/Ph ratio indicates suboxic conditions, which can be correlated with the high ratio of Ca/Mg that implies flooding (Kelly

et al., 2017) as the influx of floodwater can cause an increase in the dissolved oxygen content within the peatland.

- **GDGTs**

This section follows a period of *M. flexuosa* expansion and the sample comes from a palaeoenvironemnt with high Ca/Mg ratio, deep flooding events and input from aquatic vegetation (Kelly et al., 2017) which is also supported by P_{aq} increased values. At this depth, we see peaks in all GDGTs.

isoGDGTs

The increase in isoGDGT-0 suggests the (re)establishment of archaeal methanogenic community and restart of methanogenesis at the site, which led to substrate availability seen as peaks in anaerobic methanotrophs due to possible Euryarchaea group development (i.e. increase in isoGDGTs 1-4; also see Figure 25-ternary diagram). Crenarchaeaol and isoGDGT-5 also peak at this point. As crenarchaeol is an indicator for aerobic or oxygen-rich settings and based on its concentrations seen in ternary diagram in Figure 25, it is mainly produced in-situ in the lake environment at the site. A lake-like setting would allow concomitant anaerobic CH_4 production at depth and oxidation at/near surface. IsoGDGT-5 was recently discovered in mesophilic peatlands with pHs below 5.1 and possible constant increasing temperature (Naafs et al., 2018b) however, its occurrence here can suggest that it may also be synthesized by a lake-living producer.

The MI index also indicates that the site was actively producing CH_4 and although archaeol concentrations are not available for this depth, it is expected to see a similar increase in its concentration. Thus, CH_4 was probably transported via bubbles in the water column towards the surface and emitted to the atmosphere.

brGDGTs

All brGDGTs peak at this depth, a signal that corresponds to a lake-like environment (Figure 25). Furthermore, in adjacent terrestrial settings, the increase in brGDGT-Ib, -Ic, -IIa and –IIIa biomarkers specific to heterotrophic anaerobic bacteria is also expected due to further substrate input from tree (i.e. palm) roots.

The calibrated temperatures are also seen to increase, to a value of 25.7°C (±4.7°C) while pH values increase slightly to 3.88 (±0.8), a value that matches present day measured pH during the dry season.

- **Hopanes**

Most hopanes (i.e. C_{27}-hop, C_{30}-hop, C_{31}-hop; Figure 73) increase in concentrations in this lake-like palaeoenvironment, however, this is not mirrored by the concentrations of diploptene and diplopterol. Depending on the depth of the lake, aerobic bacteria could have been dispersed through the entire water column given high oxygen content (Kelly et al., 2017) and able to consume a part of the CH_4 emitted from the anoxic bottom. If true, the $\delta^{13}C$ signature of mentioned hopanes should show depleted values for this depth, comparted to adjacent samples, as seen for example in Lake Rotsee (Naeher et al., 2013).

- **FA**

At this depth, most short chain FA have constant concentrations or slight decrease from the previous depth. As the palaeoenvironment shifted to an aquatic setting, the surrounding area was probably waterlogged with high water tables, maintaining the anoxic conditions at depth. Both iso- and brGDGTs increase at this depth are suggesting high CH_4 production and possible anaerobic CH_4 consumption, respectively. The decrease in C18:1ω9 and C18:1ω7 indicate a potential decrease in type II methanotrophs that can be correlated to the CH_4 fast emission pathway and bypass of methanotrophy.

70-78 cm

- **n-Alkanes**

This depth is dominated by odd long-chain n-alkanes that peak at n-C_{29} (Figure 70). The CPI has a similar value from the previous depth, bearing a strong terrestrial signal with input from higher plants, also seen in the P_{aq} ratio (i.e. below 0.05). The Ph/Pr ratio is close to 1, indicating subanoxic to anoxic conditions probably caused by longer flooding episodes or waterlogged conditions, with minor shifts in the water table position between above and below surface.

- **GDGTs**

This depth is characterized by palm swamp vegetation and by seasonal floods (Kelly et al, 2017). The main input is from brGDGTs that is also seen in surface samples, with isoGDGTs making up less than 5% of the total GDGTs.

isoGDGTs

The decrease in isoGDGTs 0-5 is also mirrored by crenarchaeol. It appears that although the site was mainly anoxic (i.e. low crenarchaeol concentrations; Pr/Ph anoxic to subanoxic), the restricted methanogen community (i.e. low isoGDGT-0 concentration) did not allow further anaerobic methanotrophs to develop (i.e. low isoGDGTs 1-4 concentrations).

Several possible explanations exists for this signal: i) as the top section (no sample available, Figure 65) is characterized by shallow flood depths, it is also possible that water tables fluctuated between the dry and wet season, with the palaeosurface of the peat exposed to oxygen which could have caused isoGDGTs to degrade faster than brGDGTs (Schouten et al., 2013 and references therein), however, this does not explain the low concentrations of crenarchaeol; ii) a change in substrate for methanogenesis under anoxic conditions; iii) competition between anaerobic bacteria and archaea domains. While archaea are known to be highly adapted to extreme conditions (i.e. low pH), heterogenic anaerobic bacteria would be capable of similar adaptations (e.g. Acidobacteria) and could have been advantaged by substrate availability, anoxic conditions and increasing temperatures.

brGDGT

BrGDGT-Ia and -Ic are seen to increase in concentration, supporting competitive relationships between archaea and bacteria domains in the anaerobic part of the peat. As suggested above, Acidobacteria could have dominated at this depth since it is an important brGDGT-Ia producer. However, brGDGT-Ib and –IIa decrease, possible signifying competitive relationships even within the same domain. Calibrated pH at this location has a value of 3.47 (±0.8) while calibrated temperatures of 27°C (±4.7°C), above measured present day temperatures (Table 7).

- **Hopanes**

Hopanes decrease in concentrations from the previous depth and this cannot be correlated to the increase in brGDGTs, indicating again that at least in this setting, anaerobic bacteria are not an important source of hopanes. It is likely that water tables were high, not allowing a stable aerobic bacteria community to develop. Only βα C_{29}-hop increases in concentration, however this is probably due to the medium-high degree of peat maturation.

- **FA**

This depth is marked by a slight increase in the concentration of several short chain FAs, however, monosaturated FA peak at this point simultaneously. As isoGDGT-0 responsible

for CH_4 production decreases to a very low concentration, type II aerobic methanotrophs could have switched to CO_2 consumption, and their $\delta^{13}C$ signature could be highly enriched (i.e. less depleted in ^{13}C) at this depth, in contrast to the below sample.

Surface

- **n-Alkanes**

At the surface of SJO there is a bimodal distribution in terms of avergae n-alkanes from 4 samples (Figure 69). Here, short chain n-alkanes with no odd over even preference dominate in the first range, with a high input from n-C_{19} and n-C_{20} are seen in the average, however n-C_{19} dominates in 3 of the 4 samples. Since there is not a pronounced even/odd preference to suggests present day thermal degradation (i.e. fire; Eckmeier and Wiesenberg, 2009), n-fatty acids hydrogentaion (e.g. Welte and Ebhardt, 1968, Welte and Waples, 1973) or an odd/even preference to indicate algal input (e.g. Gelpi et al., 1970), a cause for this distribution could be the lack of biodegradation of fresh organic matter at surface and a n-alkane input from microbial organisms (i.e. yeast, fungi; Weete, 1972). As this n-alkane distribution is seen in all three peatlands at surface, it is possibly due to the lack of biodegradation of less resistent shorter n-alkanes (Singh et al., 2011) and concomitent input from microbes living in the surface, oxic-rich layers.

In the range of long n-alkanes, there is a odd/even preference distribution that is also seen in the mid-chain lenghts, with the highest input from n-C_{29} and n-C_{31} (Figure 69). This indicates an input from higher plants, in agreememnt with the short-pole present day vegetation, CPI and P_{aq} values that both indicate the presence of terrestrial and vascular, decay resistent vegetation. The Pr/Ph ratio is below 1, indicating anoxic conditions for the dry season when surface samples were collected. Indeed, in this peatland, even during the dry season, the water table is only 4.7 cm below surface (Teh et al., 2017), thus allowing waterlogged conditions to persists. ACL decreases towards the surface, suggesting relatively colder and/or wetter conditions even during the dry season experienced by vegetation (Figure 73).

- **GDGTs**

No relative input differences between isoGDGTs and brGDGTs is seen in the three analysed surface samples. All GDGTs show decreasing concentrations, below 1 µg/g in the case of isoGDGTs and with a maxim of 122 µg/g in the case of brGDGTs, indicating present day homogenous physical parameters.

IsoGDGTs

Overall, very low concentrations of isoGDGTs are indicative of low CH_4 production in surface samples (i.e. low isoGDGT-0) together with a limited community of anaerobic methanogenic archaea (i.e. isoGDGTs 1-4). Furthermore, no archaeol was found in any of the 4 surface samples. This is due to fluctuating water table values between the wet and dry season. Teh et al. (2017) reported values of 26.9 cm above surface for the wet season and -4.7 cm, below surface, during the dry season. Since samples were collected during the dry season, it is expected that organic matter was still fresh at the surface and decomposition was mainly due to aerobic bacteria and other organisms (i.e. fungi). Since considerably higher CH_4 efflux was measured during the wet season (Teh et al., 2017, Table 5), CH_4 is being produced in the peat from a few cm below surface to further depths. This can be due to the fact that, although at the surface there is a higher availability of organic matter, it may not be yet decomposed in substrate suitable for methanogenesis (i.e. shallower depths suitable for methanogenesis compared to surface even during wet season).

BrGDGTs

BrGDGT-Ia is the most abundant of the isoprenoidal GDGTs, with concentrations between 31 and 122 µg/g. This could be due to biomarkers that persisted from the wet into the dry season, indicating the anaerobic bacteria community present during the former one and/or that anaerobic decomposition continues in restricted anaerobic water pools or microsites. This is supported by the hydraulic conductivity model ran by Kelly et al. (2016), which indicated that even during a dry period of 30 days, water level would remain high at the surface although water loss would be experienced around the margins of the peatland.

Given one potential source of brGDGT-Ia, discussed in several cases in this study, that of aerobic *Acidobacteria*, with many mesophilic species living in oxic environments (Sinninghe Damsté et al., 2014), the presence of brGDGT-Ia at surface in relative low concentrations can be an indicator of present-day anoxia. However, at least at SJO, brGDGT-Ia may not indicate an aerobic producer. Teh et al. (2017) reported water tables below the surface (i.e. 4.7 cm below), thus, if a clear relationship between brGDGT-Ia and the presence of an oxic layer was true in these settings, we would expect to see higher concentrations, as in the case of surface BVA. Furthermore, between the three peatlands, SJO has the highest levels of dissolved oxygen (%; Table 7), thus a clearer relationship should be apparent in this peatland. However, the possibility cannot be dismissed as there is a gap between sample collection and Teh et al. (2017) report and the surveyed area can differ.

Calibrated pH values are between 4.04 and 4.15 (±0.8) with temperatures just below the upper limit of saturation for the MAATpeat calibration (Naafs et al., 2017a) at 28.7-28.9°C (±4.7°C) within the ranges reported by Teh et al. (2017).

It is also interesting that measured present day surface pH during the dry season was lower than the pH recorded during the wet season (Teh et al., 2017), which indicates that SJO is receiving part of water from ground/river sources despite its domed structure.

- **Hopanes**

Most hopanes were not identified in surface samples. The average diploptene concentration increases, however, in surface samples and it varies between 2.9 and 40.7 μg/g, indicating the heterogenic nature of its distribution. The variations in diploptene concentrations can be due to microtopographic features (i.e. hallows, hummocks, pools) that influence the position of water table and relationships between oxic and anoxic layers. It is thus possible, that palaeomicrotopography played an important role in the past, and that, overall the peaks and troughs seen in concentrations are not entirely peatland characteristic, but site-specific characteristic. More specifically, given the raised dome topography of SJO peatland, it would be of interest to see how biomarkers vary in concentrations between centre and margins that are characterized by *M. felxuosa* vegetation (Kelly et al., 2017).

Only two samples contained diplopterol, with similar concentrations (i.e. 0.32 μg/g and 0.27 μg/g) and since diplopterol was present in the sample that contained the highest concentration of diploptene (i.e. 40.7 μg/g), is an indicator that diplopterol surface concentrations are less variable. The ββ C_{27}-hop, αβ C_{31}-hop S isomers and hopane are present in trace concentrations at surface, indicating a present-day restricted bacteria community and fast biological R configuration degradation to the S isomer (MacKenzie et al., 1980; Inglis et al., 2018 and references therein). Although the hopane-calibrated pH (Inglis et al., 2018) could not be calculated for surface sample, the values reported by Teh et al. (2017) are 4.88 and 3.8 for the wet and dry season, respectively. As the samples were collected during the dry season, a pH value of 3.8 is close to calibrated down core values.

Thus, at this location, it is possible that recent pHs are lower during the dry season due to less input from ground and floodwaters, however, a different or secondary mechanism is probably dominant, since the topography of the peatland is domed and probably receives most of its water from atmospheric sources (Lähteenoja et al., 2009a).

- **FA**

With one exception, surface samples have lower or constant concentrations than what is recorded down-core indicating that lack of biodegradation at this site, and possible, microtopography and water table position influence on the size of the bacteria community. The difference in CH_4 fluxes between the dry and wet season (Teh et al., 2017; table 5) indicates efficient CH_4 oxidation during the dry season. Thus, by comparing the concentrations of the two monosaturated biomarkers at the surface to the two peaks down-core, we can interpret the depths of 70-78 cm and 206-214 cm as periods of efficient CH_4 oxidation, and a possible mixed isotopic signal due to evidence of little to no CH_4 efflux and a potential switch to CO_2 consumption during those times.

Implications of type II methanotrophs biomarkers

Very similar to QT peatland, SJO is characterized by nutrient poor and acidic conditions, due to its domed shaped, which allows it to be fed mainly by atmospheric precipitations (Lähteenoja et al., 2009b, Kelly et al., 2017). The presence of type II methanotrophs in quantifiable amounts is thus characteristic to this site. Furthermore, although possibly coeluting on the GC-MS chromatogram, the DMDS derivatisation method (see subchapter 2.4.2.1.) showed evidence of C18:1ω9, C18:1ω7 and most importantly, C18:1ω8 (possibly cis- since no other isomer eluted) biomarkers at the surface, while in core samples, mass spectra for C18:1ω9 (cis- and trans-) and C18:1ω7 were found. The presence of C18:1ω8, although not in quantifiable amounts, is highly specific of type II methanotrophs (Nichols et al., 1985; Bowman et al., 1991, 1993; Bodelier et al., 2009) due to the unusual position of the double bond between C8 and C9.

4.3.1. SJO peatland synthesis

Peat at SJO accumulated under different shifts in the environment and hydrological regimes. The lowermost CPI has a high value, comparable to the ones recorded in present day surface samples, indicating that the peat started forming under higher plants, has a low maturity, is poorly oxidised and that n-alkanes are well preserved in SJO-1 pollen zone. The following decrease in CPI, recorded for SJO-2 zone was most likely caused by a shift in vegetation, with reduced higher plants in the proximity of the coring site, and herbaceous taxa depicted through the pollen record (Kelly et al., 2017). The following increase in CPI indicates the recalcitrant nature and an odd/even predominance that corresponds to higher plants (Figure 73.1.).

Further biomarker proxies, such as Pr/Ph ratio indicate that pollen zones SJO-1 and SJO-3 experienced suboxic conditions (Figure 73.5.), probably due to the oscillating nature of the water table or less intense flood events. Remaining pollen zones are characterized by anoxic conditions, as depicted through ratio values less than or around 1. The P_{aq} proxy depicts a lake-like setting, with emergent macrophytes in pollen zone SJO-3. This is also noticed by Kelly et al. (2017) in the pollen record that described the palaeovegetation as a "marginal and/or floating mat". Furthermore, due to relatively high values in the Pr/Ph ratio, it is likely that the lake or pool had a well-oxygenated surface or that the water was frequently replaced during flood events.

The peak in hopanes is also recorded in the same pollen zone (i.e. SJO-3), indicating again the high dissolved oxygen content of the lake/pool during aquatic vegetation development and potential for aerobic oxidation in the water column. However, hopanes show decreasing or trace values in further pollen zones, bearing very low concentrations in surface samples, indicating anoxic and waterlogged conditions at present. In the sample available from this pollen zone (i.e. SJO-3), fatty acids (FA) indicative of microbial biomass are seen to decrease in concentration, however, given the inferred oxygen-rich lake-like environment, it is likely that they were oxidised by other microbes with the return of anoxic conditions in further pollen zones. A similar trend is seen in iso- and brGDGTs that peak or increase in concentrations at this point. The same trend is expected for archaeol concentrations. As they are indicative of anaerobic microbes, it is likely that the bottom of the lake and peat accumulating just below were highly anoxic and could allow anaerobic microbes to decompose organic matter. Thus, as both methanogens and anaerobic methanotrophs biomarkers increase in concentrations, while monosaturated FA show decreasing

concentrations at this point, it is expected that a greater part of the produced CH_4 was consumed in-situ, anaerobically, while the remaining CH_4 was mainly delivered to the atmosphere via ebullitions, in bubble-form, and thus, less substrate was available for aerobic methanotrophs in the oxic parts of the lake. The increase in monostaurated FA in the following pollen zone, SJO-4, indicates a lower potential for CH_4 consumption in lake-like settings at SJO, as CH_4 by-passes aerobic oxidation processes.

At SJO, GDGT-calibrated pH indicates again a higher value in the lowermost sample, however, slightly acidic than the one recorded in QT-1, as SJO-1 sample is already representative of a peatland (i.e. high organic matter content). The pH further decreases towards the surface, where the calibrated average value is of 4.04. This correlates well with instrumental data recorded by Teh et al. (2017), who reported a pH value of 3.8 for the dry season. The hopane-calibrated pH correlates well for samples in pollen zones SJO-3 and SJO-4, however, surface values could not have been calculated as required hopanes were not identified (see subchapter 1.7.3.4.). Calibrated temperatures indicate increasing values towards present, peaking in surface samples at a value of 28.9°C while reported instrumental data show dry season temperatures at 24.8°C.

5. Buena Vista (4°14’ S, 73°12’ W)

5.1. Introduction

At Buena Vista (BVA), peat accumulates in a (borderline) neutral pH and nutrient-rich environment under present day forested vegetation (Teh et al., 2017; Lähteenoja et al., 2009b; Figure 76). The maximum peat depth at BVA was measured at 290 cm (Lähteenoja et al., 2009a) and the deepest peat sample available for this study comes from a depth range of 266-275 cm. Less is known about this peatland, however available data coupled with biomarker studies indicate that BVA might be the most interesting peatland of the three with regards to the microbial community and CH_4 cycle.

Vegetation type	Site name	Nutrient status*	Latitude (S)	Longitude (W)	Plots	Flux chambers
Forested	Buena Vista	Rich	4°14'45.60"	73°12'0.20"W	9	74
Forested (short pole)	San Jorge (centre)	Poor	4°03'35.95"S	73°12'01.13"W	3	26
Forested (short pole)	Miraflores	Poor	4°28'16.59"S	74° 4'39.95"W	16	142
M. flexuosa Palm Swamp	Quistococha	Intermediate	3°49'57.61"	73°12'01.13"	119	433
M. flexuosa Palm Swamp	San Jorge (edge)	Intermediate	4°03'18.83"S	73°10'16.80"W	6	81
Mixed palm swamp	Charo	Rich	4°16'21.80"S	73°15'27.80"W	8	56
*After Householder et al. 2012, Lahteenoja et al. 2009a, and Lahteenoja et al. 2009b						

Figure 76 Buena Vista peatland geographical location,vegetation type and nutrient status (Teh et al., 2017).

1. Site description, location and geology

BVA peatland is located near the Tamshiyacu-Tahuayo River, which flows into the Amazon (Valderrama, 2013) and 55 km from Iquitos (Figure 77). The flat topography of this area

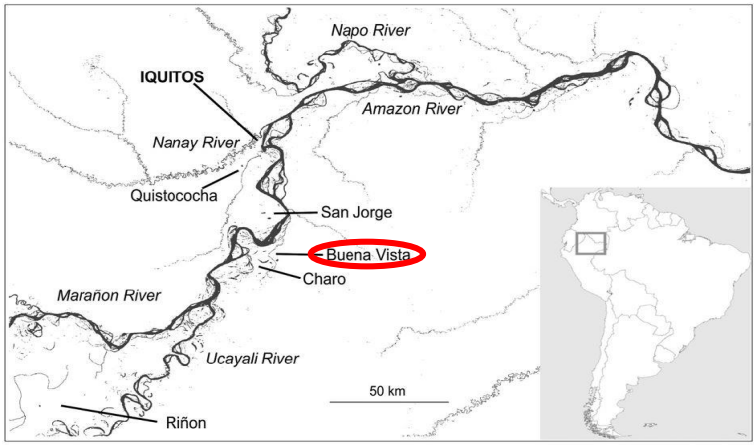

Figure 77 Buena Vista location (highlighted) with respect to the Amazon River and Iquitos locality (Lähteenoja, 2009b). Notice location of QT and SJO.

allows the region to be annually flooded (Kelly et al., 2014; Valderrama, 2013), confirmed by high Ca/Mg value relative to rainwater (Lähteenoja et al., 2009b).

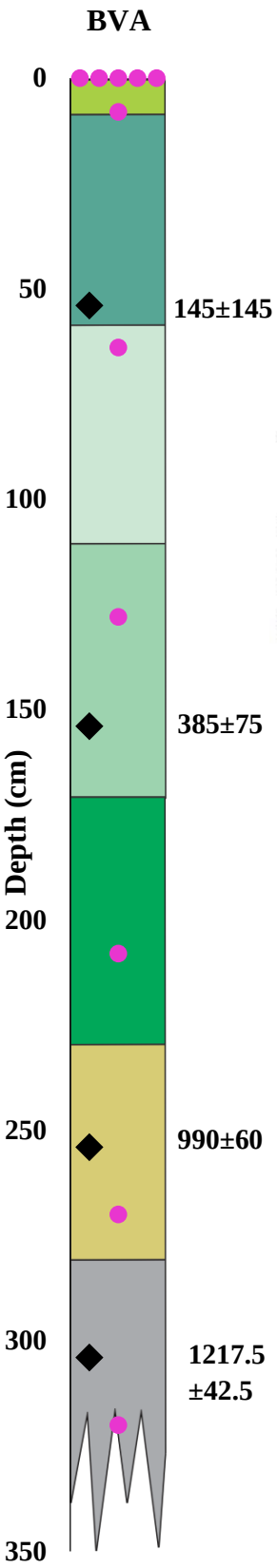

Figure 79 BVA core representations with sample depth.

2. Age model and peat accumulation rates

The bottom of a different peat core (300-308 cm) was dated at 1217.5±42.5 cal yr BP (1950). The sections between 250-258 cm, 150-158 cm and 50-58 cm were dated at 990±60, 385±75 and 145±145 cal yr BP, respectively. Based on this, the mean peat accumulation rate was calculated at **2.5 ±0.1 mm/yr** (Lähteenoja et al., 2009a). A summary of the data and varying peat accumulation rates can be found below:

Study site, core code, and sample depth (cm)	Radiocarbon age	Cal yr BP (1950)	LOI (%)	C content (%)	Dry bulk density (g cm^{-3})	Interval for which the accumulation rates were calculated (cm)	Peat accumulation rate (mm yr^{-1})
Buena Vista							2.50 ± 0.10
BQ15, 50–58 cm	*165 ± 25*	*145 ± 145*	–	–	–	–	–
BQ15, 150–158 cm	340 ± 20	385 ± 75	–	–	–	0–154	4.00 ± 0.80
BQ15, 250–258 cm	1070 ± 25	990 ± 60	–	–	–	154–254	1.65 ± 0.29
BQ15, 300–308 cm	1260 ± 25	1217.5 ± 42.5	–	–	–	254–304	2.20 ± 0.78

Figure 78 Radiocarbon ages at BVA and peat accumulation rate (Lähteenoja et al., 2009a).

3. Vegetation, core and samples

At Buena Vista the main vegetation is forested type with a few species of *M. felxuosa* (Valderrama et al., 2013; Lähteenoja et al., 2009a). No pollen records are available yet for BVA, thus the biomarker data will provide the first attempt to characterise vegetation and environmental changes at this location.

The core extends down into an underlying light-grey clay unit (i.e. 332-340 cm). Samples (circles) available for analysis are depicted in the adjacent figure (Figure 79) with their relative depths and age of radiocarbon samples (diamonds).

Peat here has the same general character as the rest in PMFB and, until the depth of 100 cm; peat is composed of plant material, fine roots with few wood fragments (Lähteenoja et al., 2009a; Kelly et

al., 2014). The humification index was between H6 and H7 (Kelly et al., 2014).

4. Present day vegetation and environmental data

Five surface samples are available from the area. Teh et al. (2017) reported peat temperatures of 26.1°C and 24.7°C between the wet and dry season, respectively, with pH between 5.88 and 6.31.

Table 11 Physical parameters at present at BVA peatland (Teh et al., 2017). Notice higher CH4 effluxes during the dry season when water table depth is below surface.

Forested vegetation season	**Peat-T°C**	**Air-T°C**	**Conductivity (µS/m$^{2)}$**	**Dissolved O_2 (%)**	**WT level (cm)**	**pH**	**CH_4 C/m^2/day**
Wet season	26.1±0.1	28.8 ±0.7	79.0 ±5.9	0.2 ±0.1	**110.8 ±9.3**	5.88 ±0.15	**6.7 ± 1.0**
Dry season	24.7±0.0	26.4 ±0.3	75.9 ±5.7	18.9 ±4.4	**-13.2 ±0.7**	6.31 ±0.04	**47.2± 5.4**

The floristic diversity is higher than in the other two peatlands, with 42 species reported by Kelly et al. (2014) making less than 70% of the total individuals. No *M. flexuosa* or *M. armata* were identified by Kelly et al., (2014) however, other studies have reported a few individuals (Valderrama et al., 2013; Lähteenoja et al., 2009a) in other parts of this peatland.

Present day CH_4 emissions are higher during the dry season (i.e. 47.2 CH_4-C/m^2/day; Table 8) when water table levels are below surface (i.e. -13.2 cm). A proposed explanation for this can be found in the interpretation subchapter 5.3. A summary of the other parameters can be found in the tables below (Tables 8, 9 and 10; Teh et al., 2017).

5. Geochemistry and K

Due to its flat topography and proximity to the Amazon River, the site is periodically flooded by nutrient-enriched black-waters (Table 10). A summary of the main nutrient can be found in the table below. The Ca/Mg values are also above those of rain water, thus the peatland has been described as minerotrophic (Lähteenoja et al., 2009b)

Table 12 Geochemical parameter averages from two depths (60-64 cm and 50-54 cm) at BVA (Kelly et al., 2014).

Buena Vista Forested vegetation	**Ca (g/kg dry peat)**	**K (g/kg dry peat)**	**Mg (g/kg dry peat)**	**P (g/kg dry peat)**
2 sampling depths: 60-64cm 50-54cm	17.4 (17.14-17.66)	2.13 (1.89-2.37)	1.73 (1.65-1.81)	0.39 (0.36-0.41)

Hydraulic conductivity at BVA remains relatively constant between depths of 50 and 90 cm (Kelly et al., 2014; Table 11).

Table 73 Modelled hydraulic conductivity of peat at two different depths (Kelly et al., 2014).

Depth within peat column	**Buena Vista (K estimates)**
50 cm	0.00664 cm/s
90 cm	0.00624 cm/s

5.2. Results

5.2.1 n-Alkanes

Individual n-alkane concentrations/sample (µg/g) are depicted in Figure 82. N-alkanes were identified in the range of n-C_{16} and n-C_{33}. Surface n-alkanes in the 5 samples have a total mass of 4443.9 µg, while their sum in 6 core samples is of 1594 µg.

At BVA, n-alkane concentrations vary between various depths, with the maximum recorded in the concentration of n-C_{29} and n-C_{31} in the same sample, for the depth of 60-68 cm, with values of 238.3 µg/g and 207.6 µg/g, respectively. At all depths apart from surface, long-chain n-alkanes dominate with a strong input from n-C_{29} and n-C_{31}, even at 8 cm below surface. In the surface samples, there is a high input from short chain n-alkanes with no preferred distribution.

The CPI peaks in surface samples, with an average value of 15.04 and decreases in steps towards the bottom of the core, reaching a value of 3.27 (Figure 85.1.). P_{aq} shows the opposite trend, however its values are below 0.1, thus always indicating a terrestrial environment (Figure 85.2.). The ACL mainly reflects the same changes depicted in CPI however, the lowest value is recorded in the 0-8 cm sample (i.e. 29.09) and not at depth, while the peak is recorded at the depth of 266-275 cm (i.e. 30.13). Similar trends to ACL are seen in P_{wax}, however values are between 0.92 and 0.98, with the minimum and maxima recorded in the 0-8 cm and at surface, respectively (Figure 85.3. and 85.4.).

The Pr/Ph ratio at the BVA site has a bottom core value of 1.77 recorded at the depth of 336 cm and decreases to values between 0.89-1.53 recorded up-core (Figure 85.5.). The depth of 336 cm also marks the base of the peat-core, and represents an organic-poor layer, made of grey clays and silts, thus, not representative of the peats found at BVA site.

5.2.2. GDGTs

In terms of GDGTs, isoGDGTs represent only 17% of the overall input in combined samples, with the remaining 83% being made up by brGDGTs (Figure 80). Surface samples have very low isoGDGT concentrations, below 3% of corresponding isoGDGTs concentrations. A larger variation is seen in core samples, with the relative input of isoGDGTs fluctuating between 2% and 38%, with a peak value of 144 µg/g.

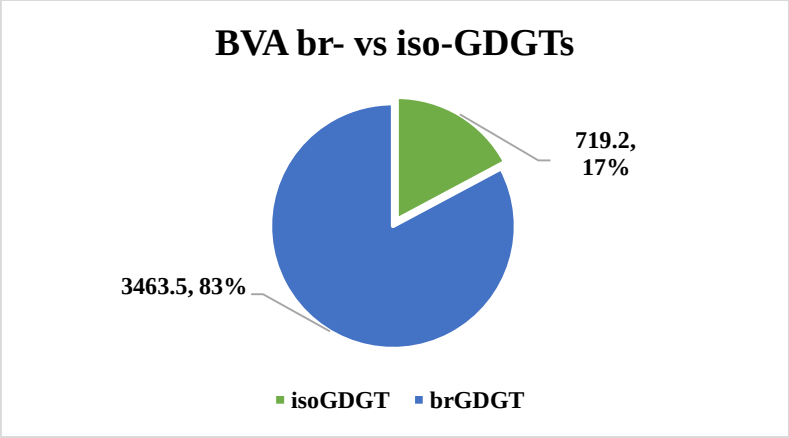

Figure 80 Relative total input of brGDGTs and isoGDGTs at BVA.

In terms of isoGDGT profiles (Figures 81 and 86.1.-86-4.), their concentrations start from close to trace values at depth of 332-340 cm, increase and reach their peak at the depth of 266-275 cm then decrease in steps until concentrations close to 0 µg/g at the depth of 60-68 cm. Their concentrations recover in the sample just before surface, with values of 136 µg/g in the case of isoGDGT-0, the most abundant isoGDGT.

BrGDGTs (Figures 81 and 86.7.-86.10.) show increasing concentration from the depth of 332-340 cm, reach a first peak at the depth of 204-212 cm then decrease in concentrations at the same depth as isoGDGTs, however their decrease is less pronounced. Similarly, to isoGDGTs, brGDGTs increase towards surface, peaking in the horizon below present-day peat surface (i.e. 0-8 cm).

Overall, calibrated pHs are between 3.9 and 5.16 (±0.8) and calibrated temperatures between 23.79°C and 26.9°C (±4.7°C), with a possible colder period recorded between 204 and 124 cm (Figures 86.11. and 86.12.).

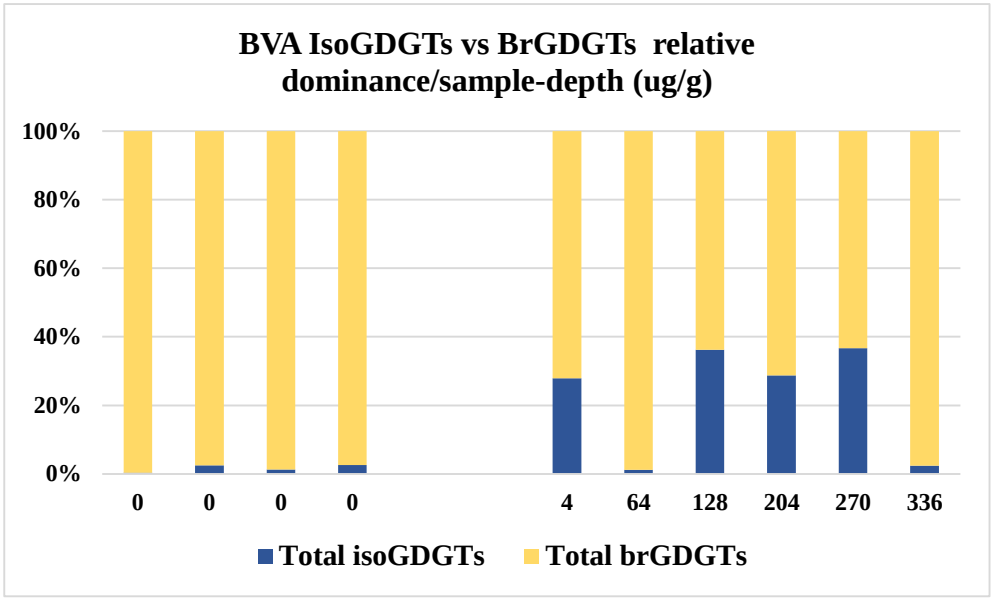

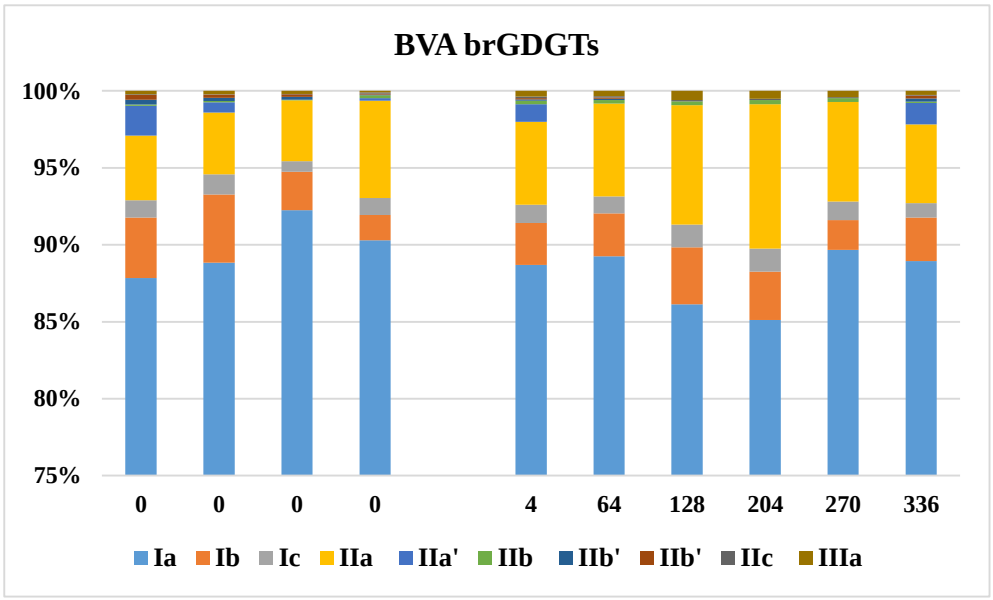

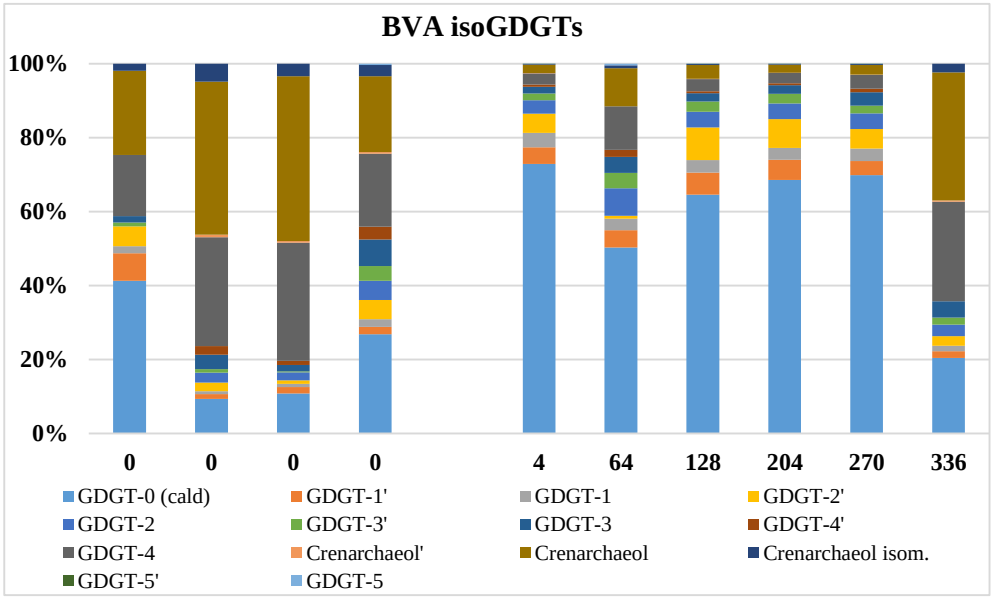

Figure 81 GDGTs relative distribution at BVA with depth (x axis representing depth in cm).

n-Alkanes

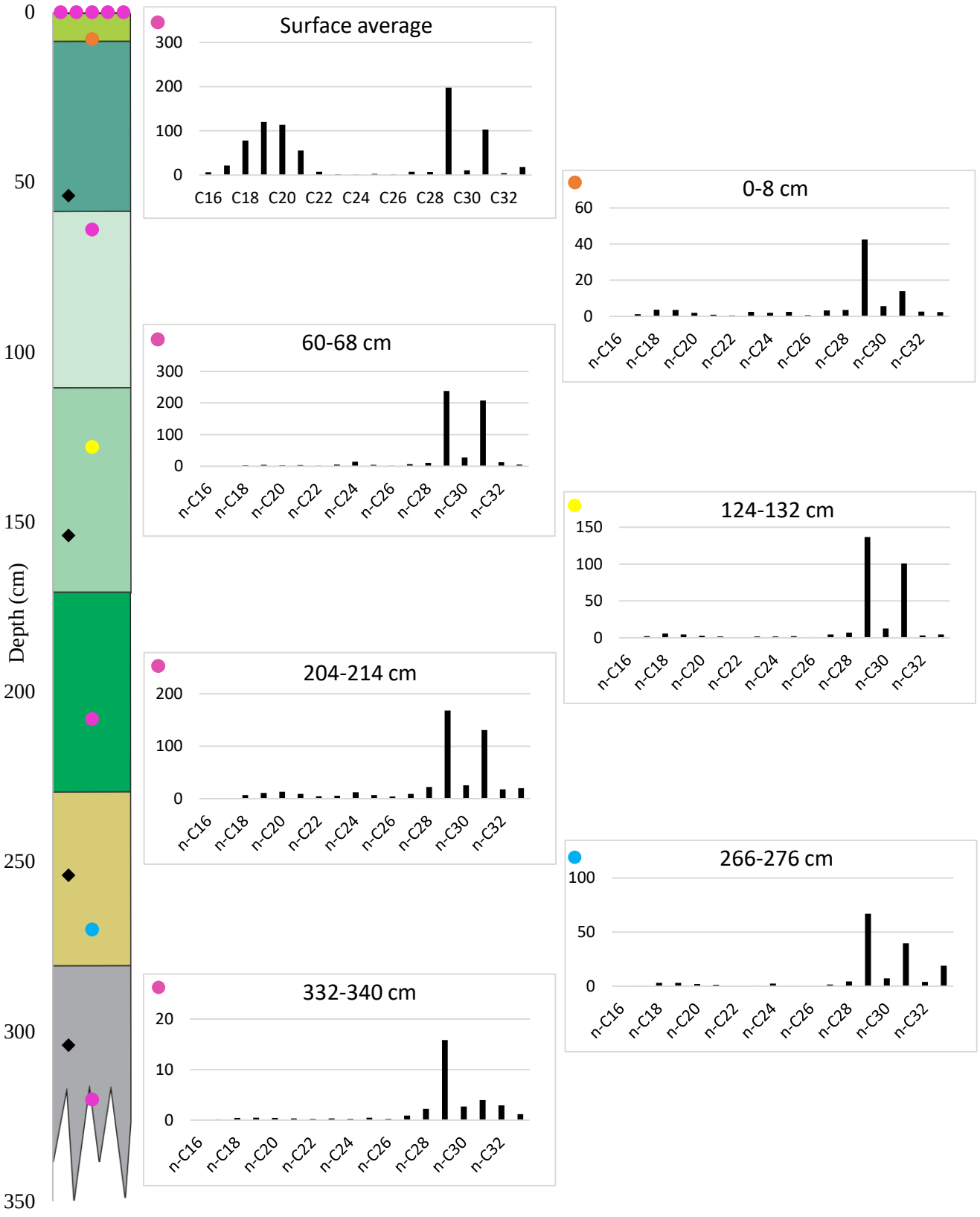

Figure 82 Individual n-Alkane concentrations (µg/g) with depth (cm) recorded at BVA. Notice sample coloring links with depth for the right hand side plots.

Figure 83 Fatty acids concentrations (µg/g) with depth at BVA. X axis represents n-alkanes while y axis, concentration.

5.2.3. Hopanes

Hopanes at BVA show two peaks in concentrations, one seen at the depth of 266-275 cm and one at a depth of 60-68 cm. In both cases, αβC_{31}-hop is the most abundant one, reaching concentrations of 8.58 μg/g and 18.33 μg/g, respectively. Diploptene is only seen to increase in concentration in the 266-275 cm section and does not mirror the increase seen in other hopanes towards surface, however, diploptene peaks again in surface samples. The ββ configuration dominates in the case of C_{27}-hop and C_{29}-hop, while for C_{31}-hop, αβ is the dominant stereoisomer. Diplopterol values show an increase at the depth of 266-275 cm, reaching peak concentrations of 30.4 μg/g, have stable concentrations around 20 μg/g for the depth where hopanes increase (i.e. 124-132 cm and 60-68 cm) and decrease towards surface, reaching minimum concentrations of 0.4 μg/g.

5.2.4. Fatty acids

At BVA, saturated FA occur within the range of C_{11}-C_{36}, with a total concentration across 5 surface samples and 5 core samples of 5403.5 μg/g (Figure 83). Overall, higher concentrations of FA occur in the surface samples compared to depth, and, at all depths, even FA have higher concentrations than odd adjacent FA.

In terms of branched short chain FA, at BVA the iso- and anteiso- isomers were identified only for C15:0 and C17:0 in the range of interest. Apart from anteisoC17:0, they show similar trends to their saturated isomers. AnteisoC17:0 (aC17:0; Figure 87.8.) shows a decoupling in concentration trends from its isomers, with a relative increase in concentration at the depth of 124-132 cm to a value of 0.64 μg/g. Furthermore, saturated FA in the range of C14-C18 increase in concentration from depth towards the surface, with a sharp increase seen in surface samples (Figure 87). The highest concentration at surface within this range is recorded in C16:0, that of 46.02 μg/g. Unlike shorter unsaturated FAs that do not show much variation between depths of 0-8 cm and 124-132 cm, C18:0 shows a relative decrease in concentration at the depth of 0-8 cm. In terms of individual concentrations, until the depth of 124-132 cm C22:0 has the highest overall concentration; after this depth, it is equalled by C24:0 and exceeded by C23:0.

BVA shows a complex variety in terms of its monosaturated FA (Figures 84 and 87.10.). For example, as at the other two locations, both C18:1ω7 and C18:1ω9 are present and show similar trends. They start with a concentration of 1.8 μg/g and 1.44 μg/g, respectively, decrease until the depth of 124-132 cm and peak in values just before surface, with concentrations of 3.62 μg/g and 3.12 μg/g, respectively. Concentration graphs are

represented in Figure 87. Based on DMDS method (see subchapter 2.4.2.1.), surface samples contained the following monosaturated FA with 18C: **C18:1ω9c, C18:1ω7c, C18:1ω7t; C18:1ω5c; C18:1ω5t; C18:1ω8c; C18:1ω8t.** In core samples, only **C18:1ω7, C18:1ω8 and C18:1ω9** were identified (Figure 84), probably in their cis- configuration. The implications of these biomarkers are discussed in subchapter 1.7.4.

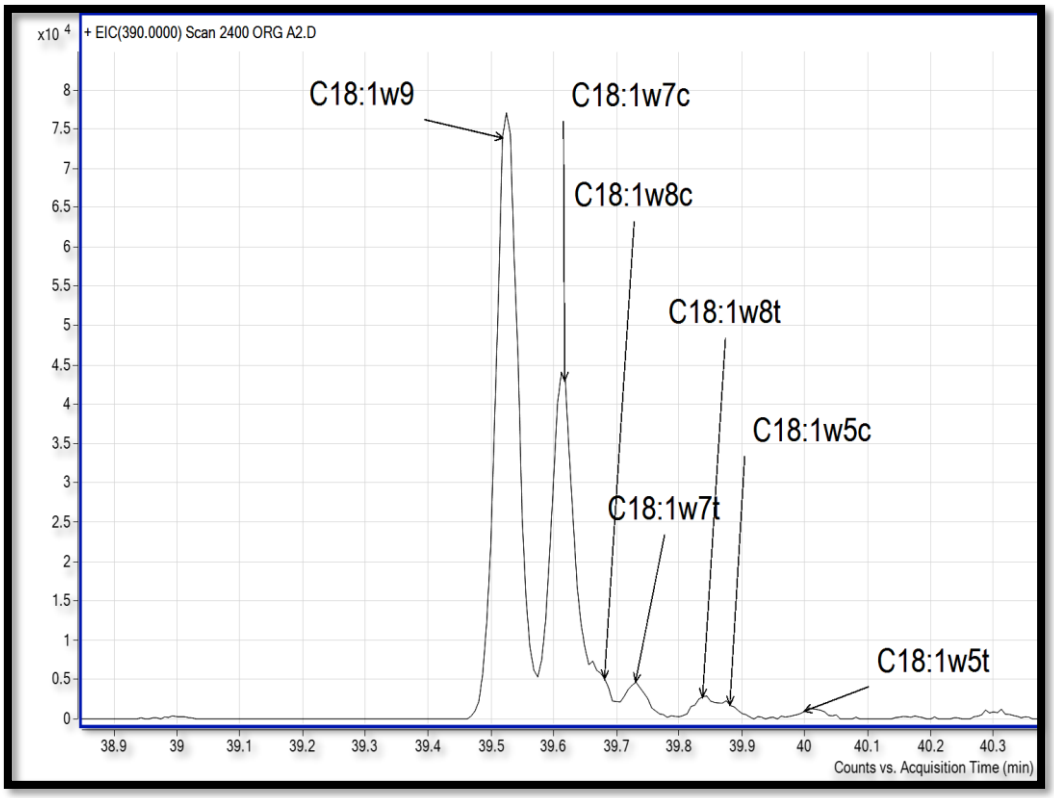

Figure 84 Example of higher diversity in monosaturated C18:1 fatty acids seen through the DMDS method ayt BVA in a surface sample. Notice cis- isomer eluting before trans-isomer.

Furthermore, and one of the most interesting features at BVA, is the presence of monosaturated FA with 16 carbons. They were identified based on the DMDS method in surface samples, and based on their retention times at a depth of 124-132 cm (i.e. on GC-FID). Thus, their concentrations at surface are between 0.08 and 0.53 µg/g., while at the depth of 124-132 cm, of 0.113 µg/g. Due to their low concentration in core samples, the DMDS method did not reveal any results in order to aid their identification. However, at surface, the following isomers were identified: **C16:1ω7c, C16:1ω7t; C16:1ω5c; C16:1ω5t; C16:1ω8t; C16:1ω8c**.

n-Alkane proxies and hopanes

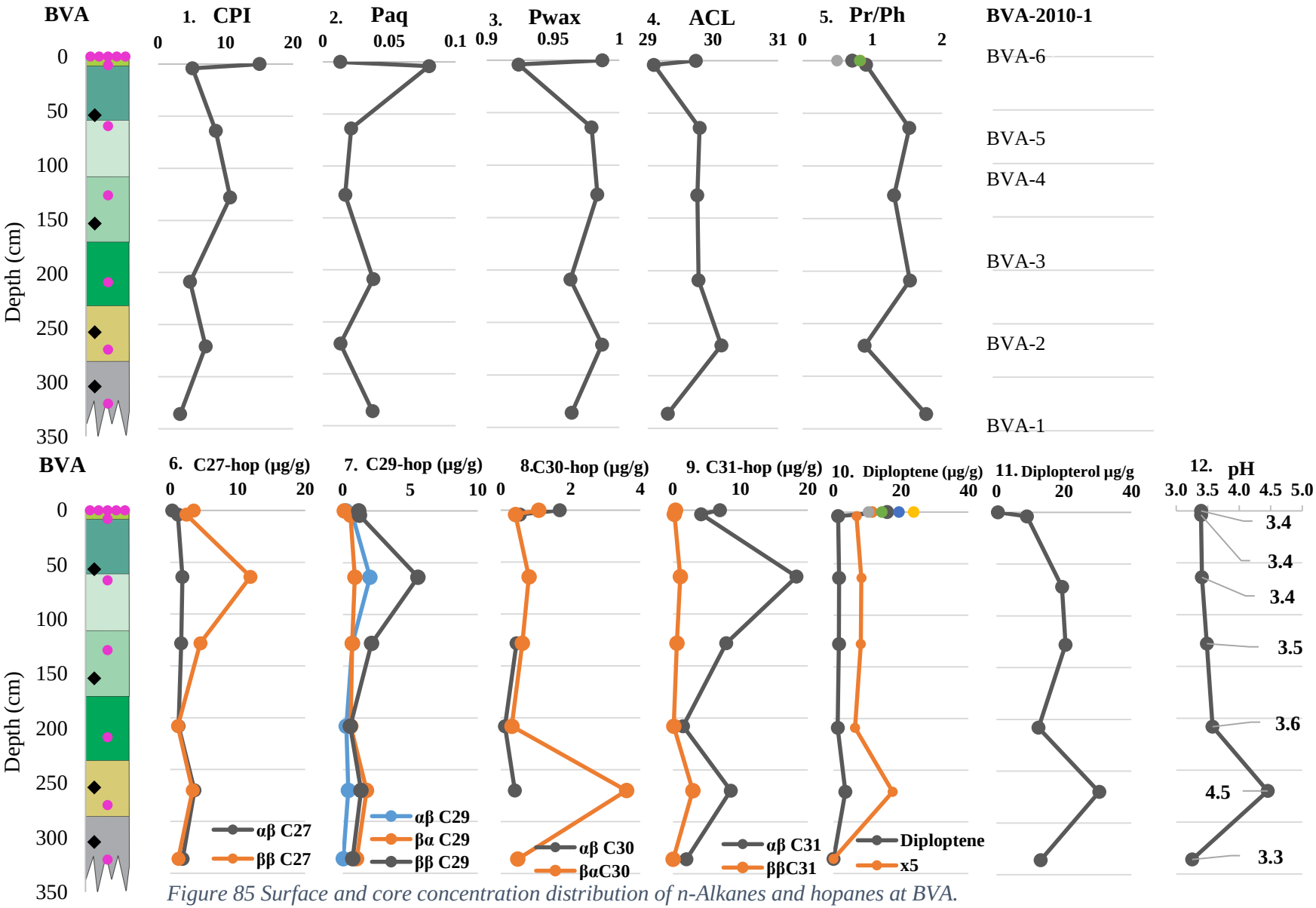

Figure 85 Surface and core concentration distribution of n-Alkanes and hopanes at BVA.

iso- and brGDGTs

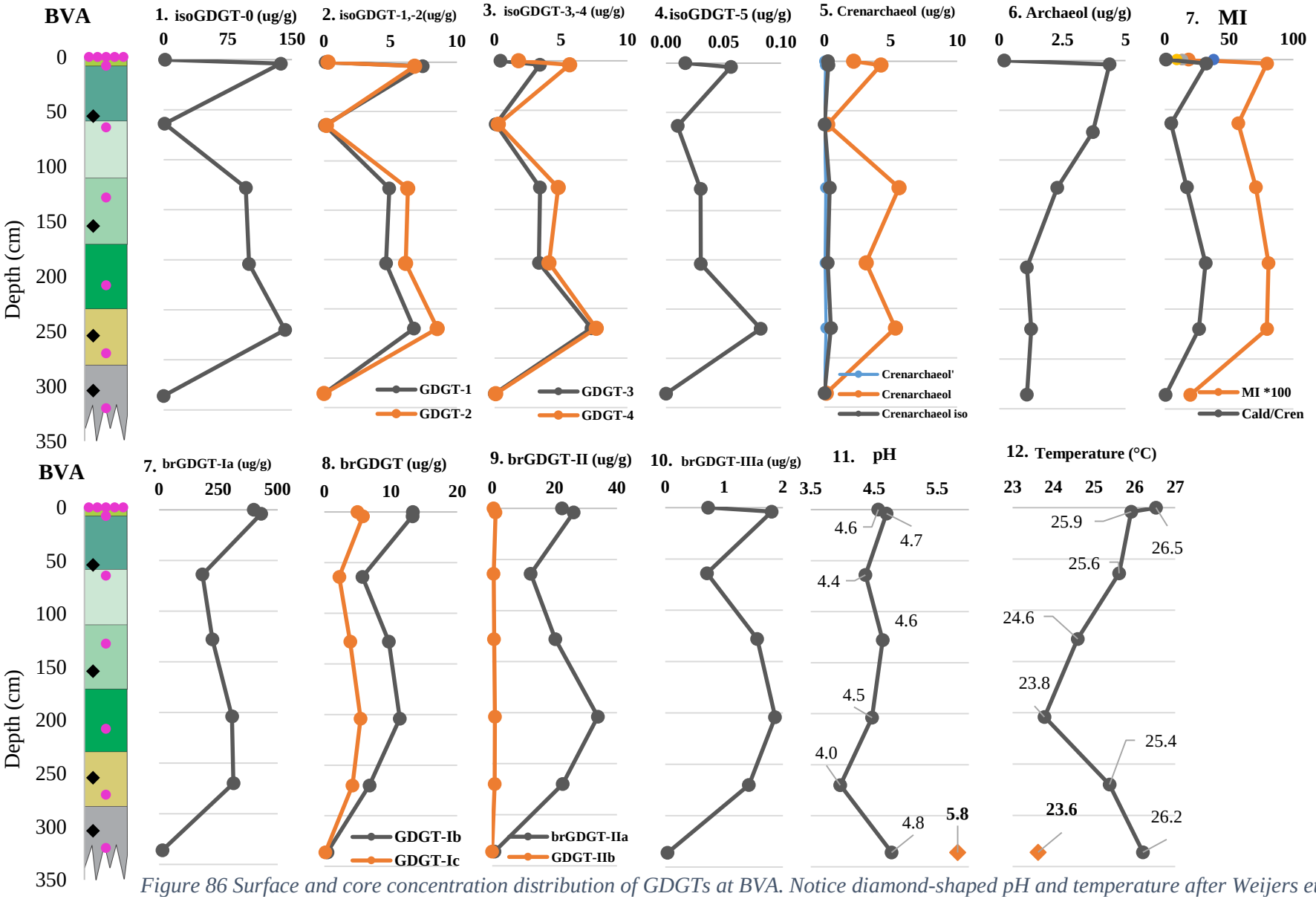

Figure 86 Surface and core concentration distribution of GDGTs at BVA. Notice diamond-shaped pH and temperature after Weijers et al. (2007)

Fatty acids

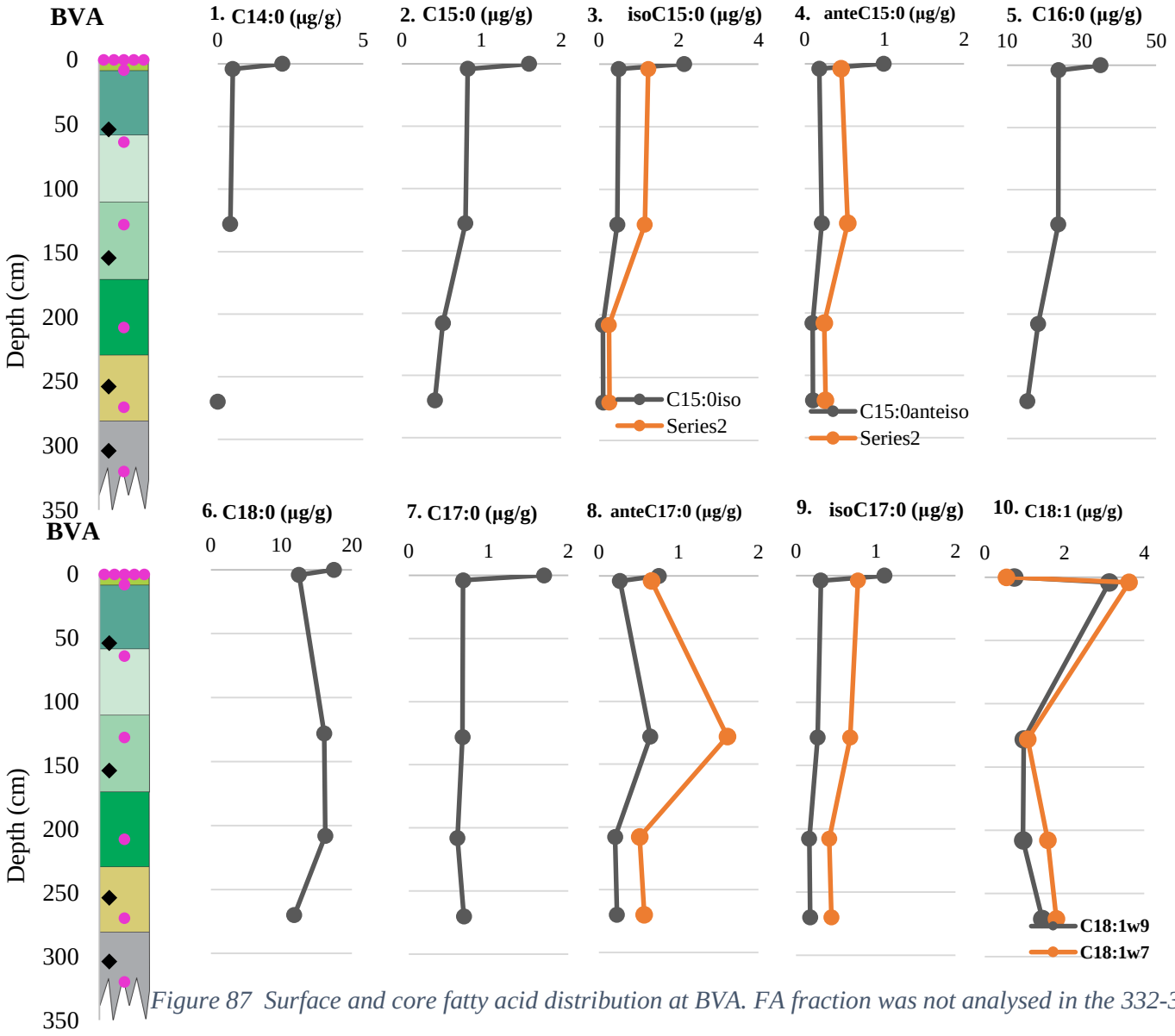

Figure 87 Surface and core fatty acid distribution at BVA. FA fraction was not analysed in the 332-340 cm sample.

Table 14 Summary of BVA results and observations.

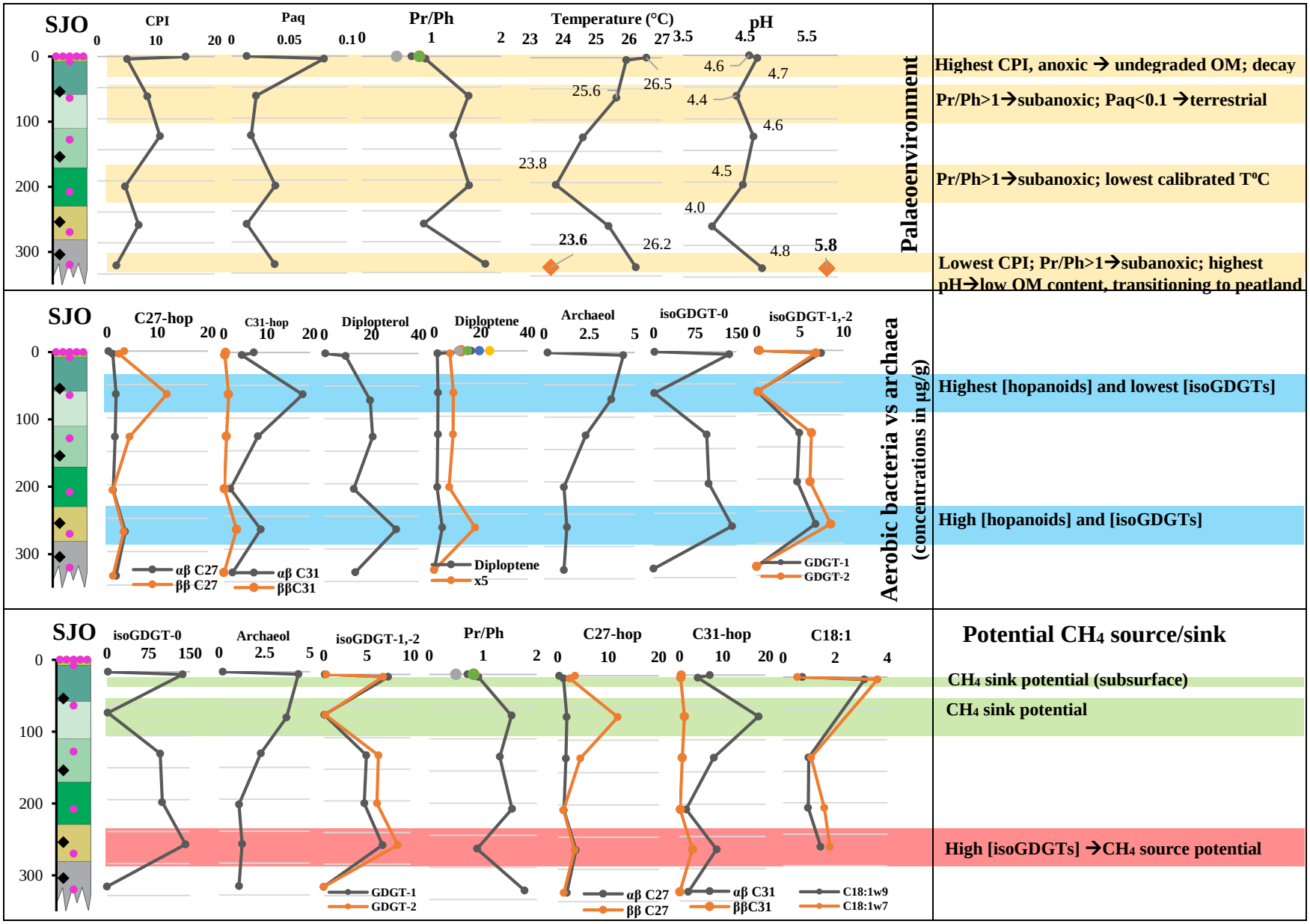

5.3. Interpretation

332-340 cm (BVA-1)

- **n-Alkanes**

The n-alkanes at this depth (BVA-1) come from a clay rich sample, located below the first peat deposits, which indicates a low energy environment and, as at QT, it can be indicative of a lake-like setting. However, due to the absence and relative low concentrations of short chain n-alkanes characteristic to lakes and no aquatic signal seen in P_{aq} proxy (i.e. P_{aq} below 0.1, at a value of 0.03), the palaeoenvironment was probably a flood plain, a terrestrial environment, at a greater distance from Amazon's palaeochannel, only affected during flood events. The signal seen in longer chain n-alkanes, although it does not show a strong odd/even predominance (Figure 82), indicates possibly allochtochonous input from higher plants carried by Amazon floods. The relatively high Pr/Ph ratio (1.77) value indicates suboxic to oxic conditions and correlates with an exposed low-energy terrestrial environment.

- **GDGTs**

IsoGDGTs

Most isoGDGTs show concentrations of less than 0.1 µg/g, with only isoGDGT-4 (i.e. 0.104 µg/g) and crenarchaeol (0.134 µg/g) slightly above this value. This indicates that the environment was lacking required substrate and could not support an extensive archaea community. The predominantly oxic setting, with access to high nutrients, low organic matter content and neutral pH was thus less fitted for microbial development.

BrGDGTs

BrGDGT-Ia has a relatively higher concentration, with a value of 14.8 µg/g however, since sediments were transported by floodwaters, the value is less likely to indicate in-situ production. Thus, peat-calibrations for temperature (i.e. 26.2°C±4.7°C) and pH (i.e. 4.8±0.8) will not yield accurate values. In this case, as in QT's bottom sample, soil calibrations proposed by Weijers et al. (2007a) could be more suited for this environment (see subchapter 1.7.2.3.), given a calibrated pH value at 5.82, slightly higher and more characteristic of a flood plain, with a calibrated temperature at 23.6°C, several degrees lower than the peat-GDGT calibration (Naafs et al., 2018b).

- **Hopanes**

As hopanes are attributed mainly to prokaryote cell membranes (Ourisson et al, 1987), they are probably again not produced in-situ and represent input from adjacent soils and/or were transported via floodwaters.

At this location, although the palaeoenvironment is similar to the bottom of the core at QT, the hopane calibrated pH value of 3.25 (±1.4) is lower than expected suggesting again the allochthonous nature of hopanes, and indicating that the GDGT soil calibration (Weijers et al., 2007a) may be closer to the real value.

- **Fatty acids**

No FA were identified for this depth. Coupled with the occurrence of hopanes, it is likely that FA existed at this depth yet were removed by biodegradation, as seen in part at the surface of QT and SJO and core samples.

266-275 cm (BVA-2)

- **n-Alkanes**

An increase in the concentration of long-chain n-alkanes is seen at this depth with a strong odd/even predominance (Figure 82), indicating mainly input from higher plants, and a possible establishment of forested vegetation after approximatively 300 years from the previous sample (i.e. accumulation rate 2.20±0.78 mm/yr, Lähteenoja et al., 2009a). This is also seen in the trends of CPI and P_{wax} (and P_{aq}) that indicate the presence of less labile and more decay resistant organic matter source (Baker et al., 2016 and references therein). The ACL also increases from the previous depth, peaking at this point, suggesting drier and/or warmer conditions than experienced in the up core samples (see following discussion). The Pr/Ph ratio indicates anoxic conditions however, the value is slightly below 1, thus subanoxic for parts of the year. At this depth, waterlogged conditions that initiated peat accumulation persisted or the peatland was seasonally flooded, which could also explain the Pr/Ph ratio and the increase in hopanes at this depth.

- **GDGTs**

Both iso- and brGDGTs increase in concentrations with the onset of peat accumulation, which also suggests frequent waterlogged conditions and anoxic/subanoxic conditions.

IsoGDGTs

IsoGDGTs have the highest relative contribution to the GDGT pool, with isoGDGT-0 dominating at this depth (141 μg/g). This indicates an increased input from methanogenic archaea under anaerobic conditions, which led to a further increased in the contribution of anaerobic methanotrophs represented by isoGDGT 1-4. However, there is a slight decrease in archaeol concentrations, which does not mirror the isoGDGT-0 (caldarchaeol) values in order to confirm the existence of an active methanogen community. Since archaeol is recalcitrant in nature (see subchapter 1.7.3.), while isoGDGTs are more susceptible to aerobic degradation (Schouten et al., 2003 and references therein), other analytical techniques need to be applied (i.e. carbon isotopic signatures) in order to say whether the peatland was already acting as a CH_4 source and whether isoGDGT-0 in this setting is an indicator of methanogenesis. However, in previous peatlands there was a good correlation between the relative increases in isoGDGT-0 and archaeol (see QT and SJO interpretations), indicating that isoGDGT-0 producers are (at least in part) representative of the methanogenic community.

Crenarchaeol concentration increase suggests either that the top parts of the peat were frequently exposed to oxygen or that water table oscillated between above surface at least during the wet season and below during the dry season for approximatively 35 years (i.e. 8 cm of sample; accumulation rates of 2.5mm/yr, Lähteenoja et al., 2009a). This is also seen as a peak in the MI values, at 94.8 (Figure 86.7.). There is also an increase in isoGDGT-5 and this can be due to the overall increase and stability of the archaeal community that included its producers or to an increase in temperature (i.e. also ACL increase) on the background of stable pHs (Naafs et al., 2018b). Indeed, this is true for a basal temperature of 23.6ºC (Weijers et al., 2007a), characteristic of a soil sample.

BrGDGTs

BrGDGTs also increase in concentrations, supporting anaerobic overall conditions and development of an anaerobic bacteria community. BrGDGT-Ia is the dominant brGDGT, characteristic of tropical peatlands (Naafs et al., 2017a). At this depth, vegetation was probably adapted to waterlogged conditions.

Calibrate pH values are in the range of 4.77-3.17, with an average at 4.0, indicating that although the peatland was annually flooded, high water tables and precipitation did not allow for pH increase and that the main water source was atmospheric precipitations. Calibrated temperature is at 25.3°C (±4.7°C), within the range of present day measured temperatures.

- **Hopanes**

This depth represents a peak in the concentration in all hopanes relative to adjacent samples. The peaks are also recorded in diploptene and diplopterol. As no pollen data exists for this peatland, it is difficult to appreciate the variations in water table and effect of vegetation on microbes. However, given the discussed increase in crenarchaeol (Figure 86.5.), which suggests that at least the top of the peatland was frequently exposed to oxygen, aerobic bacteria were able to develop in a relatively stable acrotelm between flood events during the dry season.

The peaks in diploptene and diplopterol that have the highest concentrations at this depth (i.e. 3.5 and 30.4 µg/g, respectively) indicate their recalcitrant nature, however they cannot be correlated with methanotrophy due to their diverse aerobic and anaerobic producers (Rohmer et al., 1984; Hartner et al., 2005). For this depth, it would be interesting to analyse diplopterol and diploptene carbon isotopic signatures, as they would indicate the role of bacteria in CH_4 consumption at BVA.

The hopane-calibrated pH is at 4.45 (±1.4), peaking at this depth also suggesting a thicker or more stable acrotelm.

- **FA**

At this depth, short chain FA are dominated by C16:0 and C18:0 indicating bacterial input however, the iso- and anteiso- isomers of C15:0 and C17:0, C18:1ω9 and C18:1ω7 have very low concentrations implying low CH_4 consumption rates and that the peatland had a high potential of acting as a CH_4 source. As isoGDGT-0 peaks at this depth indicating an extensive methanogen community, the lack of suitable substrate cannot be the main reason for low concentrations of biomarkers indicating type II methanotrophs, thus, a further driver is needed. It is also possible that given the high degree of peat maturation at this depth indicated by a peak in βα C_{30}-hop, that FA were also subject to diagenesis in the reducing environment or consumed by microbes, a process that preferentially takes place in the case of short chain and unsaturated FA (Disnar et al., 2005; Cranwell et al., 1981 and references therein).

204-212 cm (BVA-3)

- **n-Alkanes**

There is a further increase from the previous depth in the concertation of long-chain n-alkanes however, the odd/even preference is maintained and, with a low, undifferentiated input from short- and medium-chain n-alkanes, indicate a strong terrestrial signal, from vascular vegetation. The slight decrease in CPI is due to relative higher concentrations of long-chain even n-alkanes, thus a change in vegetation is also possible and can be confirmed through pollen analysis. Although the Pr/Ph ratio indicates a suboxic setting, bearing a higher value than at the previous depth, it can also be due to plant-adaptations to anoxic conditions, with the ability to transport oxygen to lower depths and CH_4 to the atmosphere, a process which was also seen at QT and SJO.

The overall increase in n-alkanes, with n-C_{29} and n-C_{31} peaking at this depth, higher input from short and mid-chain n-alkanes can indicate changes in the hydrological regime, possibly explaining the lower CPI and an expected vegetation shift.

- **GDGTs**

IsoGDGTs

At this depth, the main isoGDGTs (0-4) shows a slight decrease in concentration, which is also mirrored by crenarchaeol and isoGDGT-5. Although it is difficult to assess what might have caused this decrease or change in the archaea community without vegetation changes, n-alkanes indicate a possible change in the hydrological regime (and potentially, in vegetation). Furthermore, there is an increase in biomarkers specific of anaerobic bacteria (i.e. brGDGTs) and a decrease in biomarkers that indicate aerobic bacteria (i.e. hopanes, diplopterol). This can indicate that the flooding regime increased in frequency, and that BVA was under permanent waterlogged or periodic flooded conditions. Due to the implied decrease in oxic degradation in the top parts of the peat, it is possible that anaerobic decomposition and production of substrate for methanogenesis was slower, affecting isoGDGT-0 producers and leading to a decrease in anaerobic methanotrophs (isoGDGT 1-4). Furthermore, the decrease in isoGDGT-5 can also indicate a decrease in temperature or shift in pH (Naafs et al., 2018b), confirmed by brGDGTs-based calibrations.

BrGDGTs

BrGDGTs increase (i.e. GDGT-Ib, -Ic, -IIa, -IIIa) or remain at stable concentrations (brGDGT-Ia), although this stability can only be apparent, it can also indicate that overall

environmental conditions were favourable for anaerobic bacteria community development. Calibrated pH is at 4.46 (±0.8) while calibrated temperatures at 23.79°C (±4.7°C), the lowest temperature for this location which could have had an impact on microbial activity and thus, their concentrations. As discussed above, this can correlate to the decrease seen in isoGDGT-5.

- **Hopanes**

The following decrease in hopane concentrations supports the assumed change in the hydrological regime, from seasonal or periodic flooding to permanent waterlogged conditions, during which the bacteria community was restricted to oxic microsites or developed for short periods in the oxic top layer. The calibrated pH indicates a decrease, with a value of 3.57 (±1.4), within the error range of GDGT-calibrated pH, supporting increased precipitations and waterlogged conditions. However, a drop in temperature can also lead to a decrease in the microbial activity.

- **FA**

Saturated FA maintained their concentrations and a further decrease is seen in monosaturated FAs indicating biodegradation or unfavorable conditions (mainly anoxic) for aerobic methanotrophs.

124-132 cm (BVA-4)

- **n-Alkanes**

The palaeoenvironment at this depth is similar to the one described above: a terrestrial waterlogged setting with input from vascular vegetation. Some vegetation species probably disappeared at this point as we see less input from short chains and even carbon n-alkanes or, this can indicate less biodegradation and microbial reworking, which could have led to the increase seen in CPI, P_{wax} and ACL ratios. A slight decrease in Pr/Ph ratio potentially suggests a higher frequency or duration of floods, waterlogged conditions and less space for aerobic microbes development which was previously discussed.

- **GDGTs**

IsoGDGTs

IsoGDGTs show similar concentrations to the previous depth. The stability of microbial community can be again only apparent given the large time gap between the two depths,

however, it is also possible that between 204 and 124 cm similar environmental conditions occurred. For the two depths, archaeol biomarker increases in concentration supporting an increase in the methanogen community however, this increase could postdate the palaeoenvironment that this depth represents in terms of vegetation (i.e. n-Alkane input) as methanogenesis can continue at depth under favourable conditions. Crenarchaeol increases in concentration which can be due to incorporation of peat that deposited during several drier periods (i.e. 8 cm thick sample, representing approximatively 32 years of continuous deposition at the rate of 2.5mm/yr, Lähteenoja et al., 2009a).

BrGDGTs

BrGDGTs decrease in concentrations can be due to competitive relationships or, if Acidobacteria is a main brGDGT-Ia producer (Weijers et al., 2009a), to less acidic conditions. The GDGT-calibrated pH for this depth is at 4.63 (±0.8), slightly higher than in the previous section but still supporting to some extend this interpretation. The temperature also increases to a calibrated value of 24.6°C (±4.7°C).

- **Hopanes**

Hopanes start to increase in concentrations, and peak in the following sample, at the 60-68 cm horizon. Although the increase cannot be correlated and considered continuous due to the low resolution of samples and the age difference between the two depths, similar factors probably led to these increases. Since crenarchaeol also increases in concentration and the vegetation was probably adapted to waterlogged conditions, the area around root systems could have been oxygen-rich and able to support aerobic communities (see subchapter 1.5.2.). Furthermore, as the present-day flat topography of the peatland supports periodic flood events, this could have also been true in the past, thus, it is also possible that a shift in precipitation led to reduced flooding and waterlogged conditions during the dry season.

However, the hopane-calibrated pH value is at 3.5 (±1.4), not indicating again a decrease in the precipitation regime.

- **FA**

FA have slightly higher concentrations at this depth, following the increase seen in hopanes, with a peak in anteisoC17:0. This supports the interpretation of an active bacteria community for that time. However, monosaturated FA have similar or lower concentrations (C18:1ω7) from the previous depth, thus indicating a low potential for CH_4 consumption.

60-68 cm (BVA-5)

- **n-Alkanes**

The overall increase in the input of n-C_{29} and n-C_{31} from the previous depth, suggests again a terrestrial environment. Pr/Ph ratio has a value above 1.5 indicating suboxic conditions and thus, a fluctuating nature of the water table, less frequent and shorted flood events or even a drier period, confirmed by further biomarkers. The CPI value decreases slightly due to possible microbial reworking of organic matter or change in vegetation.

- **GDGTs**

At this depth, there is a pronounced decrease in isoGDGTs, mirrored brGDGTs.

IsoGDGTs

IsoGDGTs reach trace concentrations indicating a possible collapse in the methanogen and anaerobic methanotroph communities (i.e. isoGDGT 0-4). However, archaeol input continues to increase.

The decoupling seen between isoGDGT-0 (caldarchaeol) and archaeol implies that either isoGDGT-0 might not be related to a methanogen community or that methanogens in this peatland do not biosynthesise a high amount of caldarchaeol for their membrane structure. This interpretation is also supported by the fact that within the archaea domain, archaeosomes (although not a methanogen), for example, can have membranes composed of only monopole archaeol in a bilayered configuration **or** bipolar caldarchaeol (isoGDGT-0) lipid in a monolayered structure (Kaur et al., 2015; Benvegnu et al., 2009). Since only archaeol was found in methanogen cultures (e.g. Sprott et al., 1990; Koga et al., 1998) as well as in environments where CH_4 is produced (Pancost et al., 2000), and caldarchaeol's methanogen origin was assessed primary based on the isotopic signature of byphytanes (Schouten et al., 2013 and references therein; Pancost et al., 2003), it can be likely, that in this peatland, isoGDGT-0 is not a methanogen indicator and that carbon isotopic measurements should be employed alongside isoGDGT-0 source assessments.

What is also interesting is the collapse in isoGDGTs 1-4 that were assigned to anaerobic archaeal methanotrophs. This could indicate that producers of isoGDGTs 1-4 are obligate in nature and that they utilize CH_4 produced in very close proximity since some CH_4 is still expected to be generated at depth. Furthermore, methanogenesis in higher just below water table (e.g. Pancost et al., 2011; Zheng et al., 2014), thus, if this palaeosetting experienced a drier period, a drop in the water table could have restricted methanogenesis to previous

substrate depleted depths. However, despite this proposed highly oxic setting, crenarchaeol lipid which characterise ammonium-oxidising Thaumarchaeota under oxic conditions (Schouten et al., 2103 and references therein), is also seen to decrease in concentrations indicating overall reduced oxygen, thus a combination of factors is expected, even a possible shift in (local) vegetation to herbaceous taxa given the relative drier period. This shift was also seen to affect microbial communities at QT (see QT-4b).

BrGDGTs, although decrease in concentrations across all profiles, are still relatively abundant, with brGDGT-Ia's concentration, the most common brGDGT in peat-accumulating environments (Naafs et al., 2018a), at 182 µg/g. BrGDGTs could have been thus restricted to anoxic microsites.

Calibrated pH value is at 4.36 (±0.8), while calibrated temperatures at 25.6°C (±4.7°C).

- **Hopanes**

The increase in hopanes supports the interpretation of a drier period or a thick and constant acrotelm. The increase in mainly seen in ββ hopanes, thus indicating an active and extended aerobic bacteria community and the lack of diagenesis (i.e. immature peat). There is also a decrease in brGDGTs for these two depths and a minimum concentration recorded in isoGDGTs for 60-68 cm, again, implying a stable and thick acrotelm, decomposition of organic matter and possible a higher CH_4 consumption. The present day flat topography of the peatland that supports periodic flooding events could have also sustained this conditions in the past, thus, it is possible that a shift in the precipitation led to reduced flooding and waterlogged conditions

The hopane-calibrate pH is at 3.4, similarly to the previous depth.

0-8 cm (BVA-6)

- **n-Alkanes**

There is a decrease in the relative input of long-chain n-alkanes just below the surface, however, at this depth, n-C_{29} dominates. The vegetation was probably the same as at present, thus indicating that the present-day forested vegetation is characterized by both n-C_{29} and n-C_{31}, with a higher input from the former and that the transition to this vegetation type took place after the depth of 60-68 cm (where both n-alkanes dominate). The CPI is relatively constant from the previous depth, with a slight increase in ACL. Pr/Ph ratio decreases, below

1 indicating anoxic conditions and, as the dissolved oxygen % was recorded for the top 15 cm of the peat (Teh et al., 2017), bearing a value of 18.9%, similar thus to that recorded in the surface sample, it indicates that for higher Pr/Ph values in the past, the dissolve oxygen % was higher than this present-day value.

- **GDGTs**

As this sample comes from the fresh peat just below the surface, it is highly useful in understanding bioaccumulation, biomarkers' relative concentrations between frequently the air-exposed organic matter at the surface and more degraded organic matter below. All GDGTs concentrations increase in this horizon, indicating possible higher microbial activity due to less degraded organic matter.

IsoGDGTs

IsoGDGTs return to relatively high concentrations. Although a decoupling between isoGDGT-0 and archaeol was seen at depth, below surface both biomarkers have relative high values. CH_4 is likely produced in the anoxic part of the peat, just before surface, in the mesotelm (Pancost et al., 2011). Several studies (Pancost et al., 2011; Huguet et al. 2013) done in boreal peatlands have related this part of a peatland to the highest methanogen activity based on biomarker concentrations due to the existence of readily available substrate for methanogenesis.

All isoGDGT (0-5) peak in this horizon. IsoGDGT-0, a proposed biomarker for methanogen community, has a concentration slightly lower than what was recorded at a depth of 266-275 cm. If the two depths are similar in terms of methanogenic community size and species, then the signal seen at 266-275 cm can be considered a palaeosignal, with very little input from subsequent active communities and accumulation over time. The increase in isoGDGTs 1-4 indicate a growing anaerobic methanotroph community, due to abundant substrate provided from methanogens. The presence of isoGDGT-5 in relative higher concentrations than at previous depths can be an indicator of sustained acidic conditions and increase in temperatures (Naafs et al., 2018b). Crenarchaeol also increases in concentration from previous depth. This concurrent increase in the top 10 cm of the peatland suggests the oscillating nature of the water table or present day accumulation and an active aerobic microbial community.

BrGDGTs

BrGDGTs mirror the increase in isoGDGTs, peaking in concentrations at this depth, highlighting the overall waterlogged nature of BVA. Since GDGTs core lipids are decay-resistant (Huguet et al., 2010; Lengger et al., 2014), the relative highest concentrations at this depth implies that environmental conditions were most favourable for brGDGTs. Today, BVA is characterized by high nutrient input (i.e. minerotrophic setting); it is possible that the input of nutrient from secondary sources (i.e. ground- or floodwater) is a process that did not affected previous depths. Input of nutrients such as K, Mg and P (Table 8) are expected to provide additional substrate for methanotrophy in the aerobic layer or can enhance anaerobic bacteria population size, a hypothesis supported by peaks in brGDGTs-Ib, -IIa, -IIb and –IIIa.

Calibrated pH for this depth is at 4.69 (±0.8) while calibrated temperatures at 25.91°C (±4.7°C).

- **Hopanes**

The following decrease in hopane concentrations are probably related to present-day environmental conditions. The flat topography at BVA implies waterlogged conditions and periodic flood events from nutrient-rich water (Lähteenoja et al., 2009b), leading to a reduced acrotelm, that restricts the development of the aerobic bacteria community. The water table oscillated between above and below surface, with the acrotelm reaching a maximum thickness of 13 cm (Teh et al., 2017). The calibrated pHs of 3.39 (±1.4) are well below present day measured values of 6.31 recorded during the dry season when samples were collected (Teh et al., 2017), however, this hopane-based pH calibration is mainly restricted to acidic environments and may not be suitable for a peatland like BVA (Inglis et al., 2018).

- **FA**

At this depth, an increase in concentrations is seen in medium and long-chain FA, however, short branched and saturated short chain FA have a similar or lower concentration from the previous sample. Monosaturated FA peak at this depth, just below surface, which corresponds to the relative position of the water table during the dry season (i.e. approximatively 13 cm below the surface). Monosaturated biomarkers with 18 carbons are indicators of type II methanotrophs that are known to prefere the interface between the oxic and anoxic layers, where CH_4 availability is greatest (Pancost et al., 2011). Thus, a higher

methanotroph concentration, probably also indicating the present day living community is expected and it is confirmed by this increase just before surface.

Surface samples

- **n-Alkanes**

The availability of samples from just below and from the surface provides information on the rate of biodegradation and (enhanced) microbial activity at the surface of the peatland. As the samples were collected during the dry season, the acrotelm was approximatively 13 cm in thickness (Teh et al., 2017). Similarly, to the previous two peatlands, there is a relative increase in short chain n-alkanes, suggesting that short chain n-alkanes are further biodegraded and that this process takes place in a relatively short time. Again, long-chain n-alkanes display an odd/even preference, specific to a forested vegetation. Pr/Ph ratio indicates anoxic to suboxic conditions that correspond to a value of 18.9% of dissolved oxygen. However, the complete data set published by Teh et al. (2017) shows high discrepancies between two consecutive dry seasons with values below 0.5% for 2012 and for 2013 values between 0.1 and 90% (Website 15).

- **GDGTs**

All isoGDGTs decrease in concentration, reaching almost trace values. This is explained by the fact that samples were collected from the surface of BVA, in contact with air. Only one of the four analysed surface samples shows isoGDGT-0 with a concentration of 5.17 µg/g, which is probably due to the (micro)topography of the sampling location (i.e. possible a hallow structure). Since surface samples are expected to be more often exposed to aerobic conditions, we see relatively higher concentrations of crenarchaeol, a biomarker for ammonia-oxidizing Thaumarchaeota (Zheng et al., 2015). IsoGDGT-5 was found in trace concentrations (0.067 µg/g) in only 1 of the 4 samples, indicating its slow accumulation rate over time and specific environmental conditions in which it occurs (see Naafs et al., 2018b).

However, higher concentrations seen in brGDGTs suggest the waterlogged or seasonal flooded character of this peatland and, potentially, the more competitive nature of anaerobic bacteria compared to archaea at colonizing fresh organic matter under (even short-lasted) anaerobic conditions. This observation is probably best supported by the necessity of only several types of substrate required for methanogenesis, which might have not been available at this time (Hanson and Hanson, 1996). Thus, as observed in other settings (e.g. Megonigal

et al., 2014), methanogens are constricted by other microbes and by their ability to provide required substrate (acetate, methanol, CO_2, see subchapter 1.2.1.). As seen in the previous sample, methanogenesis probably starts just below surface, after the onset of organic matter decay.

One further explanation for this increase can be due to an aerobic source for brGDGT-Ia (and potentially further brGDGTs in unidentified sources). Sinninghe Damsté et al. (2011) discovered two aerobic Acidobacteria that produced brGDGT-Ia and from thereon several other studies agreed on the aerobic or facultative nature of some Acidobacteria (Pankratov et al., 2012; Kielak et al., 2016), thus, implying that the presence of this biomarker can also indicate aerobic settings. Since samples were collected during the dry season, when the water tables, at least at this site, were below surface (Teh et al., 2017) and since the phyla is highly diverse and common in acidic settings such as peatlands (Sinninghe Damsté et al., 2011 and references therein; Jones et al., 2009), the possibility of an aerobic producer should be further investigated in PMFB.

Calibrated pHs are between 5.16 and 3.9 (±0.8), while present day measured pH during the dry and wet seasons are at 6.31 and 5.88, respectively (Teh et al., 2017). It can suggest that since the time of peat core collection (2010) and time of instrumental measurements collection (2012-2014; Teh et al., 2017; Website 15), pH increased in value. Calibrated temperatures are between 25.6°C and 26.9°C (±4.7°C), while instrumental temperatures for this location are at 24.7°C for the dry season and 26.1°C for the wet one, thus, within the error range, implying relatively accurate values for calibrated temperatures down-core based on GDGTs concentrations.

- **Hopanes**

As expected, hopanes increase in concentration at the surface, due to readily available oxygen and organic matter. The hopane-calibrated pH is at 3.4 (±1.4), not matching instrumental measurements (Teh et al., 2017).

- **FA**

Surface samples have overall higher concentrations of FA across all ranges and isomers apart from monosaturated FA which are seen to decrease slightly in concentration. Furthemore, although the average is reported in Figure 87.10., C18:1ω7 and/or C18:1ω9 are not found in all surface samples, indicating, unlike at depth, an uneven distribution, and possible subsequent accumulation over periods of fluctuating water tables.

Implications of type I and type II biomarkers and present day effluxes

Both core and surface samples contain biomarkers specific of type II methanotrophs. Although only concentrations of C18:1ω7 and C18:1ω9 were quantifiable through GC-FID, the DMDS method revealed further compounds specific of type II methanotrohps at surface, together with evidence of type I. Thus, in terms of monosaturated C18 FA, the following biomarkers were found: **C18:1ω5c,t; C18:1ω7c,t; C18:1ω8c,t** and **C18:1ω9**. The higher diversity of monosaturated isomers indicates a possible more diverse methanotroph community than in the other two peatlands. Furthermore, in terms of monosaturated FA with 16C, DMDS method revealed the following configurations: **C16:1ω5c, t; C16:1ω7c, t** and **C16:1ω8c, t**.

The high diversity of monosaturated FA also can potentially indicate a higher diversity or a larger methanotroph community. However, by taking into account CH_4 efflux measurements reported by Teh et al. (2017), we see that there are higher CH_4 effluxes during the dry season (i.e. 47.2±5.4 mg CH_4-C/m^2/d) when the water is also below surface (-13.2 cm) compared to the wet season. The occurrence of higher overall CH_4 emissions during a period of (potentialy) high and active methanotroph community can however be explained through a main pathway of CH_4 release from this peatland. Thus, one explination can be that, due to lower water tables, at depth, this will be experienced as a drop in the hydrostatic pressure. This pressure decrease during the dry season could allow CH_4 bubbles to form and be released via ebbulition to the surface, bypassing most of the methanotrophy zone (see subchapter 1.5. and references). This proccess was also observed by Teh et al. (2017) at sites with forested vegetation, characteristic to present day BVA. Thus, this can explained the possible presence of type II methanotrophs that are facultative in nature, meaning that they can also survive on CO_2 substrate in the complete absence of CH_4, however, since there are also biomarkers indicative of type I methanotrophs, which are obligate in nature, there is a high chance that part of the CH_4 is being consumed as well in-situ.

From this particular case, it appears that high water tables can have in fact a negative impact on CH_4 emissions, with higher water tables actually restricting ebbulition and thus, mitigating high CH_4 fluxes from this peatland. This is further indicated by the 6-7 times lower effluxes during wet season, when water tables at this site have been measured at 110.9 ±9.3 cm above the surface. Much of the CH_4 movement at depth is possibly restricted by the imposed water pressure and, it can be consumed in-situ by anaerobic methanotrophs or, if the water table decrease happends gradually, part of it can be released by diffusion and oxidized. However, due to the large difference in water table height between the dry and wet

season, it is less possible for diffusion to take place at the same time with the existance of an oxic peat layer and active methanotroph community.

This case shapes itself as a potential research question that needs to be further investigated. Here, it would be of interest to understand how the three main pathways of CH_4 transport take place and which one dominates, how much CH_4 is being produced at depth and if indeed the water table depth has an effect on the prefered pathway to surface; what is the required drop in water table and hydrostatic pressure to allow CH_4 to aggregate into bubbles and be release to the surface; when does the main fluxes of CH_4 occur with resprect to the shift in water table depth (i.e. fast drop-fast release relationship) and, furthermore, the potential of CH_4 consumption during the dry season in the oxic layer, the time lag between increase in oxygen levels and increase in the methanotroph population. Furthermore, the flat topography at BVA also implies its flood-prone character and minerotrophic nature. The presence of river-brought nutrient to the peatland during the wet season can also be accountable for the (potentially) higher methanotroph community and occurrence of type I methanotrophs, indicating again the importance of high water tables, however this time river flood-generated.

5.3.2. Buena Vista peatland synthesis

Although pollen records are not yet available for BVA peatland, biomarker data and present day instrumental parameters allowed palaeoenvironment descriptions in terms of relative vegetation and hydrological changes. As a summary, n-alkane-based proxies such as CPI with values mainly below 10 with a strong odd/even signal in individual n-alkane profiles, indicate that peat here accumulated mainly under higher plants. Herbaceous taxa were inferred in the 60-68 cm sample (BVA-5), and based on other proxies discussed below, the increase seen towards the surface given the prominent terrestrial and higher plants signals implies that the organic matter is better preserved towards recent. This could be correlated to the suboxic/subanoxic signal seen in the Pr/Ph ratio, that mainly shows values above 1, which suggests that the peatland's surface was frequently exposed to air, and that waterlogged conditions or flooding was somewhat restricted at this site, compared to QT and SJO. In zone BVA-2 (Figure 85), we notice a slight relative increase in CPI from adjacent zones at the same depth where Pr/Ph indicate anoxic conditions. The indices suggest that waterlogging had an effect on organic matter preservations and that in up-core samples, the water table fluctuated in the past, leading to organic matter reworking. The P_{aq} proxy at this site does not record an aquatic signal in the analysed samples, thus, at this site, no lake-

like environment is inferred and we do not expect to find ppollen indicating aquatic species in our future analyses.

Hopanes concentrations show two peaks, one in zone BVA-2 and one in zone BVA-5 (Figure 85). This can be due to longer periods when the peat surface was exposed to the atmosphere, allowing a thicker acrotelm development and thus, space for aerobic bacteria development, also indicated by the increase in crenarchaeol in zone BVA-2. However, for zone BVA-5, there appears to be an overall collapse in the microbial community, in both anaerobic and aerobic species represented by GDGTs. Thus, it is expected that this depth was exposed longer to air, which restricted CH_4 production in the substrate-rich horizon, leading to a further collapse in the anaerobic and aerobic methanotrophic communities.

Both iso- and brGDGTs appear to be present the same trends in concentration, indicating similar responses to changes in the hydrological regime and available substrate. Thus, we see an increase in GDGTs from zone BVA-1 characterized by clayey deposits with low organic matter, to zone BVA-2 where peat accumulation started, a decoupling in the following zone BVA-3, where only brGDGTs continue to increase as a possible consequence of competitive relationships, and a decrease in both GDGTs types that reach a trough in zone BVA-5. Both iso- and brGDGTs increase afterwards in concentrations, indicating CH_4 production and a high potential for consumptions that minimise again in surface samples.

Inferred pH values indicate that, similar to QT, the peat started accumulating in a pH neutral environment, as zone BVA-1 is represented by a terrestrial, low energy environment, represented by a poor organic matter clayey unit. Thus, BVA-1 is characterized by a 5.8 pH calculated through Weijers et al. (2007) soil calibration, while the following zone show progressively acidic pHs. The pHs in zone BVA-2 to BVA-6 and surface samples have been calculated using GDGTs (Naafs et al., 2017a), and show values between 4.0 and 4.7 (±0.8). Surface pH average was calculated at 4.6, more acidic than present day instrumental values (i.e. 6.31). Calibrated temperatures indicate that peat started accumulating during a relatively warmer period (26.2±4.7°C), similar to present day conditions. Lowest temperatures are recorded in pollen zone BVA-3 (i.e. 23.8°C±4.7°C), and are seen to increase after this point. Present day instrumental temperature during the dry season, 24.7°C are within the error range of calibrated temperatures of 25.9±4.7°C.

6. Discussion

6.2. Biomarker differences between peatlands and heterogeny at the surface

- **n-Alkanes**

The biomarker distribution at the surface of the sites allow us to not only validate that they are recording modern signals within the peatland, but also assess different vegetation types and processes occurring among the three sites. We observe that the summed average of n-alkanes at surface for QT and SJO are similar, with 754.76 µg and 748.53 µg, respectively, while BVA has a lower summed average of 456.89. This can indicate a higher microbial reworking at BVA at the surface, facilitated by an increased acrotelm thickness during the dry season (Figures 88 and 89).

Vegetation Type	Peat Temperature (°C)		Air Temperature (°C)		Conductivity (µS m^{-2})		Dissolved Oxygen (%)		Water Table Level (cm)		pH	
	Wet Season	Dry Season	Wet Season	Dry Season	Wet Season	Dry Season	Wet Season	Dry Season	Wet Season	Dry Season	Wet Season	Dry Season
Forested	26.1 ± 0.1a	24.7 ± 0.0a	28.8 ± 0.7a	26.4 ± 0.3a	79.0 ± 5.9a	75.9 ± 5.7a	0.2 ± 0.1a	18.9 ± 4.4a	110.8 ± 9.3a	-13.2 ± 0.7a	5.88 ± 0.15a	6.31 ± 0.04a
Forested (short pole)	25.2 ± 0.0b	24.8 ± 0.1a	27.6 ± 0.1b	27.5 ± 0.1b	21.0 ± 0.0b	48.5 ± 4.8b	4.4 ± 0.0a	33.1 ± 2.6b	26.9 ± 0.5b	-4.7 ± 0.4b	4.88 ± 0.01b	3.8 ± 0.03b
M. flexuosa Palm Swamp	25.6 ± 0.6c	25.3 ± 0.1b	26.3 ± 0.1c	26.4 ± 0.1a	45.9 ± 2.1c	51.9 ± 1.8b	19.4 ± 1.3b	17.3 ± 1.5a	37.2 ± 1.7c	6.1 ± 1.3c	5.04 ± 0.03c	5.49 ± 0.03c
Mixed Palm Swamp	26.0 ± 0.0a	25.0 ± 0.1ab	26.1 ± 0.1c	28.2 ± 0.3b	100.0 ± 0.2d	206.4 ± 4.2c	0.0 ± 0.0a	0.0 ± 0.0c	183.7 ± 1.7d	-2.4 ± 0.3b	6.1 ± 0.03a	6.82 ± 0.02d

Figure 88 Showing main physical parameters at surface in the three peatlands (Teh et al., 2017). Forested vegetation=BVA Forested (short pole)=SJO; M.felxuosa palm swamp=QT.

Vegetation type can have a further impact on the organic matter input and preservation. While all three peatlands have high concentrations of short chain n-alkanes, n-C_{27} is present in higher concentrations only at QT. Furthermore, the long-chain n-alkane concentrations at QT (i.e. n-C_{27}, n-C_{29} and n-C_{31}, sum averaged concentrations=163.7 µg) is lower than at SJO and BVA (i.e. n-C_{29} and n-C_{31}, sum of averaged concentrations=237 µg and 308 µg, respectively). The high relative concentration of n-C_{27} can be a signature of present-day vegetation at QT, *M. flexuosa* palm vegetation. Indeed, at QT, n-C_{27} becomes the predominant biomarker after the depth of 240 cm (QT-4b; Figure 58), when pollen of Arecaceae *Mauritia t.* becomes abundant in the pollen record. However, the distribution of

long-chain n-alkanes can also be influenced by climatic factors or different producers, and thus the signatures of individual vegetation species need to be analysed.

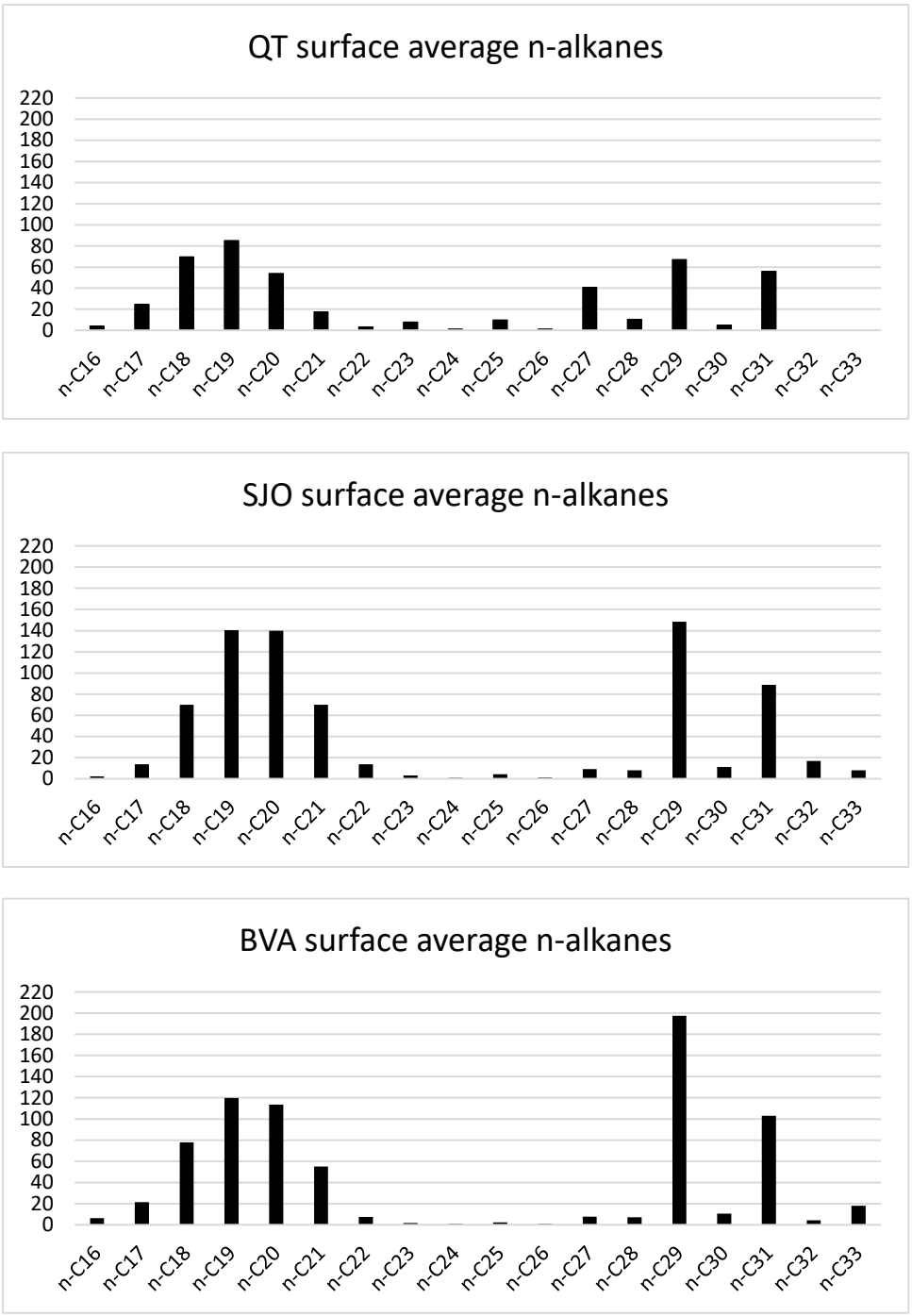

Figure 89 N-alkane average concentrations at the surface of the three peatlands.

Overall, the three peatlands show a similar distribution of short chain n-alkanes, for QT with a peak in n-C19, SJO, with two peaks for n-C19 and n-C20, and at BVA peaking again at n-C19 (Figure 89). However, BVA and SJO have higher concentrations in that range, indicating less bacterial reworking or degradation-resistent organic matter. As the three

peatlands have different vascular vegetations types at present, based solely on n-alkane signatures and concentration, no clear distinctions can be made between the three.

- **GDGTs**

Given that each sample represents a combination of 5 distinct points within a 400 m^2 area (square Figure 90; see subchapter 2.1.), the differences seen at the surface could be mainly due to the relative location within the sampling area and probably less by microtropography of individual samples that could have skewed the results (i.e. hummocks and lawns structures

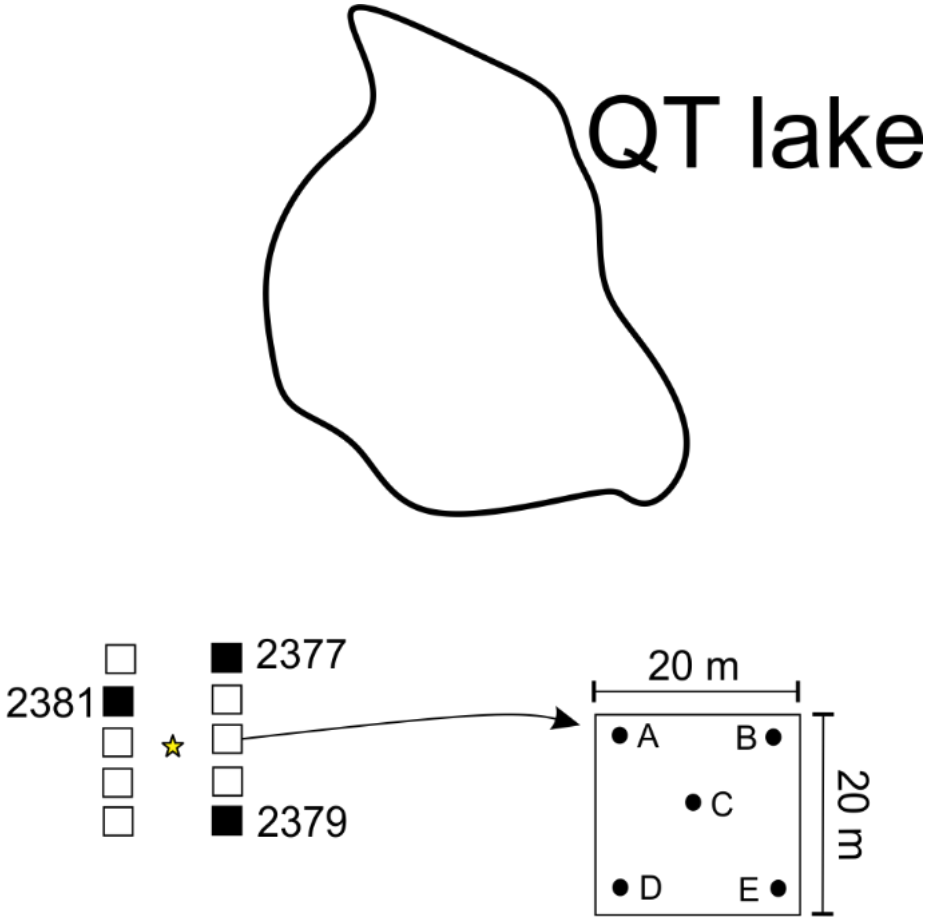

Figure 90 Relative distance of analysed samples (black squares) from QT lake and sampling strategy described in subchapter 2.1. (not to scale). The core location is marked by the star. The distance between core location and lake margin is of approximative 0.8 km. Notice that for a sample (id numbers), 5 different parts of a subplot were sampled from a 20m x 20m area and combined.

are known to be relatively raised structures, above the water table, while hollows are below the water table, which can influence the br/isoGDGT distribution). Indeed, at QT, they appear to vary in relative concentration with distance from the Qusitococha Lake. Sample 2377 is the closest sample to the lake, followed by sample 2381 and finally, by sample 2379,

which is the furthest (Figure 90). Although this might be an apparent trend, variations in water table depth could be expected with distance from a standing water body.

Thus, in sample 2377 there is a lower brGDGT input compared to isoGDGTs which could mean: i) a drier area due to either lower water tables or a raised micro-topography or ii) higher fluctuations in water table depths (i.e. higher hydraulic conductivity) which could be due to lake proximity. Samples 2381 and 2379 are further away from the lake, and represent either relatively wetter areas or experience less variability in water table fluctuations.

6.3. Biomarkers and palaeoenvironmental changes

A suite of biomarkers employed here (i.e. n-alkanes; n-acids GDGTs) were used as proxies for determining palaeoenvironment, climate and vegetation variability as they were exploited as proxies in numerous studies. The availability of pollen records in two of the studied peatlands (i.e. QT and SJO, Roucoux et al., 2013; Kelly et al., 2017) provided a framework in assessing the suitability of biomarker research in these recently discovered peatlands.

We found that n-alkane biomarkers successfully depicted changes in the type of vegetation input downcore, and more importantly, changes between aquatic and terrestrial inputs. Furthermore, they were successful in determining shifts from terrestrial to lake-like, marginal fen and/or floating mat vegetation settings at QT and SJO, which have also been reconstructed through palynology by Roucoux et al. (2013). This signal was recognized in samples with a relatively higher input of n-alkanes specific to aquatic species (i.e. peaks in n-C_{21}, n-C_{23} and n-C_{25}; Ficken et al., 2000) depicted through P_{aq} ratio. For example, at QT, at a depth of 380-388 cm, P_{aq} has a value of 0.288, the highest in the section together with a peak in the concentrations of n-C_{21} n-alkane. This indicates the presence of emergent macrophytes and thus, of an aquatic setting that was also depicted through pollen records. Furthermore, ACL and P_{wax} proxies that are also based on n-alkane composition suggest an increase in humidity and/or precipitation at this point, and the presence of long-chain n-alkanes with an odd/even predominance present within the same sample, indicate that terrestrial higher plants were already present at the site, not far from the core's location. n-Alkane relative concentrations and employed proxies further track changes depicted through pollen (Roucoux et al., 2013), indicating the waterlogged and flood prevailing conditions, the presence of higher plants and a return to an aquatic lake-like setting or high depths and

flood durations at the depth of 120-128 cm. At SJO, we also see an increase in P_{aq} ratio at the depth of 140-148 cm, a period described as a shift from terrestrial to marginal/floating mat vegetation (Kelly et al., 2017). The Pr/Ph proxy, although rarely employed in peatland settings (see however Zulkifley et al., 2015), indicated changes between subanoxic and anoxic settings, allowing us to make interpretations on the hydrological regime and tested the ratio against vegetation taxa depicted through pollen. Having demonstrated the suitability of n-alkanes in depicting shifts in environment and flooding/waterlogged conditions, we then infer that at BVA, the third peatland for which a pollen record is not yet developed, there were no shifts between terrestrial and aquatic settings after the onset of peat deposition as long-chain n-alkanes with an odd/even distribution dominate over the short and medium length n-alkanes. Furthermore, based on the availability of surface and a shallow core sample between 0-8 cm, we could also comment on the degree and speed of decomposition of organic matter at the site, which we hypothesis that is the same in the other two peatlands, based on higher overall concentrations seen in short n-alkanes at surface. Thus, due to high temperatures all year round that lead to high and active microbial communities, fresh organic matter (i.e. mainly leaves) is quickly degraded at the surface, even during waterlogged conditions.

The n-alkanes inferrences also correlated with pollen records with respect to primary producers. For example, a correlation was made between the increase in n-alkane n-C_{32} and the increase in pollen from a fern species, *Davalliaceae nephrolepis* at QT and SJO. Since there are no biomarker signatures of this fern, we infer that it can be one of the producers of this n-alkane and plan to test this in future studies.

Furthermore, GDGTs were analysed due to their use in determining relative inputs from bacteria and archaea communities within peatlands and soils (Weijers et al., 2007b; Schouten et al., 2013; Naafs et al., 2018), which were tied to temperature and pH variations. Although the pH in these settings can be qualitatively assessed based on the developmental history of the peatland (i.e. expected to become more acidic towards present), the recent peat-specific pH calibrations (Naafs et al., 2017a) provided an ideal background to test pre-existing theories and potential shifts from an atmospheric to a river-flood hydrological regime or between wetter and drier periods. Thus, we see that QT and BVA evolved from (an almost) pH neutral settings, and transitioned towards more acidic pHs upcore (Figure 92). Furthermore, at the surface QT and SJO, calibrated GDGT pH values are within the error range of available present-day pH field measurements provided by Teh et al. (2017). We see that at the surface of QT, instrumental reported pH is 5.04 during the dry season, whereas

the calibrated surface pH is of 5.0 (±0.8). At SJO, the reported dry season pH was of 3.8 (Teh et al., 2017) and the calibrated value of 4.04 (±0.8), again, within the error range. At BVA, calibrated pH is lower than expected and a clear difference is seen between the reported value for the dry season, 6.31, and calibrated pH, 4.5. It is thus expected that in this peatland, calibrated down-core pH could be more on the positive error side and thus, corrections can be applied downcore. However, the peat specific calibrations were proven to work better in acidic peatlands and since BVA has currently an almost neutral pH given the high input from floodwaters, we argue that before applying further pH specific calibrations at this location, calibrated pHs of surface samples from both the dry and the wet seasons need to be assessed against instrumental pHs.

In terms of calibrated temperatures, we see a very good correlation between instrumental present-day temperatures and calibrated ones. For example, at QT, Teh et al. (2017) reported a surface air temperature of 26.4°C, while our calibrated temperature average was at 25.92°C (±4.7°C). Furthermore, instrumental temperatures at SJO and BVA were 27.5°C and 26.4°C, respectively (Teh et al., 2017) whereas calibrated temperatures are 28.9°C and 26.5°C (±4.7°C), respectively.

The good correlations seen between present-day measured pH and temperatures and calibrated parameters (with pH exception at BVA), indicate that downcore calibrated values are also accurate (within the error range), allowing for a broader characterization of the three sites. Thus, since core temperatures and pHs were also calculated, it would be interesting to see that if, since the initiation of peat deposition at the three sites, basin-scale or continental scale climate changes affected the peat deposition, and consequently, if large scale climatic variations can be depicted in the peat record.

6.3.2. Synchronous climatic events depicted by biomarkers

Given the ages of peat deposits in PMFB, with the oldest peat deposit in this study having a calibrated age of of 2100-1990 cal yr BP (Roucoux et al., 2013), they could have been affected mainly by two global events: The Little Ice Age (LIA), which occurred between approx. 1400-1900 yr A.D. (Diaz et al., 2011) or 1350-1800 yr A.D. (Bernal et al., 2016) and by the Medieval Climate Anomaly (MCA), which took place between 950-1400 A.D. (Diaz et al., 2011). For example, during the LIA, as depicted by the proxy records in Bernal et al. (2016), the area experienced an overall drier period between 1700 and 1800 AD,

followed by a relatively wetter period between 1700 and 1350 AD. The climatic differences between the two intervals are mainly caused by external forcing factors, and show different amplitudes when interacting with regional factors (Diaz et al., 2011 and references therein). Understanding the importance of climate factors that dominate the hydrology cycle during late Holocene in Peru arrives from the importance of Amazon's tributaries and their hydrological regimes in peat formation and accumulation in PMFB (Bustamante et al., 2016 and references therein).

Thus, during the MCA (950-1400 A.D.), as depicted in Figure 91, most parts of Peru, and PMFB, experienced a drier period and low South American Summer Monsoon (SAMS; Diaz et al., 2011; Bustamante et al., 2016), however, as depicted from lacustrine sediments, central Chile experienced higher moisture and precipitation (Diaz et al., 2011 and references therein). Furthermore, during the MCA, tropical Pacific recorded lower temperatures, similar to La Nina events and environmental parameters (Cobb et al., 2003).

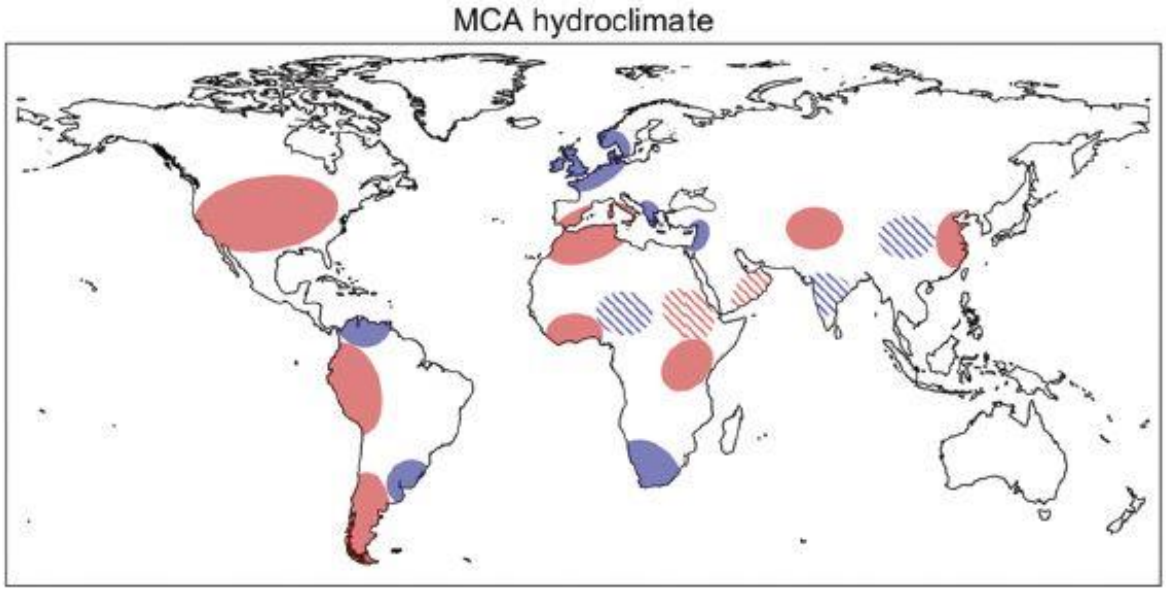

Figure 91 Map of the world indicating the response of different regions during the Medieval Climate Anomaly (950-1400 AD) relatively to 20th century averages. Peru, where PMFB is located, experienced a drier period (red), while the north of the South American continent a wetter period (Diaz et al.,2011).

The speleotherm from Shatuca cave (Bustamante et al., 2016) put in context with previous studies indicates a drier period before and around 2 ka (b2k, age before present, taking the present as 2000 AD) in between two wetter periods.

For example, at BVA, the lowest GDGT calibrated temperature (i.e. 23.8°C±4.7°C) occurs at the depth of 204-212 cm. This, correlated with deposition rates and radiocarbon dates provided by Lähteenoja et al. (2009a), took place around 724 yr bp (cal yr bp-extrapolated

age), which on Figure 94 (Bernal et al., 2016) and corresponds to a drier climate with temperatures recovering from a relative colder period.

Again, at QT, the lowest GDGT calibrated temperature (i.e. 22.08°C) is recorded in the 348-356 cm sample, that was deposited around 2057 yr bp (calibrated for 353 cm), during a relatively wet period, however, the regional $\delta^{18}O$ values display on Figure 93 throughs during the time of deposition, indicating less evaporations and possible, lower temperatures. On the other hand, the highest calibrated temperature at QT (i.e. 27.43°C±4.7°C) occur in the sample that comes from a depth of 120-128 cm, which was extrapolated to an age of 834

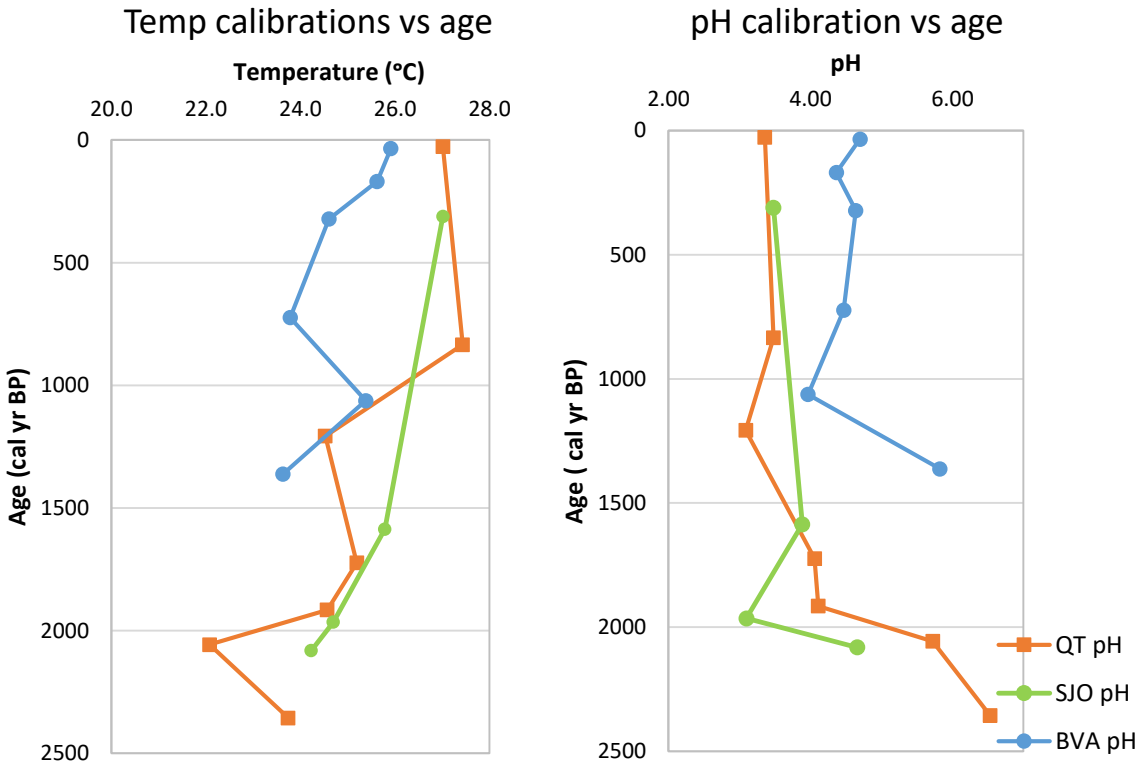

Figure 92 Calibrated temperatures and pH in relationship with extrapolated deposition ages at the three peatlands.

cal yr bp (Figure 94). This corresponds to a period of less negative $\delta^{18}O$ values, potentially indicating a peak in temperatures in the area. Moreover, not taking into account regional temperature records, overall temperatures in the three peatlands appear to have the same trend, increasing towards present.

The pH can also be influenced by the amount of precipitation or by local factors like input from secondary sources (i.e. floodwater and groundwater). To test this, the lowest calibrated pH at BVA (i.e. 4.0) is recorded at the depth of 266-275 cm, that correlated to an approximate age of 1062.6 yr bp. This occurs within the MCA, however, during a relatively wetter period,

going from colder to relatively warmer temperatures (i.e. Sr/Ca and $\delta^{18}O$ proxy graphs). Thus the relatively higher amount of precipitation that occurred during this period can explain the drop in pH seen at BVA, a peatland with a low topography, that even at the time of deposition, would have been influenced by floodwaters and thus, relatively higher pHs. The lowest calibrated pH at QT (i.e. 3.09) corresponds to an age of 1207 yr bp. Based on data provided by Diaz et al., 2011, this occurs during a relatively wetter period, with possibly higher precipitations that allowed a drop in the pH.

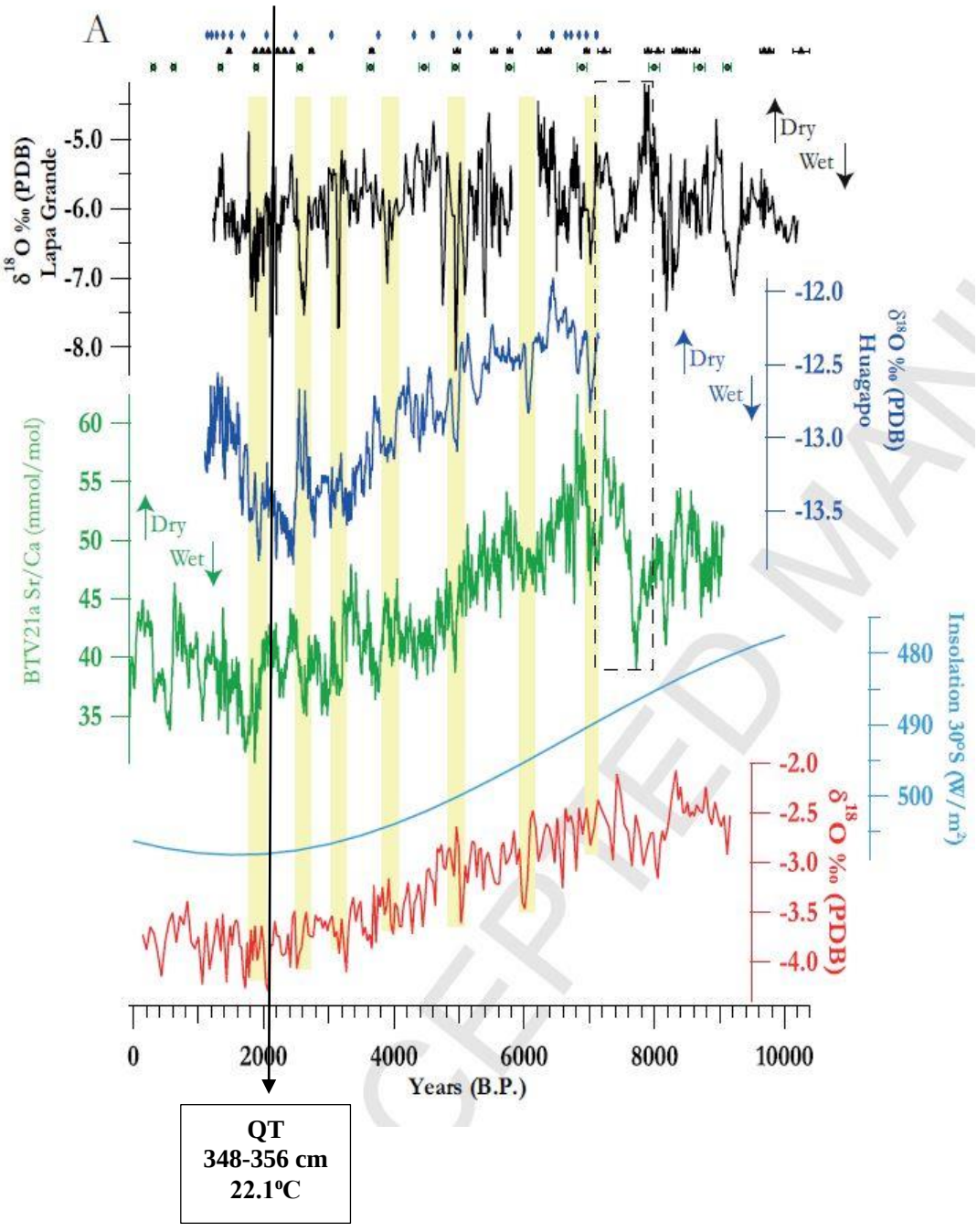

Figure 93 Various poxies across South America continent indicating dry and wet periods Bernal et al., 2016).

During and after MCA (1400-1900 AD), we see a correlation between BVA and QT, however both indicating more acidic conditions during a relatively dry period (Figures 91 and 92). Overall, the pH across the three peatlands show similar trends, decreasing towards more acidic pHs towards present. Thus, several correlations can be made between calibrated pHs and temperatures and regional to continental climatic changes over the last 2200 cal yr BP. However, peat initiation within this environment is likely caused by the lateral migration of rivers (Lähteenoja et al., 2009a) and consequently, pH changes can be due to the proximity from the closest river and thus, flooding regime and peatland evolution (i.e. dome-shaped ombrotrophic).

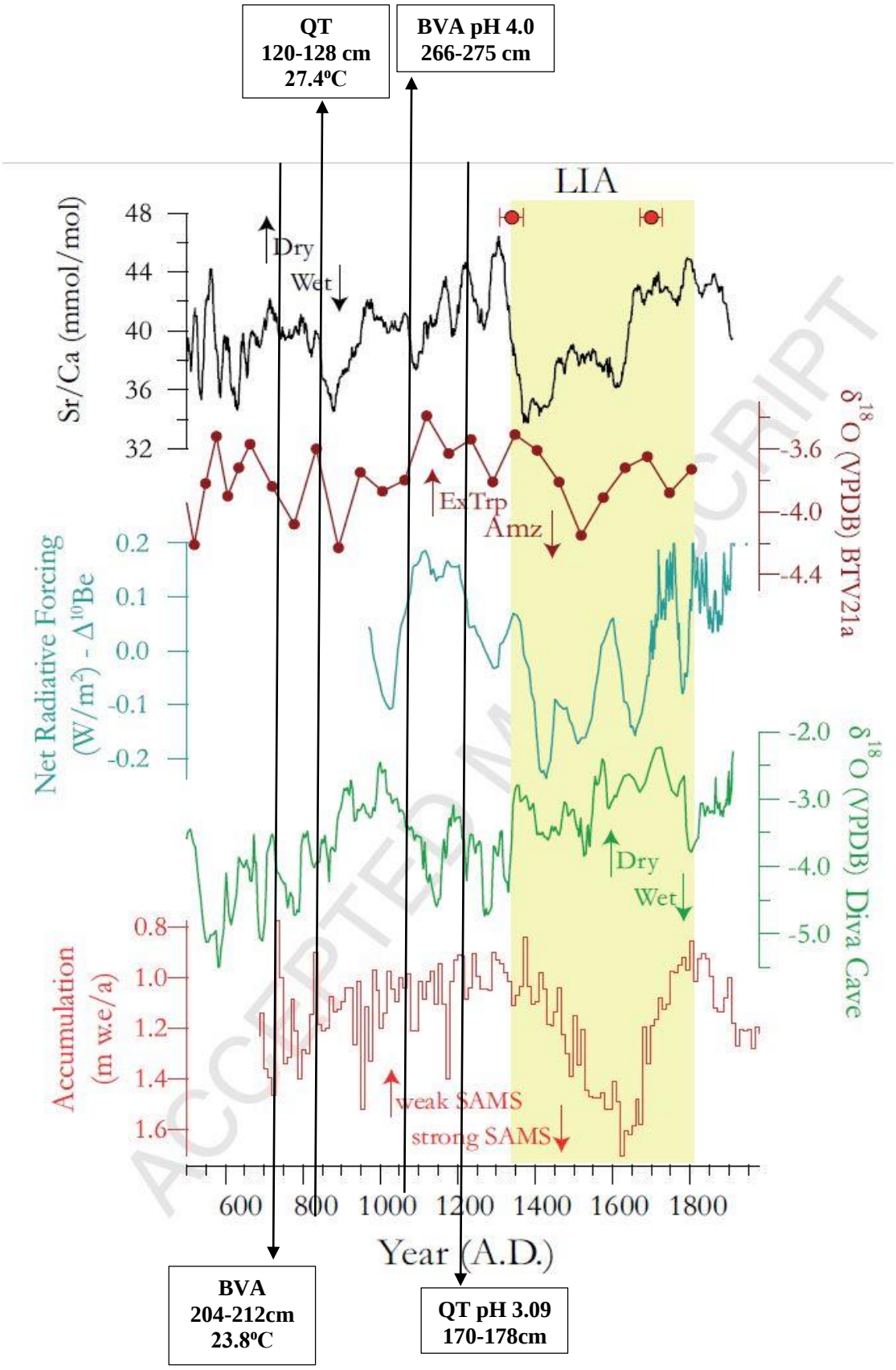

Figure 94 Various poxies across South America continent indicating dry and wet periods (Bernal et al., 2016) with plotted calibrated pH and temperatures.

6.4. Potential of biomarkers to track changes in CH_4 cycle

Having demonstrated the potential of n-alkanes to track vegetation and hydrological changes within these peatlands, the following aim employed a suite of biomarkers capable of describing and quantifying microbial changes within different vegetation assemblages and physical conditions. Thus, GDGTs concentrations were used in order to differentiate between (mainly) anaerobic bacteria (i.e. brGDGTs) and archaea (i.e. isoGDGTs) communities, and certain isoGDGTs employed to differentiate between different groups of archaea, for example, based on previously published literature, isoGDGT-0 and archaeol were used as a biomarker to indicate the methanogen community, while isoGDGTs 1-4, the anaerobic methanotroph community. Crenarchaeol within the brGDGTs, was employed as a biomarker that indicated oxic condition as it is being biosynthesized by ammonia-oxidizing *Thaumarchaeota* and isoGDGTs-5 and -6 have been recently proposed to occur in acid peatland with constant pH and possibly increase in concentrations with increasing temperatures (Naafs et al., 2018b). Hopanes and hopanoid biomarkers (i.e. diploptene and diplopterol) were employed in order to understand (mainly) changes in aerobic bacteria community. Several fatty acid lipids were used as they can indicate several microbes while the monosaturated fatty acids with 16 and 18 carbons can be indicative of aerobic methanotrophs and can be used to distinguish between the two types.

Thus, in all three peatlands, we demonstrated or commented on the relationship between both aerobic and anaerobic microbes and heights of the water table. Overall we see a good correlation between the concentration of anaerobic archaea and anaerobic bacteria and the inferred hydrological regime through n-alkanes or pollen records. For example, at QT, there is a good correlation between concentrations of isoGDGT-0 and archaeol, both known to indicate methanogenic communities. We also see a consequent increase during inferred times of high methanogenic activity in the anaerobic methanotroph community (i.e. isoGDGT 1-4), and from here on, we could infer the high availability of substrate (i.e. CH_4) for the latter group. Furthermore, there is a negative correlation between the concentrations of isoGDGTs and brGDGTs, and for example at QT for the depth of 120-128 cm, we see a collapse in the isoGDGTs 0-4 and archaeol concentrations, and peaks in brGDGTs, hopanes and diplopterol, with the highest concentrations recorded in brGDGT-Ia (i.e. 1909 µg/g). This was explained through a different type of source for brGDGT-Ia, aerobic *Acidobacteria* that, if proven correct, would infer that at the site there was a thicker (and constant) oxic layer at the surface capable of sustaining a large aerobic microbial community, and support

the biosynthesis of hopanoids. Furthermore, the calibrated palaeotemperature was highest at this point (i.e. 27.43°C), possibly enhancing bacteria activity. A further possibility would be the occurrence of a lake-like setting or a pool at the site as depicted through P_{aq} at this depth, that could allow hopanoids and brGDGTs producers to live in the oxygen-rich waters while restricting the input from anaerobic archaea and methanogen development. At the same depth we also see an increase in C18:1ω9 input, a biomarker characteristic for type II methanotrophs, and from here on we can infer that at least during this time, CH_4 effluxes were reduced at the site.

On the contrary, at SJO we see a positive correlation between the concentrations of iso- and brGDGTs, with both increasing or decreasing at the same depth. This can be explained through the increase in methanogen community mass able to provide readily available substrate for anaerobic methanotrophy during a time of relative lower or fluctuating water tables as there is also an increase in aerobic bacteria.

At BVA, we see the same overall positive correlation between iso- and br-GDGTs, indicating a close relationship between CH_4 producers and anaerobic consumers. Hopanes appear to peak in concentrations at a depth (i.e. 60-68 cm), during a time of low concentrations in GDGTs, thus the negative relationship between the two can be explained through a relatively thicker oxic layer at the palaeosurface of the peatland. Furthermore, at BVA there appears to be decoupling between archaeol concentrations and isoGDGT-0, which was not seen the previous two peatlands. Here we see archaeol gradually increasing in concentration towards recent, peaking just below the surface which can indicate that the methanogenic community increased slowly in size, and that the peak seen at the surface indicates that only recently CH_4 production has increased at BVA. However, the presence at the surface of BVA of biomarkers that potentially indicate type I and type II methanotrophs.

6.5. Relationship between vegetation type, CH_4 effluxes and methanotroph community sizes

In several instances, inferred shifts in CH_4 effluxes and methanotroph community were explained by referring to vegetation-mediated CH_4 emissions. For example, at QT, in the 348-356 cm sample, the increase in oxygen content depicted through an increase in the Pr/Ph ratio during waterlogged conditions can be due to the presence of aerenchyma adaptations

in plants. Furthermore, the increase in hopanoids at QT in the 120-128 cm sample can be explain through the existence of plant waterlogged adaptations-aerenchyma tissues. This could have provided enough oxygen for further hopane input at this depth if the roots from the above peat sections penetrated to this depth.

It also possible that pneumatophore adaptations in *M. flexuosa* provide an important pathway for CH_4 release to the atmosphere at all depths and locations where *M. flexuosa* occurs as a positive relationship between the density of pneumatophores and CH_4 was also recognized by van Lent et al. (2018). This would be seen in the biomarker records as an increase in methanogenic community and a decrease in anaerobic and aerobic methanotrophs, due to a lack of substrate. However, since type II aerobic methanotrophs are facultative, they can also consume CO_2 during periods of low CH_4 emissions, compound specific isotope signatures will prove useful to determine if: i) the initial isotope signature is methanotroph specific and ii) if changes occur in the type of carbon incorporated (i.e. ^{13}C vs ^{12}C) during periods of inferred high anoxia, pneumatophore and aerenchyma adaptations.

Although indirectly related to CH_4 effluxes, we also observed a high rate of organic matter decay in the top 8 cm compared to surface samples based on concentrations of fatty acids and n-alkanes. Thus, the quality and quantity of litter input has a strong impact on the methanogen communities that also rely on the presence of other micorbes to provide with required substrate. The rapid breakdown and decomposition at surface and subsequent decay at depth, probably limits the availability of suitable methanogenesis substrates at depth, even during periods of low water tables, when stored organic matter is exposed to oxic decay.

6.6. Assessing the relationship between diploptene and aerobic methanotrophy

Diploptene is a hopanoid biomarker biosynthesized by a wide range of bacteria (see subchapter 1.4.3.5.). Since one of the aims of this project was to assess the use of diploptene as a novel proxy for CH_4 effluxes together with its $\delta^{13}C$ signatures, the compound was one of the first to be identified and its changes in concentrations evaluated against first pollen, then other biomarker data. There is little to no evidence solely based on the relationships between concentration changes in diploptene and other biomarkers related to

methanogenesis and methanotrophy, that diploptene can be used as an indicator for CH_4 consumption.

At QT, diploptene is seen to increase gradually towards surface and does not mirror the peaks in hopanes and diplopterol seen at this location. Furthermore, hopanes and diplopterol are seen to reach trace concentrations in surface samples, whereas diploptene, although decreases in concentration, it is still less than half of its concentrations recorded down core.

At SJO, diploptene increases towards the surface, while diplopterol decreases in the same direction. Here, it can be argued that there is a relationship between the two based on the overall anoxic conditions at SJO, some of the oxygen from diplopterol could have been removed and thus, transformed to hopane (i.e. C_{30}-hop) and later to diploptene, by the addition of a double bound. However, there is little evidence to support this theory, and it is more probable that, although both are produced by aerobic bacteria, there is no relationship between the two.

Finally, only at BVA there is a peak in diploptene at two different depths, at the surface and at 266-275 cm. The increase at surface can be due to the existence of a thicker aerobic layer (acrotelm) during the dry season, and thus, more input from bacteria, however, the increase seen at depth (Figure 85.10.) also occurs during peaks in C_{30}-hop and C_{31}-hop. Hence, a certain (weakly positive) correlation can be made between diploptene and other bacteria membrane biomarkers and diploptene's recalcitrant potential. However, the increase is still minor and can be also caused by the fact that this sample contained 9 cm instead of 8 cm of the peat core, and thus represent a longer period of deposition during which conditions could have been favorable for diploptene biosynthesis, similarly to present day conditions at the surface of BVA. Advice on how to confirm (or invalidate) the potential of diploptene as a biomarker for methanotrophy is discussed in the following sections.

7. Conclusion and further research

Here we presented the first multibiomarker study within newly discovered Amazonian peatlands, in the PMFB (Lähteenoja et al., 2009 a, b) with the primary aim to assess the potential of vegetation- and microbial-related biomarkers in tracking past changes in the environment. Given the nature of available samples, we tested the applicability of a suite of biomarkers in three different peatlands, QT, SJO and BVA, characterized at present by different vegetation types (i.e. black-water seasonally flooded forest, short pole and *M. flexuosa* palm swamp) and hydrological regimes. We showed that there is a good correlation between shifts in biomarkers concentrations and vegetation successions at QT and SJO and commented on inter-site variations between the three peatlands. We set the scene for further high-resolution investigations into past CH_4 efflux changes and of biomarkers in tracking shifts in microbial communities, with a focus on methanogen and methanotroph communities. Water table depths, input of nutrients, the frequency of floods and present-day vegetation with discussed waterlogged adaptation were proven to influence CH_4 production, emission pathways and consumption and should be taken into account in future studies. Furthermore, we argue that addressing this gap in knowledge represented by past CH_4 cycles will provide further insights into strategies of conservations and human impact mitigations.

7.2. Research aims and conclusions

All 4 set aims (see subchapter 1.8.) were reached and new observations and recommendations for future work arised during this research. As our first and most important aim was to evaluate the suitability of biomarker research in these newly discovered peatlands, we have analysed samples from both the surface and downcore, and have compared data with pollen record (where available) and with present-day environmental parameters. We measured the concentrations of n-alkanes, known to be biosynthesised by vegetation and tracked changes in their concentrations. Furthermore, we tested a suite of biomarkers proxies known to depict changes in organic matter degradation level (i.e. CPI), shifts between terrestrial and aquatic vegetation (i.e. P_{aq}) as well as between different species and genera (i.e. ACL and P_{wax}), fluctuations between oxic and anoxic settings within the peatland (i.e. Pr/Ph). The availability of pollen recores at two of the sited (i.e. QT and SJO) allowed us to validate their suitability at sites where other proxies are absent, encouraging the use of biomarkers as a stand-alone method. These proxies were further applied to the third site,

BVA, allowing us to base interpretations of palaeoenvironment changes solely on them. A final validation of this stand-alone approach will be offered by future pollen analysis at BVA, from samples coming from the same core. We expect that pollen analysis will confirm that, at least for the depths analysed in this study, no lake-like environment occurred at the site and that the vegetation was mainly terrestrial. Furthermore, as discussed in subchapter 5.3., we expect BVA to have had in the past a similar hydrological regime to that which occurs at present. As the overall topography of BVA in flat, at present the water table depths oscillates between above and below surface depending on the season (i.e. wet and dry seasons, respectively). A similar behaviour is inferred for the past, since the Pr/Ph ratio has values greater than 1 in the middle part of the core, indicating that the peatland was exposed to oxic conditions periodically.

The identified gap in knowledge regarding past CH_4 emissions and the potential of these three peatlands to act as CH_4 sink or sources was also possible to investigate as a second aim through biomarker analysis. Given the proven potential of some biomarkers to provide information on the relative contribution of lipids from methanogens and methanotrophs, we have also related them to other palaeoenvironment biomarkers or proxies in order to distinguish CH_4 production and consumption potential in the absence of compound specific isotopic analysis . Thus, our data shows that CH_4 production varies greatly between the three peatlands in the past, and confirms present-day measurements and trends. For QT, CH_4 production was likely more reduced in the past and increased towards the present in a step-like fashion. Here, we see that isoGDGT-0 (Figure 58.1.), a biomarker for methanogens, has the highest concentrations in the surface samples, with the next highest concentrations recorded at the depth of 20-28 cm, where CH_4 production is still likely to take place at the present given favourable conditions. In the same samples, the anaerobic methanotrophic community is comparable to those from the past (i.e. isoGDGT-2, -3, -4), with isoGDGT-1 decreasing in surface samples. This, coupled with CH_4 efflux measurements (Teh et al., 2017), implies that QT produced in the past less than 28.3±2.6 mg CH_4-C/m^2/day. Similarly, for BVA, although the peatland shows trace concentrations of isoGDGT-0 in surface samples (Figure 86.1., expected from Teh et al., 2017 dry season measurements), the sample from just below surface where CH_4 production most likely takes place (i.e. 0-8 cm), has the highest concentration of isoGDGT-0 in the last 725 yr bp (Figure 92 correlated with Figure 86.1.). This peatland appears to have acted as a CH_4 sink around 322 yr bp, when the methanogen and anaerobic methanotrophic communites collapsed while biomarkers of aerobic bacteria peaked in concentrations (i.e. for depth 60-68 cm). However, this is not true across all three peatlands at present, as at the surface of SJO, isoGDGT-0 reaches trace

concentrations together with isoGDGTs 1-4, while diploptene is surface average increases in concentration. Based on this data, SJO appears to have a higher potential for CH_4 consumption at this site at present. The same can be inferred from measurements published by Teh et al. (2017), from where we see a large difference in the CH_4 between the wet and dry season at SJO, with lower CH_4 emissions in the latter. It is likely that, given the dome-shaped topography of SJO, the peatland has at present a smaller input GHG effluxes compared to QT and BVA, at least during the dry season. This needs further investigation of subsurface samples where methanogenesis is likely to occur yet, it is likely that parts of PMFB will respond differently to changes in climate and hydrology and a better understanding of their future behaviour is needed.

In order to understand further past behaviours of the the three peatlands from a CH_4, as a third aim, we have correlated and investigated past climate and vegetation from a CH_4 production/consumption potential point of view. In terms of potential climatic drivers for large CH_4 emissions, water-table position, and consequently, sustained precipitation and flooding events appear to have an important role, however its effect has different responses in the three peatlands. For example, at BVA, during the dry season, when the water table was 13 cm below surface, higher emissions were noticed (Teh et al., 2017) yet at the surface trace concentrations of isoGDGT-0 and archaeol were found, whereas just below surface (i.e. 0-8 cm), the second highest concentrations of isoGDGT-0 was found (i.e. methanogen biomarker). The biomarkers in the subsurface peat are most likely representative of non-living methanogens from the previous wet season (i.e. recalcitrant in nature) with only a fraction possibly belonging to living methanogens in anoxic microsites, thus indicating the high potential of the peatland to produce CH_4 during anoxic conditions. However, the fact that the dry season has higher emissions compared to the wet season indicates that a secondary or different CH_4 emission pathway takes place apart from diffusion-ebullition. At BVA, the drop in water-table was thus associated with a decrease in hydrostatic pressure at depth and a higher efflux of CH_4 that by-passed methanotrophy in the relatively thick oxic layer. Further studies should assess the impact of water table on ebullition during the dry season, relating both atmospheric and hydrostatic pressure. On the contrary, QT and SJO have considerably lower CH_4 effluxes during the dry season. SJO peatland may also have a stable below-surface water table during the dry season (Teh et al., 2017) and hence, we see trace concentrations of isoGDGT-0 in the surface samples, indicating that a lower water table might lead to less emissions. At QT, the water table was recorded above surface even during the dry season, and although isoGDGT-0 peaks in surface samples, CH_4 effluxes are smaller

than in the wet season (Teh et al., 2017), leading us to propose anaerobic CH_4 consumption as well as aerobic consumption in oxic micropores.

Also related to the hydrological regime, the pH was found to have an impact on the types of methanotrophs present at each site. The proximity to the Amazon and the frequency of flood events can also have an impact on the microbial community size since they can deliver nutrient-rich waters compared to atmospheric precipitations. At present, since BVA has an overall flat topography and it is annualy flooded by river water (Kelly et al., 2014; Valderrama, 2013), has at the present a border-line neutral pH, biomarkers indicative of type I methanotrophs were identified along type II. As type I methanotrophs are obligate in nature, they have a higher potential to reduce the CH_4 emissions from this peatland. Apart from BVA, evidence of type I methanotrophs was also found at QT, in trace amounts, at a depth of 120-128 cm, however the calibrated-pH was acidic (i.e. 3.48± 0.8), but the depth recorded the highest calibrated temperature at the site, which might also have an influence of the size of the methanotroph community. Further observations relating temperature and the size of microbail communities were less obvious and no correlations could be made thus, we expect that, compared to the pH, temperature will play a less important role in the future, under predicted climate change scenarios.

The fourth aim regarded the assessment of diploptene's concentration as a proxy to depict changes in CH_4 efflux. Although preliminary data indicated that diploptene increases in concentration during periods of high CH_4 emissions which led to , the measurements were done in a different setting characterized by different environmental parameters. In these environments, there was no correlations between diploptene concentration or trends and other CH_4-related biomarkers. However, in proposed further research, we discuss another way to reassess this potential in these settings (see subchapter 7.1.3.).

7.3. Further research suggestions

This study investigates for the first time the ability of biomarkers to depict changes in environment, vegetation and microbail community in recently discovered Amazonian peatlands. Having meet the first 4 set aims, our final objective is to encourage a high resolution investigation using these proxies as a stand-alone methode and recommend further steps to whole our understanding of these environments.

7.2.1. Compound specific isotopic analysis

The first further step is to perform compound specific isotope analysis of various biomarkers, in order to confirm their methanotroph origin and potential of their producers for consuming CH_4 in these settings. Thus, we hypothesised that in these settings monosaturated fatty acids with 16 and 18 carbons (i.e. C16:1 and C18:1) are indicative of type I and II methanotrophs, respectively. Since type I is obligate in nature, on the assumption that it is the (main) producer of C16:1 fatty acids, its isotopic signature would be highly depleted in ^{13}C, while the signature C18:1 fatty acids, can indicate a mixed signal, since type II methanotrophs can consume both CO_2 and CH_4. Furthermore, based on discussed literature, we assigned isoGDGTs 1-4 to anaerobic methanotrophs, and this assumption can be confirmed by assessing their carbon isotopic signature.

Diploptene, which was initially considered a biomarker that can indicate aerobic methanotroph communities, due to its occurrence in membranes of a wide range of bacteria (see subchapter 1.4.3.5.), is expected to have a lighter isotopic signature than biomarkers representative of vegetation (i.e. n-alkanes). However, given that bulk isotopic signatures for various depth are known for QT (Roucoux et al., 2013), diploptene signatures can be compared to those of vegetation within the same sample, and if proven to be slightly depleted, its methanotroph origin can be further investigated.

Furthermore, through stable isotope analysis, fractionations factors can be calculated, allowing interpretations on specific pathways of anaerobic degradations and CH_4 production. It can provide relative quantification and distinguish between CH_4 production pathways (i.e. aceticlastic or hydrogenotrophic, see subchapter 1.2.1.) and different substrates used for methanogenesis (i.e. root exudates or soil OM) if isotopically different. In this case, peat incubation experiments are no longer necessary in determining CH_4 incorporation pathways (Blaser and Conrad, 2016).

7.2.2. High resolution biomarker records

We argue that vegetation-specific biomarkers can trace changes in the hydrological regimes and input sources, being able to differentiate between terrestrial and aquatic species, input from higher plants compared to microbial masses. Moreover, we have demonstrated a close correlation between temperature, acidity and anaerobic microbes (i.e. GDGTs) in order to estimate (within the error ranges) palaeoenvironmental changes. The use of hopane-calibrated pH (Inglis et al., 2018) provides a proxy that can be employed to describe conditions characteristic of the acrotelm and presence of aerobic microbes, in the absence of GDGT data.

Finally, the relationships between archaea and bacteria, CH_4 cycle and influences from hydroecology can be traced at a higher resolution with the use of the suite of biomarkers presented here, thus assuring a more detailed understanding of the palaeoenvironment. However, since peatlands in PMFB differ in terms of several key physical and chemical parameters (i.e. pH, dissolved oxygen content, topography, water sources, hydraulic conductivity, see Teh et al., 2017; Kelly et al., 2017), it is recommended that biomarker analysis is performed in both minerotrophic and ombrotrophic peatlands. With regard to an increased resolution in two such peatland, further questions can be answered: What is the rate of change of the microbial community during periods of environmental change and/or instability? How does the different input from flood water and atmospheric precipitations impact the relative community size of archaea and bacteria? What are the main long-terms drivers of the CH_4 cycle in the different types of peatlands and which factors limit CH_4 production or CH_4 effluxes in each setting? A high resolution record can answer these questions and, more importantly, can investigate the activity of methanogens in subsurface samples or anoxic/oxic microsites.

7.2.3. Recommended sampling strategies

Surface samples analysed in this study provided a level of uncertainty regarding concentration of and occurrence of biomarkers under present-day conditions. As surface samples were collected in 2010 with the primary aim of pollen analysis, they were less suitable for biomarker analysis. As explained in subchapter 2.1., 5 different surface samples were collected and combined from an area of 400 m^2, making up one surface sample analysed in this study. We recognised that both vegetation- and microbial-specific

biomarkers can vary at surface based on specific microtopography, position of water table, vegetation growing at the site and adaptations to waterlogged conditions specific to some species. For example, at surface, both type II and I (C18:1 and C16:1, respectively), indicative of different microenvironments based on studies done on their occurrences, were found within the same sample suggesting that probably only a few of the 5 collection points had type I while the others, type II and thus, even within a 400 m^2 surface conditions are not homogenous. Furthermore, concentrations of other biomarkers such as n-alkanes, hopanes and GDGTs varied across the 4 or 5 analysed surface samples within the same peatland however, it is not clear if the 400 m^2 area had different proprieties than a neighbouring 400 m^2 area, or if the differences were collection point specific (i.e. one of the 5 collection points that made a sample had a higher/lower concentration that skewed the overall result once sample was homogenised).

We recommend that further surface sampling strategies avoid combining samples and take into account peatland topography, vegetation gradients and landscape components (i.e. proximity to lakes, rivers, terraces). For example, surface sampling in nutrient-poor minerotrophic peatlands like QT can be done on a transect from the Amazon river to the middle of the peatland and on a transect moving away from Quistococha lake or other main features, towards the middle of the peatland. This would allow a wider understanding of the influences of water table depth and nutreient content over microbial communities. We expect that correlations will arise at surface regarding occurrence of type I methanotrophs biomarkers and proximity to river compared to proximity to Quistococha lake and interior or opposing margins of the QT peatland. Furthermore, vegetation growing at each site, microtopography features (i.e. hummocks, hallows) and position of water table depth should be recorded for further correlations regarding relative input from aerobic and anaerobic bacteria and archaea. Ombrotrophic and domed peatlands like SJO can be viewed as two separated peatlands if vegetation occurring in the centre is different from that around the margins. A surface transect can be crossed between the edges and centre of the peatland, passing thus through various vegetations zones and hydrological conditions. Finally, minerotrophic peatlands like BVA that are frequently flooded by nutrient-rich river waters can follow the same sampling strategy as at QT.

Finally, it is yet uncertain if similar biomarker concentrations are to be expected from another core within the same peatland yet we expect that ratios and trends will be similar when investigating occurrences of oxic or anoxic conditions, input from terrestrial and aquatic species in close vicinity of the initial cores and relative changes microbial

community sizes if these are unaffected by the occurrence of, for example, pneumatophores. In order to confirm this hypothesis, two cores are recommended to be taken from a restricted area (e.g. 200-400 m^2) and one core from a distnat area within the same peatland. This way we can generalize results from a single core from an individual peatland to a wider area or we can comment on intra-peatland heterogenies. Moreover, domed peatland that display distinct marginal characteristic from centre might require two cores, one dealing with the domed centre, usually above water table depth, and one from the margins that are periodically below water table depth.

7.2.4. Recommended biomarkers for a higher resolution record

Although all 5 fractions were analysed (i.e. Total Acid fraction-A2; Total Neutral fraction-N1, N2, N3 and N4; see subchapter 2.4.), only a small fraction of present biomarkers were further investigated as their either belong to specific producers used for palaeoenvironmental reconstruction or they enter proxy ratios used for a similar aim. Thus, solely for palaeoenvironmental interpretations, we recommend the use of N1 fraction as it contains both n-alkanes, branched and cyclic alkanes as well as hopane fraction (see Table 2). While **alkanes** and proxies based on them have the ability to track changes in hydrological regime, vegetation, water table depths and fluctuation frequencies, **hopanes** can indicate the size of aerbic bacteria community and, in the absence of N4 fraction analysis possibility, hopanes can be employed in a pH-related proxy, allowing to access fast trends in palaeoacidity in the environment (i.e. hop-C31; see subchapter 1.7.3.4.).

Research looking into correlating palaeoenvironmental changes to consequent shifts in the microbial communities can further employ analysis of diplopterol and archaerol (N3 fraction), GDGTs (N4 fraction) and fatty acids (A2 fraction). Furthermore, analysis of GDGTs can focuse on brGDGTs such as **Ia, Ib, Ic, IIa, IIb, IIc, IIIa, IIa', IIb' and IIIa'** that are employed in palaeoacidity and palaeotemperature proxies (Naafs et al., 2017a). Fatty acid analysis might be restricted to short chain fatty acids and **monosaturated fatty acids** with 16 and 18 carbons as the later can indicate the presence and relative size of type I and type II methanotrophs, respectively. All these biomarkers and their associated proxies are discussed in subchapter 1.7. and are further summarized in Table 2.

7.2.5. Test the applicability of further biomarkers and vegetation-specific biomarkers

N-alkanols (i.e. alcohols) are also indicative of shifts in vegetation and can be applied to identify the input of some species that occurred at QT and BVA. For example, embryophyte (i.e. subaerial terrestrial plants) are known to synthesize n-alkanols in the range of C_{22}-C_{28} (Eglinton and Hamilton, 1967; Zheng et al., 2009); n-alkanols from heathers and sedges like Ericaceae and Cyperaceae, respectively, peak at C_{30} (Ficken et al., 1998; Pancost et al., 2002), while lichens produce high concentrations of C_{28} alkanols (Ficken et al., 1998). Aquatic macrophytes show high concentrations of n-alkanols with 22 and 24 carbons, while aquatic algae in the range of C_{16}-C_{22}, similarly to photosynthetic bacteria (Volkman et al., 1998). The distribution of n-alkanol signatures can be tested against pollen palaeorecords or tested from vegetation samples of modern vegetation. Furthermore, other biomarkers indicating vascular plant input, such as sterols (i.e. campesterol, stigmasterol, sitosterol) and oleanoids can be analysed in order to achieve further information about shifts in vegetation and their relative input to the peat content (Volkman et al., 1986; 1998).

Fatty acids with different levels of unsaturation were also used to infer the relative input of fungi, protozoans, cyanobacteria to the peat (e.g. Boschker and Middelburgh, 2002). It would be thus interesting to understand more about the microbes that perform organic matter decomposition, their roles in providing further substrate for methanogenesis and further the carbon cycle and how fast they adapted or changes in distribution during shifts in the environment or hydrology.

Furthermore, based on published pollen records for QT and SJO, input of n-C_{32} in the n-alkane fraction was correlated with the appearance of *Davalliaceae Nephrolepis,* a fern species, at both sites, an assumption than can be further tested. The biomarker composition of different parts of present-day vegetation (i.e. leaves, bark, roots) can provide information on past organic sources in the absence of pollen records and vegetation macrofossils.

7.2.6. Surface peat incubation experiments

Present-day peat incubation experiments coupled with biomarker techniques could provide a way to answer questions about the microbial community response to shifts in pH, water table location and rate of decay of organic matter, compared to present day (i.e. control) conditions. An increase/decrease in pH experiment considered in the acrotelm, can track the

increase in isoGDGT-Ia in order to confirm (aerobic) Acidobacteria source. Furthermore, since at the surface of BVA, pH conditions are close to neutral (i.e. 5.88 and 6.31 for wet and dry seasons), it would be interesting to see what effect a further increase/decrease in pH would have on this site, providing thus data for peatland and river banks conservation attempts.

7.4. Contribution to the knowledge gap

This study represents the first multibiomarker approach for characterizing the recently discovered Amazonian peatlands, and the first attempt to understand shifts in CH_4 emissions in the past, setting thus the scene for higher resolution studies in peatlands developed in Pastaza-Marañón Foreland Basin, N Peru.

We have provided and validated with present-day instrumental measurements the first peatland-specific palaeoacidity and palaeotemperature records for this region (Naafs et al., 2017a), adding thus to both our understanding of conditions that prevailed in the past and to further land management and conservation strategies. Discussing past records of CH_4 emissions potential from the three peatlands provided further indicators that should be considered when deciding on preservation practices. For example, data suggests that pH might have an impact on the type of methanotrophs present in surface samples, with relatively higher pH values allowing the development of type I methanotrophs, known to be obligate in nature, thus providing a higher potential for CH_4 consumption. Furthermore, fluctuations in water table depth and, more likely, the speed at which the drop occurs can have an impact on the CH_4 primary emission pathway, with a fast drop capable of lowering the hydrostatic pressure at depth of peat column and release CH_4 in bubble form directly to the atmosphere, a process known as ebullition. While Teh et al. (2017) also recognised this process, it was not related to river banks conservation and flooding mitigation strategies. We encourage further data collection on ebullution occurrence and water table drop episodes and suggest that a sustained (even high) water table that is known to be the primary cause of CH_4 anoxic production, can still allow CH_4 consumption in the top oxic parts or oxic microsites than frequent fluctuations in catotelm thickness.

This biomarker approach coupled with pollen analysis (Roucoux et al., 2013; Kelly et al., 2017) also allowed to tie vegetation successions to collapses in key-components of microbial communities responsible for CH_4 cycling. For example, at QT, we see a decrease in biomarkers of both aerobic and anaerobic microbial communities during periods when

herbaceous taxa dominated. While a drop is expected in anaerobic microbes given a drop in water table depth and prevailing oxic conditions, we argued that the decrease in aerobic biomarkers can be due to poor substrate availability (i.e. less root exudates) provided by herbaceous taxa compared to woodland taxa. This occurs twice in the record at QT in the available samples and, since herbaceous taxa was replaced by forested and palm swamp vegetation with roots systems that most likely extended to this depth, this signal was conserved in the palaeorecord, offering an argument against continuous and synchronous accumulation, allowing biomarkers to be used as an accurate tool in palaeoenvironment reconstructions. Furthermore, the occurrence of waterlogged-adapted species in the palaeorecord (i.e. such as *M.flexuosa*) was also linked to lower concentrations seen in some biomarkers adapted to anoxic conditions. As such plants can transport oxygen from the atmosphere to the area around root-systems, lower peat accumulation rates after the establishment of such species can also be a consequence of higher decay rates in the presence of oxygen from 260 cm upwards and subsequent increase in aerobic bacteria biomarkers (i.e. hopanes, diplopterol, fatty acids). Although these observations were done on limited samples that span 20-35 years (i.e. 8 cm thickness), a higher resolution investigation can test this hypothesis in order to incorporate it into strategies that look at reducing CH4 emission at a peatland-scale.

8. References

A

1. **Abbott**, M.B., Seltzer, G.O., Kelts, K.R., Southon, J., 1997b. Holocene paleohydrology of the tropical Andes from lake records. Quat. Res. 47, 70-80.
2. **Abbott**, M.B., Wolfe, B.B., Wolfe, A., Seltzer, G., Aravena, R., Mark, B.G., Polissar, P.J., Rodbell, D.T., Rowe, H.D., Vuille, M., 2003. Holocene paleohydrology and glacial history of the central Andes using multiproxy lake sediment studies. Palae-ogeogr. Palaeoclimatol. Palaeoecol. 194, 123-138.
3. **Absy**, M L, 1982, Quaternary palynologlcal stu&es in the Amazon Basin In Prance, G T (ed), Biological Dzverstficatlon in the Tropics, pp 67-73 Columbia University Press, New York
4. **Absy**, M.L. and **Hammen**, T., 1976. Some palaeoecological data from Rondonia, southern part of the Amazon Basin. *Acta Amazonica*, *6*(3), pp.293-299.
5. **Ageta**, H. and **Arai**, Y., 1983. Fern constituents: pentacyclic triterpe- noids isolated from Polypodium niponicum and P. formosanum. Phytochemistry 22 (8), 1801-1808.
6. **Allan**, J. and **Douglas**, A. G., 1977, Variations in the content and distribution of n-alkanes in a series of Carboniferous vitrinites and sporinites of bituminous rank, Geochim Cosmochim Acta 41, pp. 1223-1230.
7. **Andersen**, R., Chapman, S.J. and Artz, R.R.E., 2013. Microbial communities in natural and disturbed peatlands: a review. *Soil Biology and Biochemistry*, *57*, pp.979-994.
8. **Andersson**, R.A. and **Meyers**, P.A., 2012, Effect of climate change on delivery and degradation of lipid biomarkers in a Holocene peat sequence in the Eastern European Russian Arctic, Org. Geochem. 53, pp. 63–72.
9. **Aniceto**, K., Moreira-Turcq, P,Cordeir, R.C.F.P., Quintana, I. T. B., 2014, Holocene paleohydrology of Quistococha Lake (Peru) in the upper Amazon Basin. Influences on carbon accumulations, Palaeogeogr.Palaeoclimatol. Palaeoecol., 415, pp. 165-174
10. **Anthony**, C., 1982. The Biochemistry of the Methylotrophs. Academic Press, New York.
11. **Amaral**, J.A. and **Knowles**, R., 1995. Growth of methanotrophs in methane and oxygen counter gradients. FEMS Microbiol. Lett. 126, pp. 215–220.
12. **Arai**, H., Hadi, A., Darung, U., Limin, S.H., Hatano, R. & Inubushi, K., 2014a, A methanotrophic community in a tropical peatland is unaffected by drainage and forest fires in a tropical peat soil. Soil Science and Plant Nutrition, 60, pp. 577–585.
13. **Artz**, R.R., Chapman, S.J., Campbell, C.D., 2006. Substrate utilisation profiles of microbial communities in peat are depth dependent and correlate with whole soil FTIR profiles. Soil Biol. Biochem. 38 (9), pp. 2958–2962.
14. **Aselmann**, I., and **Crutzen**, P., 1989, Global distribution of natural freshwater wetlands and rice paddies, their net primary productivity, seasonality and possible methane emissions. Journal of Atmospheric Chemistry, 8, pp. 307–358
15. **Atlas**, R.M., 1981. Microbial degradation of petroleum hydrocarbons: an environmental perspective. Microbiol. Rev. 45, pp.180–209.
16. **Auguet**, J.C., Montanie, H., Hartmann, H.J., Lebaron, P., Casamayor, E.O., Catala, P. and Delmas, D., 2009, Potential Effect of Freshwater Virus on the Structure and Activity

of Bacterial Communities in the Marennes-Oleron Bay (France). Microb. Ecol., 57, pp. 295-306

17. **Avery**, G., Shannon, R., White, J., Martens, C., Alperin, M., 1999. Effect of seasonal changes in the pathways of methanogenesis on the d13C values of pore water methane in a Michigan peatland. Global Biogeochemical Cycles 13, 475–484
18. **Ayari**, A., Yang, H., Wiesenberg, G.L.B., Xie, S., 2013. Distribution of archaeal and bacterial tetraether membrane lipids in rhizosphere-root systems in soils and their implication for paleoclimate assessment. Geochemical Journal 47, 337– 347.

B

19. **Bai**, L., Smuts, J., Schenk, J., Cochran, J. and Schug, K.A., 2018. Comparison of GC-VUV, GC-FID, and comprehensive two-dimensional GC–MS for the characterization of weathered and unweathered diesel fuels. *Fuel*, *214*, pp.521-527.
20. **Baker**, A., Routh, J. and Roychoudhury, A.N., 2016, Biomarker records of palaeoenvironmental variations in subtropical Southern Africa since the late Pleistocene: Evidences from a coastal peatland. Palaeogeography, palaeoclimatology, palaeoecology, 451, pp.1-12.
21. **Batjes**, N.H., Dijkshoorn, J.A., 1999, Carbon and nitrogen stocks in the soils of the Amazon Region. Geoderma 89, pp.273–286.
22. **Bellisario**, L.M., Bubier, J.L., Moore, T.R., Chanton, J.P., 1999. Controls on CH4 emissions from a northern peatland. Global Biogeochemical Cycles 13, pp. 81–91.
23. **Bernal**, J. P., Cruz, F. W., Stríkis, N. M., Wang, X., Deininger, M., Catunda, M.C. A., Ortega-Obregón, C., Cheng, H., Edwards, R. L., Auler, A.S.., 2016, High-resolution Holocene South American monsoon history recorded by a speleothem from Botuverá Cave, Brazil. Earth Planet. Sci. Lett. **450,** pp. 186–196
24. **Beckmann**, M., Sheppard, S.K. and Lloyd, D., 2004. Mass spectrometric monitoring of gas dynamics in peat monoliths: effects of temperature and diurnal cycles on emissions. *Atmospheric Environment*, *38*(39), pp.6907-6913.
25. **Bender**, M., **Conrad**, R., 1992. Kinetics of CH4 oxidation in oxic soils exposed to ambient air or high CH4 mixing ratios. FEMS Microbiol. Ecol. 101, 261–270.
26. **Bender**, M., **Conrad**, R., 1995. Effect of CH4 concentrations and soil conditions on the induction of CH4 oxidation activity. Soil Biol. Biochem. 27, 1517–1527.
27. **Benvegnu** T, Lemie`gre L, Cammas-Marion S. (2009). New generation of liposomes called archaeosomes based on natural or synthetic archaeal lipids as innovative formulations for drug delivery. Recent pat Drug Deliv Formul 3:206–20.
28. **Bernal**, J.P., Cruz, F.W., Stríkis, N.M., Wang, X., Deininger, M., Catunda, M.C.A., Ortega-Obregón, C., Cheng, H., Edwards, R.L. and Auler, A.S., 2016. High-resolution Holocene South American monsoon history recorded by a speleothem from Botuverá Cave, Brazil. *Earth and Planetary Science Letters*, *450*, pp.186-196.
29. **Bédard**, C. and **Knowles**, R., 1989. Physiology, biochemistry, and specific inhibitors of CH4, NH4+, and CO oxidation by methanotrophs and nitrifiers. Microbiological reviews, 53(1), pp.68-84.

30. **Berndmeyer**, C., Thiel, V., Schmale, O., Wasmund, N. and Blumenberg, M., 2014. Biomarkers in the stratified water column of the Landsort Deep (Baltic Sea). Biogeosciences, 11(23), pp.7009-7023.
31. **Bianchi**, T.S. and Canuel, E.A., 2011. *Chemical biomarkers in aquatic ecosystems*. Princeton University Press.
32. **Bird**, C.W., Lynch, J.M., Pirt, F.J., Reid, W.W., 1971. Steroids and squalene in Methylococcus capsulatus grown on methane. Nature 230, 473–475.
33. **Blaga**, C.I., Reichart, G.J., Heiri, O., Sinninghe Damsté, J.S., 2009. Tetraether membrane lipid distributions in water-column particulate matter and sediments: a study of 47 European lakes along a north–south transect. Journal of Paleolimnology 41, 523–540.
34. **Blair**, N.E. and Aller, R.C., 1995. Anaerobic methane oxidation on the Amazon shelf. *Geochimica et Cosmochimica Acta*, *59*(18), pp.3707-3715.
35. **Blaser**, M. and **Conrad**, R., 2016. Stable carbon isotope fractionation as tracer of carbon cycling in anoxic soil ecosystems. Current opinion in biotechnology, 41, pp.122-129.
36. **Blumer**, M. and **Thomas**, D., 1965, Phytadienes in zooplankton, Science, Vol. 149, 1148-1149.
37. **Blumer**, M., Mullin, M.M., Thomas, D.W., 1963. Pristane in zooplankton. Science 140, 974
38. **Blumer**, M., Mullin, M.M., Thomas, D.W., 1964. Pristane in the marine environment. Helgol. Meeresunters 10, 187-201.
39. **Bodelier**, Paul LE, Marie-José Bär Gillisen, Kees Hordijk, Jaap S. Sinninghe Damsté, W. Irene C. Rijpstra, Jan AJ Geenevasen, and Peter F. Dunfield. "A reanalysis of phospholipid fatty acids as ecological biomarkers for methanotrophic bacteria." The ISME journal 3, no. 5 (2009): 606.
40. **Boschker**, H.T.S. and **Middelburg**, J.J., 2002. Stable isotopes and biomarkers in microbial ecology. FEMS Microbiology Ecology, 40(2), pp.85-95.
41. **Bost**, F.D., Frontera-Suau, R., McDonald, T.J., Peters, K.E. and Morris, P.J., 2001. Aerobic biodegradation of hopanes and norhopanes in Venezuelan crude oils. *Organic Geochemistry*, *32*(1), pp.105-114.
42. **Bowman**, J.P., Skerratt, J.H., Nichols, P.D., Sly, L.I., 1991, Phospholipid fatty acid and lipopolysaccharide fatty acid signature lipids in methane-utilizing bacteria. FEMS Microbiol. Ecol. 85, 15–22.
43. **Bowman** J. P., Sly L. I., Nichols P. D., and Hayward A. C., 1993, Revised taxonomy of the methanotrophs—Description of Methyl- obacter Gen Nov, emendation of Methylococcus, validation of Methylosinus and Methylocystis species, and a proposal that the Family Methylococcaceae includes only the group I methanotrophs. Int. J. Syst. Bacteriol. 43, 735–753.
44. **Brown,** L.R., 1987, Oil degrading microorganisms. Chem Eng Prog October 35–40
45. **Buch**, R.T. and McInerney, F.A., 2013, Leaf wax n-alkane distribution in and across modern plants: implications for paleoecology and chemotaxonomy Geochim. Cosmochim. Acta, 117 (2013), pp. 161-179
46. **Bull**, I.D., Parekh, N.R., Hall, G.H., Ineson, P., Evershed, R.P., 2000. Detection and classification of atmospheric methane oxidizing bacteria in soil. Nature 405, 175–178.

47. **Bush**, M.B. and Cohnvaux, P.A., 1988, A 7000-year pollen record from the Amazonian lowlands, Ecuador Vegetatto, 76, 141-154
48. **Bush** M.B., Silman M.R., Listopad M.C.S. , 2007, A regional study of Holocene climate change and human occupation in Peruvian Amazonia. Journal of Biogeography, 34, 1342–1356
49. **Bustamante**, M.G., Cruz, F.W., Vuille, M., Apaéstegui, J., Strikis, N., Panizo, G., Novello, F.V., Deininger, M., Sifeddine, A., Cheng, H. and Moquet, J.S., 2016. Holocene changes in monsoon precipitation in the Andes of NE Peru based on δ 18 O speleothem records. *Quaternary Science Reviews*, *146*, pp.274-287.
50. **Bush**, R.T. and McInerney, F.A., 2013. Leaf wax n-alkane distributions in and across modern plants: implications for paleoecology and chemotaxonomy. *Geochimica et Cosmochimica Acta*, *117*, pp.161-179.
51. **Bohn**, T.J., Melton, J.R., Ito, A., Kleinen, T., Spahni, R., Stocker, B., Zhang, B., Zhu, X., Schroeder, R., Glagolev, M.V., Maksyutov, S., Brovkin, V., Chen, G., Denisov, S.N., Eliseev, A.V., Gallego-Sala, A., McDonald, K.C., Rawlins, M.A., Riley, W.J., Subin, Z.M., Tian, H.Q., Zhuang, Q., Kaplan, J.O., 2015. WETCHIMP-WSL: inter- comparison of wetland methane emissions models over West Siberia. Biogeosciences 12, pp. 3321-3349.
52. **Boschker**, H.T.S. and Middelburg, J.J., 2002. Stable isotopes and biomarkers in microbial ecology. FEMS Microbiology Ecology, 40(2), pp.85-95.
53. **Bray**, E.E. and **Evans**, E.D., 1961. Distribution of n-paraffins as a clue to recognition of source beds. Geochimica et Cosmochimica Acta, 22(1), pp.2-15.
54. **Briggs**, D.E.G. and **Summons**, R.E., 2014. Ancient biomolecules: Their origins, fossilization, and role in revealing the history of life. Bioessays 36, 482-490
55. **Brooks**, J.D., Gould, K. and Smith, J.W., 1969, Isoprenoid hydrocarbons in coal and petroleum, Nature, 222 (1969), pp. 257-259

C

56. **Caforio**, A. and **Driessen**, A.J., 2017. Archaeal phospholipids: Structural properties and biosynthesis. Biochimica et Biophysica Acta (BBA)-Molecular and Cell Biology of Lipids, 1862(11), pp.1325-1339.
57. **Cai**, Y., Zheng, Y., Bodelier, P.L., Conrad, R., Jia, Z., 2016. Conventional methanotrophs are responsible for atmospheric methane oxidation in paddy soils. Nat. Commun. 7, 11728.
58. **Caldwell**, S.L., Laidler, J.R., Brewer, E.A., Eberly, J.O., Sandborgh, S.C., Colwell, F.S., 2008. Anaerobic oxidation of methane: mechanisms, bioenergetics, and the ecology of associated microorganisms. Environ. Sci. Technol. 42, 6791–6799.
59. **Calvo** E., Pelejero C., Logan G. A. and De Deckker P. (2004) Dust- induced changes in phytoplankton composition in the Tasman Sea during the last four glacial cycles. Paleoceanography 19(2), PA2020
60. **Caraco** N.F. and Cole J.J. 1994. Human impact on nitrate export: an analysis using major world rivers. Ambio 28: 167–170.
61. **Castañeda**, I. S. and Schouten, S., 2011, A review of molecular organic proxies for examining modern and ancient lacustrine environments. Quat. Sci. Rev. 30, 2851–2891

62. **Chappe**, B., Michaelis, W., Albrecht, P., Ourisson, G., 1979. Fossil evidence for a novel series of archaeabacterial lipids. Naturwissenschaften 66, 522–523.
63. **Chappe**, B., Michaelis, W., Albrecht, P., 1980. Molecular fossils of Archaebacteria as selective degradation products of kerogen. In: Douglas, A.G., Maxwell, J.R. (Eds.), Advances in Organic Geochemistry 1979. Pergamon Press, Oxford, pp. 265–274.
64. Chambers, F. M., Beilman, D. W. and Yu, Z., 2011, Methods for determining peat humification and for quantifying peat bulk density , organic matter and carbon content for palaeostudies of climate and peatland carbon dynamics. *Mires Peat* **7,** pp. 1–10.
65. **Charman**, D.J., 2002, Peatlands and environmental change, John Wiley, Chichester
66. **Chasar**, L.S., Chanton, J.P., Glaser, P.H., Siegel, D.I., 2000b. Methane concentration and stable isotope distribution as evidence of rhizopheric processes: comparison of a fen and bog in the Glacial Lake Agassiz peatland complex. Annals of Botany 86, 655–663.
67. **Cheng**, B., Chen, F., Zhang, J., 2013. Palaeovegetational and palaeoenvironmental changes since the last deglacial in Gonghe Basin, northeast Tibetan Plateau. J. Geogr. Sci. 23, 136–146.
68. **Chowdhury**, T.R. and **Dick**, R.P., 2013. Ecology of aerobic methanotrophs in controlling methane fluxes from wetlands. Applied Soil Ecology 65, 8-22.
69. **Clymo**, R.S., 1984. Sphagnum-dominated peat bog: a naturally acid ecosystem. Proceedings of the Royal Society of London 305, 487–499.
70. **Clymo** RS, Turunen J, Tolonen K (1998) Carbon accumulation in peatland. Oikos 81:368–388
71. **Clymo**, R.S. and **Pearce**, D.M.E., 1995. Methane and carbon dioxide production in, transport through, and efflux from a peatland. *Phil. Trans. R. Soc. Lond. A*, *351*(1696), pp.249-259.
72. **Clymo**, R.S. and **Williams**, M.M.R., 2012. Diffusion of gases dissolved in peat pore water. *Mires & Peat*, *10*.
73. **Cobb**, K. M., C. D. Charles, H. Cheng, and R. L. Edwards, 2003: El Niño/Southern Oscillation and tropical Pacific climate during the last millennium. Nature, **424,** 271–276.
74. **Cohnvaux**, P A, Miller, M C, Lm, K -B, Stelnitz-Kannan, M and Frost, I (1985) Discovery of permanent Amazon lakes and hydrauhc disturbance in the upper Amazon river Nature, 313, 42-45
75. Comas, X., Slater, L. and Reeve, A., 2008. Seasonal geophysical monitoring of biogenic gases in a northern peatland: Implications for temporal and spatial variability in free phase gas production rates. *Journal of Geophysical Research: Biogeosciences*, *113*(G1).
76. **Coulthard**, T. J., Baird, A. J., Ramirez, J., and Waddington, J. M., 2009, Methane dynamics in peat: Importance of shallow peats and a novel reduced-complexity approach for modeling ebullition, in: Geophysical Monograph Series, edited by: Baird, A. J., Belyea, L. R., Comas, X., Reeve, A. S., and Slater, L. D., Vol. 184, 173– 185, American Geophysical Union,Washington, D. C.
77. **Cowardin**, L. M., Carter, V., Golet, F. C., and LaRoe, E. T., 1979, Classification of wetlands and deepwater habitats of the United States, U.S. Fish and Wild- life Service, Office of Biological Services, FWS/OBS-79/31, Washington, DC
78. **Cranwell**, P. A., 1973, Chain length distribution of n-alkanes from lake sediments in relation to postglacial environmental change, Freshwater Biol., 3, 259–265.

79. Cranwell, P.A., 1981, Diagenesis of free and bound lipids in terrestrial detritus deposited in a lacustrine sediment, Org Geochem Vol.3, pp. 79-89

80. **Cruz** Jr, F.W., Burns, S.J., Karmann, I., Sharp, W.D., Vuille, M., Cardoso, A.O., Ferrari, J.A., Dias, P.L.S. and Viana Jr, O., 2005. Insolation-driven changes in atmospheric circulation over the past 116,000 years in subtropical Brazil. *Nature*, *434*(7029), p.63.

D

81. **Dargie**, G., Lewis, S., Lawson, I., Mitchard, E., Page, S., Bocko, Y., and Ifo, S., 2017, Age, extent and carbon storage of the central Congo Basin peatland complex. Nature, 542,86–90
82. **Davidson**, N., 2014, How much wetland has the world lost? Long-term and recent trends in global wetland area. Marine and Freshwater Research, 65, 934–941.
83. Davies, K.L., Pancost, R.D., Edwards, M.E., Anthony, W., Katey, M., Langdon, P.G. and Chaves Torres, L., 2016. Diploptene δ 13 C values from contemporary thermokarst lake sediments show complex spatial variation. *Biogeosciences*, *13*(8), pp.2611-2621.
84. **Denich**, T. J., Beaudette, L. A., Lee, H. & Trevors, J. T. (2003). Effect of selected environmental and physico-chemical factors on bacterial cytoplasmic membranes. J Microbiol Methods 52, 149–182.
85. **De Granville**, J. J. Aperçu Sur La Struture Des Pneumatophores De Deux Espèces Des Sols Hydromorphes En Guyane. ORSTOM. série Biol. 3–22 (1974).
86. **de Granville** J-J, 1969, Aperçu sur la structure des Pneumatophores de 2 espèces des sols hydromorphes: Mauritia flexuosa L. et Euterpe oleracea Mart. (Palmae) - généralisation au système respiratoire racinaire d'autres palmiers. Dissertation, Centre Orstom de Cayenne
87. **De Jonge**, C., Hopmans, E.C., Stadnitskaia, A., Rijpstra, W.I.C., Hofland, R., Tegelaar, E., Sinninghe Damsté, J.S., 2013. Identification of novel penta- and hexamethy- lated branched glycerol dialkyl glycerol tetraethers in peat using HPLC–MS2, GC–MS and GC–SMB-MS. Org. Geochem. 54, 78–82.
88. **de Lange**, G., **Brumsack**, H.-J., 1998. The occurrence of gas hy- drates in Eastern Mediterranean mud dome structures as indi- cated by pore-water compositionHenriet, J.-P., Mienert, J. (Eds.), Gas Hydrates: Relevance to World Margin Stability and Climate Change, Special Publications, vol. 137. Geological Society, London, pp. 167–175.
89. **De Rosa**, M., Gambacorta, A., Minale, L. and Bu'Lock, J.D., 1971. Bacterial triterpenes. Journal of the Chemical Society D: Chemical Communications, (12), pp.619-620.
90. **Dedysh**, S. N., 2002, Methanotrophic bacteria of acidic sphagnum peat bogs, Microbiology, 71, 638–650
91. **Dedysh**, S.N., Belova, S.E., Bodelier, P.L., Smirnova, K.V., Khmelenina, V.N., Chidthaisong, A., Trotsenko, Y.A., Liesack, W. and Dunfield, P.F., 2007. Methylocystis heyeri sp. nov., a novel type II methanotrophic bacterium possessing 'signature'fatty acids of type I methanotrophs. International journal of systematic and evolutionary microbiology, 57(3), pp.472-479.
92. **Dedysh**, S.N. and Dunfield, P.F., 2011. Facultative and obligate methanotrophs: how to identify and differentiate them, Method Enzymol 495B: 31–44.

93. **Diaz**, H.F., Trigo, R., Hughes, M.K., Mann, M.E., Xoplaki, E., Barriopedro, D., 2011. Spatial and temporal characteristics of climate in Medieval Times revisited. Bulletin of the American Meteorological Society 92, 1487–1500
94. **Didyk**, B.M., Simoneit, B.R.T., Brassell, S.C., and Eglinton, G., 1978, Organic geochemical indicators of palaeoenvironmental conditions of sedimentation, Nature, 272 (1978), pp. 216-222
95. **Dinel**, H., Schnitzer, M., Mehuys, G.R., 1990. Soil lipids: origin, nature, contents, decomposition and effect on soil physical properties. In: Bollag, J.M., Stotzky, G. (Eds.), Soil Biochemistry. Marcel Dekker, New York, pp. 397–427.
96. **Dirghangi**, S.S., Pagani, M., Hren, M.T. and Tipple, B.J., 2013. Distribution of glycerol dialkyl glycerol tetraethers in soils from two environmental transects in the USA. Organic Geochemistry, 59, pp.49-60.
97. **Dise**, N. B. and **Verry**, E. S., 2001, Suppression of peatland methane emission by cumulative sulfate deposition in simulated acid rain, Bio- geochemistry, 53, 143–160, 2001
98. **Disnar**, J.R., Stefanova, M., Bourdon, S. and Laggoun-Défarge, F., 2005. Sequential fatty acid analysis of a peat core covering the last two millennia (Tritrivakely lake, Madagascar): diagenesis appraisal and consequences for palaeoenvironmental reconstruction. *Organic Geochemistry*, *36*(10), pp.1391-1404.
99. **Dixon**, M.J.R., Loh, J., Davidson, N.C., Beltrame, C., Freeman, R., Walpole, M., 2016, Tracking global change in ecosystem area: the wetland extent trends index. Biol. Conserv. 193, 27–35.
100. **Dommain**, R., Cobb, A.R., Joosten, H., Glaser, P.H., Chua, A.F.L., Gandois, L., Kai, F.-M., Noren, A., Salim, K.A., Su'ut, N.S.H., Harvey, C.F., 2015. Forest dynamics and tip-up pools drive pulses of high carbon accumulation rates in a tropical peat dome in Borneo (South- east Asia). Geophys. Res. Biogeosci. 120, 617–640.
101. **Draper**, F.C., 2015. Carbon storage and floristic dynamics in Amazonian peatland ecosystems. PhD Thesis. University of Leeds, U.K.
102. **Draper**, F.C.H., Roucoux, K.H., Lawson, I.T., Mitchard, E.T.A., Honorio Coronado, E.N., Lähteenoja, O., Montenegro, L.T., Valderrama Sandoval, E., Zaráte, R., Baker, T.R., 2014. The distribution and amount of carbon in the largest peatland complex in Ama- zonia. Environ. Res. Lett. 9, 124017
103. Drew, M.C., He, C.J. and Morgan, P.W., 2000. Programmed cell death and aerenchyma formation in roots. *Trends in plant science*, *5*(3), pp.123-127.
104. **Duan**, Y., C. Y. Wang, C. Y. Zheng, B. X. Wu, and G. D. Zheng, 2008, Geochemical study of crude oils from the Xifeng oilfield of the Ordos basin, China, J. Asian Earth Sci., 31, 341–356
105. **Dubroeucq** D, Volkoff B, 1998, From oxisols to spodosols and histosols: evolution of the soil mantles in the Rı´o Negro Basin (Amazonia). Catena, 32, 245–280.
106. **Dugan**, P. J. (Ed.). 1993. Wetlands under Threat. Mitchell Beazley, London
107.

E

108. **Eley,** Y.L. and **Hren**, M.T., 2018, Reconstructing vapor pressure deficit from leaf wax lipid molecular distributions, Scientific Reports 8, Article number 2967, Nature

109. **Eckmeier**, E., and **Wiesenberg**, G. L. B., 2009, Short-chain n-alkanes (C16-20) in ancient soil are useful molecular markers for prehistoric biomass burning. Journal of Archaeological Science, 36(7), 1590–1596.
110. **Eglinton**, G., Scott, P.M., Belsky, E., Burlingame, A.L., Calvin, M., 1964. Hydrocarbons of biological origin in a one-billion-year-old-sediment. Science 145, 263–264.
111. **Eglinton**, G. & Calvin, M. (1967). Chemical fossils. Scientific American 216,32-43.
112. **Espinoza Villar** JC, Guyot JL, Ronchail J, Cochonneau G, Naziano F, Fraizy P, Labat D, de Oliveira E, Ordonez JJ, Vauchel P., 2009b, Contrasting regional discharge evolutions in the Amazon basin (1974-2004). Journal of Hydrology 375: 297–311.
113. **Elvert** M, Suess E, Greinert J, Whiticar MJ (2000) Archaea mediating anaerobic methane oxidation in deep-sea sediments at cold seeps of the eastern Aleutian subduction zone. Organic Geochemistry 31, 1175–1187.
114. **Eva**, H.D., Belward, A.S., De Miranda, E.E., Di Bella, C.M., Gond, V., Huber, O., Jones, S., Sgrenzaroli, M. and Fritz, S., 2004. A land cover map of South America. *Global Change Biology*, *10*(5), pp.731-744.

F

115. **Ficken**, K. J., Li, B., Swain, D. L., and Eglinton, G, 2000, An n -alkane proxy for the sedimentary input of submerged/floating freshwater aquatic macrophytes. Organic Geochemistry, 31, pp. 745–749.
116. **Field**, C.B., Barros, V.R., Dokken, D.J., Mach, K.J., Mastrandrea, M.D., Bilir, T.E., Chatterjee, M., Ebi, K.L., Estrada, Y.O., Genova, R.C. and Girma, B., 2014. IPCC, 2014: Climate change 2014: Impacts, adaptation, and vulnerability. Part A: Global and sectoral aspects. Contribution of working group II to the fifth assessment report of the intergovernmental panel on climate change.
117. **Finlayson**, C. M., and **Davidson**, N. C. 1999. Summary report. In 'Global review of wetland resources and priorities for wetland inventory'. (Eds C.M. Finlayson and A.G. Spiers.) pp. 1–15. Supervising Scientist Report 144/Wetlands International Publication 53. (Supervising Scientist: Canberra, Australia.)
118. **Finne** G. and **Matches**, J.R., 1976, Spin-labeling studies on the lipids of psychrophilic and psychrotrophic, and mesophilic Clostridia. J. Bacteriol. 125, 211
119. **Fischer**, W.W., Summons, R.E. and Pearson, A., 2005. Targeted genomic detection of biosynthetic pathways: anaerobic production of hopanoid biomarkers by a common sedimentary microbe. Geobiology, 3(1), pp.33-40.
120. **Frostegård**, Å., Tunlid, A. and Bååth, E., 1993. Phospholipid fatty acid composition, biomass, and activity of microbial communities from two soil types experimentally exposed to different heavy metals. Applied and Environmental Microbiology, 59(11), pp.3605-3617.

G

121. **Gaines**, S. M., G. Eglinton, and J. Rüllkolter. 2009. Echoes of life—What fossil molecules reveal about earth history. Oxford University Press, New York
122. **Gauci**, V., Dise, N., and Fowler, D.2002, Controls on suppres- sion of methane flux from a peat bog subjected to simu- lated acid rain sulfate deposition, Global Biogeochem.

123. **Gauci**, V., Matthews, E., Dise, N., Walter, B., Koch, D., Granberg, G., and Vile, M, 2004, Sulfur pollution suppression of the wetland methane source in the 20th and 21st centuries, Proceedings of the National Academy of Sciences of the United States of America, 101, 12583–12587, 2004
124. **Gelpi** E, Schneider H, Mann J, Oró J, 1970, Hydrocarbons of geochemical significance in microscopic algae. Phytochemistry 9:603–612
125. **Girguis**, P.R., Orphan, V.J., Hallam, S.J. and DeLong, E.F., 2003. Growth and methane oxidation rates of anaerobic methanotrophic archaea in a continuous-flow bioreactor. Applied and environmental microbiology, 69(9), pp.5472-5482.
126. **Gola,** M. R., Karger, M., Gazda, L. abd Grafka, O., 2013, Organic geochemistry of Upper Carboniferous bituminous coals and clastic sediments from the Lublin Coal Basin (Poland), Acta Geologica Polonica, Vol.63, No. 3, pp.425-442
127. González-Vila, F.J., 1995. Alkane biomarkers. Geochemical significance and application in oil shale geochemistry. In *Composition, Geochemistry and Conversion of Oil Shales* (pp. 51-68). Springer, Dordrecht.
128. **Goossens**, H., Due, A., de. Leeuw, J.W., van De Graaf, B. and Schenk, P.A., 1988, The Pristane Formation Index, a new molecular maturity parameter - A simple method to assess maturity by pyrolysis/evaporation-gas chromatography of unextracted samples, Geochim. Cosmochim. Acta, 52, pp. 1189-1193
129. **Goulding** M., Barthem R. and Ferreira E., 2003, The Smithsonian Atlas of the Amazon. Smithsonian Books, Washington, DC, p. 255.
130. **Graham**, D.W., Chaudhary, J.A., Hanson, R.S., Arnold, R.G., 1993. Factors affect- ing competition between Type-I and Type-II methanotrophs in two-organism, continuous-flow reactors. Microb. Ecol. 25, 1–17.
131. **Guckert**, J.B., Hood, M.A. and White, D.C., 1986. Phospholipid ester-linked fatty acid profile changes during nutrient deprivation of Vibrio cholerae: increases in the trans/cis ratio and proportions of cyclopropyl fatty acids. *Applied and environmental microbiology*, *52*(4), pp.794-801.
132. Guyot, J.L., Jouanneau, J.M., Soares, L., Boaventura, G.R., Maillet, N. and Lagane, C., 2007. Clay mineral composition of river sediments in the Amazon Basin. *Catena*, *71*(2), pp.340-356.

H

133. **Hanson**, R.S., Hanson, T.E., 1996, Methanotrophic bacteria.Microbiol. Rev. 60, 439–471.
134. **Härtner**, T., Straub, K.L. and Kannenberg, E., 2005. Occurrence of hopanoid lipids in anaerobic Geobacter species. FEMS Microbiology Letters, 243(1), pp.59-64.
135. **Heindel**, K., Birgel, D., Brunner, B., Thiel, V., Westphal, H., Gischler, E., Ziegenbalg, S.B., Cabioch, G., Sjövall, P. and Peckmann, J., 2012. Post-glacial microbialite formation in coral reefs of the Pacific, Atlantic, and Indian Oceans. Chemical Geology, 304, pp.117-130.
136. **Hess**, L.L., Melack, J.M., Affonso, A.G., et al., 2015. Wetlands of the lowland Amazon basin: extent, vegetative cover, and dual-season inundated area as mapped with JERS-1 syn- thetic aperture radar. Wetlands 35, 745–756.

137. **Hoefs**, M.J.L., Schouten, S., de Leeuw, J.W., King, L.L., Wakeham, S.G., Sinninghe Damsté´, J.S., 1997. Ether lipids of planktonic archaea in the marine water column. Appl. Environ. Microbiol. 63, 3090–3095.
138. **Hoffmann**, B., Kahmen, A., Cernusak, L.A., Arndt, S.K. and Sachse, D., 2013. Abundance and distribution of leaf wax n-alkanes in leaves of Acacia and Eucalyptus trees along a strong humidity gradient in northern Australia. Organic geochemistry, 62, pp.62-67.
139. **Hornibrook**, E. R. C., W. S. Longstaffe, and W. S. Fyfe, 1997, Spatial distribution of microbial methane production pathways in temperate zone wetland soils: Stable carbon and hydrogen isotope evidence, *Geochim. Cosmochim. Acta*, **61**, 745–753.
140. **Hornibrook**, E. R. C., Longstaffe, F. J., and Fyfe, 2000a, W. S.: Evolu- tion of stable carbon isotope compositions for methane and car- bon dioxide in freshwater wetlands and other anaerobic environ- ments, Geochim. Cosmochim. Acta, 64, 1013–1027.
141. **Hornibrook**, E. R. C., Longstaffe, F. J., and Fyfe, W. S.. 2000b, Fac- tors influencing stable isotope ratios in CH4 and CO2 within subenvironments of freshwater wetlands: Implications for delta- signatures of emissions, Isot. Environ. Healt. S., 36, 151–176.
142. **Hinrichs**, K.U., Hayes, J.M., Sylva, S.P., Brewer, P.G. and DeLong, E.F., 1999. Methane-consuming archaebacteria in marine sediments. Nature, 398(6730), p.802-805
143. **Hinrichs**, K.U., Summons, R.E., Orphan, V., Sylva, S.P. and Hayes, J.M., 2000. Molecular and isotopic analysis of anaerobic methane-oxidizing communities in marine sediments. Organic Geochemistry, 31(12), pp.1685-1701.
144. **Hinrichs**,K.U. ,Hmelo,L.K. and Sylva, S.P., 2003, Molecular fossil record of elevated methane levels in late Pleistocene coastal waters, Science, 299, pp. 1214-1217
145. **Hoehler**, T.M., Alperin, M.J., Albert, D.B., Martens, C.S., 1994. Field and laboratory studies of methane oxidation in an anoxic sediment – evidence for a methanogen-sulfate reducer consortuim. Glob. Biogeochem. Cycles 8, pp. 451–463
146. **Householder**, J.E., Janovec, J.P., Tobler, M.W., Page, S., Lähteenoja, O., 2012, Peatlands of the Madre de Dios river ofPeru: distribution, geomorphology, and habitat diversity.Wet- lands 32, 359–368.
147. **Hu**, S., Niu, Z., Chen, Y., Li, L. and Zhang, H., 2017, Global wetlands: Potential distribution, wetland loss, and status, Sci. Total Environ., 586, pp. 319–327
148. **Huguet**, A., Gocke, M., Derenne, S., Fosse, C., Wiesenberg, G.L.B., 2013. Root-associated branched tetraether source microorganisms may reduce estimated paleotemperatures in subsoil, Chemical Geology 356, p. 1-10
149. Huguet, A., Fosse, C., Laggoun-Défarge, F., Delarue, F. and Derenne, S., 2013. Effects of a short-term experimental microclimate warming on the abundance and distribution of branched GDGTs in a French peatland. *Geochimica et Cosmochimica Acta*, *105*, pp.294-315.
150. **Huguet**, A., Fosse, C., Laggoun Défarge, F., Toussaint, M.L., Derenne, S., 2010, Occurrence and distribution of glycerol dialkyl glycerol tetraethers in a French peat bog. Organic Geochemistry 41, 559–572.
151. **Huang**, X., Meyers, P.A., Xue, J., Gong, L., Wang, X. and Xie, S., 2015. Environmental factors affecting the low temperature isomerization of homohopanes in acidic peat deposits, central China. Geochimica et Cosmochimica Acta, 154, pp.212-228.

152. **Huizer**, S., Karaoulis, M. C., Essink, G. H. P. O., and Bierkens, M. F. P, 2017, Water Resources Research. Water Resources Research, 53, 1–23.

153. **Hunt**, J. H. 1996. Petroleum geochemistry and geology, 2nd ed. Freeman, New York.

I

154. **Immirzi** CP, Maltby E, Clymo RS, 1992, The Global Status of Peatlands and their 9 Role in Carbon Cycling. A report for Friends of the Earth by the Wetlands 10 Ecosystems Research Group, Department of Geography, University of Exeter, UK. 11 Friends of the Earth, London

155. **Inglis**, G.N., Naafs, B.D.A., Zheng, Y., McClymont, E.L., Evershed, R.P. and Pancost, R.D., 2018. Distributions of geohopanoids in peat: Implications for the use of hopanoid-based proxies in natural archives. *Geochimica et Cosmochimica Acta*, *224*, pp.249-261.

156. **IPCC**, Team, C.W., Pachauri, R.K. and Meyer, L.A., 2014. IPCC, 2014: climate change 2014: synthesis report. Contribution of Working Groups I. *II and III to the Fifth Assessment Report of the intergovernmental panel on Climate Change. IPCC, Geneva, Switzerland*, *151*.

J

157. **Jahnke**, L.L., Summons, R.E., Hope, J.M., Des Marais, D.J., 1999, Carbon isotopic fractionation in lipids from methanotrophic bacteria: II. The effects of physiology and environmental parameters on the biosynthesis and isotopic signatures of biomarkers. Geochim. Cosmochim. Acta 63, 79–93

158. **Jauhiainen** J, Silvennoinen H, Könönen M, Limin S, Vasander H (2016) Management driven changes in carbon mineralization dynamics of tropical peat. Biogeochemistry 129:115–132.

159. **Jenks**, M.A. and **Ashworth**, E.N., 1999, Plant epicuticular waxes: function production and genetics. In: Janick, J. (Ed.), Horticultural Reviews, vol. 23, pp. 1–68.

160. **Jones**, R. T., et al. 2009. A comprehensive survey of soil acidobacterial diversity using pyrosequencing and clone library analyses. ISME J. 3:442–453.

161. **Junk**, W.J., Piedade, M.T., Wittmann, F., Schöngart, J. and Parolin, P. eds., 2010. *Amazonian floodplain forests: ecophysiology, biodiversity and sustainable management* (Vol. 210). Springer Science & Business Media.

162. **Junk**, W.J., 1983. Ecology of swamps on the middle Amazon. In: Gore, A.J.P. (Ed.), Mires: swamp, bog, fen and moor, regional studies; Ecosystems of the World 4B. Elsevier, Amsterdam, the Netherlands, pp. 269–294.

K

163. **Kahn** F. and **Mejia** K., de Castro A, 1988, Species richness and density of palms in terra firme forests ofAmazonia. Biotropica 20, pp.266–269

164. **Kahn**, F. and **Granville**, J., 1992. Palms in forest Ecosystems of Amazonia. Springer Verlag, Heidelberg.
165. **Kaneda** T., 1991, Iso- and anteiso-fatty acids in Bacteria: biosynthesis, function, and taxonomic significance. Microbiol. Mol. Biol. Rev. 55, 288–302.
166. **Kannenberg**, E.L. and Poralla, K., 1999. Hopanoid biosynthesis and function in bacteria. Naturwissenschaften, 86(4), pp.168-176.
167. **Kanner**, L.C., Burns, S.J., Cheng, H., Edwards, R.L., Vuille, M., 2013. High-resolution variability of the South American summer monsoon over the last seven millennia: insights from a speleothem record from the central Peruvian Andes. Quat. Sci. Rev. 75, pp. 1-10
168. **Kates** M. (1993) Membrane lipids of archaea. In The Biochemistry of Archaea (Archaebacteria) (eds. M. Kates, D. S. Kushner, and A. T. Matheson), pp. 261–295. Elsevier Science, New York.
169. **Kaur**, G., Mountain, B.W., Stott, M.B., Hopmans, E.C., Pancost, R.D., 2015. Temperature and pH control on lipid composition of silica sinters from diverse hot springs in the Taupo Volcanic Zone, New Zealand. Extremophiles 19, 327–344.
170. **Keddy**, P., Fraser, L., Solomeshch, A., Junk, W., Campbell, D., Arroyo, M., and Alho, C., 2009, Wet and wonderful: The world's largest wetlands are conservation priorities. BioScience, 59, 39–51.
171. **Kellner**, E., Waddington, J.M. and Price, J.S., 2005. Dynamics of biogenic gas bubbles in peat: Potential effects on water storage and peat deformation. *Water Resources Research, 41*(8).
172. **Kelly**, T.J., Baird, A.J., Roucoux, K.H., Baker, T.R., Honorio Coronado, E.N., Ríos,M., Lawson, I.T., 2014. The high hydraulic conductivity of three wooded tropical peat swamps in Northeast Peru: measurements and implications for hydrological function. Hydrol. Process. 28, 3373–3387.
173. **Kelly**, T.J., Lawson, I.T., Roucoux, K.H, Baker, T.R., Jones, T.D. and Sanderson, K.N., 2017, The vegetation history of an Amazonian domed peatland, Palaeogeography, Palaeoclimatology, Palaeoecology, 468, pp. 129–141
174. **Kieft,** T. L., Ringelberg D. B. and White D. C., 1994, Changes in ester-linked phospholipid fatty acid profiles of subsurface bacteria during starvation and desiccation in a porous medium. Applied and Environmental Microbiology 60, 3292-3299.
175. **Kielak**, A. M., Cipriano, M. A. P., & Kuramae, E. E., 2016, Acidobacteriastrains from subdivision 1 act as plant growth-promoting bacteria. Archives of Microbiology, 198(10), 987–993.
176. **Kito**, M., and Pizer, L.I. (1969) Purification and regulatory properties of biosynthetic L-glycerol 3-phosphate dehydro- genase from Escherichia coli. J Biol Chem 244: 3316–3323.
177. **Klavins**, M., Sire, J., Purmalis, O. and Melecis, V., 2008, Approaches to estimating humification indicators for peat, Mires and Peat, 3, 7
178. **Knief**, C., Lipski, A. and Dunfield, P.F, 2003, Diversity and Activity of Methanotrophic Bacteria in Different Upland Soils, APPLIED AND ENVIRONMENTAL MICROBIOLOGY, Vol. 69, No. 11, pp. 6703-6714
179. **Knapp**, Daniel R., 1979, Handbook of Analytical Derivatization Reaction; pages 10, 10; Wiley & Sons; New York, 1979.

180. **Koelbener**, A., Ström, L., Edwards, P. J. & Olde Venterink, H., 2010, Plant species from mesotrophic wetlands cause relatively high methane emissions from peat soil. Plant Soil 326, 147–158.
181. **Koga,** Y., Kyuragi T, Nishihara M, Sone N. 1998b. Did archaeal and bacterial cells arise independently from non-cellular precur- sors? A hypothesis stating that the advent of membrane phospholipid with enantio- meric glycerophosphate backbones caused the separation of the two lines of descent. Journal of Molecular Evolution 46:54–63.
182. **Koh**, H.-S., C. A. Ochs, and K. Yu. 2009. Hydrologic gradient and vegetation controls on CH4 and CO2 fluxes in a spring-fed forested wetland. Hydrobiologia 630: 271–286.
183. **Kool**, D.M., Talbot, H.M., Rush, D., Ettwig, K., Sinninghe Damsté, J.S., 2014. Rare bacteriohopanepolyols as markers for an autotrophic, intra-aerobic methanotroph. Geochimica et Cosmochimica Acta 136, 114-125.
184. **Kuhn**, T.K., Krull, E.S., Bowater, A., Grice, K. and Gleixner, G., 2009, The occurrence of short chain n-alkanes with an even over odd predominance in higher plants and soils, Organic Geochemistry 41, pp. 88-95

L

185. **Lappalainen,** E., 1996. Global Peat Resources. International Peat Society Jyskä.
186. **Langworthy**, T.A., Holzer, G., Zeikus, J.G., Tornabene, T.G., 1983. Iso- and anteiso-branched glycerol diethers of the thermophilic anaerobe Thermodesulfotobacterium commune. Syst. Appl. Mi- crobiol. 4, 1–17.
187. **Lawrence**, B.A. and Zedler, J.B., 2013, Carbon Storage by Carex stricta Tussocks: A Restorable Ecosystem Service?, Wetlands, 2013, Volume 33, Issue 3, pp 483–493
188. **Lähteenoja**, O., Page, S., 2011. High diversity of tropical peatland ecosystem types in the Pastaza-Marañón basin, Peruvian Amazonia. J. Geophys. Res. 116, G02025.
189. **Lähteenoja**, O., Ruokolainen, K., Schulman, L., Oinonen,M., 2009a. Amazonian peatlands: an ignored C sink and potential source. Glob. Chang. Biol. 15, 2311–2320.
190. **Lähteenoja**, O., Ruokolainen, K., Schulman, L., Alvarez, J., 2009b. Amazonian floodplains harbour minerotrophic and ombrotrophic peatlands. Catena 79, 140–145.
191. **Lähteenoja**, O., Reátegui, Y.R., Räsänen, M., Torres, D.D.C., Oinonen, M. and Page, S., 2012. The large A mazonian peatland carbon sink in the subsiding P astaza-M arañón foreland basin, P eru. *Global Change Biology*, *18*(1), pp.164-178.
192. **Lähteenoja**, O., Reátegui, Y.R., Räsänen, M., Torres, D.D., Oinonen, M., Page, S., 2012. The large Amazonian peatland carbon sink in the subsiding Pastaza-Marañón foreland basin, Peru. Glob. Chang. Biol. 18, 164–178.
193. **Lähteenoja**, O., Flores, B., Nelson, B., 2013. Tropical peat accumulation in Central Amazo- nia. Wetlands 33, 495–503.
194. **Laing**, C.G., Shreeve, T.G. and Pearce, D.M., 2010. The fine scale variability of dissolved methane in surface peat cores. *Soil Biology and Biochemistry*, *42*(8), pp.1320-1328.
195. **Lengger**, Sabine K; Hopmans, Ellen C; Sinninghe Damsté, Jaap S; Schouten, Stefan (2014): Fossilization and degradation of archaeal intact polar tetraether lipids in ODP Site 201-1229 sediments. PANGAEA, Supplement to: Lengger, SK et al. (2014): Fossilization and degradation of archaeal intact polar tetraether lipids in deeply buried marine sediments (Peru Margin). Geobiology, 12(3), 212-220

196. **Lawrence**, B.A. and Zedler, J.B., 2011. Formation of tussocks by sedges: effects of hydroperiod and nutrients. Ecological Applications, 21(5), pp.1745-1759.
197. **Lawso**n, I.T., Jones, T.D., Kelly, T.J., Honorio Coronado, E.N., Roucoux, K.H., 2014. The geo- chemistry of Amazonian peats.Wetlands 34, 905–915
198. **Le Mer**, Jean, and Pierre Roger. "Production, oxidation, emission and consumption of methane by soils: a review." *European Journal of Soil Biology* 37, no. 1 (2001): 25-50.
199. **Lijmbach**, G., 1975, Proceedings of the 9th World Petroleum Congress, 2, Applied Science Publishers, London, 1975, 357–369.
200. **Lim**, K.L., Pancost, R.D., Hornibrook, E.R., Maxfield, P.J. and Evershed, R.P., 2012. Archaeol: an indicator of methanogenesis in water-saturated soils. Archaea, 2012.
201. **Loomis**, S.E., Russell, J.M., Heureux, A.M., D'Andrea, W.J. and Damsté, J.S.S., 2014. Seasonal variability of branched glycerol dialkyl glycerol tetraethers (brGDGTs) in a temperate lake system. *Geochimica et Cosmochimica Acta*, *144*, pp.173-187.
202. **Luo**, G., Yang, H., Algeo, T. J., Hallmann, C. and Xie, S., 2018, Lipid biomarkers for the reconstruction of deep-time environmental conditions, Earth Science Reviews, In Press
203. **Lupascu**, M., Wadham, J.L., Hornibrook, E.R.C. and Pancost, R.D., 2014. Methanogen biomarkers in the discontinuous permafrost zone of Stordalen, Sweden. Permafrost and Periglacial Processes, 25(4), pp.221-232.

M

204. **Mackenzie**, A.S., Patience, R.L., Maxwell, J.R., Vandenbroucke, M. and Durand, B., 1980. Molecular parameters of maturation in the Toarcian shales, Paris Basin, France—I. Changes in the configurations of acyclic isoprenoid alkanes, steranes and triterpanes. *Geochimica et Cosmochimica Acta*, *44*(11), pp.1709-1721.
205. **Maia,** L.A., 1997, Influência do pulso de inundação na fisiologia, fenologia e produçao de frutos de Hevea spruceana (Euphorbiaceae) e Eschweilera tenuifolia (Lecythidaceae), em área inundável de igapó da Amazônia central. Unpublished Ph.D. Thesis, INPA/FUA Manaus, p 186
206. **Maltchik**, L., 2003, Three new wetlands inventories in Brazil. Interciencia 28(7), pp. 421–423
207. **Marengo**, J.A., 1998. Climatologia de la zona de Iquitos, Peru. In: Kalliola, R., Flores Paitan, S. (Eds.), Geoecologia y desarrollo amazonico: studio intergrado en la zona de Iquitos, Peru. Annales Universitatis Turkuensis Ser A, 114. University of Turku, Finland, pp. 35–57.
208. **Martens**, C.S. and Klump, J.V., 1980. Biogeochemical cycling in an organic-rich coastal marine basin—I. Methane sediment-water exchange processes. *Geochimica et Cosmochimica Acta*, *44*(3), pp.471-490.
209. **Marzi**, R., Torkelson, B.E. and Olson, R.K., 1993, A revised carbon preference index, Org. Geochem., Vol. 20, No. 8, pp. 1303-1206
210. **Mathews**, E., and I. **Fung**. 1987. Methane emission from natural wetlands: global distribution, area and environmental characteristics of sources. Global Biogeochem. Cycles 1:61–86

211. **Maxfield**, P.J., Hornibrook, E.R.C. and Evershed, R.P., 2006. Estimating high-affinity methanotrophic bacterial biomass, growth, and turnover in soil by phospholipid fatty acid 13C labeling. Applied and environmental microbiology, 72(6), pp.3901-3907.
212. **Megonigal**, J.P., Hines, M.E. and Visscher, P.T.,2014, Anaerobic metabolism: linkages to trace gases and aerobic processes, edited by: Schlesinger, WH. *Biogeochemistry*, *8*.
213. **Meyers**, P.A., Takemura, K., 1997. Quaternary changes in delivery and accumulation of organic matter in sediments of Lake Biwa, Japan. Journal of Paleolimnology 18, 211–218.
214. **Meyers**, P. A. 2003. Application of organic geochemistry to paleolimnological reconstructions: a summary of examples from the Laurentian Great Lakes. Organic Geochemistry 34: 261–290.
215. **McClymont**, E., Pendall, E. & Nichols, J. E., 2010, Stable isotopes and organic geochemistry in peat: Tools to investigate past hydrology, temperature and biogeochemistry. PAGES news 18, 15–18
216. **McIntyre**, C.P., Harvey, P.M., Ferguson, S., Wressnig, A.M., Snape, I. and George, S.C., 2007. Determining the extent of weathering of spilled fuel in contaminated soil using the diastereomers of pristane and phytane. Organic Geochemistry, 38(12), pp.2131-2134.
217. **Melton**, J.R., Wania, R., Hodson, E.L., Poulter, B., Ringeval, B., Spahni, R., Bohn, T., Avis, C.A., Beerling, D.J., Chen, G. and Eliseev, A.V., 2013. Present state of global wetland extent and wetland methane modelling: conclusions from a model intercomparison project (WETCHIMP). Biogeosciences, 10, pp.753-788.
218. **Ménot**, G. and **Bard**, E., 2010. Geochemical evidence for a large methane release during the last deglaciation from Marmara Sea sediments. Geochimica et Cosmochimica Acta, 74(5), pp.1537-1550.
219. **Miettinen**, J., Liew, S.C., 2010. Degradation and development of peatlands in Peninsular Malaysia and in the islands of Sumatra and Borneo since 1990. Land Degradation & Development 21, 285e296.
220. **Michaelis**, W., Albrecht, P., 1979. Molecular fossils of archaebacteria in kerogen. Naturwissenschaften 66, 420-422
221. **Mills**, C.T., Slater, G.F., Dias, R.F., Carr, S.A., Reddy, C.M., Schmidt, R. and Mandernack, K.W., 2013. The relative contribution of methanotrophs to microbial communities and carbon cycling in soil overlying a coal-bed methane seep. FEMS microbiology ecology, 84(3), pp.474-494.
222. **Mitch,** W.J. and **Gosselink**, J.G., 2000, The value of wetlands: importance of scale and landscape setting, Ecological Economics, Vol. 35, Issue 1, pp.25-33
223. **Mitsch**, W.J., and **Gosselink**, J.G., 2007. Wetlands, 4th edition. John Wiley & Sons, Inc, Hoboken, New Jersey.
224. **Mohialdeen**, I.M., Hakimi, M.H. and Al-Beyati, F.M., 2015. Biomarker characteristics of certain crude oils and the oil-source rock correlation for the Kurdistan oilfields, Northern Iraq. Arabian Journal of Geosciences, 8(1), pp.507-523.
225. **Morales-Olmedo**, M., Ortiz, M. and Sellés, G., 2015. Effects of transient soil waterlogging and its importance for rootstock selection. *Chilean journal of agricultural research*, *75*, pp.45-56.
226. **Moustafa**, Y. M. and **Morsi**, R. E.. 2012, Chapter 9: Biomarkers. Chromatogr. Its Appl. 165–186

227. **Moquet**, J.S., Crave, A., Viers, J., Seyler, P., Armijos, E., Bourrel, L., Chavarri, E., Lagane, C., Laraque, A., Casimiro, W.S.L. and Pombosa, R., 2011. Chemical weathering and atmospheric/soil CO2 uptake in the Andean and Foreland Amazon basins. Chemical Geology, 287(1-2), pp.1-26.
228. **Moldowan**, J.M., Seifert, W.K. and Gallegos, E.J., 1985, Relationships between petroleum composition and depositional environment of petroleum source rocks. AAPG Bulletin, 69, 1255−1268.
229. **Morales-Olmedo**, M., Ortiz, M., & Sellés, G. (2015). Effects of transient soil waterlogging and its importance for rootstock selection. Chilean Journal of Agricultural Research, 75(August), 45–56.
230. **Morgan**, J. and C. **Winstanley**. 1997. Microbial biomarkers. p. 331–352. In J. van Elsas, J. Trevors, and E. Wellington (eds.) Modern Soil Microbiology. Marcel Dekker, Inc., New York, USA.
231. **Morgan** J.A.W., and Winstanley, C, 1997, Microbial biomark- ers. (in) Modern soil microbiology. (eds. J.D van Elsas, J.T. Trevors, E.M.H. Wellington) Marcel Dekker. Inc., New York, pp 331-348

N

232. **Naafs**, B.D.A., Inglis, G.N., Zheng, Y., Amesbury, M.J., Biester, H., Bindler, R., Pancost, R.D., 2017a. Introducing global peat-specific temperature and pH calibrations based on brGDGT bacterial lipids. Geochimica et Cosmochimica Acta 208, 285– 301.
233. **Naafs**, B.D.A., Rohrssen, M., Inglis, G.N., Lähteenoja, O., Feakins, S.J., Collinson, M.E., Kennedy, E.M., Singh, P.K., Singh, M.P., Lunt, D.J. and Pancost, R.D., 2018b, High temperatures in the terrestrial mid-latitudes during the early Palaeogene. Nature Geoscience, p.1.
234. **Naeher**, S., Niemann, H., Peterse, F., Smittenberg, R.H., Zigah, P.K. and Schubert, C.J., 2014. Tracing the methane cycle with lipid biomarkers in Lake Rotsee (Switzerland). *Organic geochemistry*, *66*, pp.174-181.
235. **Naeher**, S., Peterse, F., Smittenberg, R.H., Niemann, H., Zigah, P.K., Schubert, C.J., 2014. Sources of glycerol dialkyl glycerol tetraethers (GDGTs) in catchment soils, water column and sediments of Lake Rotsee (Switzerland) – implications for the application of GDGT-based proxies for lakes. Organic Geochemistry 66, 164–173.
236. **Naiman**, R.J., Decamps, H. and McClain, M.E., 2010, Riparia: Ecology, Conservation, and Management of Streamside Communities, Elsevier
237. **Naeher**, S., Niemann, H., Peterse, F., Smittenberg, R.H., Zigah, P.K., Schubert, C.J., 2014. Tracing the methane cycle with lipid biomarkers in Lake Rotsee (Switzerland). Organic Geochemistry 66, 174-181
238. **Navale**, V., 1994. Comparative study of low and high temperature hydrous pyrolysis products of monoglycerol diether lipid from archaebacteria. J. Anal. Appl. Pyrolysis 29, 33-43.
239. **Nichols**, J.E., Booth, R.K., Jackson, S.T., Pendall, E.G., Huang, Y., 2006. Paleohydrologic reconstruction based on n-alkane distributions in ombrotrophic peat. Organic Geochemistry 37, 1505–1513.

240. **Nichols**, J.E., Walcott, M., Bradley, R.S., Pilcher, J., Huang, Y., 2009. Quantitative assessment of precipitation seasonality and summer surface wetness using ombrotrophic sediments from an Arctic Norwegian peatland. Quaternary Research 72, 443–451.
241. **Nichols**, J.E., Peteet, D.M., Moy, C.M., Castañeda, I.S., McGeachy, A., Perez, M., 2014. Impacts of climate and vegetation change on carbon accumulation in a south- central Alaskan peatland assessed with novel organic geochemical techniques. The Holocene 24, 1146–1155.
242. **Nichols**, P.D., Glen A, S., Antworth, C.P., Hanson, R.S. and White, D.C., 1985. Phospholipid and lipopolysaccharide normal and hydroxy fatty acids as potential signatures for methane-oxidizing bacteria. FEMS Microbiology Letters, 31(6), pp.327-335.
243. **Nicholson**, B., 1997. Aguajal Swamp Forests of the Peruvian Amazon. In: Rieley, J.O., Page, S.E. (Eds.), Biodiversity and sustainability of tropical peatlands. Samara Publishing Ltd., Tresaith, Cardigan, Wales, pp. 267–270.
244. **Niemann**, H. and Elvert, M., 2008. Diagnostic lipid biomarker and stable carbon isotope signatures of microbial communities mediating the anaerobic oxidation of methane with sulphate. Organic Geochemistry, 39(12), pp.1668-1677.
245. **Nishihara**, M., and Koga, Y. (1995) Sn-glycerol-1-phosphate dehydrogenase in Methanobacterium thermoautotrophi- cum – key enzyme in biosynthesis of the enantiomeric glycerophosphate backbone of ether phospholipids of Archaebacteria. J Biochem 117: 933–935.
246. **Nwadinigwe**, C. A. & **Alumona**, T. N., 2018, Assessment of n-alkanes and acyclic isoprenoids (geochemical markers) in crudes: A case study of Iraq and Niger delta, Nigeria. Egypt. J. Pet. **27,** 111–116

O

247. **Orata**, F., 2012, Derivatization Reactions and Reagents for Gas Chromatography Analysis, Advanced Gas Chromatography - Progress in Agricultural, Biomedical and Industrial Applications, Dr. Mustafa Ali Mohd (Ed.), ISBN: 978-953-51-0298-4, InTech
248. **Ourisson**, G., Rohmer, M. and Poralla, K. (1987) Prokaryotic hopanoids and other sterol surrogates. Ann. Rev. Microbial. 41, 301-333.
249. **Ourisson**, G., Albrecht, P., 1992. Hopanoids 1. Geohopanoids: the most abundant natural products on Earth? Acc. Chem. Res. 25, 398– 402.
250. **Oppermann** B.I., Michaelis W., Blumenberg M., Frerichs J., Schulz H.M., Schippers A., Beaubien S.E., Krüger M., 2010, Soil microbial community changes as a result of long-term ex- posure to a natural CO_2 vent. Geochimica et Cosmochimica Acta 74, 2697–2716.
251. **Quintana-Cobo**, I., Moreira-Turcq, P., Cordeiro, C. R., Aniceto, K.Crave, A., Fraizy, P., Moreira, L.S., Contrera, J.M. de A. D., Turcq, B., 2018, Dynamics of floodplain lakes in the Upper Amazon Basin during the late Holocene, Geoscience 350, pp. 55-64

P

252. **Page**, S.E., Rieley, J.O. and Wüst, R., 2006. Lowland tropical peatlands of Southeast Asia. *Developments in Earth Surface Processes*, *9*, pp.145-172.

253. **Page**, S.E., Rieley, J.O., Banks, C.J., 2011. Global and regional importance of the tropical peatland carbon pool. Glob. Chang. Biol. 17, 798–818.
254. **Pancost**, R.D., Sinninghe Damsté´, J.S., de Lint, S., van der Maarel, M.J.E.C., Gottschal, J.C., 2000a. Biomarker evidence for wide-spread anaerobic methane oxidation in Mediterranean sediments by a consortium of methanogenic archaea and bacteria. Appl. Environ. Microbiol. 66, 1126–1132.
255. **Pancost**, R.D., van Geel, B., Baas, M., Sinninghe Damsté, J.S., 2000a. D13C values and radiocarbon dates of microbial biomarkers as tracers for carbon recycling in peat deposits. Geology 28, 663–666.
256. **Pancost**, R.D., Sinninghe Damsté, J.S., 2003. Carbon isotopic compositions of prokaryotic lipids as tracers of carbon cycling in diverse settings. Chemical Geology 195, 29–58.
257. **Pancost**, R.D., Hopmans, E.C., Sinninghe Damsté´, J.S., and the MEDINAUT Shipboard Scientific Party, 2001b. Archaeal lipids in Mediterranean Cold Seeps: molecular proxies for anae- robic methane oxidation. Geochim. Cosmochim. Acta 65, 1611–1627.
258. **Pancost**, R. D., Baas M., van Geel B. and Sinninghe Damsté´ J. S., (2003) Response of an ombrotrophic bog to a regional climate event revealed by macrofossil, molecular and carbon isotopic data. Holocene 13, 921–932.
259. **Pancost**, R. D., McClymont, E.L., Bingham, E.M., Roberts, Z., Charman, D.J., Hornibrook, E.R., Blundell, A., Chambers, F.M., Lim, K.L. and Evershed, R.P., 2011. Archaeol as a methanogen biomarker in ombrotrophic bogs. Organic Geochemistry, 42(10), pp.1279-1287.
260. **Pankratov**, T.A., Kirsanova, L.A., Kaparullina, E.N., Kevbrin, V.V. and Dedysh, S.N., 2012, Telmatobacter bradus gen. nov., sp. nov., a cellulolytic facultative anaerobe from subdivision 1 of the Acidobacteria, and emended description of Acidobacterium capsulatum Kishimoto et al. 1991, International Journal of Systematic and Evolutionary Microbiology (2012), 62, 430–437
261. **Patt**, T. E., Cole, G. C. and Hanson, R. S. (1976). Int. J. Syst. Bad. 26, 226-229.
262. **Payne**, R.J. and Blackfold, J.J., 2008, Peat humification and climate change: a multi-site comparison from mires in south-east Alaska, Mires and Peat, 3(09), pp. 1-11
263. **Peters**, K.E. and Moldowan, J.M., 1991. Effects of source, thermal maturity, and biodegradation on the distribution and isomerization of homohopanes in petroleum. Organic geochemistry, 17(1), pp.47-61.
264. **Pearson** A, Brocks JJ, Budin M (2003) Phylogenetic and biochemical evidence for sterol synthesis in the bacterium, Gemmata obscuriglobus. Proceedings of the National Academy of Sciences of the United States of America 100, 15,352–15,315,357
265. **Pease**, T.K., van Vleet, E.S., Barre, J.S., 1992. Diphytanyl glycerol ether distributions in sediments of the Orca Basin. Geochimica et Cosmochimica Acta 56, 3469–3479.
266. **Pease**, T.K., Van Vleet, E.S., Barre, J.S., Dickins, H.D., 1998. Simulated degradation of glyceryl ethers by hydrous and flash pyrolysis. Org. Geo- chem. 29, 979-988
267. **Pennington**, T.D., Reynel, C., Daza, A., 2004. Illustrated Guide to the Trees of Peru. David Hunt, Sherborne, UK (848 pp.)
268. **Peltzer**, E.T., and **Gagosian**, R.B., 1989. Organic geochemistry of aerosols over the Pacific Ocean. Chemical Oceanography 10, 282–338.

269. **Peters**, K. E., C. C. Walters, and J. M. Moldowan (2005), The Biomarker Guide, Cambridge Univ. Press, Cambridge, U. K.
270. **Piotrowska-Seget**, Z. and **Mrozik**, A., 2003. Signature lipid biomarker (SLB) analysis in determining changes in community structure of soil microorganisms. *Polish Journal of Environmental Studies*, *12*(6)
271. **Pihlatie** M., Ambus P., Rinne J., Pilegaard K., Vesala T., 2005, Plant-mediated nitrous oxide emissions from beech (Fagus sylvatica) leaves. New Phytol 168:93–98.
272. **Pitcher**, A., E. C. Hopmans, S. Schouten, and J. S. Sinninghe Damsté´. 2009. Separation of core and intact polar archaeal tetraether lipids using silica columns: insights into living and fossil biomass contributions. Org. Geochem. 40:12–19.
273. **Poynter**, J.G., Farrimond, P., Robinson, N. and Eglinton, G., 1989. Aeolian-derived higher plant lipids in the marine sedimentary record: Links with palaeoclimate. In Paleoclimatology and paleometeorology: modern and past patterns of global atmospheric transport (pp. 435-462). Springer, Dordrecht.
274. **Prahl**, F.G., Hayes, J.M., Xie, T.-M., 1992. Diploptene: an indicator of terrigenous organic carbon in Washington coastal sediments. Limnol. Oceanogr. 37, 1290±1300
275. **Prigent**, C., Papa, F., Aires, F., et al., 2007. Global inundation dynamics inferred from mul- tiple satellite observation, 1993-2000. J. Geophys. Res. Atmos. 112, 1103–1118.
276. **Pu**, Y., Zhang, H., Wang, Y., Lei, G., Nace, T. and Zhang, S., 2011, Climatic and environmental implications from n-alkanes in glacially eroded lake sediments in Tibetan Plateau: An example from Ximen Co, Chinese Science Bulletin, Vol. 56, No. 14, pp. 1503-1510
277. **Putkinen**, A., Juottonen, H., Juutinen, S., Tuittila, E.S., Fritze, H. and Yrjälä, K., 2009. Archaeal rRNA diversity and methane production in deep boreal peat. FEMS microbiology ecology, 70(1), pp.87-98.
278. **Purvaja**, R., Ramesh, R. & Frenzel, P, 2004, Plant-mediated methane emission from an Indian mangrove. Glob. Chang. Biol. **10,** 1825–1834

Q

279. **Quintana-Cobo**, I., Moreira-Turcq, P., Cordeiro, R.C., Aniceto, K., Crave, A., Fraizy, P., Moreira, L.S., Contrera, J.M.D.A.D. and Turcq, B., 2018. Dynamics of floodplain lakes in the Upper Amazon Basin during the late Holocene. *Comptes Rendus Geoscience*, *350*(1-2), pp.55-64.

R

280. **Rieley**, G., Collier, R.J., Jones, D.M., Eglinton, G., Eakin, P.A., Fallick, A.E., 1991, Sources of sedimentary lipids deduced from stable carbon-isotope analyses of individual compounds. Nature 352, pp. 425–427.
281. **Räsänen** M.E., Salo J, Jungnert H, Pittman LR (1990) Evolution of the western Amazon lowland relief: impact of Andean foreland dynamics. Terra Nova 2:320–332
282. **Räsänen**, M.E., Salo, J.S., Jungner, H., 1991. Holocene floodplain lake sediments in the Amazon: 14C dating and palaeoecological use. Quaternary Science Reviews 10, 363–372

283. **Räsänen** M, Neller R, Salo J, Jungner H (1992) Recent and ancient fluvial deposition systems in the Amazonian foreland basin, Peru. Geol Mag 129:293–306
284. **Rieley**, G., Collier, R.J., Jones, D.M., Eglinton, G., Eakin, P.A. and Fallick, A.E., 1991. Sources of sedimentary lipids deduced from stable carbon-isotope analyses of individual compounds. Nature, 352(6334), p.425.
285. **Ries-Kautt**, M., Albrecht, P., 1989. Hopane-derived triterpenoids in soils. Chemical Geology, 76, pp. 143-151
286. **Risatti**, J.B., Rowland, S.J., Yon, D.A., Maxwell, J.R., 1984. Stereochemical studies of acyclic isoprenoids XII. Lipids of methanogenic bacteria and possible contributions to sedi- ments. Organic Geochemistry 6, 93–104
287. **Rohmer**, M., Bouvier, P. and Ourisson, G., 1979. Molecular evolution of biomembranes: structural equivalents and phylogenetic precursors of sterols. *Proceedings of the National Academy of Sciences*, *76*(2), pp.847-851.
288. **Rohmer**, M., Bouvier-Nave, P. and Ourisson, G., 1984. Distribution of hopanoid triterpenes in prokaryotes. Microbiology, 130(5), pp.1137-1150.
289. **Rohmer**, M., Bisseret, P., Neunlist, S., 1992. The hopanoids, prokaryotic triterpenoids and precursors of ubiquitous molecular fossils. In: Moldowan, J.M., Albrecht, P., Philp, R.P. (Eds.), Biological Markers in Sediments and Petroleum. Prentice-Hall, New Jersey, pp. 1 –17.
290. **Rontani**, J.F. and Bonin, P., 2011, Production of pristane and phytane in the marine environment: role of prokaryotes. Research in microbiology, 162(9), pp.923-933.
291. **Rosell-Melé**, A., Moraleda-Cibrian, N., Cartro-Sabate, M., Colomer-Ventura, F., Mayor, P., Orta-Martinez, M., 2018, Oil pollution in soils and sediments from the Northern Peruvian Amazon. Sci. Total Environ. 610–611, 1010–1019
292. **Rush**, D., Sinninghe Damsté, J.S., Poulton, S.W., Thamdrup, B., Garside, A.L., Acuña González, J., Schouten, S., Jetten, M.S.M., Talbot, H.M., 2014. Anaerobic ammonium-oxidising bacteria: A biological source of the bacteriohopanetetrol stereoisomer in marine sediments. Geochimica et Cosmochimica Acta 140, 50-64.
293. **Russi**, D., ten Brink, P., Farmer, A., Badura, T., Coates, D., Fòrster, J., Kumar, R., and Davidson, N., 2013, The Economics of Ecosystems and Biodiversity for Water and Wetlands, IEEP: London
294. **Ruokolainen**, K., Schulman, L., Tuomisto, H., 2001. On Amazonian peatlands. International Mire Conservation Group Newsletter 2001, 8–10.

S

295. **Saenz**, J.P., Grosser, D., Bradley, A.S., Lagny, T.J., Lavrynenko, O. Broda, M. and Simons, K., 2015, Hopanoids as functional analogues of cholesterol in bacterial membranes, PNAS, Vol. 112, np.38., pp. 11971-11976
296. **Sahm**, H., Rohmer, M., Bringer-Meyer, S., Sprenger, G.A. and Welle, R. (1993) Biochemistry and physiology of hopanoids in bacteria. Adv. Microbial Physiol. 35, 247-273.
297. **Sauer**, T. and **Boehm**, P., 1991, The use of defensible analytical chemical measurements for oil spill natural resource damage assessment. Proceedings of the International Oil Spill Conference, March 3–7, San Diego, CA. American Petroleum Institute, Washington, DC, 1991, p 363.

298. **Schouten** S., Hopmans E.C., Schefuß E., Sinninghe Damsté J.S., 2002. Distributional variations in marine crenarchaeotal membrane lipids: a new tool for reconstructing ancient sea water temperatures? Earth and Planetary Science Letters 204, 265-274
299. **Schouten** S., Hopmans E. C. and Sinninghe Damsté´ J. S. (2013), The organic geochemistry of glycerol dialkyl glycerol tetraether lipids: a review, Org. Geochemistry, 54, pp. 19-61
300. **Scott**, R.P.W., 2003. Gas chromatography. book 2 Chrom-Ed Book Series. The Reese-Scott Partnership.
301. **Sebacher**, D. I., R. C. Harriss, K. B. Bartlett, S. M. bacheL and S.S. Grice, 1986, Atmospheric methane sources: Alaskan tundra bogs, an alpine fen, and a subarctic real marsh, Tellus, 1-10
302. **Sessions**, A.L., Zhang, L., Welander, P.V., Doughty, D., Summons, R.E. and Newman, D.K., 2013. Identification and quantification of polyfunctionalized hopanoids by high temperature gas chromatography–mass spectrometry. Organic geochemistry, 56, pp.120-130.
303. **Shah**, S.R., Mollenhauer, G., Ohkouchi, N., Eglinton, T.I. and Pearson, A., 2008. Origins of archaeal tetraether lipids in sediments: Insights from radiocarbon analysis. Geochimica et Cosmochimica Acta, 72(18), pp.4577-4594.
304. **Sinninghe Damsté**, J.S., Hopmans, E.C., Pancost, R.D., Schouten, S., Geenevasen, J.A.J., 2000, Newly discovered non-isoprenoid dialkyl diglycerol tetraether lipids in sediments. Journal of the Chemical Society, Chemical Communications 23, 1683–1684.
305. **Sinninghe Damsté**, J.S., Rijpstra, W.I.C., Hopmans, E.C., Weijers, J.W.H., Foesel, B.U., Overmann, J., Dedysh, S.N., 2011. 13,16-Dimethyl octacosanedioic acid (iso-diabolic acid): a common membrane-spanning lipid of Acidobacteria subdivisions 1 and 3. Applied and Environmental Microbiology 77, 4147– 4154.
306. **Sinninghe Damsté**, J.S., Rijpstra, W.I.C., Schouten, S., Fuerst, J.A., Jetten, M.S.M., Strous, M., 2004. The occurrence of hopanoids in planctomycetes: implications for the sedimentary biomarker record. Organic Geochemistry 35, 561-566.
307. **Sinninghe Damsté**, J.S., Rijpstra, W.I.C., Hopmans, E.C., Schouten, S., Balk, M., Stams, A.J.M., 2007. Structural characterization of diabolic acid-based tetraester, tetraether and mixed ether/ester, membrane-spanning lipids of bacteria from the order Thermotogales. Archives of Microbiology 188, 629–641.
308. **Shaw**, S.P. and **Fredine**, C.G., 1956. Wetlands of the United States. USDA Fish Wildl. Serv.,Circ. 39, 67 pp.
309. **Sjodin** A.L., Lewis W.M. Jr and Saunders J.F. III 1997. Denitrification as a component of the nitrogen budget for a large plains river. Biogeochem. 39: 327–342.
310. **Smith**, K. E. and Luna, T. O., 2013, Radial oxygen loss in wetland plants: potential impacts on remediation of contaminated sediments. J. Environ. Eng. 139, 496–501
311. **Spencer-Jones**, C., 2016. Novel concepts derived from microbial biomarkers in the Congo System: Implications for continental methane cycling, PhD Thesis
312. **Suszczynski**, E. F., 1984, The peat resources of Brazil, in Proceedings of the 7th International Peat Congress, Dublin, Ireland, vol.1,pp.468–492, Int. Peat Soc., Jyväskylä, Finland.

313. **Stefanakis**, S., Akratos, C., Tsihrintzis, V, 2014, Vertical flow constructed wetlands: eco-engineering systems for wastewater and sludge treatment. Amsterdam, Netherlands. Elsevier Science. pp. 392.
314. **Strack**, M., Kellner, E. and Waddington, J.M., 2005. Dynamics of biogenic gas bubbles in peat and their effects on peatland biogeochemistry. *Global Biogeochemical Cycles*, *19*(1).
315. **Sturt**, H.F., Summons, R.E., Smith, K., Elvert, M. and Hinrichs, K.U., 2004. Intact polar membrane lipids in prokaryotes and sediments deciphered by high-performance liquid chromatography/electrospray ionization multistage mass spectrometry—new biomarkers for biogeochemistry and microbial ecology. Rapid Communications in Mass Spectrometry, 18(6), pp.617-628.

T

316. **Takahashi,** H., Yamauchi, T., Colmer, T.D. and Nakazono, M., 2014. Aerenchyma formation in plants. In *Low-Oxygen Stress in Plants* (pp. 247-265). Springer, Vienna.
317. **Talbot**, G., Topp, E., Palin, M.F., Masse, D.I., 2008. Evaluation of molecular meth- ods used for establishing the interactions and functions of microorganisms in anaerobic bioreactors. Water Res. 42, 513–537
318. **Teh**, Y. A., Murphy, W. A., Berrio, J.-C., Boom, A., and Page, S. E., 2017, Seasonal variability in methane and nitrous oxide fluxes from tropical peatlands in the Western Amazon basin. Biogeosciences Discussions, (February), 1–39.
319. **Teixidor**, P. and Grimalt, J.O., 1992. Gas chromatographic determination of isoprenoid alkylglycerol diethers in archaebacterial cultures and environmental samples. Journal of Chromatography A, 607(2), pp.253-259.
320. **Theisen**, A.R. and Murrell, J.C., 2005, Facultative methanotrophs revisited. J. Bacteriol. 187, 4303–4305.
321. **Thormann**, M.N., Currah, R.S., and Bayley, S.E. 2003. Succession of microfungal assemblages in decomposing peatland plants. Plant Soil, 250: 323–333.
322. **Taipale**, S., Jones, R.I. and Tiirola, M., 2009. Vertical diversity of bacteria in an oxygen-stratified humic lake, evaluated using DNA and phospholipid analyses. Aquatic Microbial Ecology, 55(1), pp.1-16.
323. **Treibs**, A., 1934, The occurrence of chlorophyll derivatives in an oil shale of the upper Triassic, Annalen, Vol. 517, 103-114.
324. **Trotsenko**, Y.A., Khmelenina, V.N., 2005. Aerobic methanotrophic bacteria of cold
325. ecosystems. FEMS Microbiol. Ecol. 53, 15–26.
326. **Twenhofel**, W. H., Principles of Sedimentation, McGraw-Hill, New York, 1926.
327. **Twenhofel**, W. H., Principles of Sedimentation, McGraw-Hill, New York, 1951

U

328. **Updegraff**, K, Pastor J, Bridgham S.D., Johnston C.A., 1995, Environmental and substrate controls over carbon and nitrogen mineralization in northern wetlands. Ecol Appl 5:151–163.

V

329. **Valderrama**, E. H., 2013, Floristics and above-ground biomass in peatlands in Peruvian lowland Amazonia, Loreto, Peru. Department of Biology, Msc. Thesis
330. **Vaksmaa**, A., Lüke, C., Van Alen, T., Vale, G., Lupotto, E., Jetten, M.S. and Ettwig, K.F., 2016. Distribution and activity of the anaerobic methanotrophic community in a nitrogen-fertilized Italian paddy soil. *FEMS microbiology ecology*, *92*(12).
331. **Van Graas**, G., De Leeuw, J.W., Schenk, P.A. and Haverkamp, J., 1981, Kerogen of Toarcian shales of the Paris Basin A study of its maturation by flash pyrolysis techniques, Geochim. Cosmochim. Acta, 45 (1981), pp. 2465-2474
332. **Virapongse** A, Endress BA, Gilmore MP, Horn, C., Romulo, C., 2017, Ecology, livelihoods, and management of the Mauritia flexuosa palm in South America. Glob Ecol Conserv 10:70–92
333. **van Dongen**, B.E., Talbot, H.M., Schouten, S., Pancost, R.D., 2006. Well preserved Paleogene and Cretaceous biomarkers from the Kilwa area, Tanzania. Organic Geochemistry 37, 539-557.
334. **van Lent**, J., Hergoualc'h, K., Verchot, L., Oenema, O., & van Groenigen, J. W., 2018, Greenhouse gas emissions along a peat swamp forest degradation gradient in the Peruvian Amazon: soil moisture and palm roots effects. Mitigation and Adaptation Strategies for Global Change, 1–19.
335. **van Noordwijk**, M., Martikainen, P., Bottner, P., Cuevas, E., Rouland, C. and Dhillion, S.S., 1998. Global change and root function. *Global change biology*, *4*(7), pp.759-772.
336. **van Winden**, J. F., Talbot, H. M., De Vleeschouwer, F., Reichart, G. J., and Sinninghe Damsté, J. S., 2012, Variation in methanotroph-related proxies in peat deposits from Misten Bog, Hautes-Fagnes, Belgium. *Organic Geochemistry*, *53*, 73–79.
337. **Venterink**, H.O., Hummelink, E. and Van den Hoorn, M.W., 2003. Denitrification potential of a river floodplain during flooding with nitrate-rich water: grasslands versus reedbeds. *Biogeochemistry*, *65*(2), pp.233-244.
338. **Volkman**, J., 2003. Sterols in microorganisms. Applied microbiology and Biotechnology, 60(5), pp.495-506.
339. **Volkman**, J.K., 2005. Sterols and other triterpenoids: source specificity and evolution of biosynthetic pathways. Organic Geochemistry, 36(2), pp.139-159.

W

340. **Wahyunto**, Ritung, S., Subagjo, H., 2003. Peta Luas Sebaran Lahan Gambut dan Kandungan Karbon di Pulau Sumatera/Maps of Area of Peatland Distribution and Carbon Content in Sumatera, 1990e2002. Wetlands International e Indonesia Programme & Wildlife Habitat Canada (WHC).
341. **Wahyunto**, Ritung, S., Subagjo, H., 2004. Peta Sebaran Lahan Gambut, Luas dan Kandungan Karbon di Kalimantan / Map of Peatland Distribution Area and Carbon Content in Kalimantan, 2000e2002. Wetlands International - Indonesia Programme & Wildlife Habitat Canada (WHC)
342. **Walker**, T. S., Bais, H. P., Grotewold, E. & Vivanco, J. M. Root exudation and rhizosphere biology. Plant Physiol. 132, 44–51 (2003).

343. **Wang**, M., Zhang, W. and Hou, J., 2015, Is average chain length of plant lipids a potential proxy for vegetation, environment and climate change? Biogeosciences Discuss, Vol. 12, pp. 5477-5501
344. **Waterway**, M. J., K. T. Martins, A. Dabros, A. Prado, and M. J. Lechowicz. 2016. Ecological and evolutionary diversification within the genus Carex (Cyperaceae): Consequences for community assembly in subarctic fens. Systematic Botany 41: 558–579.
345. **Weete**, D., 1972, Aliphatic hydrocarbons of the fungi, Phytochemistry, 11 (1972) ,pp. 1201-1205
346. **Weijers**, J.W., Schouten, S., van der Linden, M., van Geel, B. and Sinninghe Damsté, J.S., 2004. Water table related variations in the abundance of intact archaeal membrane lipids in a Swedish peat bog. *FEMS Microbiology Letters, 239*(1), pp.51-56.
347. **Weijers**, J. W., 2007, Soil-derived branched tetraether membrane lipids in marine sediments: reconstruction of past continental climate and soil organic matter fluxes to the ocean. Geologica Ultraiectina **275; PhD Thesis**
348. **Weijers**, J.W., Schouten, S., Hopmans, E.C., Geenevasen, J.A., David, O.R., Coleman, J.M., Pancost, R.D. and Sinninghe Damsté, J.S., 2006a. Membrane lipids of mesophilic anaerobic bacteria thriving in peats have typical archaeal traits. *Environmental Microbiology, 8*(4), pp.648-657.
349. **Weijers** J. W. H., Schouten S., Spaargaren O. C. and Sinninghe Damsté´ J. S. (2006b) Occurrence and distribution of tetraether membrane lipids in soils: implications for the use of the TEX86 proxy and the BIT index, Org. Geochem. 37, 1680-1693.
350. **Weijers**, J.W.H., Schefub, E., Schouten, S., Sinninghe Damsté, J.S., 2007a. Coupled thermal and hydrological evolution of tropical Africa over the last deglaciation. Science 315, 1701–1704.
351. **Weijers**, J.W.H., Schouten, S., Van Den Donker, J.C., Hopmans, E.C. and Sinninghe Demste, J.S., 2007b, Environmental controls on bacterial tetraether membrane lipid distribution in soils Geochim. Cosmochim. Acta, 71, pp. 703-713
352. **Welte**, D.H. and **Ebhardt**, G., 1968. Distribution of long-chain n-paraffins and n-fatty acids in sediments from the Persian Gulf. Geochimica et Cosmochimica Acta 32, 465–466
353. **Welte**, D.H., Waples, D.W., 1973. Über die Bevorzugung geradzahliger n-Alkane in Sedimentgesteinen. Naturwissenschaften 60, 516–517.
354. **Whalen**, S.C., 2005, Biogeochemistry of methane exchange between natural wetlands and the atmosphere. Environmental Engineering Science, 22, pp. 73–94
355. **Winkler**, M. G., and **DeWitt**, C. B. (1985). Environmental impacts of peat mining: documentation for wetland conservation. Environmental Conservation 12, 317–330.
356. **White**, D.C., Davis, W.M., Nickels, J.S., King, J.D., Bobbie, R.J., 1979. Determination of the sedimentary microbial biomass by extractable lipid phosphate. Oecologia 40, 51–62.
357. **Whittenbury**, R., Phillips, K.C. and Wilkinson, J.F., 1970. Enrichment, isolation and some properties of methane-utilizing bacteria. Microbiology, 61(2), pp.205-218.
358. **Whiteoak**, K. and **Binney**, J., 2012, Literature Review of the Economic Value of Ecosystem Services that Wetlands Provide Final Report. Financ. Econ. Consult. ABN 66, 79.

359. **Winton**, R.S., Flanagan, N. and Richardson, C.J., 2017. Neotropical peatland methane emissions along a vegetation and biogeochemical gradient. *PloS one*, *12*(10), p.e0187019.

X

360. **Xie**, S., Liu Populin, T., Biedermann, M., Grob, K, Moret, S. and Conte, L.,2004, Relative hopane content confirming the mineral origin of hydrocarbons contaminating foods and human milk, Food Additives and Contminants, Vol.21, No.9, pp. 893-904
361. **Xi**e, S., Liu, X.L., Schubotz, F., Wakeham, S.G. and Hinrichs, K.U., 2014. Distribution of glycerol ether lipids in the oxygen minimum zone of the Eastern Tropical North Pacific Ocean. Organic Geochemistry, 71, pp.60-71.

Y

362. **Yavitt**, J.B., Lang, G.E. and Downey, D.M., 1988. Potential methane production and methane oxidation rates in peatland ecosystems of the Appalachian Mountains, United States. *Global Biogeochemical Cycles*, *2*(3), pp.253-268.
363. **Younes**, M. A., and R. P. **Philp** (2005), Source rock characterization based on biological marker distributions of crude oils in the southern Gulf of Suez, Egypt, J. Pet. Geol., 28, 301–317,
364. **Yusta-Garcia**, R., Orta-Martínez, M., Mayor, P., Gonzalez-Crespo, C., Rosell-Mele, A., 2017. Water contamination from oil extraction activities in Northern Peruvian Amazonian rivers. Environ. Pollut. 225, pp. 370–380

Z

365. **Zehnder**, A.J., Brock, T.D., 1980. Anaerobic methane oxidation: occurrence and ecology. Appl. Environ. Microbiol. 39, 194–204.
366. **Zell**, C., Kim J.-H., Moreira-Turcq P., Abril G., Hopmans E. C., Bonnet M.-P., Lima Sobrinho R. and Sinninghe Damsté´ J. S., 2013a, Disentangling the origins of branched tetraether lipids and crenarchaeol in the lower Amazon River: implications for GDGT-based proxies. Limnol. Oceanogr. 58, 343–353.
367. **Zell**, C., Kim, J.H., Hollander, D., Lorenzoni, L., Baker, P., Silva, C.G., Nittrouer, C. and Damsté, J.S.S., 2014. Sources and distributions of branched and isoprenoid tetraether lipids on the Amazon shelf and fan: Implications for the use of GDGT-based proxies in marine sediments. Geochimica et Cosmochimica Acta, 139, pp.293-312.
368. **Zelles**, L. 1999. Fatty acid patterns of phospholipids and lipopolysaccharides in the characterisation of microbial communities in soil: a review. Biology and Fertility of Soils 29, 111–129.
369. **Zhang**, Y.G., Zhang, C.L., Liu, X.L., Li, L., Hinrichs, K.U. and Noakes, J.E., 2011. Methane Index: a tetraether archaeal lipid biomarker indicator for detecting the instability of marine gas hydrates. Earth and Planetary Science Letters, 307(3), pp.525-534.

370. **Zheng**, Y., Singarayer, J.S., Cheng, P., Yu, X., Liu, Z., Valdes, P.J. and Pancost, R.D., 2014. Holocene variations in peatland methane cycling associated with the Asian summer monsoon system. Nature communications, 5, p.4631.

371. **Zheng**, Y., Li, Q., Wang, Z., Naafs, B. D. A., Yu, X., & Pancost, R. D.,2015, Peatland GDGT records of Holocene climatic and biogeochemical responses to the Asian Monsoon. Organic Geochemistry, 87, 86–95.

372. **Zigah**, P.K., Oswald, K., Brand, A., Dinkel, C., Wehrli, B. and Schubert, C.J., 2015. Methane oxidation pathways and associated methanotrophic communities in the water column of a tropical lake. Limnology and Oceanography, 60(2), pp.553-572.

373. **Zulkifley**, M. T. M., Ng, T. F., Abdullah, W. H., Raj, J. K., Shuib, M. K., Ghani, A. A., and Ashraf, M. A., 2015, Geochemical Characteristics of a Tropical Lowland Peat Dome in the Kota Samarahan-Asajaya Area, West Sarawak, Malaysia, Environ. Earth Sci., 73, 1443–1458.

Websites

Website 1:

Global Distribution of Wetlands (Last accessed: 07-10-2018)

https://www.nrcs.usda.gov/wps/portal/nrcs/detail/soils/use/?cid=nrcs142p2_054021

Website 2: Aerial roots (Last accessed: 17-11-2018)

https://www.mindenpictures.com/search/preview/buriti-palm-mauritia-flexuosa-tree-showing-root-structure-in-rainforest/0_00762505.html

Website 3: Pneumatophores (Last accessed: 17-11-2018)

https://www.examplesof.net/2013/09/example-of-pneumatophores.html#.W_ABYej7TIU

Website 4: Main Amazon effluents on South America continental scale (Last accessed: 17-11-2018)

https://en.wikipedia.org/wiki/Amazon_basin

Website 5: Pristane molecule (Last accessed 17-11-2018)

https://en.wikipedia.org/wiki/Pristane

Website 6: Phytane molecule (Last accessed 17-11-2018)

https://en.wikipedia.org/wiki/Phytane

Website 7: Archaeal and eukaryotic/bacteria phospholipids (Last accessed 17-11-2018)

https://www.khanacademy.org/science/biology/bacteria-archaea/prokaryote-structure/a/prokaryote-structure

Website 8: Main divisions of proteroarchaeota

https://en.wikipedia.org/wiki/Proteoarchaeota

Website 9: Membrane spanning character-Slide 10 (Last accessed 17-11-2018)

https://www.slideshare.net/RajanKumar16/membrane-dynamics

Website 10: Archaeol structure (Last accessed 17-11-2018)

https://en.m.wikipedia.org/wiki/File:Archaeol.png

Website 11: Proteobacteria classification (Last accessed 17-11-2018)

https://alchetron.com/Proteobacteria

Website 12: Bacteria membrane structure (Last accessed 17-11-2018)

https://www.khanacademy.org/science/high-school-biology/hs-cells/hs-the-cell-membrane/a/structure-of-the-plasma-membrane

Website 13: Hopane numbering (Last accessed 17-11-2018)

http://summons.mit.edu/biomarkers/biomarker-classification/lipids/isoprenoids/polycyclic-isoprenoids-with-concatenated-ring-system/hopanoids/

Website 14: Trans- and cis- FA examples (Last accessed 18-11-2018).

https://en.wikipedia.org/wiki/Fatty_acid

Website 15: Teh et al., (2017) supporting data set-CEDA Archive (Last accessed 25-11-2018)

http://catalogue.ceda.ac.uk/uuid/a416be296ccc40ad983a98c30fb291ee?jump=related-anchor&search_url=%2F%253Fq%253Dtropical%2Bpeatland%26sort_by%253D